

**SYNTHESIS OF SMALL MOLECULE ANTAGONISTS AT THE ANDROGEN  
RECEPTOR FOR PROSTATE CANCER TREATMENT AND EFFORTS TOWARD AN  
ENANTIOSELECTIVE CO(II)-CATALYZED CYCLOPROPANATION**

by

Serene Tai

B.S. Chemistry, Tennessee Technological University, 2015

Submitted to the Graduate Faculty of the  
Kenneth P. Dietrich School of Arts and Sciences in partial fulfillment  
of the requirements for the degree of  
Master of Science

University of Pittsburgh

2018

UNIVERSITY OF PITTSBURGH  
DIETRICH SCHOOL OF ARTS AND SCIENCES

This thesis was presented

by

Serene Tai

It was defended on

November 14<sup>th</sup>, 2017

and approved by

Dr. Paul Floreancig, Professor, Department of Chemistry

Dr. Peng Liu, Assistant Professor, Department of Chemistry

Thesis Advisor: Dr. Peter Wipf, Distinguished University Professor, Department of Chemistry

Copyright © by Serene Tai

2018

**SYNTHESIS OF SMALL MOLECULE INHIBITORS OF ANDROGEN RECEPTOR  
FOR PROSTATE CANCER TREATMENT**

Serene Tai, MS

University of Pittsburgh, 2018

This thesis describes the synthesis of fluorinated cyclopropane analogues to enhance the metabolic stability of a previously published lead candidate for prostate cancer treatment. A structural unique motif such as the bicyclo[1.1.0]pentane was also incorporated to investigate its potential as cyclopropane bioisostere. Preliminary results from liver microsome and luciferase assays suggested that fluorinations on the cyclopropane carbon atoms have little impact on the metabolic stability. However, fluorination on other labile sites showed enhanced metabolic stability while retaining compound potency. An enantioselective route to improve the original racemic synthesis of these analogues was also investigated. The key step was a Co(II)-salen catalyzed enantioselective *cis*-cyclopropanation of an olefin with ethyl diazoacetate to provide the cyclopropyl amide in 98% *ee* over three high-yielding steps.

## TABLE OF CONTENTS

<b>1.0</b>	<b>SYNTHESIS OF SMALL MOLECULE ANTAGONISTS AT THE NUCLEAR ANDROGEN RECEPTOR FOR PROSTATE CANCER TREATMENT .....</b>	<b>1</b>
<b>1.1</b>	<b>INTRODUCTION .....</b>	<b>1</b>
<b>1.1.1</b>	<b>Prostate cancer.....</b>	<b>1</b>
<b>1.1.2</b>	<b>Androgen receptor (AR) and androgen.....</b>	<b>2</b>
<b>1.1.3</b>	<b>Androgen deprivation therapy (ADT).....</b>	<b>6</b>
<b>1.1.4</b>	<b>High-throughput screening (HTS).....</b>	<b>9</b>
<b>1.1.5</b>	<b>Development of lead compound JJ-450.....</b>	<b>10</b>
<b>1.1.6</b>	<b>Metabolic stability of JJ-450.....</b>	<b>12</b>
<b>1.1.7</b>	<b>Fluorine improves metabolic stability in small molecule drugs .....</b>	<b>13</b>
<b>1.2</b>	<b>RESULTS AND DISCUSSION .....</b>	<b>15</b>
<b>1.2.1</b>	<b>Synthesis of fluorinated cyclopropane analogues of JJ-450 .....</b>	<b>15</b>
<b>1.2.1.1</b>	<b>Fluorination and trifluoromethylation at the benzylic position .....</b>	<b>15</b>
<b>1.2.1.2</b>	<b>Fluorination and trifluoromethylation at the <math>\alpha</math>-carbonyl position.</b>	<b>16</b>
<b>1.2.1.3</b>	<b>Synthesis of gem-difluorocyclopropane analogues.....</b>	<b>18</b>
<b>1.2.2</b>	<b>Bicyclo[1.1.1]pentane (BCP) as a bioisostere in medicinal chemistry .....</b>	<b>23</b>
<b>1.2.2.1</b>	<b>Design and synthesis of BCP analogues .....</b>	<b>25</b>

1.2.3	Configuration determination of cyclopropane analogues.....	28
1.2.3.1	Determination of relative configuration .....	28
1.2.3.2	Determination of absolute configuration .....	30
1.2.4	Biological data.....	34
1.2.5	Conclusion .....	40
2.0	EFFORTS TOWARD AN ENANTIOSELECTIVE CO(II)-CATALYZED CYCLOPROPANATION .....	41
2.1	INTRODUCTION .....	41
2.1.1	Synthetic route toward JJ-450 and its analogues .....	41
2.1.2	Enantioselective <i>cis</i> -cyclopropanation.....	42
2.2	RESULTS AND DISCUSSION .....	45
2.2.1	Design and synthesis of Co(II)-salen complexes .....	45
2.2.2	Gram-scale Co(II)-salen catalyzed asymmetric cyclopropanation .....	48
2.2.3	Proposed mechanism for asymmetric induction.....	49
2.2.4	Conclusion .....	51
3.0	EXPERIMENTAL SECTION .....	52
3.1	GENERAL PROCEDURE .....	52
3.2	EXPERIMENTAL PROCEDURES .....	53
	APPENDIX A .....	112
	APPENDIX B .....	169
	APPENDIX C .....	177
	BIBLIOGRAPHY .....	235

## LIST OF TABLES

Table 1. Attempted difluorocarbene additions to <i>cis</i> -alkene and alkyne.....	19
Table 2. Screening for <i>trans</i> -to- <i>cis</i> isomerization conditions.....	20
Table 3. Condition screening for hydrogenation of difluorocyclopropene.....	22
Table 4. Tentative absolute configuration assignment of the analogues. ....	32
Table 5. Half-life of analogues in mouse liver microsomes. ....	35
Table 6. Half-life of analogues with more stable side chains in mouse liver microsomes.....	36
Table 7. Luciferase activity of selected analogues .....	38
Table 8. Asymmetric cyclopropanation using Co(II)-salen complexes.....	47
Table 9. Crystal Data for <b>3b</b> . ....	179
Table 10. Data collection and structure refinement for <b>3b</b> . ....	179
Table 11. Atomic coordinates and equivalent isotropic atomic displacement parameters ( $\text{\AA}^2$ ) for <b>3b</b> . ....	180
Table 12. Bond lengths ( $\text{\AA}$ ) for <b>3b</b> .....	180
Table 13. Bond angles ( $^\circ$ ) for <b>3b</b> . ....	181
Table 14. Anisotropic atomic displacement parameters ( $\text{\AA}^2$ ) for <b>3b</b> . ....	181
Table 15. Hydrogen atomic coordinates and isotropic atomic displacement parameters ( $\text{\AA}^2$ ) for <b>3b</b> . ....	182

Table 16. Crystal data for <b>6a</b> .....	184
Table 17. Data collection and structure refinement for <b>6a</b> .....	184
Table 18. Atomic coordinates and equivalent isotropic atomic displacement parameters ( $\text{\AA}^2$ ) for <b>6a</b> .....	185
Table 19. Bond lengths ( $\text{\AA}$ ) for <b>6a</b> .....	186
Table 20. Bond angles ( $^\circ$ ) for <b>6a</b> .....	187
Table 21. Anisotropic atomic displacement parameters ( $\text{\AA}^2$ ) for <b>6a</b> .....	188
Table 22. Hydrogen atomic coordinates and isotropic atomic displacement parameters ( $\text{\AA}^2$ ) for <b>6a</b> .....	189
Table 23. Crystal data for <b>11a</b> .....	192
Table 24. Data collection and structure refinement for <b>11a</b> .....	192
Table 25. Atomic coordinates and equivalent isotropic atomic displacement parameters ( $\text{\AA}^2$ ) for <b>11a</b> .....	193
Table 26. Bond lengths ( $\text{\AA}$ ) for <b>11a</b> .....	194
Table 27. Bond angles ( $^\circ$ ) for <b>11a</b> .....	195
Table 28. Anisotropic atomic displacement parameters ( $\text{\AA}^2$ ) for <b>11a</b> .....	196
Table 29. Hydrogen atomic coordinates and isotropic atomic displacement parameters ( $\text{\AA}^2$ ) for <b>11a</b> .....	197
Table 30. Crystal data for <b>15</b> .....	200
Table 31. Data collection and structure refinement for <b>15</b> .....	200
Table 32. Atomic coordinates and equivalent isotropic atomic displacement parameters ( $\text{\AA}^2$ ) for <b>15</b> .....	201
Table 33. Bond lengths ( $\text{\AA}$ ) for <b>15</b> .....	202



Table 34. Bond angles ( $^{\circ}$ ) for <b>15</b> .....	203
Table 35. Anisotropic atomic displacement parameters ( $\text{\AA}^2$ ) for <b>15</b> . ....	204
Table 36. Hydrogen atomic coordinates and isotropic atomic displacement parameters ( $\text{\AA}^2$ ) for <b>15</b> .....	206
Table 37. Crystal data for (-)- <b>6b</b> . ....	208
Table 38. Data collection and structure refinement for (-)- <b>6b</b> . ....	208
Table 39. Atomic coordinates and equivalent isotropic atomic displacement parameters ( $\text{\AA}^2$ ) for (-)- <b>6b</b> . ....	209
Table 40. Bond lengths ( $\text{\AA}$ ) for (-)- <b>6b</b> . ....	210
Table 41. Bond angles ( $^{\circ}$ ) for (-)- <b>6b</b> . ....	211
Table 42. Anisotropic atomic displacement parameters ( $\text{\AA}^2$ ) for (-)- <b>6b</b> .....	212
Table 43. Hydrogen atomic coordinates and isotropic atomic displacement parameters ( $\text{\AA}^2$ ) for (-)- <b>6b</b> .....	213
Table 44. Crystal data for (-)- <b>11a</b> . ....	216
Table 45. Data collection and structure refinement for (-)- <b>11a</b> . ....	216
Table 46. Atomic coordinates and equivalent isotropic atomic displacement parameters ( $\text{\AA}^2$ ) for (-)- <b>11a</b> . ....	217
Table 47. Bond lengths ( $\text{\AA}$ ) for (-)- <b>11a</b> .....	218
Table 48. Bond angles ( $^{\circ}$ ) for (-)- <b>11a</b> . ....	219
Table 49. Anisotropic atomic displacement parameters ( $\text{\AA}^2$ ) for (-)- <b>11a</b> . ....	220
Table 50. Hydrogen atomic coordinates and isotropic atomic displacement parameters ( $\text{\AA}^2$ ) for (-)- <b>11a</b> . ....	221
Table 51. Crystal data for (-)- <b>34</b> . ....	224

Table 52. Data collection and structure refinement for (-)- <b>34</b> .....	224
Table 53. Atomic coordinates and equivalent isotropic atomic displacement parameters ( $\text{\AA}^2$ ) for (-)- <b>34</b> .....	225
Table 54. Bond lengths ( $\text{\AA}$ ) for (-)- <b>34</b> .....	227
Table 55. Bond angles ( $^\circ$ ) for (-)- <b>34</b> .....	228
Table 56. Anisotropic atomic displacement parameters ( $\text{\AA}^2$ ) for (-)- <b>34</b> .....	231
Table 57. Hydrogen atomic coordinates and isotropic atomic displacement parameters ( $\text{\AA}^2$ ) for (-)- <b>34</b> .....	233

## LIST OF FIGURES

Figure 1. Structural domains of AR.....	3
Figure 2. Crystal structure of AR DBD dimer (PDB:1R4I) .....	3
Figure 3. Crystal structure of AR LBD (PDB:1E3G).....	4
Figure 4. Structure of testosterone and DHT .....	5
Figure 5. AR signaling in prostate cells.....	6
Figure 6. Steroidal antiandrogens of the AR compared to native androgen DHT.....	7
Figure 7. Development of non-steroidal antiandrogens.....	8
Figure 8. Identification of novel antiandrogens from HTS campaign. ....	10
Figure 9. Dual luciferase reporter assay protocol .....	11
Figure 10. Hit-to-lead structural modifications and luciferase activity .....	12
Figure 11. Proposed metabolic pathways of <b>JJ-450</b> based on LCMS analyses of samples in mouse liver microsomes. ....	13
Figure 12. Development of ezetimibe via metabolic stability optimization using fluorine substituents.....	14
Figure 13. Reaction of cyclopropyl carbanion with electrophiles. ....	18
Figure 14. Bicyclo[1.1.1]pentane (BCP) as a bioisosteric replacement of a phenyl ring and an internal alkyne.....	24

Figure 15. Conventional syntheses of bridgehead 1,3-disubstituted BCP scaffolds. ....	25
Figure 16. Proposed strategy to access BCP analogues.....	25
Figure 17. Distinct coupling constants in the monofluorinated cyclopropane and X-ray structure of <b>3b</b> .....	28
Figure 18. Relative stereochemistry assignment of trifluoromethyl-substituted cyclopropane. ..	29
Figure 19. Through-space effect of the phenyl group in the <i>trans</i> -cyclopropyl ester. ....	30
Figure 20. Novel Co(II)-salen complexes <b>80-82</b> . ....	47
Figure 21. Proposed model for the conformation of the Co(IV)-carbenoid species.....	50
Figure 22. SFC chromatogram of racemic <b>5b</b> . ....	61
Figure 23. SFC resolution of (-)- <b>5b</b> . ....	62
Figure 24. SFC resolution of (+)- <b>5b</b> . ....	62
Figure 25. SFC chromatogram of racemic <b>6b</b> . ....	66
Figure 26. SFC resolution of (-)- <b>6b</b> .....	66
Figure 27. SFC resolution of (+)- <b>6b</b> .....	66
Figure 28. SFC resolution of <b>11a</b> .....	73
Figure 29. SFC resolution of (-)- <b>11a</b> .....	73
Figure 30. SFC resolution of (+)- <b>11a</b> .....	73
Figure 31. SFC chromatogram of crude racemic <b>34</b> .....	81
Figure 32. SFC resolution of (-)- <b>34</b> .....	82
Figure 33. SFC resolution of (+)- <b>34</b> .....	82
Figure 34. SFC chromatogram of racemic sample <b>78</b> .....	100
Figure 35. Enantiomeric excess of ( <b>1R,2S</b> )- <b>78</b> .....	101
Figure 36. SFC chromatogram of racemic sample of <b>79</b> .....	103

Figure 37. Enantiomeric excess of <b>(1R,2S)-79</b> .....	103
Figure 38. Enantiomeric excess of <b>(1S,2R)-78</b> .....	106
Figure 39. HPLC chromatogram of racemic sample <b>85</b> .....	109
Figure 40. Enantiomeric excess of <b>(1R,2S)-85</b> .....	109
Figure 41. HPLC chromatogram of racemic sample <b>86</b> .....	111
Figure 42. Enantiomeric excess of <b>(1R,2S)-86</b> .....	111
Figure 43. CD spectra for (-)- <b>5a</b> .....	169
Figure 44. CD spectra for (+)- <b>5a</b> .....	169
Figure 45. CD spectra for (-)- <b>5b</b> .....	170
Figure 46. CD spectra for (+)- <b>5b</b> .....	170
Figure 47. CD spectra for (-)- <b>6a</b> .....	171
Figure 48. CD spectra for (+)- <b>6a</b> .....	171
Figure 49. CD spectra for (-)- <b>6b</b> .....	172
Figure 50. CD spectra for (+)- <b>6b</b> .....	172
Figure 51. CD spectra for (-)- <b>11a</b> .....	173
Figure 52. CD spectra for (+)- <b>11a</b> .....	173
Figure 53. CD spectra for (-)- <b>15</b> .....	174
Figure 54. CD spectra for (+)- <b>15</b> .....	174
Figure 55. CD spectra for (-)- <b>17</b> .....	175
Figure 56. CD spectra for (+)- <b>17</b> .....	175
Figure 57. CD spectra for (-)- <b>34</b> .....	176
Figure 58. CD spectra for (+)- <b>34</b> .....	176
Figure 59. X-ray structural information for <i>rac</i> - <b>6a</b> . .....	183

Figure 60. X-ray structural information for <i>rac</i> - <b>11a</b> . .....	191
Figure 61. X-ray structural information for <i>rac</i> - <b>15</b> . .....	199
Figure 62. X-ray structural information for (-)- <b>6b</b> .....	207
Figure 63. X-ray structural information for (-)- <b>11a</b> .....	215
Figure 64. X-ray structural information for (-)- <b>34</b> .....	223

## LIST OF SCHEMAS

Scheme 1. Synthesis of benzylic fluorinated and trifluoromethylated analogues. ....	15
Scheme 2. Synthesis of $\alpha$ -carbonyl trifluoromethylated analogues.....	17
Scheme 3. Synthesis of analogues <b>15</b> and <b>17</b> .....	17
Scheme 4. Effort toward an electrophilic fluorination of a cyclopropyl ester.....	18
Scheme 5. Attempt to convert the <i>gem</i> -difluoroolefin to the <i>gem</i> -difluorocyclopropane .....	20
Scheme 6. Difluorocyclopropanation of alkyne <b>27</b> .....	21
Scheme 7. Revised route to difluorocyclopropene <b>33</b> and difluorocyclopropane <b>34</b> analogues ..	23
Scheme 8. Synthesis of BCP analogue <b>49</b> . ....	26
Scheme 9. Synthesis of analogue <b>58a</b> .....	26
Scheme 10. Efficient synthesis of BCP analogue <b>51</b> .....	27
Scheme 11. Synthetic route to racemic JJ-450 and chromatographic resolution .....	41
Scheme 12. Katsuki's development of an asymmetric <i>cis</i> -cyclopropanation.....	43
Scheme 13. Synthesis of Co(II)-salen complex <b>66</b> .....	45
Scheme 14. Asymmetric route for the synthesis of analogues with complex <b>66</b> .....	46
Scheme 15. Gram-scale enantioselective synthesis of analogues.....	48

## ABBREVIATIONS

ADT .....	androgen deprivation therapy
AF1 .....	activation function 1
AF2 .....	activation function 2
AR .....	androgen receptor
ARE.....	androgen response element
BCP .....	bicyclo[1.1.1]pentane
BDPPB .....	1,2-bis(diphenylphosphino)benzene
CRPC .....	castrate-resistant prostate cancer
DBD .....	DNA binding domain
DHT .....	5 $\alpha$ -dihydrotestosterone
DIPEA.....	diisopropylethylamine
DMAP.....	4-dimethylaminopyridine
DMF .....	<i>N,N</i> -dimethylformamide
DNA .....	deoxyribonucleic acid
EtOAc .....	ethyl acetate
HSP .....	heat shock protein
HTS .....	high-throughput screening
LBD.....	ligand binding domain
LBP .....	ligand binding pocket
LDA .....	lithium diisopropylamide
LHRH.....	luteinizing hormone-releasing hormone
MDFA .....	methyl 2,2-difluoro-2-(fluorosulfonyl)acetate
MLM.....	mouse liver microsome



MOMCl.....	methoxymethyl chloride
NES.....	nuclear export signal
NFSI.....	<i>N</i> -fluorobenzenesulfonimide
NLS.....	nuclear localization signal
NTD.....	N-terminal domain
Ph.....	phenyl
PMHS.....	poly(methylhydrosilane)
PSA.....	prostate specific antigen
SAR.....	structure-activity relationship
SHBG.....	sex hormone-binding globulin
T3P.....	propylphosphonic anhydride
TBAT.....	tetrabutylammonium triphenyldifluorosilane
TBBA.....	4- <i>tert</i> -butylbenzoic acid
THF.....	tetrahydrofuran
XRC.....	X-ray crystallography

## ACKNOWLEDGEMENTS

First and foremost, I owe my deepest gratitude to Dr. Wipf for giving me the opportunity to work in his lab and for his invaluable guidance and constructive criticisms. I would also like to thank Dr. Floreancig and Dr. Liu for serving on my thesis committee and for providing insightful comments that significantly improves my thesis.

I am also grateful for the stimulating discussions and motivation from all the Wipf group members past and present. In particular, I would like to thank the staff members: Taber Lewis, Desirae Crocker, and Mary Liang for their help in the lab.

I would like to express my appreciation to UPMC Enterprise and the Department of Defense for their financial support on this project. I thank our collaborators Dr. Zhou Wang's research group (UPMC) and Pharmaron for the biological data of our compounds.

Finally, I must express my very profound gratitude to my family and to my fiancé for providing me with unfailing support and continuous encouragement throughout my years of study. This accomplishment would not have been possible without them.

## **1.0 SYNTHESIS OF SMALL MOLECULE ANTAGONISTS AT THE NUCLEAR ANDROGEN RECEPTOR FOR PROSTATE CANCER TREATMENT**

### **1.1 INTRODUCTION**

#### **1.1.1 Prostate cancer**

Prostate cancer is the uncontrolled growth of cells in the prostate gland. It is the third leading cause of cancer death in men in the United States.<sup>1</sup> Recent statistics from the American Cancer Society showed that prostate cancer is the most common cancer in men – about one in seven men will be diagnosed with prostate cancer. The risk of developing prostate cancer is found to be higher in men aged 65 and older, mainly due to the changes in testosterone level with age although recently an increase in new diagnoses has been found in men below 55 years. There are often no symptoms associated with prostate cancer in the early stage, and it is only diagnosed during routine check-up through prostate-specific antigen (PSA) screening. In some cases, patients may experience pain and blood during urination, and the need to urinate more frequently when the urethra is being compressed by the tumor mass.

Long-term studies reported that most cases of early diagnosis are benign and slow-growing cancer cells that are not life-threatening.<sup>2-4</sup> Active monitoring showed that these cancer cells do not have significant progression over the years and the patients have high survival rates

even without any form of medical treatment. However, advanced stages of prostate cancer could be malignant, metastatic, and eventually cause death. Treatments for patients diagnosed with advanced prostate cancer include radical prostatectomy, radiation therapy, and androgen deprivation therapy (ADT).<sup>5</sup> Unfortunately, some patients eventually develop castration-resistant prostate cancer (CRPC), an incurable stage of cancer where the cells are resistant to hormone therapy.<sup>6</sup> Previously known as hormone-refractory prostate cancer, CRPC contributes to the majority of deaths from prostate cancer as the mean survival time is only one to two years. Almost all CRPC patients also develop metastases where the tumors rapidly spread to other organs, including bones and lymph nodes, causing extreme pain. Thus, it is important to understand the mechanism of CRPC and the elements that play a key role in its progression in order to develop an efficient treatment for CRPC.

### **1.1.2 Androgen receptor (AR) and androgen**

The prostate gland is a compound tubuloalveolar exocrine gland of the male reproductive system that is responsible for male sexual differentiation and functions. The growth and maintenance of healthy prostate cells are regulated by the androgen receptor (AR), a ligand-dependent nuclear transcription factor that belongs to the steroid hormone receptor superfamily.<sup>7,8</sup> The AR gene encodes a protein of 919 amino acids that consists of four major functional domains: (a) N-terminal domain (NTD), (b) DNA binding domain (DBD), (c) hinge region, and (d) ligand binding domain (LBD) (**Figure 1**).<sup>9</sup>

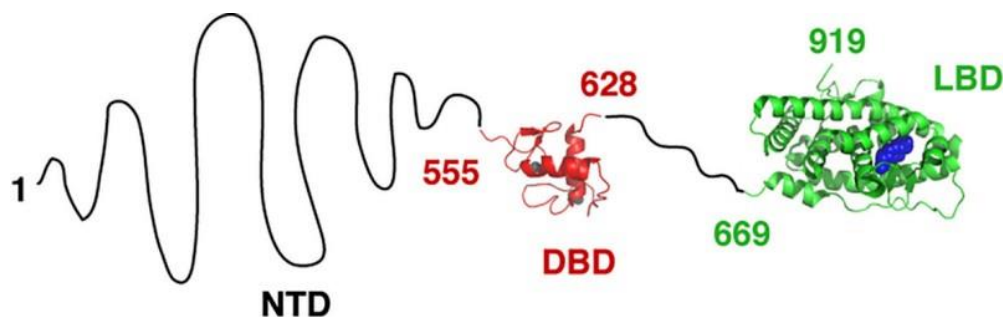


**Figure 1.** Structural domains of AR.<sup>9</sup> Copyright © 2016 American Chemical Society

The NTD consists of 555 amino acid residues, and takes up more than half the size of the AR. A combination of experimental and computational analyses suggests that the NTD exists as partially folded protein intermediate (neither full random coil nor stable globular conformation).<sup>10</sup> The intrinsic disorder of the NTD provides the flexibility that allows for binding to multiple structurally diverse protein partners. Folding is triggered by the binding event and initiates specific transcriptional functions.<sup>11</sup> The ligand-independent activation function 1 (AF1) located within the NTD is important for the transcriptional activation of the AR gene.<sup>12</sup>

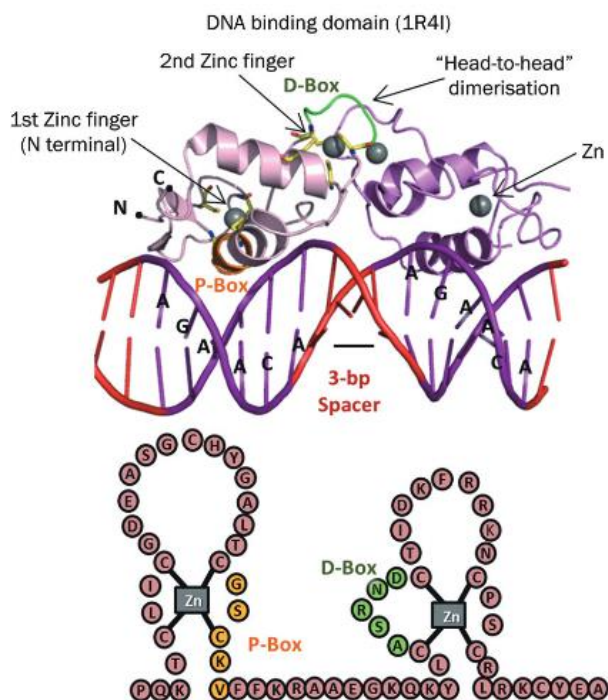


**Figure 2.** Crystal structure of AR DBD dimer (PDB:1R4I). Copyright © 2014 Nature Publishing Group

The DBD is a highly conserved cysteine-rich domain that houses 2 zinc finger domains, where the zinc ions are coordinated to four cysteine residues, respectively (**Figure 2**).<sup>13</sup> Three amino acid residues (Gly-Ser-Val) situated at the  $\alpha$ -helix of the N-terminus, named the P box, make contacts with the DNA groove at the promoter region. The AR forms a homodimeric structure when bound to the DNA. The second zinc finger contains the D box, which is a sequence of five amino acid residues (Ala-Ser-Arg-Asn-Asp) that functions as DBD/DBD binding interface during dimerization.<sup>14,15</sup> Although the main purpose of the DBD is DNA binding, studies have reported that the DBD may also be involved in other AR regulations.<sup>16-18</sup> Between the DBD and LBD is the hinge region that contains part of the nuclear localization signal (NLS) responsible for AR nuclear import. The translocation of AR (a 110kDa protein) from the cytoplasm into the nucleus is mediated by the binding of NLS to importin- $\alpha$ .<sup>19</sup>

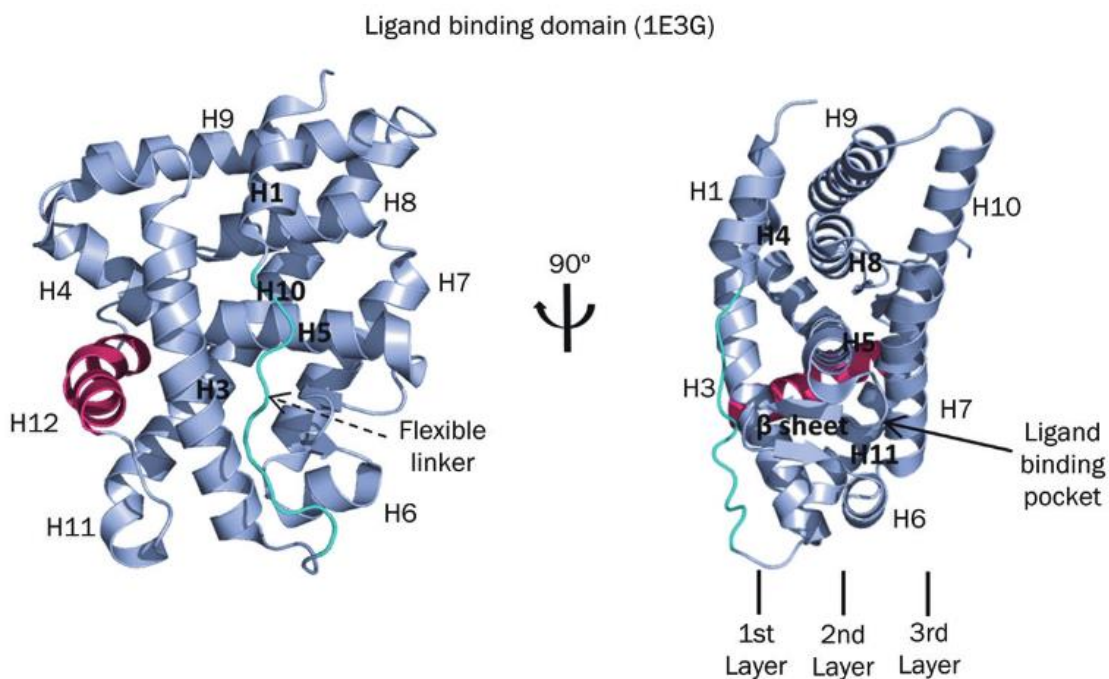


**Figure 3.** Crystal structure of AR LBD (PDB:1E3G). Copyright © 2014 Nature Publishing Group

The C-terminal LBD is made up of twelve  $\alpha$ -helices and four short  $\beta$ -strands arranged in a three-layer, antiparallel  $\alpha$ -helical sandwich fold, a feature unique to the nuclear receptor family. The X-ray crystallography (XRC) structure of the androgen-bound AR-LBD showed that there is a ligand binding pocket (LBP) buried in the helices that interacts with the ligand at H3, H5 and H11 (**Figure 3**).<sup>13,20</sup> The repositioning of H12 was observed as it acts as a ‘lid’ that closes the LBP after binding of AR agonists, possibly to prevent ligand dissociation. This conformational change also induces the formation of a hydrophobic interaction surface called activation function 2 (AF2).<sup>21</sup> Similar to AF1, the binding of coregulators to AF2 triggers the transactivation function of the AR. In contrast with other nuclear receptors, AF2 also interacts preferentially with the NTD to stabilize the AR dimer complex.<sup>22</sup> In the absence of androgen, AR is exported from the nucleus into the cytoplasm by the nuclear export signal (NES) located in the LBD.<sup>23</sup>

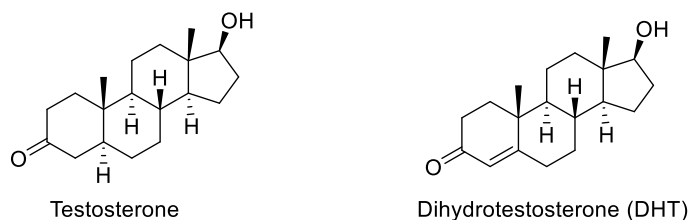


**Figure 4.** Structure of testosterone and DHT

AR activation is initiated through the binding of endogenous androgens such as testosterone and 5 $\alpha$ -dihydrotestosterone (DHT) to the LBD (**Figure 4**). Testosterones are mostly synthesized in the testes (>95%) and are bound to sex hormone binding globulin (SHBG) while circulating in the extracellular matrix.<sup>24</sup> As testosterone enters the prostatic cytoplasm, the enzyme 5 $\alpha$ -reductase readily converts testosterone to DHT, which is a more potent agonist of the AR. In the absence of androgen, the AR is mostly located in the cytoplasm as a complex with heat shock proteins (HSP-90, -70, -56) and other chaperones. The binding of DHT to the AR-

LBP results in the dissociation of heat shock proteins from the AR and induces a series of conformational changes that promote nuclear translocation. The AR homodimer interacts with the androgen response element (ARE) at the promoter region of the DNA and triggers the recruitment of coregulators to the AF1 and AF2 domains. Consequently, the docking of coregulators to AF1 and AF2 domains activates the transcription process of the target AR gene (Figure 5).<sup>13, 25-26</sup>

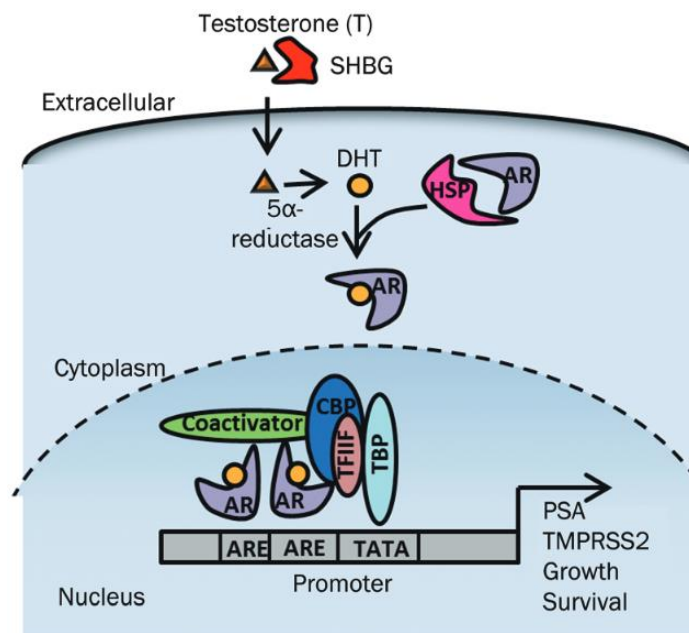


**Figure 5.** AR signaling in prostate cells.<sup>7</sup> Copyright © 2014 Nature Publishing Group

### 1.1.3 Androgen deprivation therapy (ADT)

Androgen and AR action play a vital role in the growth of cancerous prostate cells, and the suppression of androgen levels and androgen-AR interactions can impede the progression of advanced prostate cancer. Surgical castration was the conventional method of lowering androgen production prior to the development of hormone therapy. A groundbreaking discovery by Charles Huggins in 1941 in the use of chemical castration or estrogenic injection that led to



tumor regression and reduced levels of acid phosphatase (a prostate cancer marker), won him the 1966 Nobel Prize.<sup>27</sup> Since the identification of AR as a therapeutic target, steroidal and non-steroidal hormones, also called antiandrogens, have been developed to reduce androgen levels and inhibit nuclear AR signaling in prostate cancer patients, resulting in the apoptosis of androgen-dependent prostate cancer cells.

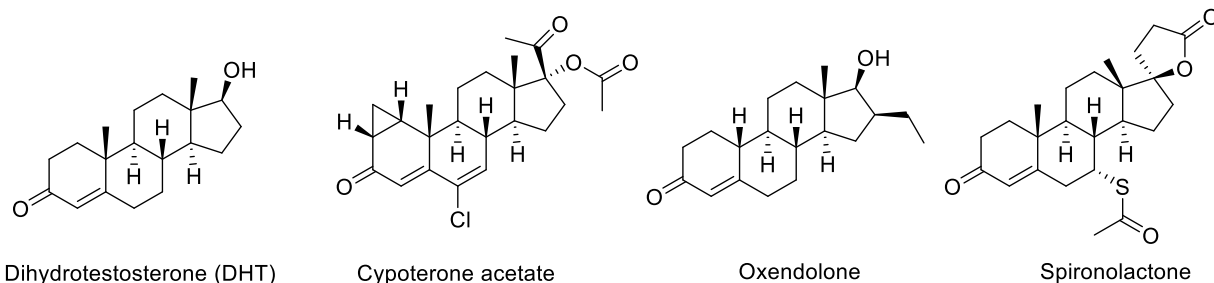


**Figure 6.** Steroidal antiandrogens of the AR compared to native androgen DHT.

Steroidal antiandrogens such as cyproterone acetate, oxendolone, and spironolactone were found to be competitive inhibitors of testosterone and DHT as they have high affinity to the AR-LBD.<sup>7, 28-29</sup> The excellent binding affinity is attributed to a common structural motif, which is a [6,6,6,5]-tetracyclic core, much like the native androgens as well as other naturally-occurring hormones (**Figure 6**). Unfortunately, this structural similarity also means that steroidal antiandrogens could be potential AR agonists and weak activators of other nuclear receptors, hence they were soon removed from prostate cancer treatment due to off-target actions and significant side effects.

In the subsequent years, more effort has been invested in the development of non-steroidal antiandrogens that possess high selectivity for AR. The antiandrogen flutamide (Eulexin) was patented by Schering-Plough Corporation, and approved by the U.S. Food and Drug Administration (FDA) in 1989, followed by bicalutamide (Casodex), and nilutamide (Nilandron) (**Figure 7a**).<sup>30-33</sup> They were approved for combined androgen blockade (CAB)

therapy in addition to luteinizing hormone-releasing hormone (LHRH) agonists, which suppress the production of luteinizing hormone (LH) and inhibit testicle testosterone synthesis. Multiple randomized trials demonstrated that patients who were administered either of these antiandrogens on top of LHRH agonists or orchiectomy showed a significant improvement in survival and progression-free survival time.<sup>34,35</sup>

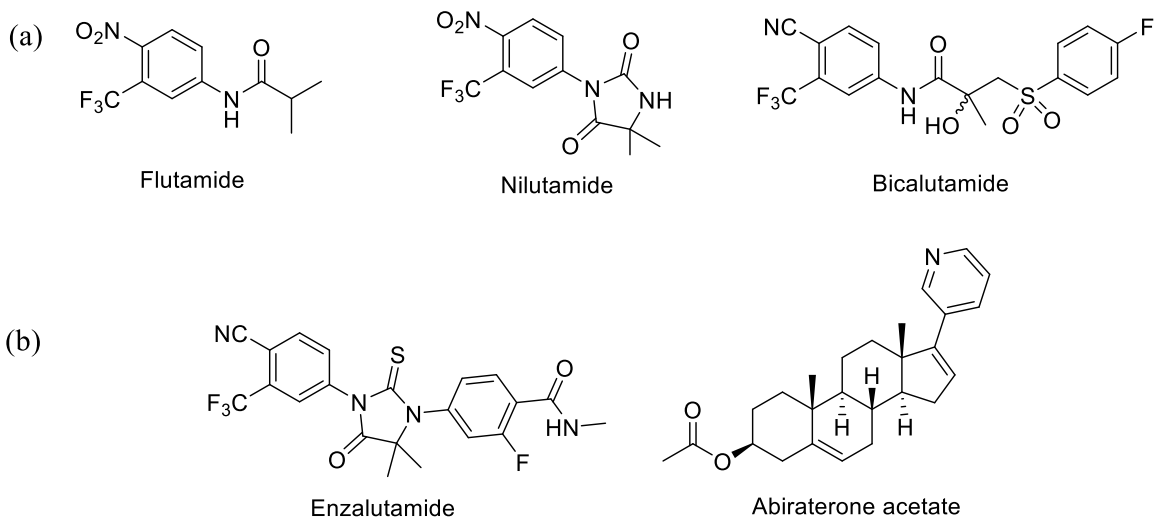


**Figure 7.** Development of non-steroidal antiandrogens. (a) First generation antiandrogen marketed for advanced prostate cancer. (b) Second generation AR inhibitors.

Some patients eventually become resistant to ADT and progress into CRPC with aggressive tumor growth. There are multiple mechanisms proposed for the initiation and propagation of CRPC, including the overexpression of the AR gene, activation of mutant AR by alternative ligands, ligand-independent AR activation via other signaling pathways, and a completely AR-independent pathway.<sup>36-38</sup> For example, studies showed that residual androgens from *in situ* tumoral synthesis and adrenal synthesis could activate the AR in CRPC cells that became hypersensitive due to lower threshold of androgens, thus amplifying AR gene expression. Literature reports suggested that amino acid substitutions from AR mutations at the LBD decreased ligand selectivity and specificity, whereby native hormones such as estrogen,

progesterone, and glucocorticoid assume the role of DHT and reactivate AR functions.<sup>7</sup> Other AR-LBD mutations also caused AR antagonists to induce an agonist role where in a specific case, a single amino acid mutation discovered during bicalutamide treatment allowed more room in the binding site to accommodate bicalutamide molecule so that it could coordinate in an agonist conformation.<sup>39</sup> In many of these cases, AR signaling kept a central role in the proliferation of CRPC.

Enzalutamide (Xtandi<sup>®</sup>) and abiraterone acetate (Zytiga<sup>®</sup>) are second generation AR inhibitors approved for CRPC treatment (**Figure 7b**).<sup>40,41</sup> Abiraterone is a steroidal CYP17A1 inhibitor, which interferes with the enzyme-catalyzed biosynthesis of androgens. Enzalutamide is a novel, more potent antiandrogen that not only competitively inhibits the binding of androgen to AR but also efficiently inhibits translocation of the AR into the nucleus.<sup>42,43</sup> Nonetheless, some cases of enzalutamide resistance have been observed.<sup>44,45</sup> Since there is no curative effect, all the treatment options for metastatic CRPC hitherto are directed toward a palliative care approach to improve the patients' quality of life and extend survival time. The crucial need for new regimens to effectively inhibit AR functions and prolong life beyond a few months continues to prompt the search for a more competent drug.

#### **1.1.4 High-throughput screening (HTS)**

Johnston *et al.* reported the first HTS that aimed to identify small molecules capable of impeding nuclear translocation in AR in CRPC cell lines.<sup>46</sup> An assay to screen 219,055 compounds from the National Institutes of Health (NIH) library was developed using C4-2 CRPC cells transfected with a green fluorescent protein tagged AR (2GFP-AR) expression vector, and the fluorescence intensities within the nucleus and cytoplasm were quantified.

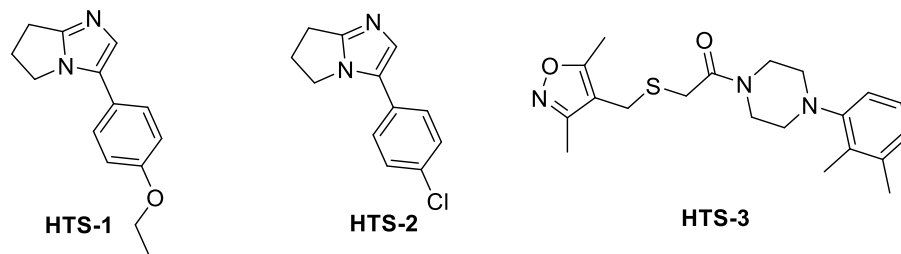


**Figure 8.** Identification of novel antiandrogens from HTS campaign.

Three small molecules were found to inhibit nuclear localization of 2GFP-AR with little or no cytotoxicity in C4-2 CRPC cell lines: treatment with **HTS-1** and **HTS-2** showed a significant shift of 2GFP-AR into the cytoplasm while treatment with **HTS-3** suggested downregulation of AR expression without cytoplasmic localization (**Figure 8**). Three hits are structurally distinct from the currently known antagonists, implying that the mechanism of inhibition could involve other components of AR signaling instead of the AR-LBP. This finding was very promising as the uncovering of the actual mechanism could open up a new strategy for CRPC drug discovery.

### 1.1.5 Development of lead compound JJ-450

After the HTS campaign, a structure-activity relationship (SAR) study on **HTS-3** was conducted by Johnson *et al.* to explore more potent analogues for nuclear localization inhibition in CRPC.<sup>47</sup> These analogues were subjected to an *in vitro* luciferase assay using CRPC C4-2 cell lines transfected with a prostate-specific antigen (PSA) promoter-driven Firefly luciferase reporter vector and a Renilla luciferase as the internal control reporter (**Figure 9**). The luciferase activity of the transfected C4-2-PSA-rl cell line was first induced by the synthetic androgen R1881. The cells were then treated with the test compounds and measured for the changes in luciferase

activity. The amount of expressed luciferase activity corresponds to the measured light intensities. Since the PSA promoter activity is a biomarker for AR transcriptional activity, the inhibition of AR by the test compounds will result in a decrease in luciferase activity. The measured androgen-driven luciferase activity was normalized to the Renilla luciferase activity.

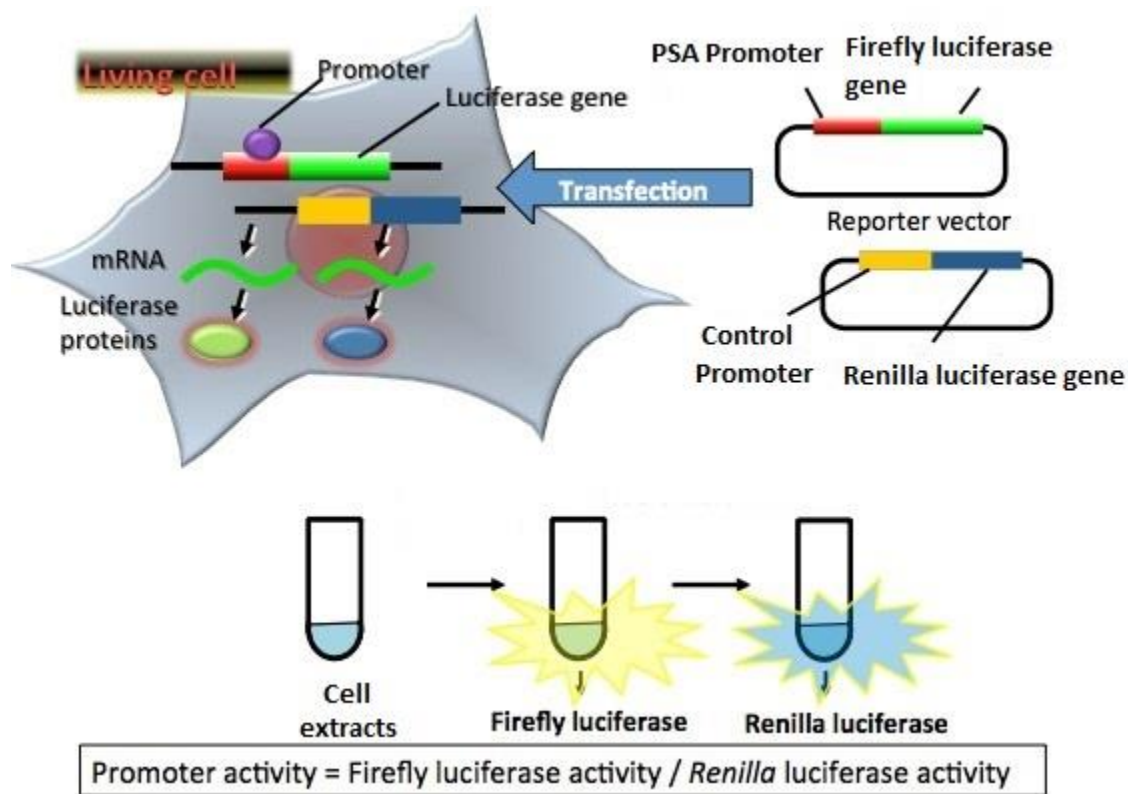
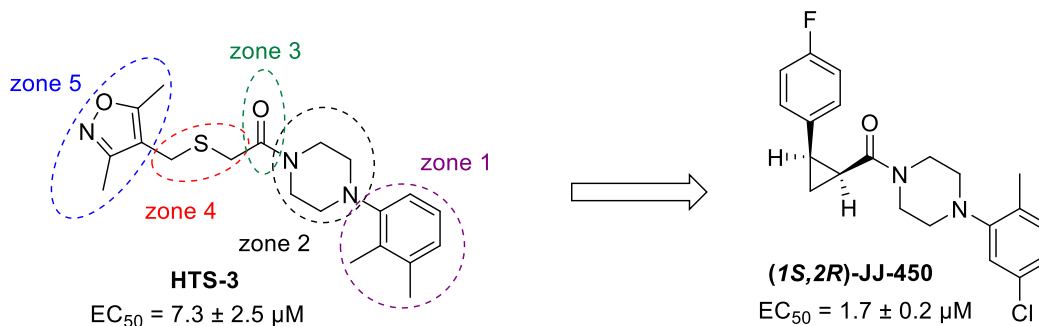


Figure 9. Dual luciferase reporter assay protocol. Copyright © American Society for Photobiology

**HTS-3** was divided into five zones for structural modifications and a total of 35 analogues were synthesized. Several structural moieties were found to be imperative for activity (**Figure 10**). The *ortho*-substitution on the phenyl group in zone 1 was important as removing the *ortho*-methyl and altering the methyl group to the *meta*- or *para*-position led to a complete loss of activity. In zone 2, replacing the piperazine with acyclic and bridged amines resulted in decreased activity, while the sterically hindered 2,6-dimethylpiperazine was found to have a 2-fold increase in activity. The carbonyl group in zone 3 was not required as a sulfonamide or

amine were tolerated at that position. The attempt to substitute the thioether linkage in zone 4 with an ether or *N*-methyl amine rendered the analogues inactive while a *cis*-cyclopropane significantly improved activity. In zone 5, substituted phenyl groups were equipotent with the 3,5-dimethylisoxazole present in the initial hit. The *cis*-cyclopropane analogue (JJ-450) was found to be 3-fold more active than the HTS hit and chiral resolution gave the more potent (*1S,2R*)-enantiomer and the 10-fold less potent (*1R,2S*)-enantiomer. The equipotency of (*1S,2R*)-JJ-450 to enzalutamide was a compelling outcome from this hit-to-lead study for the further development of a novel CRPC drug candidate.



**Figure 10.** Hit-to-lead structural modifications and luciferase activity

### 1.1.6 Metabolic stability of JJ-450

The metabolic stability assay of JJ-450 in different species of liver microsomes revealed that it has a very short half-life of 5.3 minutes in mouse liver microsomes. Preliminary metabolic stability studies using LCMS suggested that JJ-450 may undergo various oxidations and fragmentations at the cyclopropane and piperazine amide sites in mouse liver microsomes (**Figure 11**). Our approach to overcome this issue was to install fluorine atoms at these labile sites in hopes to develop analogues that are more resistant to metabolic attack.

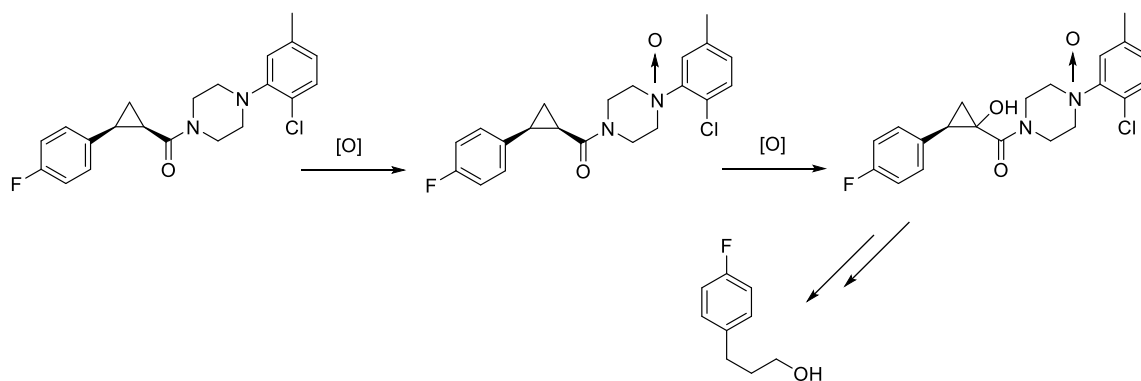


**Figure 11.** Proposed metabolic pathways of JJ-450 based on LCMS analyses of samples in mouse liver microsomes.

### 1.1.7 Fluorine improves metabolic stability in small molecule drugs

The first fluorine-containing synthetic pharmaceutical drug, fludrocortisone, was granted FDA approval in 1955 but prior to that the incorporation of fluorine into medicinal drug was unthinkable.<sup>48</sup> The lack of fluorinated natural products and the non-trivial method for laboratory fluorinations ruled out the feasibility of synthesizing fluorinated drugs. Even 15 years after the development of fludrocortisone, which was proven to have more desirable biological properties than its non-fluorinated derivative, fluorine-containing small molecule drugs only account for 2% of the pharmaceutical market in 1970.<sup>49</sup> However, the advancement of novel and safe fluorinating reagents in the 1970s facilitated the use of fluorine building blocks in drug design.<sup>50</sup> Currently, approximately 30% of the marketed pharmaceuticals contain at least one fluorine atom, including top-selling drugs such as Prozac (antidepressant), Crestor (reduces cholesterol level), and Seretide (bronchodilator).<sup>51</sup>

One of the major contributions of fluorine substitution in small molecule drugs is the increase in metabolic stability.<sup>52</sup> Various examples in the literature show that substituting the more labile C–H bond with a C–F bond helped prevent oxidative metabolism by the liver P450

cytochrome enzymes, thus extending its bioavailability without losing activity.<sup>53-55</sup> This beneficial effect is attributed to various unique properties of this most electronegative element in the periodic table:<sup>56</sup>

- the stronger bond energy of the C–F bond (485 kJ mol<sup>-1</sup> vs 413 kJ mol<sup>-1</sup>), which makes it harder to be cleaved than the C–H bond.
- the relatively small size of the fluorine atom compared to the hydrogen atom (1.47 Å vs 1.20 Å) makes it a good replacement with minimum steric disruptions.
- the highly electronegative fluorine atom (3.98 Pauling scale) can withdraw electron density of adjacent or distal bonds, thus reducing the rate of metabolism.

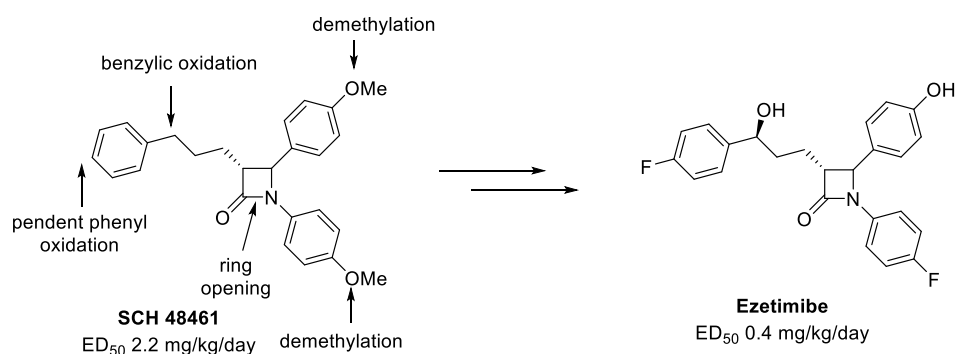


**Figure 12.** Development of ezetimibe via metabolic stability optimization using fluorine substituents.

The rational design of ezetimibe, a cholesterol lowering drug, was a proof of how the substitution with a fluorine atom improved metabolic stability and enhanced potency (**Figure 12**).<sup>57</sup> The parent molecule of ezetimibe, SCH 48461, although having modest potency, contains five major metabolically labile sites, and generates metabolites that reduce its overall potency. An intensive SAR study was conducted to probe the effects of various substitutions at the sites of detrimental metabolic oxidations, leading to ezetimibe.

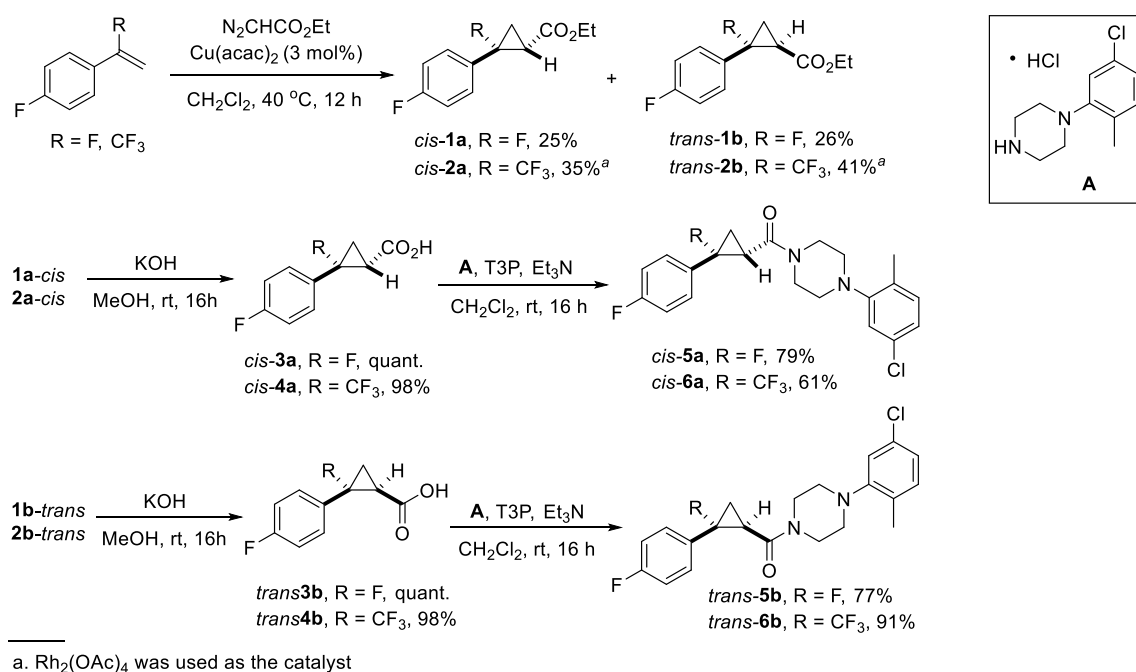


## 1.2 RESULTS AND DISCUSSION

### 1.2.1 Synthesis of fluorinated cyclopropane analogues of JJ-450

#### 1.2.1.1 Fluorination and trifluoromethylation at the benzylic position

We proposed that the target compounds can be easily prepared from a fluorinated cyclopropane carboxylate intermediate, which can be obtained from a metal-catalyzed cyclopropanation of  $\alpha$ -substituted styrene with a diazo ester based on literature precedence.<sup>58</sup>



**Scheme 1.** Synthesis of benzylic fluorinated and trifluoromethylated analogues.

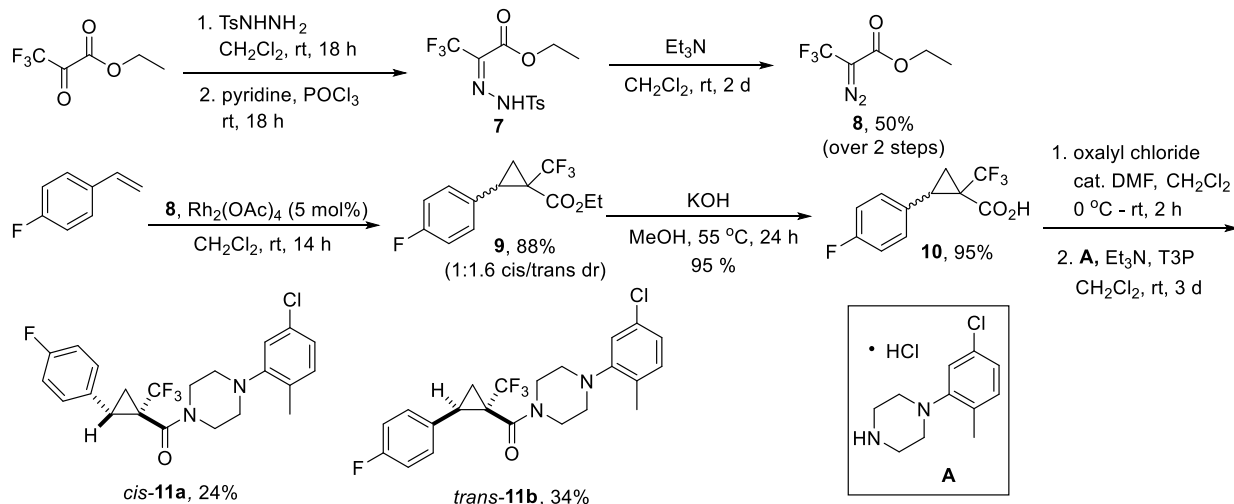
The starting material, 1-fluoro-4-(1-fluorovinyl)benzene, was synthesized according to a literature protocol and subjected to a Cu(II)-catalyzed cyclopropanation with ethyl diazoacetate to afford the cyclopropyl carboxylate as a 1:1 *cis/trans* mixture of diastereomers (with regard to the fluorine and carbonyl group according to the Cahn-Ingold-Prelog rule), which could be

separated via chromatography on SiO<sub>2</sub> (**Scheme 1**).<sup>59</sup> Base hydrolysis of the *cis*- and *trans*-cyclopropyl esters gave the respective cyclopropyl carboxylic acids without isomerization. A *n*-propanephosphonic acid anhydride (T3P)-mediated coupling with the piperazine hydrochloride salt **A** provided the final products *cis*-**5a** and *trans*-**5b** which are fluorinated at the benzylic position. The CF<sub>3</sub> analogues *cis*-**6a** and *trans*-**6a** were obtained with the same route.

It was reported that the cyclopropanation of vinyl fluoride with Cu(acac)<sub>2</sub> catalyst gave significantly better yields than with Pd- or Rh-catalysts.<sup>60</sup> However, this was not the case for the CF<sub>3</sub> analogue, as the Cu(acac)<sub>2</sub> catalyst did not promote the cyclopropanation of the alkene but only yielded fumaric and maleic esters, the homocoupling byproducts of ethyl diazoacetate. Fortunately, the desired cyclopropyl ester was obtained as a 1:1.2 *cis/trans* mixture of diastereomers in 88% yield when the cyclopropanation was carried out with Rh<sub>2</sub>(OAc)<sub>4</sub>. Diastereomers were also separable via chromatography on SiO<sub>2</sub>.

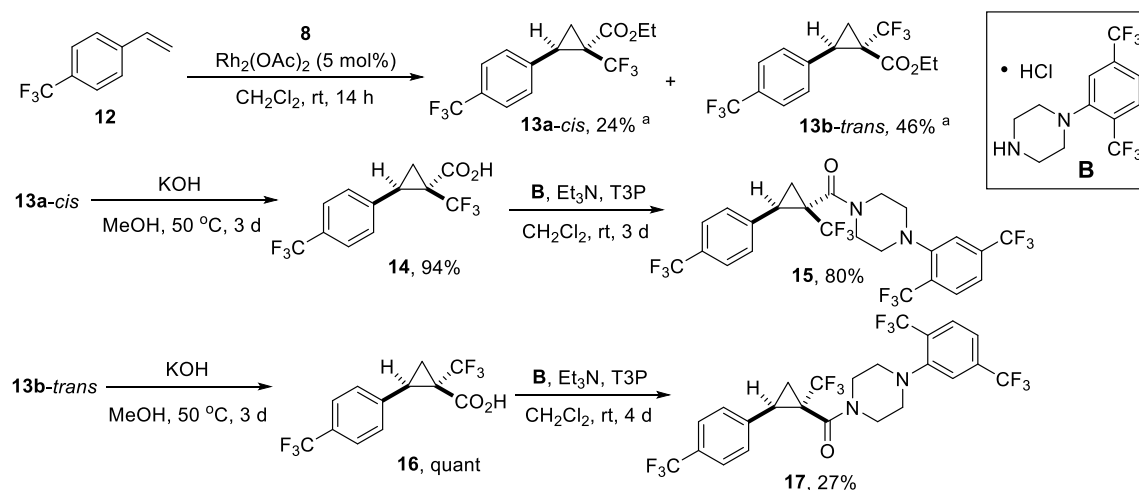
### 1.2.1.2 Fluorination and trifluoromethylation at the $\alpha$ -carbonyl position

We were motivated by the cyclopropanation with diazo ester to introduce the CF<sub>3</sub> group at the  $\alpha$ -carbonyl position by using a trifluoromethyl-substituted carbene. We were delighted to discover that carbenoid reactions based on the use of 3,3,3-trifluoro-2-diazopropionate **8** were well-precedented.<sup>61,62</sup> Diazo compound **8** was prepared from ethyl 3,3,3-trifluoropyruvate according to a literature procedure.<sup>63,64</sup> Cyclopropanation of **8** with *p*-fluorostyrene employing Rh<sub>2</sub>(OAc)<sub>4</sub> as the catalyst afforded cyclopropyl ester **9** as a 1:1.6 *cis/trans* mixture of diastereomers, and subsequent hydrolysis with base at elevated temperature proceeded smoothly to give the carboxylic acid (**Scheme 2**). Coupling with the piperazine hydrochloride salt **A** was slow due to the steric hindrance of the trifluoromethyl group but still provided *cis*-**11a** and *trans*-**11b** diastereomers, which were separated by chromatography, albeit in moderate yield.



**Scheme 2.** Synthesis of  $\alpha$ -carbonyl trifluoromethylated analogues.

Since metabolic oxidation may also occur at the benzylic positions of the two phenyl groups, we also synthesized analogues **15** and **17** (**Scheme 3**), where the benzylic positions were substituted with trifluoromethyl groups.



**Scheme 3.** Synthesis of analogues **15** and **17**.

A different approach was examined for the synthesis of  $\alpha$ -fluoro-substituted analogues as the  $\alpha$ -fluoro- $\alpha$ -diazoester is not known in the literature and would likely be unstable. Feit *et al.* reported that the reaction of cyclopropyl carbanions, derived from cyclopropyl ester, in the

presence of lithium diisopropylamide (LDA), with electrophiles afforded the corresponding trisubstituted derivative (**Figure 13**).<sup>65</sup> It is interesting to note that the product was obtained as a single diastereomer; the authors proposed that the phenyl group exerts steric hindrance to the approaching electrophile, thus favoring the electrophilic attack on the opposite face to give the *cis*-diastereomer as the sole product.

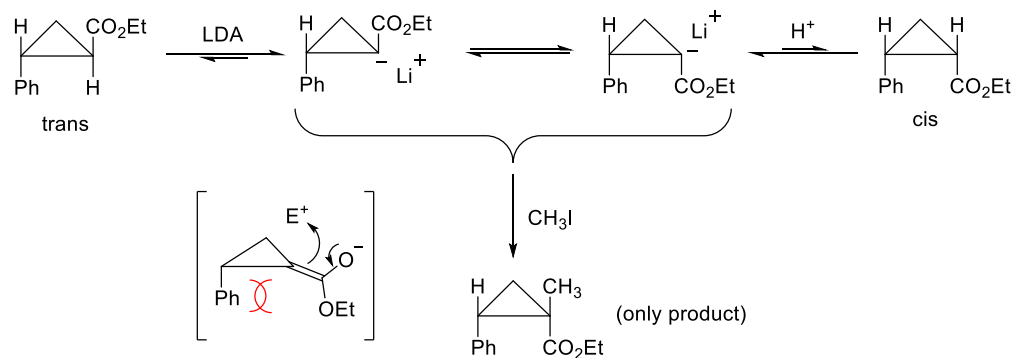
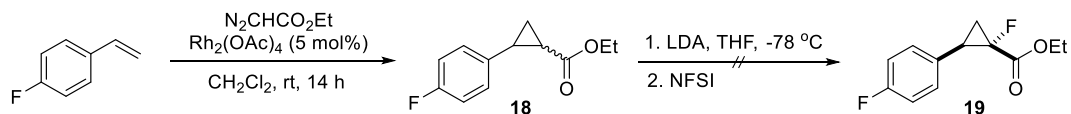


**Figure 13.** Reaction of cyclopropyl carbanion with electrophiles.

Based on the above example, we anticipated that electrophilic fluorination would generate the desired  $\alpha$ -carbonyl fluorinated product as a single diastereomer. Unfortunately, no product was detected from the reaction with *N*-fluorobenzenesulfonimide (NFSI) as the electrophile (**Scheme 4**). This target was therefore down-prioritized and we plan to revisit this reaction again using other electrophilic fluorinating reagents.



**Scheme 4.** Effort toward an electrophilic fluorination of a cyclopropyl ester.

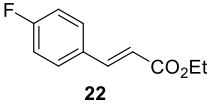
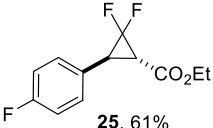
### 1.2.1.3 Synthesis of *gem*-difluorocyclopropa(e)ne analogues

The most common strategy to access the difluorocyclopropane moiety is the stereospecific addition of difluorocarbene to an electron rich/nucleophilic alkene. Various precursors to attain

difluorocarbene have been developed in the past decades and some of these methods also extended to the addition to alkyne.<sup>66-67</sup> However, many of the procedures suffer from harsh conditions (170 – 190 °C) and limited scope, or the reagents are toxic and difficult to handle (PhHgCF<sub>3</sub>). Due to the increasing demand for *gem*-difluorocyclopropanes, safer and more versatile difluorocarbene precursors have been reported in recent years.<sup>68</sup>

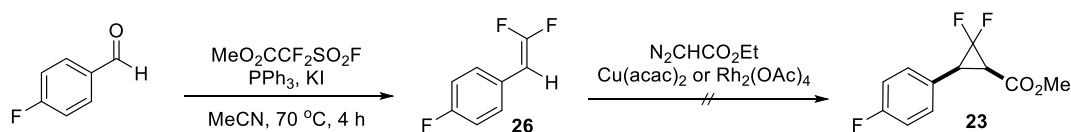
**Table 1.** Attempted difluorocarbene additions to *cis*-alkene and alkyne

Reaction scheme: *cis*-alkene **20** (4-fluorophenyl-*cis*-methyl acrylate) or alkyne **21** (4-fluorophenyl propargyl methyl ester) reacts under conditions to form *gem*-difluorocyclopropane **23** or **24**.

Entry	Substrate	Conditions	Remarks
1	<b>20</b>	BrCF <sub>2</sub> CO <sub>2</sub> Na, diglyme, 150 °C, 15 min	RSM + isomerized to <i>trans</i> -alkene
2	<b>21</b>	BrCF <sub>2</sub> CO <sub>2</sub> Na, diglyme, 150 °C, 15 min	RSM
3	<b>20</b>	MDFA, KI, TMSCl, diglyme, dioxane, 120 °C, 2 d	isomerized to <i>trans</i> -alkene + trace difluorocyclopropane
4	 <b>22</b>	MDFA, KI, TMSCl, diglyme, dioxane, 120 °C, 2 d	 <b>25</b> , 61%

We explored the options for a [2+1] cycloaddition of difluorocarbene to relatively electron-poor *cis*-alkenes bearing an ester and an electron-withdrawing *p*-fluorophenyl group. Amii and coworkers discovered the thermolysis of bromodifluoroacetate (BrCF<sub>2</sub>CO<sub>2</sub>Na), a convenient and efficient alternative to sodium chlorodifluoroacetate (ClCF<sub>2</sub>CO<sub>2</sub>Na), in a high-yielding synthesis of difluorocyclopropa(e)ne.<sup>69</sup> Unfortunately, the reaction condition was incompatible with our substrates and the *cis*-alkene was found to isomerize to the *trans*-alkene under high temperatures while there was only recovered starting material with the alkyne substrate (**Table 1**, entries 1 and 2). Dolbier and coworkers showed that *in situ* generated

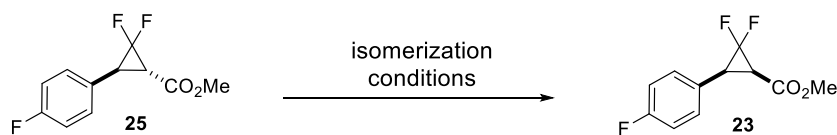
difluorocarbene from methyl 2,2-difluoro-2-(fluorosulfonyl)acetate (MDFA) under high temperature and high concentration reacts with ethyl cinnamate.<sup>70</sup> However, the *cis*-alkene again isomerized to the *trans*-alkene at high temperatures, and only trace amounts of *trans*-difluorocyclopropane were detected (entry 3). In order to prove that this result was not simply a technical failure or due to impure reagents, we treated ethyl 4-fluorocinnamate under the same conditions and found that the reaction proceeded in 61% yield (entry 4).



**Scheme 5.** Attempt to convert the *gem*-difluoroolefin to the *gem*-difluorocyclopropane.

Since MDFA can also be used in a Wittig-type difluoroolefination of aldehydes via a difluoromethylene triphenylphosphonium ylide intermediate, we attempted the reaction of 1,1-difluoroalkene **26** and ethyl diazoacetate with Cu(II) or Rh(II) catalyst but did not obtain the desired difluorocyclopropane **23** (Scheme 5).<sup>71</sup>

**Table 2.** Screening for *trans*-to-*cis* isomerization conditions

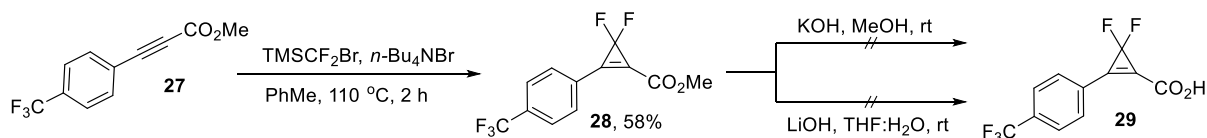


Entry	Conditions	Remarks
1	KO <sup>t</sup> Bu, PhMe, reflux	decomposition
2	KO <sup>t</sup> Bu, <i>t</i> BuOH, reflux	ester hydrolyzed
3	1. Lithium diethylamide, 2. EtOH quench	RSM
4	1. Lithium diisopropylamide, 2. EtOH quench	RSM

With the *trans*-difluorocyclopropane **25** in hand, we aimed to isomerize the *trans*-configuration to the *cis*-diastereomer **23**. Even though the *trans*-diastereomer is kinetically more

stable, the literature shows that *trans*-to-*cis* isomerization on a similar scaffold can occur to a certain extent.<sup>65</sup> Various attempts using strong bases such as potassium *tert*-butoxide and lithium diethylamide or lithium diisopropylamide, however, failed to provide the desired *cis*-diastereomer (**Table 2**).

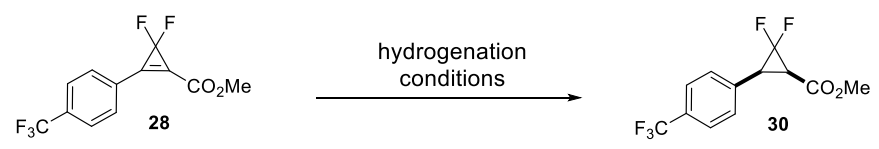
Concurrently, we began to consider other readily available precursors for difluorocarbene formation. The Rupert-Prakash reagent (TMSCF<sub>3</sub>) is known as a trifluoromethylation reagent for electrophilic substrates and only recently it was found to be a convenient source for difluorocarbene [2+1] cycloaddition to alkenes or alkynes when activated by tetrabutylammonium triphenyldifluorosilicate (TBAT) or sodium iodide.<sup>72</sup> Analogous transformations were subsequently reported by Hu and coworkers using TMSCF<sub>2</sub>Cl and TMSCF<sub>2</sub>Br.<sup>73,74</sup> We decided to employ TMSCF<sub>2</sub>Br, rather than TMSCF<sub>3</sub>, in our investigation based upon its broader substrate scope and its more environmental-friendly preparation than TMSCF<sub>2</sub>Cl. Gratifyingly, alkyne **27** was converted to the corresponding difluorocyclopropene **28** in good yield in the presence of catalytic tetrabutylammonium bromide (**Scheme 6**). Hydrolysis of the ester **28** using potassium hydroxide in methanol resulted in decomposition of the difluorocyclopropene ester. This outcome was presumably due to the conjugate addition of nucleophilic alkoxy anion, generated by hydroxide in an alcoholic solvent, on the  $\alpha,\beta$ -unsaturated ester. Lithium hydroxide in a THF/water mixture, a condition regularly employed to saponify  $\alpha,\beta$ -unsaturated esters, also failed to deliver the desired carboxylic acid.

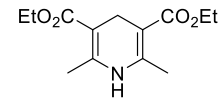


**Scheme 6.** Difluorocyclopropenation of alkyne **27**.

We then shifted our focus to screen a series of conditions for *cis*-hydrogenation of the cyclopropene. Zheng and Dolbier demonstrated that Hantzsch's ester can be used as a hydride transfer reagent in the presence of a Brønsted acid for the reduction of difluorocyclopropenyl ketone to give the corresponding cyclopropane in a *cis*-selective fashion.<sup>75</sup> However, these conditions only resulted in complete decomposition of the starting material (**Table 3**, entry 1). Lipshutz and coworkers developed a “hot” Stryker's reagent that effectively reduces  $\alpha,\beta$ -unsaturated double bonds, but our substrate **21** was found to be resistant to their optimized conditions (entry 2).<sup>76</sup>

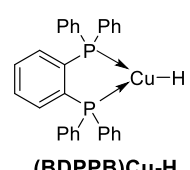
**Table 3.** Condition screening for hydrogenation of difluorocyclopropene





Hantzsch's ester

Entry	Conditions	Remarks
<b>1</b>	Hantzsch's ester, TBBA, CH <sub>2</sub> Cl <sub>2</sub> , rt, 2 d	Decomposition
<b>2</b>	Cu(OAc) <sub>2</sub> H <sub>2</sub> O, BDPPB, PMHS, <i>t</i> BuOH, PhMe, rt, 18 h	RSM
<b>3</b>	10% Pd/C (2.5 mol%), H <sub>2</sub> (balloon), EtOAc, rt, 17 h	Trace
<b>4</b>	10% Pd/C (2.5 mol%), H <sub>2</sub> (11 bar), EtOAc, rt, 17 h	<10%
<b>5</b>	<b>10% Pd/C (10 mol%), H<sub>2</sub> (6 bar), EtOAc, rt, 17 h</b>	<b>73%</b>
<b>6</b>	10% Pd/C (10 mol%), H <sub>2</sub> (5 bar), EtOH, rt, 17 h	Decomposition



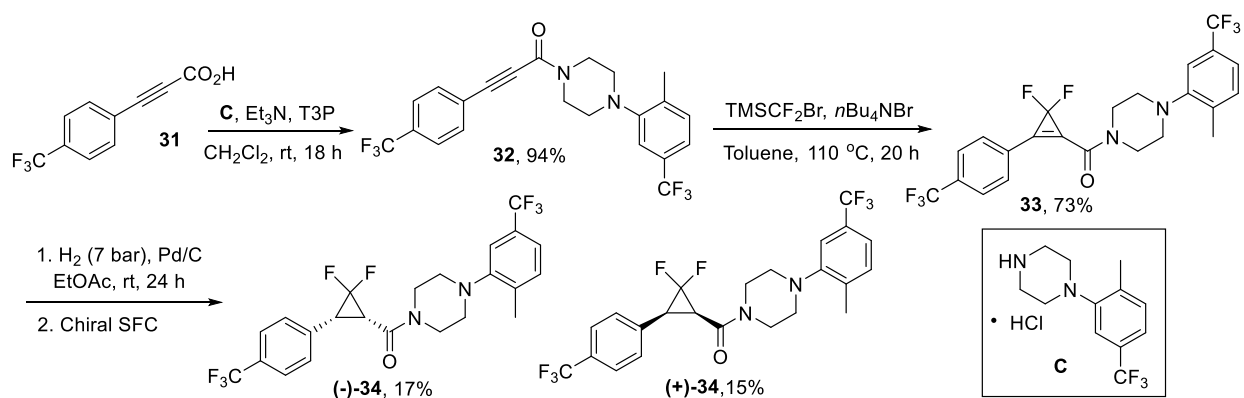
(BDPPB)Cu-H

We then proceeded to examine the feasibility of a Pd/C reduction of 1,1-difluorocyclopropene **28**. Our concern was that Pd(0) metal-insertion into the C<sub>2</sub>–C<sub>3</sub> bond of the difluorocyclopropane ring is irreversible and that bond cleavage releases the ring strain exerted by the difluoro-substituent.<sup>77</sup> To our delight, we found that a 10 mol% loading of Pd/C under 6 bar of H<sub>2</sub> pressure afforded the reduced product **30** in 73% isolated yield, though accompanied by ring-cleavage at the C<sub>2</sub>–C<sub>3</sub> bond as a minor side-product (entry 5). Unfortunately, we were



again brought to a dead-end when the subsequent hydrolysis of the difluorocyclopropane ester caused a *cis-trans* isomerization.

Because all attempts to reach the final target compound were unsuccessful, we revised our synthetic route and altered the order of bond formation. We decided to perform the T3P-mediated amide coupling prior to the formation of the difluorocyclopropane to omit the problematic ester hydrolysis step (**Scheme 7**).



**Scheme 7.** Revised route to difluorocyclopropane **33** and difluorocyclopropane **34** analogues.

We were pleased to discover that the [2+1] difluorocyclopropanation of the complex alkyne **32** proceeded well to furnish difluorocyclopropane **33**. As discussed previously, difluorocarbene addition conditions usually suffer from a narrow scope, and thus, we were very satisfied with our result as the reaction condition can be extended to the novel alkynyl amide scaffold in high yield. Reduction of the double bond with Pd/C under optimized conditions yielded the difluorocyclopropane analogue **34**, which was subjected to chiral SFC resolution.

### 1.2.2 Bicyclo[1.1.1]pentane (BCP) as a bioisostere in medicinal chemistry

Our group's ongoing interests in strained molecules prompted us to investigate the effects of incorporating a bicyclo[1.1.1]pentane (BCP) moiety in our analogues. It has been shown that

BCP is a beneficial bioisosteric replacement of the phenyl group, and significantly improves aqueous solubility, in vitro metabolic stability, and membrane permeability of several drug candidates.<sup>78-80</sup> Recently, it was reported that BCP can be a promising bioisostere of an internal alkyne (Figure 14).<sup>81</sup> However, its unique structure and reactivity pose a synthetic challenge, and there are only few reported syntheses.

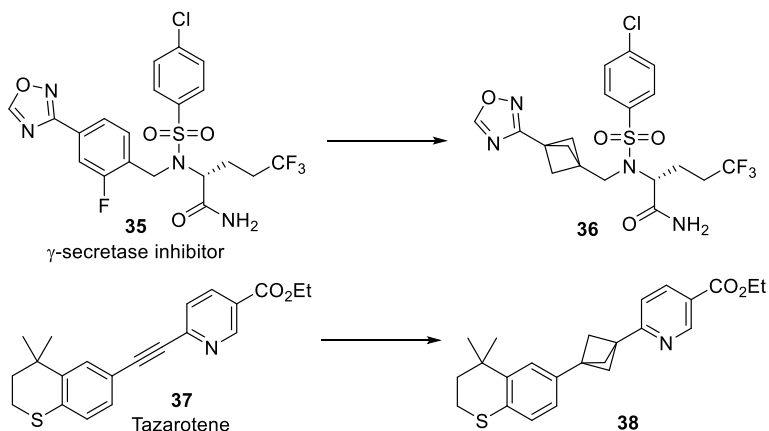


**Figure 14.** Bicyclo[1.1.1]pentane (BCP) as a bioisosteric replacement of a phenyl ring and an internal alkyne.

In pioneering studies, Wiberg and Michl showed that a bridgehead 1,3-disubstituted BCP can be accessed from a radical addition across the central bond of the [1.1.1]propellane **39** under photochemical conditions.<sup>82,83</sup> Della and deMeijere described the reaction of propellane with strong nucleophiles such as *t*-BuLi, and aryl Grignard reagents to give a 1,3-disubstituted BCP.<sup>84,85</sup> An alternative route was reported by Applequist *et al.* who utilized the addition of dichlorocarbene across the bicyclo[1.1.0]butane **45** followed by dechlorination to furnish the BCP moiety (Figure 15).<sup>86</sup>

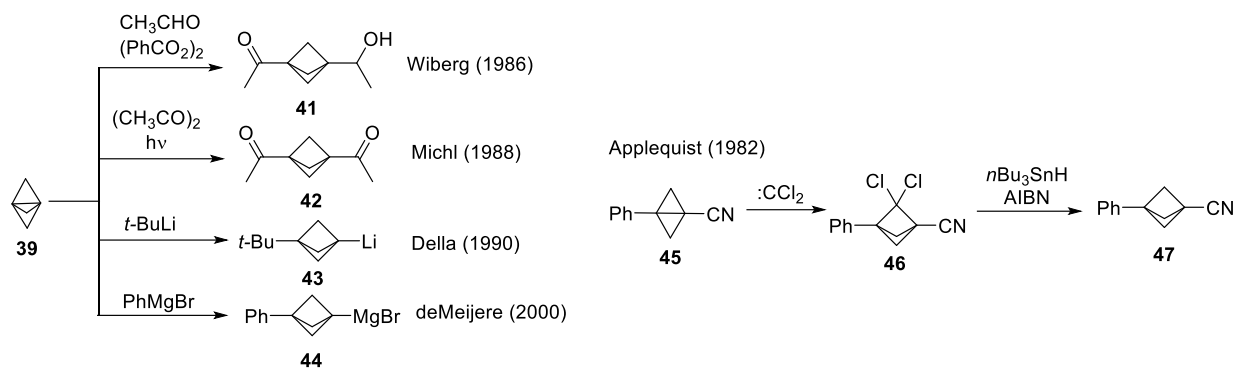


**Figure 15.** Conventional syntheses of bridgehead 1,3-disubstituted BCP scaffolds.

### 1.2.2.1 Design and synthesis of BCP analogues

We were particularly interested in two independent BCP replacements in our analogues; one for the cyclopropane ring and the other for the piperazine ring. We envisioned that BCP analogues **49** and **51** can be synthesized from a common precursor **52**, which can be obtained from a free radical addition of the aryl iodide to propellane **39** (Figure 16).<sup>87</sup>

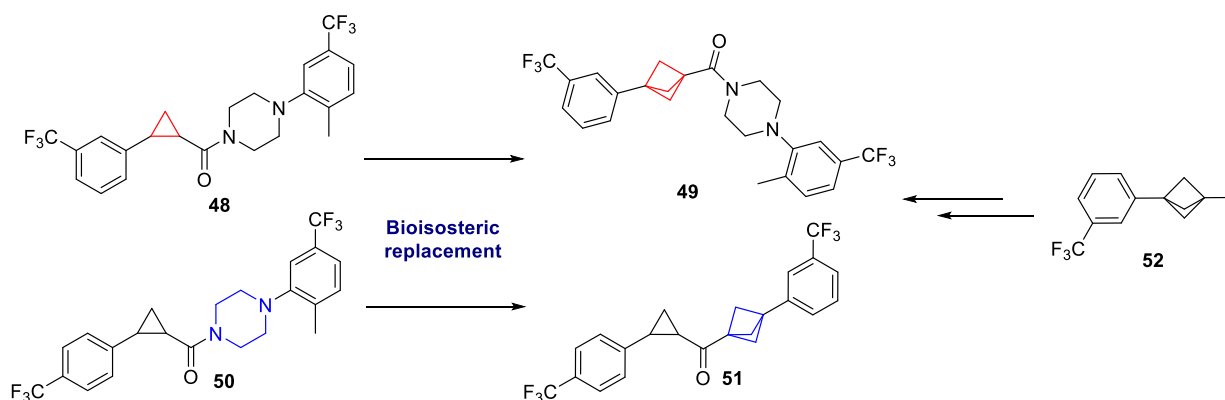
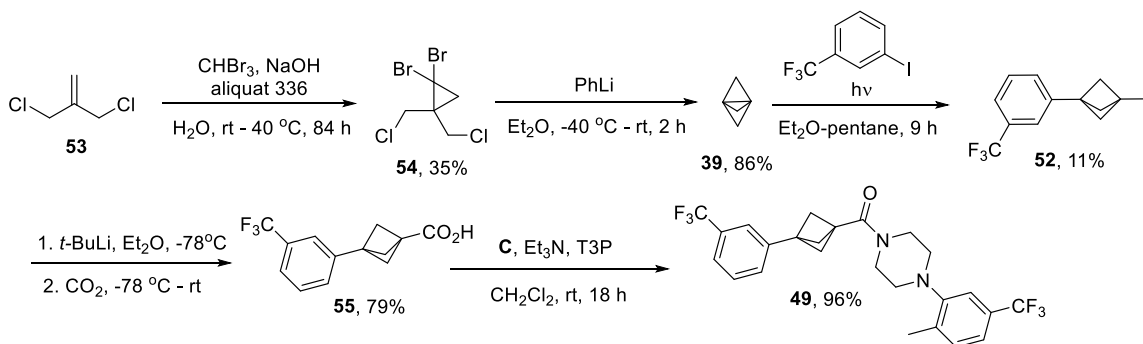


**Figure 16.** Proposed strategy to access BCP analogues.

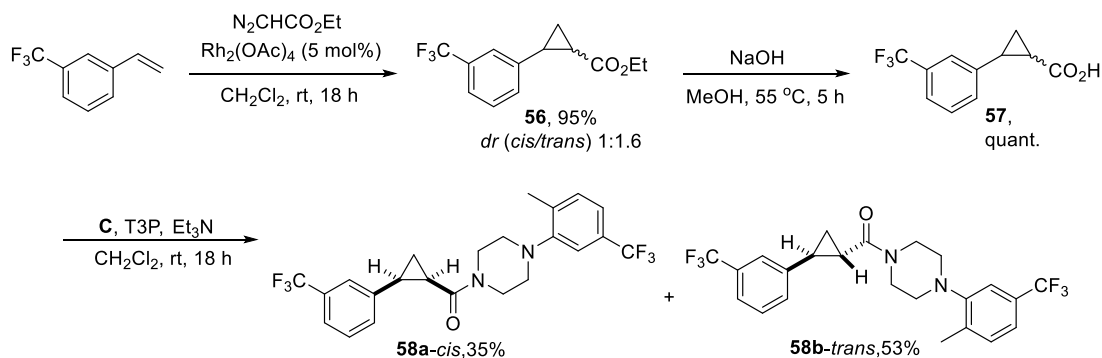
Starting from the commercially available methallyl dichloride **53**, propellane **39** was obtained via a two-step procedure involving a phase-transfer dibromocarbene addition to the olefin followed by a lithium-halogen exchange and carbenoid promoted ring-closure.<sup>88</sup> Irradiation of a solution of propellane **39** and 3-iodobenzotrifluoride with a medium-pressure Hg

lamp at 254 nm yielded the precursor **52** in low yield. Treatment of **52** with *t*-BuLi and trapping of the resulting lithium species with carbon dioxide afforded acid **55**. Finally, T3P-mediated amide formation delivered the desired analogue **49** where the cyclopropane was successfully replaced with a BCP moiety (**Scheme 8**).



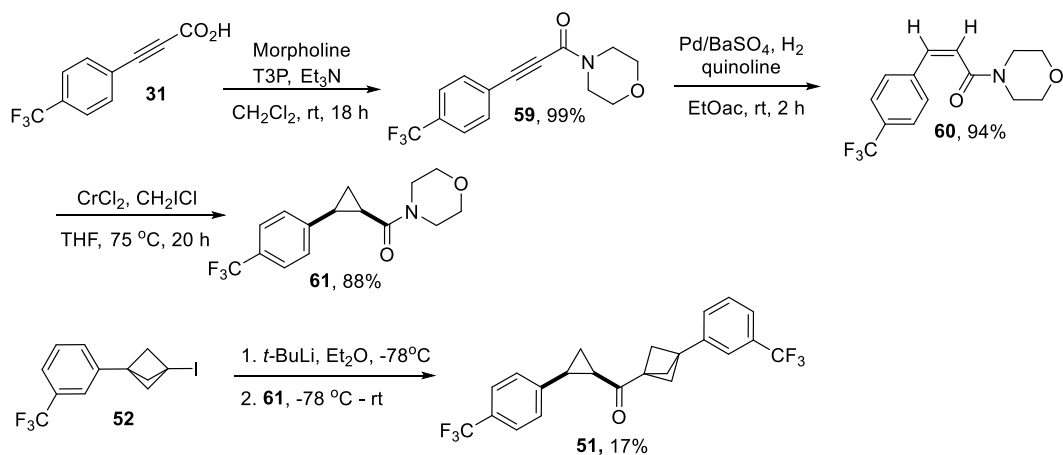
**Scheme 8.** Synthesis of BCP analogue **49**.

In order to have a more accurate direct comparison of the effect of replacing the cyclopropane with a BCP, we also synthesized the analogue where the CF<sub>3</sub> group on the phenyl ring is *meta* to the cyclopropane instead of the regular *para* position (**Scheme 9**). Starting from the Rh(II)-catalyzed cyclopropanation of 3-(trifluoromethyl)styrene, the desired *cis* product **58a** was obtained in three steps as the minor diastereomer which can be purified via normal phase chromatography.



**Scheme 9.** Synthesis of analogue **58a**.

We were inspired by the work of Concellón *et al.* to prepare the cyclopropyl ketone scaffold from the reaction of cyclopropanecarboxamides, derived from morpholine, with a series of organolithium compounds.<sup>89</sup> The intermediate cyclopropanecarboxamide **61** was obtained in three steps from the coupling of morpholine to carboxylic acid **31**, and subsequent *cis*-hydrogenation followed by stereospecific CrCl<sub>2</sub>-promoted cyclopropanation of the  $\alpha,\beta$ -unsaturated amide **60** in excellent yield (**Scheme 10**).



**Scheme 10.** Efficient synthesis of BCP analogue **51**.

We anticipated that the generation of the corresponding lithium homologue from **52** and trapping with morpholine amide **61** will provide BCP analogue **51**. While we could isolate the desired product, it appeared to be a minor compound and other unidentified major side products were also present. Various methods can be attempted to improve the yield, such as using Weinreb amide in place of morpholine amide, nickel-catalyzed reductive coupling of BCP iodide with cyclopropyl acid chloride, or transmetalation of BCP lithium species with ZnCl and subsequent acylation with cyclopropyl acid chloride. Since the compound was found to be inactive in our screen, no further effort was spent to optimize the conditions.

## 1.2.3 Configuration determination of cyclopropane analogues

### 1.2.3.1 Determination of relative configuration

The determination of the relative configuration of the cyclopropyl ester intermediates was achieved by comparing distinct NMR shifts and  $J$ -coupling constants with literature compounds, and confirmed by X-ray structure analysis of representative compounds.

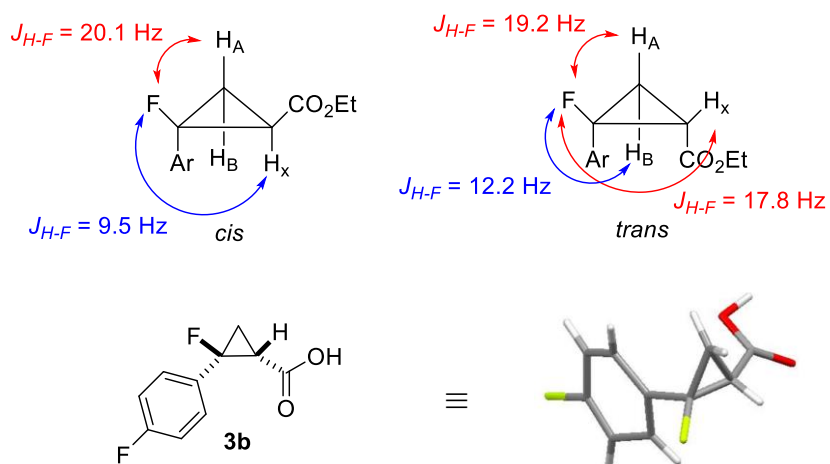


**Figure 17.** Distinct coupling constants in the monofluorinated cyclopropane and X-ray structure of **3b**.

One of the distinct features of the  $^1\text{H}$  NMR of the monofluorinated cyclopropane diastereomers is the large vicinal  $^3J_{H-F}$  coupling constant when the hydrogen and fluorine are *cis* to one another. In the *cis*-diastereomer, there is only one large  $^3J_{H-F} = 20.1$  Hz while in the *trans*-diastereomer there are two large  $^3J_{H-F}$ , indicating two vicinal hydrogens that are *cis* to the fluorine atom (**Figure 17**). In addition, the  $^{19}\text{F}$  NMR chemical shifts of the fluorine attached to *cis*- and *trans*-cyclopropane are significantly different, thus enabling an assignment of the relative configuration. The  $^{19}\text{F}$  chemical shift of the *cis*-diastereomer is at  $-184.9$  ppm while the *trans*-diastereomer is about 30 ppm downfield shifted to  $-152.6$  ppm, in agreement to literature

values.<sup>58</sup> The assignment was then confirmed by the XRC structure of the *trans*-cyclopropanecarboxylic acid **3b**.

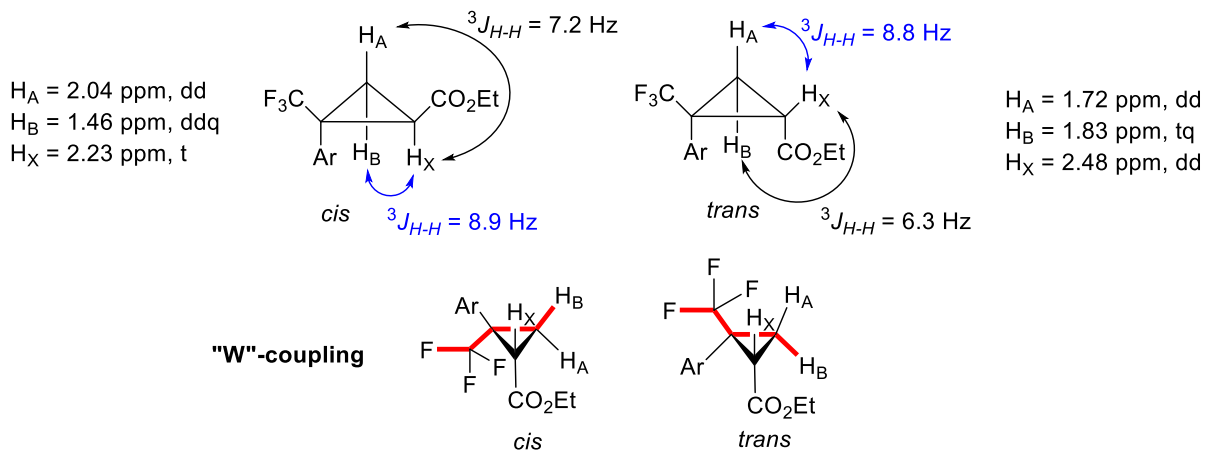


**Figure 18.** Relative stereochemistry assignment of trifluoromethyl-substituted cyclopropane.

In contrast, there was no  $^3J_{H-F}$  coupling in the  $CF_3$ -substituted cyclopropane, but we were still able to extract some information from proton chemical shifts and  $J_{H-H}$  coupling constants (**Figure 18**). In the *cis*-diastereomer, the  $H_B$  proton is the most shielded proton and thus located most upfield in the NMR spectrum. Its configuration is *cis* relative to  $H_X$  and it has a  $^3J_{H-H}$  coupling constant of 8.9 Hz, while  $H_X$  and  $H_A$  are *trans* to one another and therefore have a smaller  $^3J_{H-H}$  coupling constant of 7.2 Hz. A similar rationalization can be applied to assign the *trans*-diastereomer where  $H_A$  is the most shielded proton and the coupling constant of  $H_X$  and  $H_A$  is larger than the coupling constant of  $H_X$  and  $H_B$ . Intriguingly, the  $H_B$  proton in both diastereomers was identified to engage in a long-range "W"-coupling with the  $CF_3$  group ( $^4J_{H-F} = 1.7$  Hz in the *cis*-diastereomer and  $^4J_{H-F} = 1.8$  Hz in the *trans*-diastereomer) which led to line broadening and fine-splitting of the peaks. Consistent with literature examples, the  $^{19}F$  NMR chemical shift on the  $CF_3$ -group in the *cis*-cyclopropane (-65.5 ppm) was found at approximately 5 ppm lower field compared to the *trans*-cyclopropane (-70.7 ppm).<sup>64</sup> Analogous observations

were made for the compounds containing a CF<sub>3</sub>-substitution at the  $\alpha$ -carbonyl position; thus, the relative configurations were assigned in the same manner.

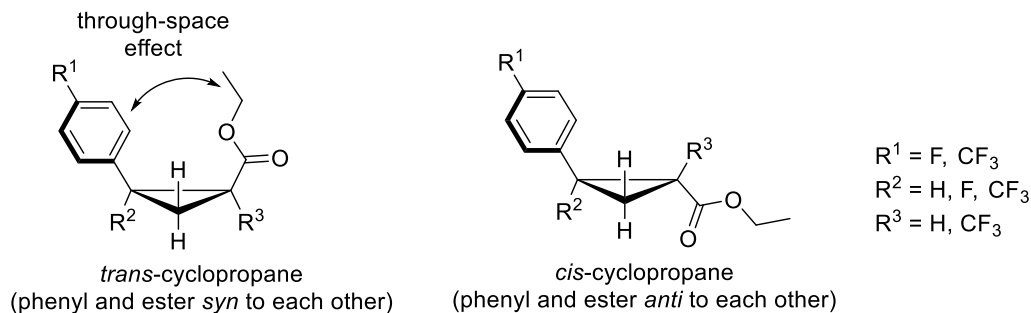


**Figure 19.** Through-space effect of the phenyl group in the *trans*-cyclopropyl ester.

Another noteworthy trend in determining the relative configuration of the cyclopropyl esters was that the chemical shift of the ester -OCH<sub>2</sub> and -CH<sub>3</sub> protons in the *trans*-cyclopropane were shifted upfield by approximately 0.3–0.4 ppm (**Figure 19**). This phenomenon can be explained by the shielding effect of the aromatic ring's circulating  $\pi$ -electrons exerted through space on the ethyl group of the ester.<sup>90</sup> The relative configurations of the final analogues were further confirmed by XRC structures of **6a**, **11a**, and **15** (**Appendix C**).

### 1.2.3.2 Determination of absolute configuration

The racemates were resolved by chiral supercritical fluid chromatography (SFC) in our lab or submitted to our collaborator for chiral high-performance liquid chromatography (HPLC) separations to deliver the pure enantiomers. The crystals of enantiomers (-)-**6b**, (-)-**11a**, and (-)-**34** were submitted to XRC for determination of absolute configuration, and the absolute structures of the other enantiomers were assigned tentatively based on the Cotton effect obtained from circular dichroism (CD) spectra and compared to (-)-**6b**, (-)-**11a**, and (-)-**34**.



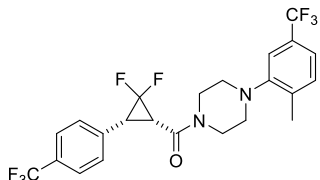
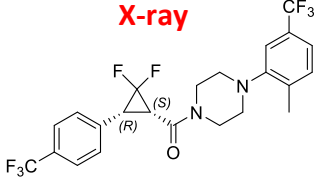
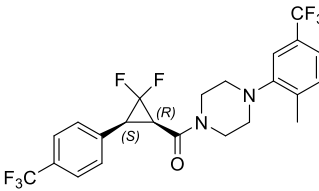
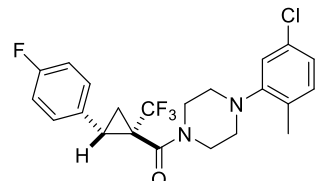
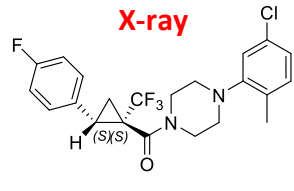
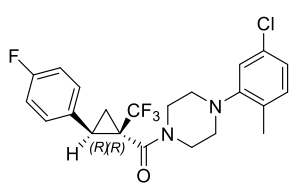
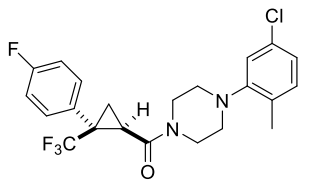
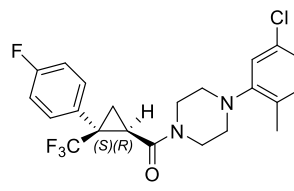
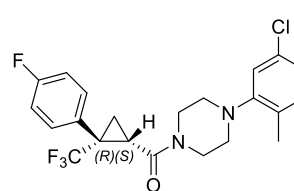
CD is the differential absorption of left and right circularly polarized light at any wavelength by a molecule containing chiral chromophores, resulting in a Cotton effect with a positive or negative sign. Molecules of identical absolute configurations should give the same Cotton effect while the Cotton effect signs for enantiomers would be opposite of each other. In our case, the substrates contain two chromophores on the cyclopropane: the aromatic ring and the amide carbonyl. We assumed that the Cotton effects observed arose from the overall interaction of these two chromophores with the circularly polarized light.

X-ray data showed that analogue (-)-**6b**, where the aromatic group and the amide are in a *cis*-configuration, has an absolute configuration of *1S,2S* and CD spectra showed that it has a negative Cotton effect with  $\lambda_{\text{max}} = 217.2$  nm (**Table 4**, entry 1). Correspondingly, the difluorocyclopropane analogue (-)-**34** has the same absolute configuration and a negative Cotton effect (entry 7). Based on this observation, we tentatively assigned the remaining substrates where the aromatic and amide are *cis* and have a negative Cotton effect with the same absolute configuration, while their corresponding enantiomers were assigned the opposite absolute configuration (entries 2-6).

Enantiomer (-)-**11a**, where the two chromophores are in a *trans*-orientation, has an absolute configuration of *1S,2S* based on the X-ray structure analysis. Its CD spectra showed a negative Cotton effect with  $\lambda_{\text{max}} = 228.2$  nm (entry 9). Accordingly, we assigned the substrates in which the chromophores are *trans* and showed a negative Cotton effect to the analogous absolute configuration as (-)-**11a** (entries 10-16).

**Table 4.** Tentative absolute configuration assignment of the analogues.

Entry	ID	Relative configuration	Optical Rotation	CD $\lambda_{\max}$ (nm)	Absolute configuration
1	6b		(-)	(-) 217.1	
2			(+)	(+) 217.6	
3	5b		(-)	(-) 220.8	
4			(+)	(+) 221.9	
5	17		(+)	(-) 224.0	
6			(-)	(+) 223.1	

Entry	ID	Relative configuration	Optical Rotation	CD $\lambda_{\max}$ (nm)	Absolute configuration
7	34		(-)	(-) 230.2	<b>X-ray</b> 
8			(+)	(+) 230.8	
9	11a		(-)	(-) 228.3	<b>X-ray</b> 
10			(+)	(+) 227.7	
11	6a		(-)	(-) 219.6	
12			(+)	(+) 216.7	

Entry	ID	Relative configuration	Optical Rotation	CD $\lambda_{\max}$ (nm)	Absolute configuration
13	5a		(-)	(-) 225.6	
14			(+)	(+) 225.1	
15	15		(-)	(-) 232.3	
16			(+)	(+) 231.8	

#### 1.2.4 Biological data

The *in vitro* metabolic stability of the analogues was analyzed via a pooled male mouse liver microsomes assay in the presence of the cofactor of P450 cytochrome enzyme, NADPH, by measuring the percent compound remaining at 0, 15, 30, 45, and 60 min via a LCMS/MS analysis. The negative control samples were prepared, by replacing NADPH with H<sub>2</sub>O, to differentiate non-metabolic related degradation of the test compounds, and a known substrate, verapamil, was used as the positive control.

**Table 5.** Half-life of analogues in mouse liver microsomes.<sup>a</sup>

Entry	ID	Structure	MLM <sup>b</sup> t <sub>1/2</sub> (min)
1 <sup>c</sup>	(-)-JJ-450		5.3
2 <sup>c</sup>	(+)-JJ-450		7.3
3	(±)-5a		n/a
4	(-)-5a	<b>(-)-5a</b>	6.8
5	(+)-5a	<b>(+)-5a</b>	28.6
6	(±)-5b		n/a
7	(-)-5b	<b>(-)-5b</b>	5.1
8	(+)-5b	<b>(+)-5b</b>	12.8
9	(±)-6a		n/a
10	(-)-6a	<b>(-)-6a</b>	7.3
11	(+)-6a	<b>(+)-6a</b>	15.0
12	(±)-6b		n/a
13	(-)-6b	<b>(-)-6b</b>	2.4
14	(+)-6b	<b>(+)-6b</b>	7.6
15	(±)-11a		n/a
16	(-)-11a	<b>(-)-11a</b>	11.2
17	(+)-11a	<b>(+)-11a</b>	2.9
18	(±)-11b		23.7
19	(-)-11b	<b>(-)-11b</b>	n/a
20	(+)-11b	<b>(+)-11b</b>	n/a

a. Data obtained from Pharmaron

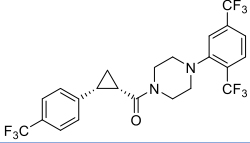
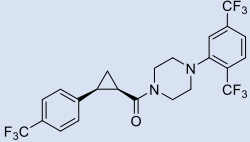
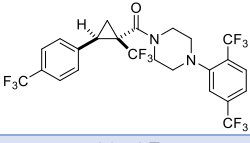
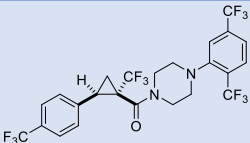
b. MLM = mouse liver microsomes

c. Synthesized by James Johnson

Compared to the lead compound JJ-450 (**Table 5**, entries 1 & 2), the addition of F- and CF<sub>3</sub>-substitutions around the cyclopropane ring had little effect in enhancing the metabolic stability of the analogues (entries 4-5, 7-8, 10-11, 13-14, 16-17, 19-20). In some cases, it was found that the addition of a CF<sub>3</sub> group decreased the metabolic stability (entries 13 & 17). This result suggested that the major metabolic sites might not be at the cyclopropane ring.

**Table 6.** Half-life of analogues with more stable side chains in mouse liver microsomes.<sup>a</sup>

Entry	ID	Structure	MLM <sup>b</sup> t <sub>1/2</sub> (min)
1 <sup>c</sup>	(-)-KT-73-454		59.4
2 <sup>c</sup>	(+)-KT-73-454		59.4
3	33		13.5
4	(-)-34		123.6
5	(+)-34		175.6
6	49		109.7
7	(±)-58a		n/a
8	(-)-58a	(-)-58a	5.0
9	(+)-58a	(+)-58a	27.6

Entry	ID	Structure	MLM <sup>b</sup> t <sub>1/2</sub> (min)
10 <sup>c</sup>	(-)-KT-76-617		227.3
11 <sup>c</sup>	(+)-KT-76-617		158.8
12	(±)-15		n/a
13	(-)-15	(-)-15	227.9
14	(+)-15	(+)-15	* d
15	(±)-17		n/a
16	(-)-17	(-)-17	457.9
17	(+)-17	(+)-17	126.4

- a. Data obtained from Pharmaron  
b. MLM = mouse liver microsomes  
c. Synthesized by Keita Takubo  
d. \* = intrinsic clearance < 0; t<sub>1/2</sub> = ∞

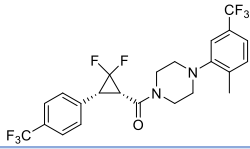
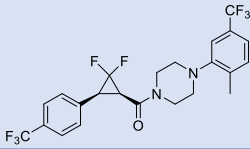
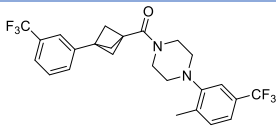
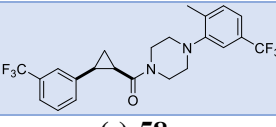
Specifically, the data suggested that the most labile sites were the aryl rings located at the terminal positions as seen in the increase in t<sub>1/2</sub> by 10-fold compared to JJ-450 when the *p*-fluoro and *m*-chloro on the phenyl groups were replaced by CF<sub>3</sub> (**Table 6**, entries 1 & 2). Accordingly, we made some alterations to the core while maintaining these highly fluorinated side chains. Interestingly, the difluorocyclopropene analogue **33** was found to be quite stable in mouse liver microsomes (entry 3), while the *gem*-difluorocyclopropane enantiomers acquired two to three times longer half-lives compared to the analogues without the *gem*-difluoro-moiety (entries 4 & 5). Finally, we were pleased to find that replacing the cyclopropane with a BCP scaffold also increased metabolic stability (entry 6 vs 8 & 9). We discovered that a further stability enhancement was achieved when all three substituents on the phenyl rings were replaced with

CF<sub>3</sub> groups (entries 10 & 11). Once the major metabolically labile terminal positions were stabilized, the addition of CF<sub>3</sub> at the  $\alpha$ -carbonyl position of the cyclopropane ring proved to deter the further propagation of metabolic attack as seen in the significant increase in half-lives (entries 14 and 16).

**Table 7.** Luciferase activity of selected analogues.<sup>a</sup>

Entry	ID	Structure	Luciferase Activity, EC <sub>50</sub> $\pm$ SD ( $\mu$ M) <sup>b</sup>
1	(-)-JJ-450 <sup>c</sup>		1.7 $\pm$ 0.2
2	(+)-JJ-450 <sup>c</sup>		15.2 $\pm$ 3.3
3	( $\pm$ )-5b		3.1 $\pm$ 0.5
4	(-)-5b	(-)-5b	3.2 $\pm$ 0.9
5	(+)-5b	(+)-5b	16.2 $\pm$ 3.8
6	( $\pm$ )-11a		5.9 $\pm$ 2.3
7	(-)-11a	(-)-11a	15.6 $\pm$ 1.7
8	(+)-11a	(+)-11a	3.9 $\pm$ 2.6
9	( $\pm$ )-11b		11.8 $\pm$ 5.7
10	( $\pm$ )-17		6.9 $\pm$ 4.6
11	(-)-17	(-)-17	9.8 $\pm$ 5.5
12	(+)-17	(+)-17	10.6 $\pm$ 3.7
13	33		18.9 $\pm$ 5.4



Entry	ID	Structure	Luciferase Activity, EC <sub>50</sub> ± SD (μM) <sup>b</sup>
14	(-)-34		13.6 ± 3.8
15	(+)-34		4.0 ± 0.3
16	49		13.3 ± 1.2
17	(±)-58a		6.5 ± 1.1
18	(-)-58a	(-)-58a	14.4 ± 1.2
19	(+)-58a	(+)-58a	10.5 ± 2.3

a. Data obtained from Department of Urology, University of Pittsburgh School of Medicine

b. Assay repeats;  $n = 2$

c. Synthesized by James Johnson

The luciferase activity of these analogues was determined and compared to JJ-450 using assay conditions developed by our collaborators using the Dual-Glo luciferase assay system (Promega). All cells were treated with compounds at concentrations of 0.2 μM, 0.8 μM, 3.2 μM, 12.8 μM, and 25 μM in triplicate wells. In this assay, the most potent analogue was compound **5b**, and the (-)-enantiomer (EC<sub>50</sub> = 3.2 μM) was more active than the (+)-enantiomer (Table 7, entry 4 vs 5). We were pleased to find that analogue (-)-17, which was one of the most metabolically stable compounds, was shown to possess moderate activity (entry 11). Interestingly, analogue **11a**, where the aryl ring and the amide are *trans* to each other, was found to be more active than the diastereomer **11b** (entry 6 vs 9). This result was in contrast with the other analogues where the more active species had a *cis* relationship between the aryl and amide moieties. The difluorocyclopropene analogue **33** maintained activity (entry 13) while the saturated difluorocyclopropane analogue (+)-34 showed better activity than **33** and (-)-34 (entry

15). It was noted that (+)-**11a** was also found to be more active than the (-)-enantiomer (entry 8 vs 7). Replacing the cyclopropane with a bicyclopentane moiety showed comparable activity in **49** (entry 16 vs 17-19).

### 1.2.5 Conclusion

A total of 32 fluorinated analogues were synthesized and tested for their microsomal metabolic stability and their ability to inhibit AR signaling in CRPC cell lines. Structurally unique scaffolds such as the gem-difluorocyclopropane and BCP were successfully incorporated following an intensive method optimization. The further expansion on the BCP analogues seemed promising but its tedious and challenging synthetic route would be a major drawback for compound derivatizations in drug development.

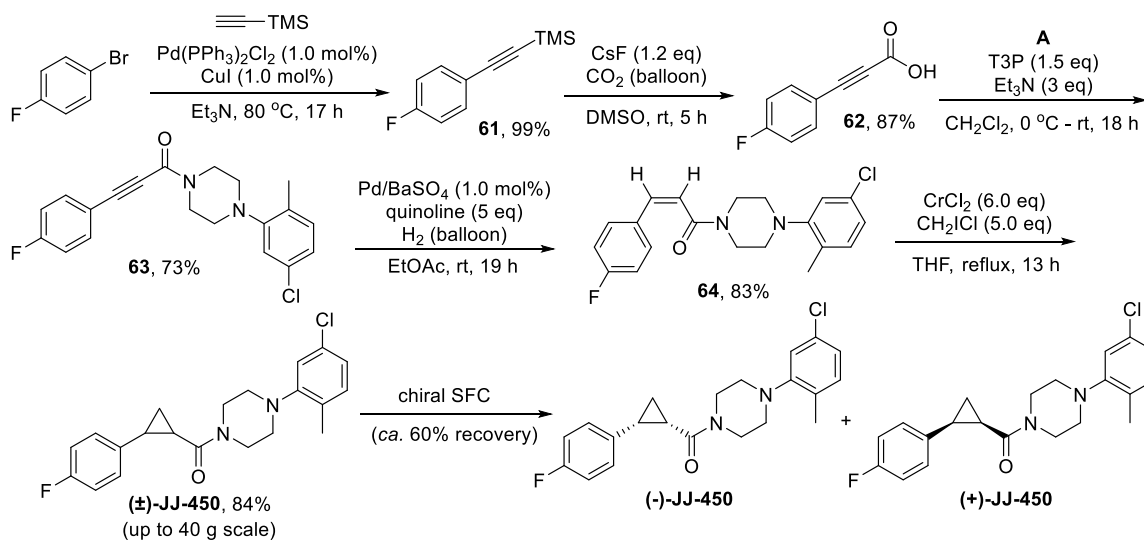
The benzylic positions on the phenyl side chains of JJ-450 were found to have a more rapid metabolism rate than the cyclopropane ring. The enhancement of metabolic stability from the addition of fluorine atoms around the cyclopropane ring was more significant when the terminal substituents were highly fluorinated. On the other hand, there was no distinctive trend in the structure-activity relationship from the luciferase assay. We found that some of the data provided by our collaborators were inconsistent and we were unable to draw a distinct correlation between the structures and measured activity. However, all the analogues were also submitted for multiple studies such as protein binding studies, dog and human liver microsome studies, as well as a cytotoxicity assay. Results from these assays are still pending, and the lead compounds for further development will be selected based on optimal properties in all assays. At the next stage, animal studies will be used to evaluate antitumor potential in the most resistant prostate cancer cell lines.

## 2.0 EFFORTS TOWARD AN ENANTIOSELECTIVE CO(II)-CATALYZED CYCLOPROPANATION

### 2.1 INTRODUCTION

#### 2.1.1 Synthetic route toward JJ-450 and its analogues

Racemic JJ-450 was synthesized over five steps, and the construction of the cyclopropane was achieved via hydrogenation of the internal alkyne **63** followed by a stereospecific CrCl<sub>2</sub>-promoted cyclopropanation of the *cis*-alkene **64** (Scheme 11).<sup>47</sup>



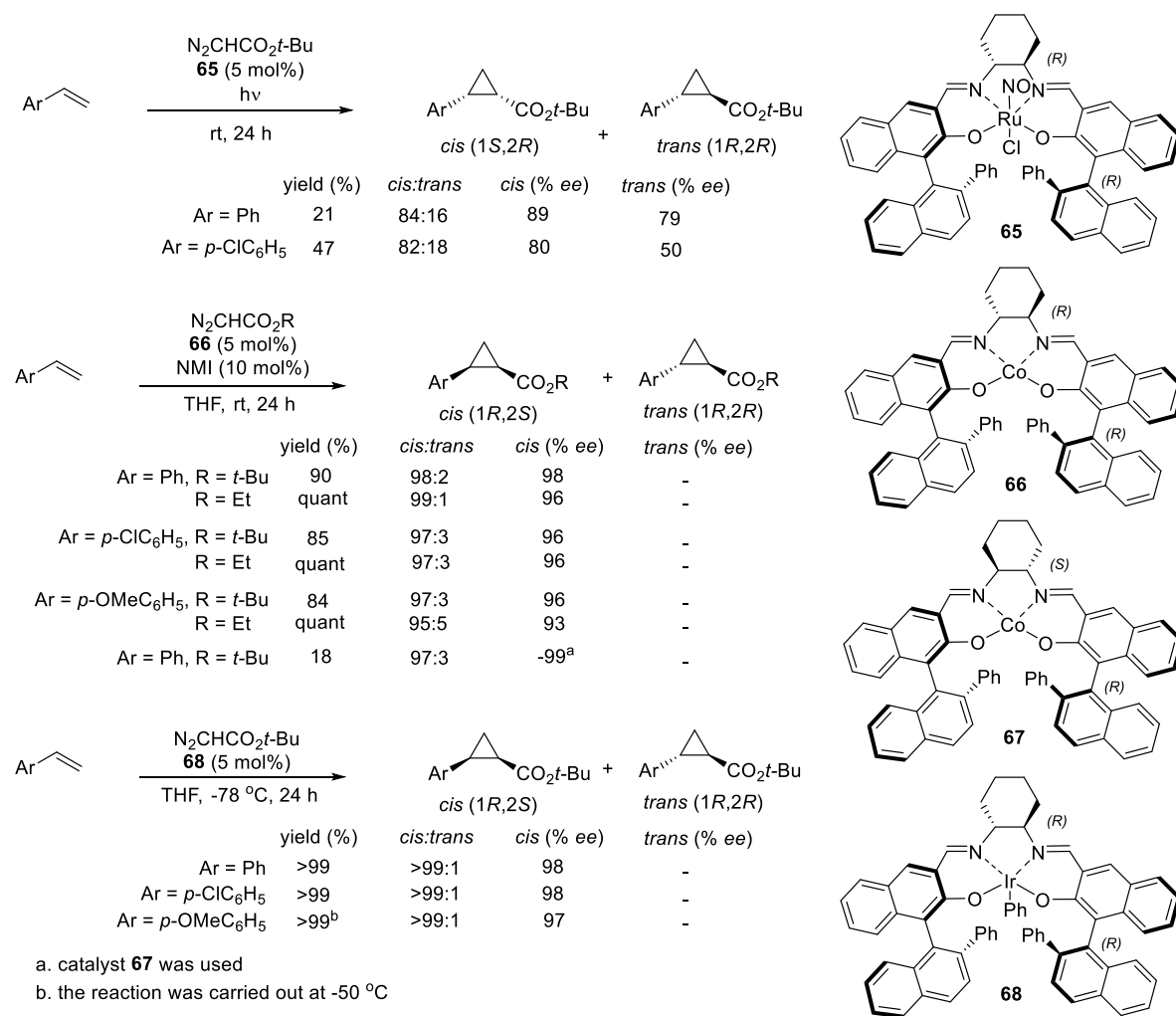
Scheme 11. Synthetic route to racemic JJ-450 and chromatographic resolution.

This process was employed for the scale-up synthesis of JJ-450 as well as analogues with a similar *cis*-1,2-disubstituted cyclopropane scaffold. However, there were a few major drawbacks that we hoped to improve. A significant amount of material was lost in the chiral separation as the recovery was only approximately 50–60%. Another disadvantage of this route was the need for a large excess of cyclopropanating reagents, CrCl<sub>2</sub> (6.0 eq) and chloriodomethane (5.0 eq). Inductively coupled plasma optical emission spectrometry (ICP-OES) analyses showed that final compounds were found to still be contaminated with chromium (1.33 ppm Cr), and had to be filtered through basic alumina multiple times to ensure complete removal of the excess chromium, which is known to be highly toxic. We aimed to develop an efficient enantioselective route to eliminate the need for chiral separation and chromium reagents in our syntheses.

### 2.1.2 Enantioselective *cis*-cyclopropanation

One of the most versatile approaches to construct 1,2-disubstituted cyclopropyl esters or cyclopropyl amides is the addition of a carbene derived from the metal-catalyzed decomposition of a diazo compound to an olefin.<sup>91, 92</sup> There is a plethora of literature devoted to catalysts that competently mediate the diastereoselective and enantioselective synthesis of *trans*-cyclopropanes.<sup>93-95</sup> On the other hand, there is still much development needed to improve the diastereoselective synthesis of the thermodynamically less favorable *cis*-cyclopropanes, and reports on asymmetric routes are scarce.<sup>96,97</sup> Katsuki's group made a major contribution in the advancement of *cis*- and enantioselective cyclopropanation using chiral Co, Ru, and Ir catalysts with simple olefins and diazoacetates (**Scheme 12**).

They reported the first highly *cis*- and enantioselective cyclopropanation using (*R,R*)-(NO<sup>+</sup>)(salen)ruthenium(II) complex **65** (up to 89% *ee*) under incandescent light.<sup>98</sup> It was hypothesized that a transient active species was generated by a ligand-dissociation induced by irradiation, as the reaction was slow and diastereoselectivity was poor when the reaction was carried out in the dark. However, the mechanism of asymmetric induction was unclear.



**Scheme 12.** Katsuki's development of an asymmetric *cis*-cyclopropanation.

Nakamura *et al.* initially developed a chiral Co(II)-salen complex for asymmetric cyclopropanation but the stereoselectivity was unsatisfactory.<sup>99</sup> Having been successful in

developing a *trans*-selective Co(III)-salen complex, Katsuki and coworkers attempted to prepare a novel Co(II)-salen complex that has the same ligand as complex **65** for a *cis*-selective cyclopropanation.<sup>100,102</sup> Indeed, the reaction using Co(II)-salen complex **66** furnished the desired *cis*-cyclopropane with an outstanding 98:2 *cis/trans* dr and 98% *ee*. The optimized conditions were applied to other *p*-substituted styrenes, and commercially available ethyl diazoacetate also delivered the corresponding *cis*-product in excellent yield and selectivity. It was interesting to note that complex **67**, which is different in the diamine chirality, delivered the *cis*-product with the opposite enantioselectivity, albeit with a sluggish reaction and much lower yield.

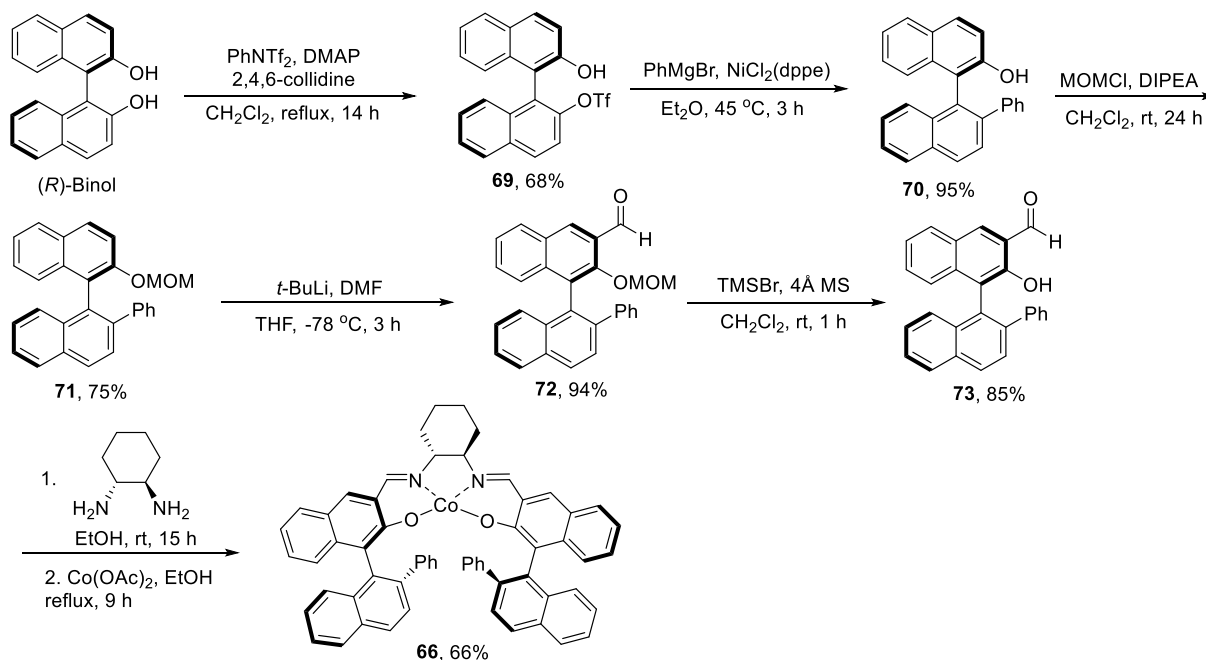
Within the Group 9 metals, Ir remained rather unexplored for this type of reaction at that time, which prompted Katsuki's group to venture into the advancement of a new class of Ir(III)-complexes.<sup>103</sup> To their delight, complex **68** was found to give the respective *cis*-isomer in quantitative yield and quintessential diastereo- and enantioselectivity when the reactions were carried out at low temperature. Unlike other Ir catalysts, this type of Ir(III)-salen complex is air stable and can be easily handled on the benchtop.

To date, the results on this topic from Katsuki's group remain the state of art and limited further discoveries have been made in the past decade for asymmetric cyclopropanations. Based on its overall performance and opportunity to fine-tune the catalyst, we selected Co(II)-salen complex **66** as a starting point for the cyclopropanation of our substrate.

## 2.2 RESULTS AND DISCUSSION

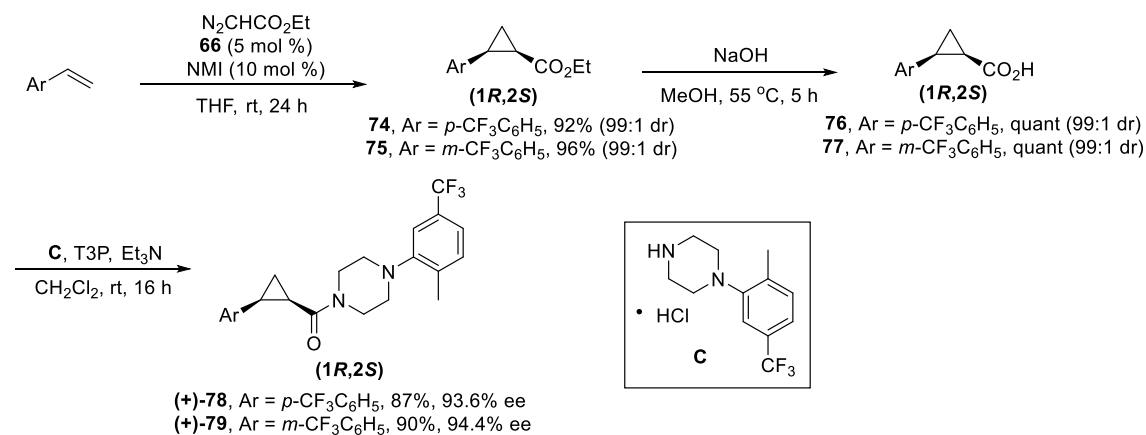
### 2.2.1 Design and synthesis of Co(II)-salen complexes

The synthesis of the salen ligand began with the treatment of commercially-available (*R*)-binol with *N*-phenylbistrifluoromethanesulfonamide to give monotriflate **69** which was subjected to a Kumada coupling with phenylmagnesium bromide in the presence of a NiCl<sub>2</sub>(dppe) catalyst (**Scheme 13**). Intermediate **70** was protected as a MOM ether **71**, then underwent a formylation reaction with DMF to give aldehyde **72**. MOM deprotection with trimethylsilyl bromide gave the free alcohol **73**, and a condensation reaction with (1*R*,2*R*)-(-)-1,2-diaminocyclohexane afforded the tetradentate salen ligand. Coordination of cobalt (II) with the salen ligand in ethanol delivered the corresponding Co(II)-salen complex **66**, which can be easily handled in air and stored in the desiccator over several months.<sup>104-105</sup>



**Scheme 13.** Synthesis of Co(II)-salen complex **66**.

We examined the efficiency of this Co(II)-salen complex in the cyclopropanation of *p*-CF<sub>3</sub> and *m*-CF<sub>3</sub> styrene. We were delighted to find that the cyclopropyl esters **74** and **75** were obtained in excellent yields and high *cis*-selectivity with a 99:1 dr (**Scheme 14**). Saponification of the ester to the corresponding carboxylic acid proceeded smoothly with retention of stereochemistry, and subsequent T3P coupling with piperazine **C** delivered the final *cis*-analogues (+)-**78** and (+)-**79**. Chiral SFC analyses revealed that the major enantiomers were obtained with enantioselectivities up to 94% *ee*. The absolute configurations were assigned by comparison of the elution order with previously analyzed samples of the same compound. This approach successfully simplified and improved the original synthesis as the enantiopure analogues can now be readily synthesized over three high-yielding steps under mild conditions without the need for additional chiral separation.



**Scheme 14.** Asymmetric route for the synthesis of analogues with complex **66**.

Motivated by these results, we proceeded to synthesize the Co(II)-salen complex that would provide the opposite enantiomer. Katsuki and coworkers noted that the enantioselectivity is dictated by the chirality of the diamine. Even though they were able to obtain excellent selectivity for the opposite enantiomer by reversing the chirality of the diamine, the reaction was



very sluggish. To explore the possibility of increasing the throughput, we decided to synthesize a Co(II)-salen complex that has both its diamine and binaphthyl chirality reversed, which is essentially the enantiomer of complex **66**. In an attempt to further improve the enantioselectivity, we also synthesized complexes **81** and **82**, where the phenyl group was replaced by the bulkier (naphthyl)phenyl substituent (**Figure 20**). We envisioned that the steric hindrance imposed by the bulkier substituent would limit the flexibility of the salen ligand and lock its transition state in a single conformation to deliver the product with high selectivity. These complexes have not been prepared or tested for their efficiency in enantioselective cyclopropanation.

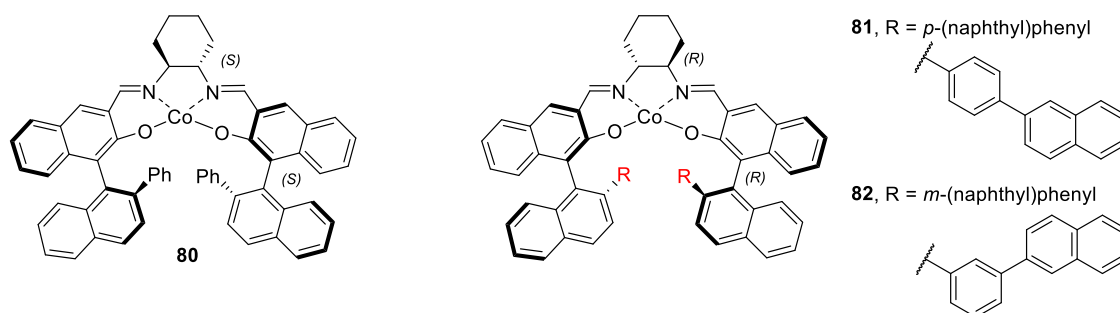


**Figure 20.** Novel Co(II)-salen complexes **80-82**.

**Table 8.** Asymmetric cyclopropanation using Co(II)-salen complexes

Entry	Catalyst	Yield of <b>74</b> (%)	<i>cis:trans</i> <b>74</b> <sup>a</sup>	% ee of <b>78</b>
1	<b>80</b>	84	95:5	93.4 <sup>b</sup>
2	<b>81</b>	99	99:1	96.8 <sup>c</sup>
3	<b>82</b>	90	99:1	96.8 <sup>c</sup>

a. Determined by <sup>1</sup>H NMR analysis

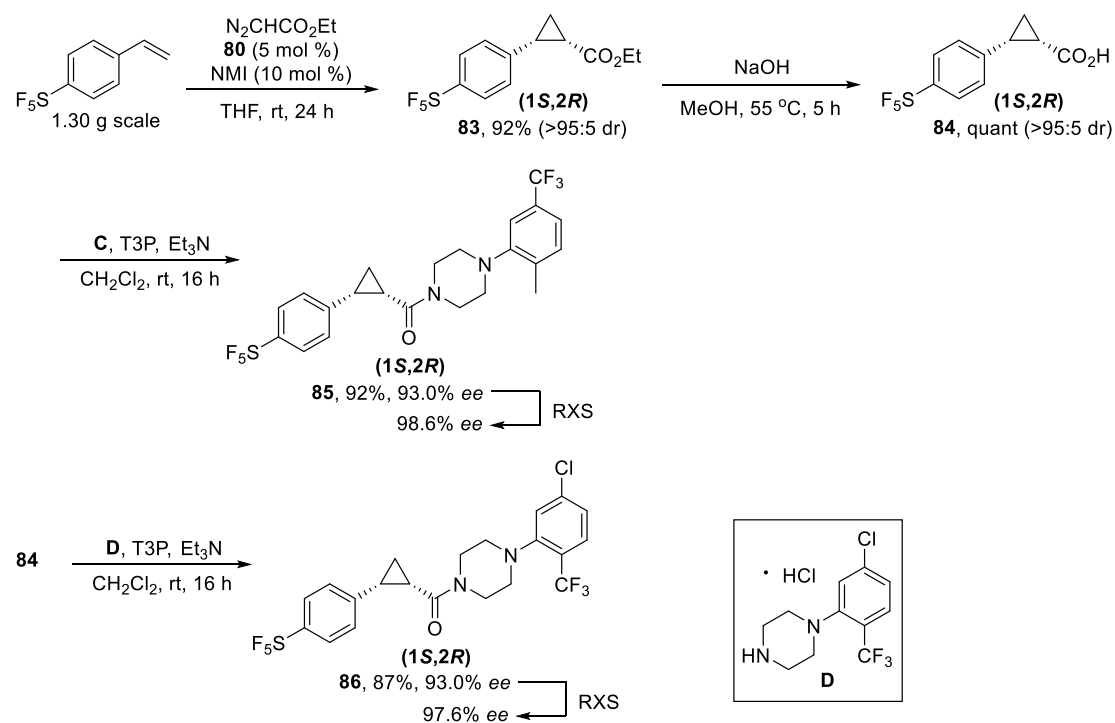
b. Absolute configuration is 1*S*,2*R*

c. Absolute configuration is 1*R*,2*S*

The novel Co(II)-salen complex **80** was synthesized analogously using (*S*)-binol and (1*S*,2*S*)-(+)-1,2-diaminocyclohexane as the chiral components. We found that the desired *cis*-cyclopropyl ester **74** was obtained in 84% yield with a 95:5 dr, a huge improvement compared to Katsuki's complex **67** in terms of isolated yield. After subsequent saponification and T3P

coupling, (-)-**78** was attained with an enantioselectivity of 93.4% *ee* (**Table 8**, entry 1). We were extremely pleased to discover that catalysts **81** and **82** showed excellent *cis*-selectivity (99:1 *dr*) and enhanced enantioselectivity of 96.8% *ee* (entries 2 and 3).

## 2.2.2 Gram-scale Co(II)-salen catalyzed asymmetric cyclopropanation



**Scheme 15.** Gram-scale enantioselective synthesis of analogues.

As a proof-of-concept, we utilized this enantioselective route for the scale up synthesis of analogues containing the pentafluorosulfanyl (SF<sub>5</sub>) moiety. The starting material 4-(pentafluorosulfanyl)styrene was obtained from the Wittig reaction of commercially available 4-(pentafluorosulfanyl)benzaldehyde according to a literature protocol. The cyclopropanation of 4-(pentafluorosulfanyl)styrene using catalyst **80** afforded cyclopropyl ester **83** in 92% yield and >95:5 *dr*. The Co(II)-complex can be recovered by trituration with hexanes and reused.

Subsequent saponification and T3P-coupling provided analogues **85** and **86** in excellent yield and *ee*. The desired enantiomer of each analogue was enriched by recrystallization from CH<sub>2</sub>Cl<sub>2</sub>/hexanes to 98.6% *ee* and 97.6% *ee* respectively. All in all, we successfully obtained 1.9 – 2.0 g of the final enantiomers over three high yielding steps.

### 2.2.3 Proposed mechanism for asymmetric induction

The mechanism for asymmetric induction in the metal-salen system was studied intensively by Katsuki's group. XRC structures of other salen-Mn(III) and salen-Co(II) have been determined.<sup>106,107</sup> Based on these results and the observed selectivity, they proposed that these salen-Co(IV) intermediates derived from their corresponding Co(II) complexes will also adopt a homologous conformation as the literature complexes.<sup>108</sup>

They assumed that the flexible salen ligand in the Co(IV)-carbenoid species will take a folded stepped-conformation, where the naphthalene rings are orthogonal (**Figure 21**). The five-membered chelate rings including the Co-ion and the two imino nitrogen atoms are assumed to adopt a half-chair conformation, and the nitrogen atoms are at an equatorial position on the cyclohexyl ring. In the (1*R*,2*R*,*R*,*R*)-**87** species derived from **66**, the ester group is shown to protrude forward due to the presence of 2''-phenyl group located at the back, which allows the olefin to approach the carbenoid over the downward naphthalene ring side along the Co-N<sub>b</sub> bond and rotate counterclockwise to attain the observed *cis*-enantioselectivity (**Figure 21**, top right).

Katsuki's group observed that switching the chirality of the diamine will give the opposite enantiomer, which is due to the change in the folding that positions the diamine in the equatorial position as shown in (1*S*,2*S*,*R*,*R*)-**88** (**Figure 21**, bottom left). The olefin now approaches the carbenoid center along the less hindered Co-N<sub>a</sub> axis over the downward

naphthalene ring. However, the approaching pathway of the olefin is obstructed by the 2''-phenyl group, thus resulted in a sluggish and low yielding reaction.

The Co(II)-salen complex **80** that we synthesized effectively solved this problem as it adopts the conformation as shown in (1*S*,2*S*,*S*,*S*)-**89** (Figure 21, bottom right). The enantioface selectivity is still controlled by the chiral diamine but the 2''-phenyl group no long protrudes toward the olefin's approaching path as it is located below the downward naphthalene ring. The olefin can now access the carbenoid center smoothly to give the *cis*-product with excellent enantioselectivity.

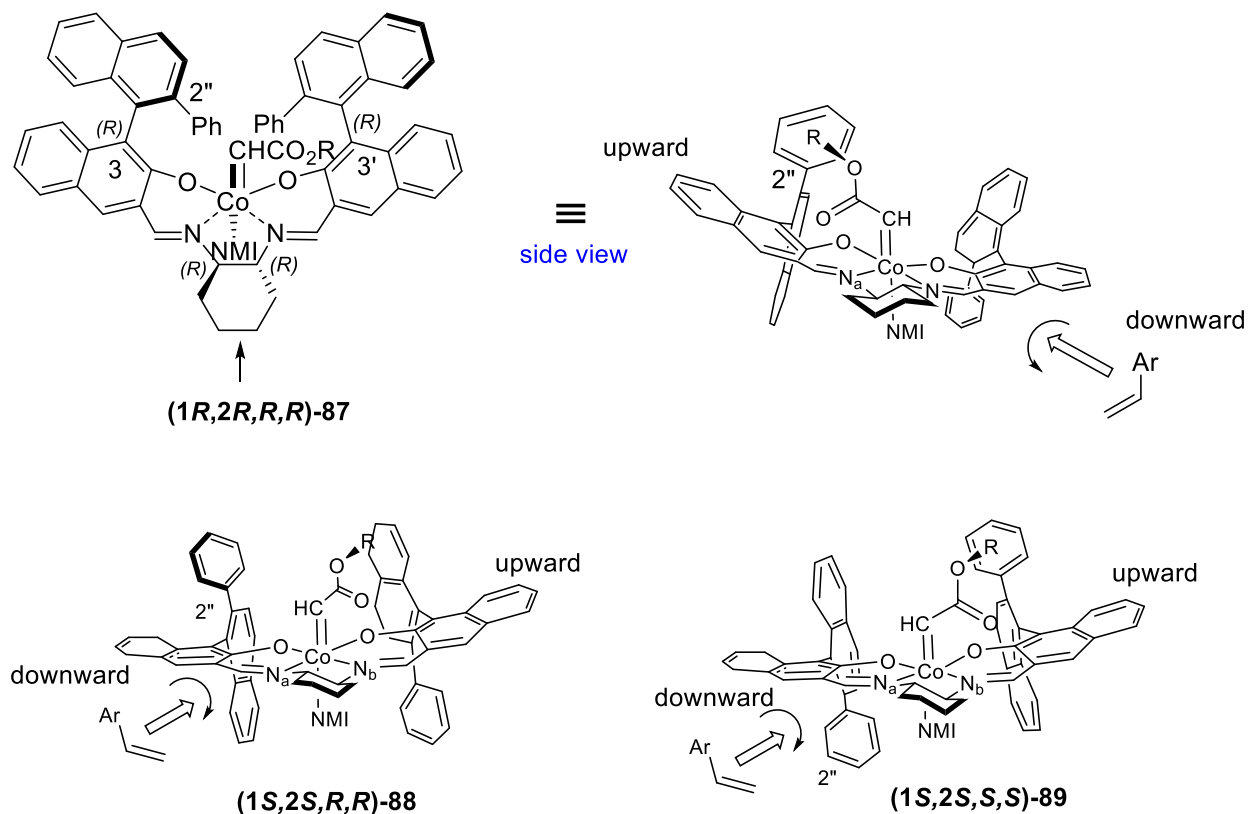


**Figure 21.** Proposed model for the conformation of the Co(IV)-carbenoid species.

## 2.2.4 Conclusion

Despite the relatively tedious synthetic route to the Co(II)-salen complexes **66** and **80 – 82**, we were able to conveniently access both enantiomers in high yields and % *ee*. The catalyst was shown to be highly efficient in providing the desired enantiomers in large scale without the need for additional chiral resolution step. The sophisticated mechanistic control of the diastereo- and enantioselectivity rendered the Co(II)-salen complex a very useful catalyst for asymmetric cyclopropanation.

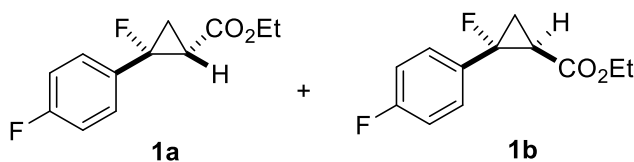
### 3.0 EXPERIMENTAL SECTION

#### 3.1 GENERAL PROCEDURE

Moisture and air-sensitive reactions were performed under a N<sub>2</sub> or Ar atmosphere and glassware used for these reactions was flamed dried and cooled under N<sub>2</sub> or Ar prior to use. THF and Et<sub>2</sub>O were distilled from sodium/benzophenone ketyl. Toluene and CH<sub>2</sub>Cl<sub>2</sub> were distilled from CaH<sub>2</sub>. CrCl<sub>2</sub> was stored and used in a glovebox. Melting points were determined using a Mel-Temp II instrument and are not corrected. Infrared spectra were determined using a Smiths Detection IdentifyIR FT-IR spectrometer. High resolution mass spectra were obtained on a Micromass UK Limited, Q-TOF Ultima API, Thermo Scientific Exactive Orbitrap LC-MS. Automated column chromatography was done using an Isco Combiflash Rf. <sup>1</sup>H and <sup>13</sup>C NMR spectra were obtained on Bruker Advance 300 MHz, 400 MHz, or 500 MHz instruments. Chemical shifts (δ) were reported in parts per million with the residual solvent peak used as an internal standard, δ <sup>1</sup>H/<sup>13</sup>C (Solvent): 7.26/77.16 (CDCl<sub>3</sub>); 2.50/39.52 (DMSO-d<sub>6</sub>); and are tabulated as follows: chemical shift, multiplicity (s = singlet, br s = broad singlet, d = doublet, br d = broad doublet, t = triplet, app t = apparent triplet, q = quartet, m = multiplet), coupling constant(s), and number of protons. <sup>13</sup>C NMR spectra were obtained at 75 MHz, 100 MHz, or 125 MHz using a proton-decoupled pulse sequence and are tabulated by observed peak. CDCl<sub>3</sub> was filtered through dried basic alumina prior to use. Thin-layer chromatography was performed using pre-coated silica gel 60

F254 plates (EMD, 250  $\mu\text{m}$  thickness) and visualization was accomplished with a 254 nm UV light and by staining with a PMA solution (5 g of phosphomolybdic acid in 100 mL of 95% EtOH) or a  $\text{KMnO}_4$  solution (1.5 g of  $\text{KMnO}_4$  and 1.5 g of  $\text{K}_2\text{CO}_3$  in 100 mL of a 0.1% NaOH solution). Chromatography on  $\text{SiO}_2$  (Silicycle, Silia-P Flash Silica Gel or SiliaFlash® P60, 40-63  $\mu\text{m}$ ) was used to purify crude reaction mixtures. Final products were of >95% purity as analyzed by RP HPLC (Alltech Prevail C-18, 100  $\times$  4.6 mm, 1 mL/min,  $\text{CH}_3\text{CN}$ ,  $\text{H}_2\text{O}$  and 0.1% TFA) with UV (210, 220 and 254 nm), ELS (nebulizer 45  $^\circ\text{C}$ , evaporator 45  $^\circ\text{C}$ ,  $\text{N}_2$  flow 1.25 SLM), and MS detection using a Thermo Scientific Exactive Orbitrap LC-MS (ESI positive). All other materials were obtained from commercial sources and used as received.

### 3.2 EXPERIMENTAL PROCEDURES



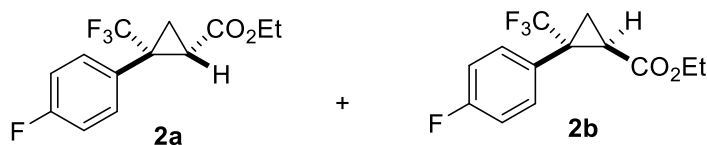
***cis*- and *trans*-Ethyl 2-fluoro-2-(4-fluorophenyl)cyclopropane-1-carboxylate (1a and 1b).**<sup>58</sup>

In a flame-dried 3-neck round-bottom flask equipped with a stir bar, reflux condenser, septum, and stopper,  $\text{Cu}(\text{acac})_2$  (64.9 mg, 0.248 mmol, 3 mol%) was dissolved in distilled  $\text{CH}_2\text{Cl}_2$  (11 mL). The solution was stirred for several minutes. A few drops of phenylhydrazine were added and the stirring continued. 1-Fluoro-4-(1-fluorovinyl)benzene (1.16 g, 8.27 mmol) was added and the mixture was heated to reflux. A solution of ethyl diazoacetate (1.48 mL, 12.4 mmol) in distilled  $\text{CH}_2\text{Cl}_2$  (22 mL) was added via syringe pump over 8 h. The solution was then heated to

reflux for an additional 4 h, after which it was cooled and diluted with CH<sub>2</sub>Cl<sub>2</sub> (150 mL). The solution was washed with saturated NaHCO<sub>3</sub> solution and distilled water (300 mL). The organic layer was dried (MgSO<sub>4</sub>), filtered, and concentrated under reduced pressure. NMR analysis of the crude product revealed a conversion of 65%. Purification of the crude product with chromatography on SiO<sub>2</sub> (1:1 CH<sub>2</sub>Cl<sub>2</sub>/hexanes) afforded a mixture of 1:1 *cis/trans* diastereomers as a yellow oil. The diastereomers were separated by chromatography on SiO<sub>2</sub> (1:2 CH<sub>2</sub>Cl<sub>2</sub>/hexanes) where the *trans*-isomer eluted first followed by the *cis*-isomer. ***cis-1a*** (474 mg, 2.10 mmol, 25%): <sup>1</sup>H NMR (500 MHz, CDCl<sub>3</sub>) δ 7.32 (dd, *J* = 8.1, 5.2 Hz, 2 H), 7.08 (t, *J* = 8.4 Hz, 2 H), 4.29-4.19 (m, 2 H), 2.28 (dt, *J* = 20.1, 7.4 Hz, 1 H), 2.15 (ddd, *J* = 9.5, 7.7, 2.7 Hz, 1 H), 1.59 (ddd, *J* = 10.5, 9.5, 7.1 Hz, 1 H), 1.30 (t, *J* = 7.1 Hz, 3 H); <sup>13</sup>C NMR (75 MHz; CDCl<sub>3</sub>) δ 167.9 (d, *J*<sub>C-F</sub> = 2 Hz), 162.9 (dd, *J*<sub>C-F</sub> = 248, 2 Hz), 133.4 (dd, *J*<sub>C-F</sub> = 22, 3 Hz), 127.3 (dd, *J*<sub>C-F</sub> = 8, 6 Hz), 115.8 (d, *J*<sub>C-F</sub> = 22 Hz), 80.7 (d, *J*<sub>C-F</sub> = 228 Hz), 61.4, 28.8 (d, *J*<sub>C-F</sub> = 12 Hz), 18.8 (d, *J*<sub>C-F</sub> = 13 Hz), 14.4; <sup>19</sup>F NMR (CDCl<sub>3</sub>, 470 MHz) δ -113.2 (s, 1 F), -184.9 (s, 1 F).

***trans-1b*** (481 mg, 2.13 mmol, 26%): <sup>1</sup>H NMR (CDCl<sub>3</sub>, 500 MHz) δ 7.48-7.44 (m, 2 H), 7.06 (t, *J* = 8.4 Hz, 2 H), 3.98-3.90 (m, 2 H), 2.56 (ddd, *J* = 17.8, 10.3, 7.6 Hz, 1 H), 1.95 (dt, *J* = 12.2, 7.3 Hz, 1 H), 1.82 (ddd, *J* = 19.2, 10.3, 7.1 Hz, 1 H), 1.04 (t, *J* = 7.1 Hz, 3 H); <sup>13</sup>C NMR (CDCl<sub>3</sub>, 125 MHz) δ 169.0 (d, *J*<sub>C-F</sub> = 2 Hz), 163.3 (dd, *J*<sub>C-F</sub> = 249, 3 Hz), 130.6 (dd, *J*<sub>C-F</sub> = 8, 4 Hz), 129.3 (dd, *J*<sub>C-F</sub> = 21, 3 Hz), 115.5 (dd, *J*<sub>C-F</sub> = 22, 2 Hz), 82.6 (d, *J*<sub>C-F</sub> = 221 Hz), 60.98, 27.9 (d, *J*<sub>C-F</sub> = 17 Hz), 16.8 (d, *J*<sub>C-F</sub> = 11 Hz), 14.14; <sup>19</sup>F NMR (CDCl<sub>3</sub>, 470 MHz) δ -111.8 (s, 1 F), -152.6 (s, 1 F).





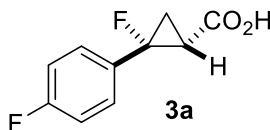
***cis*- and *trans*-Ethyl-2-(4-fluorophenyl)-2-(trifluoromethyl)cyclopropane-1-carboxylate (2a and 2b).** To a flame-dried round-bottom flask was added Rh<sub>2</sub>(OAc)<sub>4</sub> (128 mg, 0.290 mmol, 5

mol%) and 1-fluoro-4-(3,3,3-trifluoroprop-1-en-2-yl)benzene (1.20 g, 5.81 mmol) in distilled CH<sub>2</sub>Cl<sub>2</sub> (5 mL). A solution of ethyl diazoacetate (1.04 mL, 8.71 mmol) in CH<sub>2</sub>Cl<sub>2</sub> (18 mL) was added via syringe pump over 16 h at room temperature. After addition of the diazo compound, TLC analysis showed that there was still alkene present. Another 2 mol% of the Rh<sub>2</sub>(OAc)<sub>4</sub> catalyst was added and 0.5 equiv of diazo compound dissolved in CH<sub>2</sub>Cl<sub>2</sub> (10 mL) was added dropwise over 9 h. The mixture was filtered through a plug of SiO<sub>2</sub> and washed with CH<sub>2</sub>Cl<sub>2</sub>.

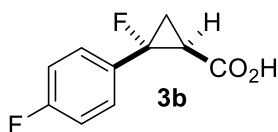
The solution was concentrated under reduced pressure and the crude mixture was purified via chromatography on SiO<sub>2</sub> (1:2 CH<sub>2</sub>Cl<sub>2</sub>/hexanes), where the *trans*-isomer eluted first followed by *cis*-isomer, as yellow oils. ***cis*-2a** (554 mg, 2.01 mmol, 35%): <sup>1</sup>H NMR (CDCl<sub>3</sub>, 500 MHz) δ 7.47 (dd, *J* = 8.6, 5.3 Hz, 2 H), 7.08-7.02 (m, 2 H), 4.32-4.18 (m, 2 H), 2.23 (t, *J* = 8.1 Hz, 1 H), 2.04 (dd, *J* = 7.2, 5.9 Hz, 1 H), 1.46 (ddq, *J* = 8.9, 5.7, 1.7 Hz, 1 H), 1.31 (t, *J* = 7.1 Hz, 3 H); <sup>13</sup>C NMR (CDCl<sub>3</sub>, 125 MHz) δ 168.0, 163.0 (d, *J*<sub>C-F</sub> = 248 Hz), 132.8 (d, *J*<sub>C-F</sub> = 9 Hz), 131.8 (d, *J*<sub>C-F</sub> = 3 Hz), 125.2 (q, *J*<sub>C-F</sub> = 276 Hz), 115.7 (d, *J*<sub>C-F</sub> = 22 Hz), 61.7, 35.0 (q, *J*<sub>C-F</sub> = 34 Hz), 27.5, 14.5 (q, *J*<sub>C-F</sub> = 2 Hz), 14.2; <sup>19</sup>F NMR (CDCl<sub>3</sub>, 471 MHz) δ -65.6 (s, 3 F), -112.4 (s, 1 F).

***trans*-2b** (662 mg, 2.40 mmol, 41%); <sup>1</sup>H NMR (CDCl<sub>3</sub>, 500 MHz) δ 7.34 (dd, *J* = 8.6, 5.3 Hz, 2 H), 7.05-7.00 (m, 2 H), 4.01-3.91 (m, 2 H), 2.48 (dd, *J* = 8.8, 6.3 Hz, 1 H), 1.83 (tq, *J* = 5.8, 1.8 Hz, 1 H), 1.72 (dd, *J* = 8.8, 5.5 Hz, 1 H), 1.07 (t, *J* = 7.1 Hz, 3 H); <sup>13</sup>C NMR (CDCl<sub>3</sub>, 100 MHz) δ 168.7, 163.0 (d, *J*<sub>C-F</sub> = 248 Hz), 133.0 (d, *J*<sub>C-F</sub> = 9 Hz), 127.4 (d, *J*<sub>C-F</sub> = 3 Hz), 125.0 (q, *J*<sub>C-F</sub> = 274 Hz), 115.6 (d, *J*<sub>C-F</sub> = 22 Hz), 61.3, 35.2 (q, *J*<sub>C-F</sub> = 34 Hz), 23.8 (q, *J*<sub>C-F</sub> = 2 Hz), 14.7 (q, *J*<sub>C-F</sub>

= 2 Hz), 14.1;  $^{19}\text{F}$  NMR ( $\text{CDCl}_3$ , 471 MHz)  $\delta$  -70.7 (s, 3 F), -112.4 (s, 1 F). A fraction containing a mixture of both diastereomers was also obtained (192 mg, 0.694 mmol, 12%).

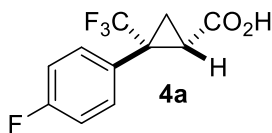


***cis*-2-Fluoro-2-(4-fluorophenyl)cyclopropane-1-carboxylic acid (3a).**<sup>58</sup> To a solution of **1a** (0.200 g, 0.884 mmol) in methanol (1.8 mL) was added KOH (0.500 g, 8.84 mmol) in methanol (4.4 mL) at 0 °C. The reaction mixture was warm to room temperature and stirred for 16 h. The mixture was poured into water and extracted with  $\text{CH}_2\text{Cl}_2$  (25 mL). The organic layer was discarded and the aqueous layer was acidified with 6 M HCl and extracted with  $\text{CH}_2\text{Cl}_2$  (2 x 25 mL). The combined organic layers were dried ( $\text{Na}_2\text{SO}_4$ ) and concentrated under reduced pressure to afford **3a** (0.171 g, 0.864 mmol, 98%) as a white solid:  $^1\text{H}$  NMR ( $\text{CDCl}_3$ , 500 MHz)  $\delta$  7.36-7.32 (m, 2 H), 7.12-7.07 (m, 2 H), 2.32 (dt,  $J = 20.1, 7.5$  Hz, 1 H), 2.18 (ddd,  $J = 9.5, 7.5, 2.2$  Hz, 1 H), 1.70 (ddd,  $J = 10.7, 9.4, 7.2$  Hz, 1 H);  $^{13}\text{C}$  NMR ( $\text{CDCl}_3$ , 125 MHz)  $\delta$  173.0, 163.0 (dd,  $J_{\text{C-F}} = 248, 2$  Hz), 132.8 (dd,  $J_{\text{C-F}} = 22, 3$  Hz), 127.5 (dd,  $J_{\text{C-F}} = 9, 6$  Hz), 115.9 (d,  $J_{\text{C-F}} = 22$  Hz), 81.3 (d,  $J_{\text{C-F}} = 229$  Hz), 28.3 (d,  $J_{\text{C-F}} = 12$  Hz), 19.3 (d,  $J_{\text{C-F}} = 12$  Hz).

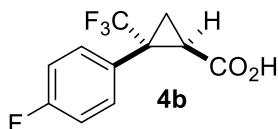


***trans*-2-Fluoro-2-(4-fluorophenyl)cyclopropane-1-carboxylic acid (3b).**<sup>58</sup> To a solution of **1b** (0.200 g, 0.884 mmol) in methanol (1.8 mL) was added KOH (0.500 g, 8.84 mmol) in methanol (4.4 mL) at 0 °C. The reaction mixture was warm to room temperature and stirred for 16 h. The mixture was poured into water and extracted with  $\text{CH}_2\text{Cl}_2$  (25 mL). The organic layer was

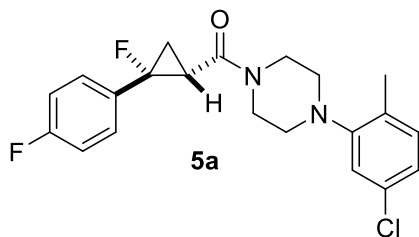
discarded and the aqueous layer was acidified with 6 M HCl and extracted with CH<sub>2</sub>Cl<sub>2</sub> (2 x 25 mL). The combined organic layers were dried (Na<sub>2</sub>SO<sub>4</sub>) and concentrated under reduced pressure to afford **3b** (0.175 g, 0.884 mmol, quant.) as a white solid: <sup>1</sup>H NMR (CDCl<sub>3</sub>, 500 MHz) δ 7.45-7.41 (m, 2 H), 7.05 (t, *J* = 8.6 Hz, 2 H), 2.52 (ddd, *J* = 17.4, 10.0, 7.5 Hz, 1 H), 1.94-1.83 (m, 2 H); <sup>13</sup>C NMR (CDCl<sub>3</sub>, 100 MHz) δ 174.3, 163.4 (dd, *J*<sub>C-F</sub> = 249, 3 Hz), 130.6 (dd, *J*<sub>C-F</sub> = 9, 4 Hz), 128.6 (dd, *J*<sub>C-F</sub> = 21, 3 Hz), 115.5 (d, *J*<sub>C-F</sub> = 22 Hz), 83.1 (d, *J*<sub>C-F</sub> = 222 Hz), 27.5 (d, *J*<sub>C-F</sub> = 17 Hz), 17.5 (d, *J*<sub>C-F</sub> = 10 Hz).



***cis*-2-(4-Fluorophenyl)-2-(trifluoromethyl)cyclopropane-1-carboxylic acid (4a).** To a solution of KOH (0.463 g, 8.25 mmol) in methanol (3.6 ml) was added **2a** (0.228 g, 0.825 mmol) in methanol (1.5 mL) at 0 °C. The reaction mixture was gradually warm to room temperature and stirred for 12 h. The mixture was poured into water and extracted with CH<sub>2</sub>Cl<sub>2</sub> (25 mL). The organic layer was discarded and the aqueous layer acidified with 6 M HCl and extracted with CH<sub>2</sub>Cl<sub>2</sub> (2 x 25 mL). The combined organic layers were dried (Na<sub>2</sub>SO<sub>4</sub>) and concentrated under reduced pressure to give **4a** (0.202 g, 0.812 mmol, 98 %) as a white solid: <sup>1</sup>H NMR (CDCl<sub>3</sub>, 500 MHz) δ 7.47 (dd, *J* = 8.6, 5.2 Hz, 2 H), 7.09-7.02 (m, 2 H), 2.28 (t, *J* = 8.0 Hz, 1 H), 2.09 (dd, *J* = 7.3, 5.9 Hz, 1 H), 1.57-1.53 (m, 1 H); <sup>19</sup>F NMR (CDCl<sub>3</sub>, 471 MHz) δ -65.3 (s, 3 F), -112.1 (s, 1 F).

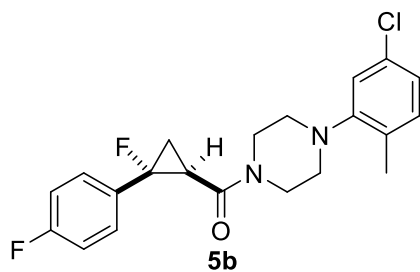


***trans*-2-(4-Fluorophenyl)-2-(trifluoromethyl)cyclopropane-1-carboxylic acid (4b).** To a solution of KOH (0.406 g, 7.24 mmol) in methanol (3.6 ml) was added **2b** (0.200 g, 0.724 mmol) in methanol (1.5 mL) at 0 °C. The reaction mixture was gradually warm to room temperature and stirred for 12 h. The mixture was poured into water and extracted with CH<sub>2</sub>Cl<sub>2</sub> (25 mL). The organic layer was discarded and the aqueous layer acidified with 6 M HCl and extracted with CH<sub>2</sub>Cl<sub>2</sub> (2 x 25 mL). The combined organic layers were dried (Na<sub>2</sub>SO<sub>4</sub>) and concentrated under reduced pressure to give **4b** (0.181 g, 0.731 mmol, 98 %) as a white solid: <sup>1</sup>H NMR (CDCl<sub>3</sub>, 500 MHz) δ 7.32 (dd, *J* = 8.3, 5.4 Hz, 2 H), 7.02 (t, *J* = 8.6 Hz, 2 H), 2.49-2.45 (m, 1 H), 1.77 (dq, *J* = 8.3, 2.9 Hz, 2 H); <sup>19</sup>F NMR (CDCl<sub>3</sub>, 471 MHz) δ -70.9 (s, 3 F), -112.1 (s, 1 F).



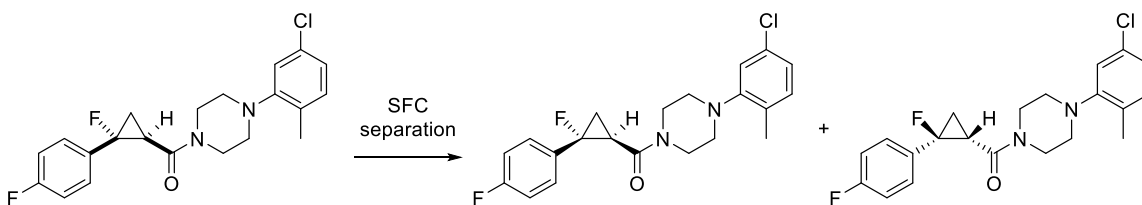
***cis*-(4-(5-Chloro-2-methylphenyl)piperazin-1-yl)((1*SR*,2*RS*)-2-fluoro-2-(4-fluorophenyl)cyclopropyl)methanone (5a).** To a solution of **3a** (0.0500 g, 0.252 mmol) in distilled CH<sub>2</sub>Cl<sub>2</sub> (2.5 mL) at 0 °C was added 1-(5-chloro-2-methylphenyl)piperazine hydrochloride (0.0750 g, 0.303 mmol) and triethylamine (0.11 mL, 0.757 mmol). The cooled solution was then treated with T3P (50 wt.% solution in EtOAc, 0.27 mL, 0.378 mmol) dropwise. The reaction mixture was stirred at 0 °C for 30 min and allowed to warm to room temperature and stirred for 16 h. The reaction was diluted with CH<sub>2</sub>Cl<sub>2</sub> (30 mL) and washed with

1 M HCl (20 mL), saturated NaHCO<sub>3</sub> (20 mL), dried (MgSO<sub>4</sub>), filtered and concentrated *in vacuo*. The crude brown oil residue was purified via chromatography on SiO<sub>2</sub> (2:3 EtOAc/hexanes) to afford **5a** (79.1 mg, 0.200 mmol, 79 %) as a white solid: Mp 110.2 – 110.8 °C (hexanes); IR (CDCl<sub>3</sub>) 2918, 2819, 1646, 1593, 1516, 1430, 1223, 831, 809, 730 cm<sup>-1</sup>; <sup>1</sup>H NMR (CDCl<sub>3</sub>, 500 MHz) δ 7.26 (m, 2 H), 7.10 (t, *J* = 7.8 Hz, 3 H), 6.98 (dd, *J* = 8.1, 1.9 Hz, 1 H), 6.93 (d, *J* = 1.8 Hz, 1 H), 4.04-4.01 (m, 1 H), 3.67-3.57 (m, 3 H), 2.92-2.79 (m, 4 H), 2.39 (dt, *J* = 20.7, 7.6 Hz, 1 H), 2.25 (s, 3 H), 2.19 (ddd, *J* = 9.8, 7.9, 4.6 Hz, 1 H), 1.63-1.58 (m, 2 H); <sup>13</sup>C NMR (CDCl<sub>3</sub>, 150 MHz) δ 164.7, 162.6 (d, *J*<sub>C-F</sub> = 248 Hz), 152.0, 133.9 (d, *J*<sub>C-F</sub> = 22 Hz), 132.2 (d, *J*<sub>C-F</sub> = 24 Hz), 132.0, 131.1, 125.6-125.5 (m), 123.8 (d, *J*<sub>C-F</sub> = 25 Hz), 119.9 (d, *J*<sub>C-F</sub> = 22 Hz), 116.2-115.9 (m), 79.9 (d, *J*<sub>C-F</sub> = 222 Hz), 52.1, 51.7, 46.2, 43.0, 30.5 (d, *J*<sub>C-F</sub> = 14 Hz), 17.7 (d, *J*<sub>C-F</sub> = 12 Hz), 17.6; <sup>19</sup>F NMR (CDCl<sub>3</sub>, 470 MHz) δ -113.88 (s, 1 F), -188.55 (s, 1 F); HRMS (ESI) *m/z* calcd for C<sub>21</sub>H<sub>22</sub>ClF<sub>2</sub>N<sub>2</sub>O ([M+H]<sup>+</sup>) 391.1383, found 391.1386.



***trans*-(4-(5-Chloro-2-methylphenyl)piperazin-1-yl)((1*S*,2*RS*)-2-fluoro-2-(4-fluorophenyl)cyclopropyl)methanone (**5b**).** To a solution of **3b** (0.0500 g, 0.252 mmol) in distilled CH<sub>2</sub>Cl<sub>2</sub> (2.5 mL) at 0 °C was added 1-(5-chloro-2-methylphenyl)piperazine hydrochloride (0.0750 g, 0.303 mmol) and triethylamine (0.11 mL, 0.757 mmol). The cooled solution was then treated with T3P (50 wt.% solution in EtOAc, 0.27 mL, 0.378 mmol) dropwise. The reaction mixture was stirred at 0 °C for 30 min and allowed to warm to room

temperature and stirred for 16 h. The reaction was diluted with CH<sub>2</sub>Cl<sub>2</sub> (30 mL) and washed with 1 M HCl (20 mL), saturated NaHCO<sub>3</sub> (20 mL), dried (MgSO<sub>4</sub>), filtered and concentrated in vacuo. The crude brown oil residue was purified via chromatography on SiO<sub>2</sub> (2:3 EtOAc/hexanes) to afford **5b** (76.0 mg, 0.195 mmol, 77 %) as a colorless oil: IR (CDCl<sub>3</sub>) 2922, 2855, 1641, 1593, 1517, 1432, 1225, 1193, 812, 735. <sup>1</sup>H NMR (CDCl<sub>3</sub>, 500 MHz) δ 7.34-7.30 (m, 2 H), 7.10-7.06 (m, 3 H), 6.97 (dd, *J* = 8.1, 2.1 Hz, 1 H), 6.74 (d, *J* = 2.1 Hz, 1 H), 3.78-3.75 (m, 1 H), 3.66 (t, *J* = 5.0 Hz, 2 H), 3.40 (ddd, *J* = 12.4, 8.6, 3.3 Hz, 1 H), 2.85-2.81 (m, 1 H), 2.77-2.73 (m, 1 H), 2.68 (ddd, *J* = 18.8, 10.9, 7.9 Hz, 1 H), 2.38 (ddd, *J* = 11.5, 8.3, 3.0 Hz, 1 H), 2.30 (dt, 1 H, *J* = 11.4, 5.7 Hz), 2.22 (s, 3 H), 2.11 (dt, *J* = 12.3, 7.6 Hz, 1 H), 1.84 (ddd, *J* = 20.6, 10.8, 7.4 Hz, 1 H); <sup>13</sup>C NMR (CDCl<sub>3</sub>, 100 MHz) δ 165.3, 162.8 (d, *J*<sub>C-F</sub> = 248 Hz), 151.8, 132.1 (d, *J*<sub>C-F</sub> = 21 Hz), 131.1, 130.6 (dd, *J*<sub>C-F</sub> = 21, 3 Hz), 127.6 (d, *J*<sub>C-F</sub> = 7 Hz), 127.5, 123.9, 119.8, 115.5 (d, *J*<sub>C-F</sub> = 22 Hz), 81.5 (d, *J*<sub>C-F</sub> = 222 Hz), 51.9, 51.6, 46.1, 42.5, 29.6 (d, *J*<sub>C-F</sub> = 13 Hz), 17.5, 16.5 (d, *J*<sub>C-F</sub> = 10 Hz); <sup>19</sup>F NMR (CDCl<sub>3</sub>, 470 MHz) δ -113.19 (s, 1 F), -164.01 (s, 1 F); HRMS (ESI) *m/z* calcd for C<sub>21</sub>H<sub>22</sub>ClF<sub>2</sub>N<sub>2</sub>O ([M+H]<sup>+</sup>) 391.1383, found 391.1384.



Racemic ***trans*-(4-(5-chloro-2-methylphenyl)piperazin-1-yl)((1*S*,2*RS*)-2-fluoro-2-(4-fluorophenyl)cyclopropyl)methanone** was separated on a SFC Chiralpak-IC semiprep (250 x 10 mm) column (30% MeOH, 7 mL/min, 220 nM, P=100) to afford (-)-**(4-(5-chloro-2-methylphenyl)piperazin-1-yl)(-2-fluoro-2-(4-fluorophenyl)cyclopropyl)methanone** (retention time 4.76 min) as a colorless oil (100% purity by ESLD): [ $\alpha$ ]<sub>D</sub><sup>20</sup> -141.9 (*c* 0.84, MeOH); <sup>1</sup>H

NMR (CDCl<sub>3</sub>, 500 MHz)  $\delta$  7.35-7.31 (m, 2 H), 7.10-7.06 (m, 3 H), 6.97 (dd,  $J$  = 8.1, 2.1 Hz, 1 H), 6.75 (d,  $J$  = 2.1 Hz, 1 H), 3.78-3.74 (m, 1 H), 3.69-3.64 (m, 2 H), 3.43-3.38 (m, 1 H), 2.85-2.81 (m, 1 H), 2.77-2.73 (m, 1 H), 2.68 (ddd,  $J$  = 18.8, 10.9, 7.9 Hz, 1 H), 2.41-2.37 (m, 1 H), 2.31 (td,  $J$  = 11.0, 5.4 Hz, 1 H), 2.22 (s, 3 H), 2.11 (dt,  $J$  = 12.3, 7.6 Hz, 1 H), 1.84 (ddd,  $J$  = 20.5, 10.8, 7.4 Hz, 1 H); HRMS (ESI)  $m/z$  calcd for C<sub>21</sub>H<sub>22</sub>ClF<sub>2</sub>N<sub>2</sub>O ([M+H]<sup>+</sup>) 391.1383, found 391.1379. The enantiomeric excess was >99% ee (SFC Chiralpak-IC (250 x 10 mm); 30% MeOH, 220 nm, 7 mL/min; retention time: 4.77 min).

**(+)-(4-(5-Chloro-2-methylphenyl)piperazin-1-yl)(-2-fluoro-2-(4-**

**fluorophenyl)cyclopropyl)methanone** (retention time 5.60 min) was obtained as a colorless oil (100% purity by ESLD):  $[\alpha]_D^{20}$  +145.1 ( $c$  0.86, MeOH); <sup>1</sup>H NMR (CDCl<sub>3</sub>, 500 MHz)  $\delta$  7.34-7.31 (m, 2 H), 7.10-7.06 (m, 3 H), 6.97 (dd,  $J$  = 8.1, 2.1 Hz, 1 H), 6.75 (d,  $J$  = 2.0 Hz, 1 H), 3.79-3.74 (m, 1 H), 3.69-3.65 (m, 2 H), 3.43-3.38 (m, 1 H), 2.85-2.81 (m, 1 H), 2.77-2.73 (m, 1 H), 2.68 (ddd,  $J$  = 18.9, 10.9, 8.0 Hz, 1 H), 2.39 (ddd,  $J$  = 11.2, 8.8, 2.6 Hz, 1 H), 2.31 (dt,  $J$  = 11.3, 5.8 Hz, 1 H), 2.22 (s, 3 H), 2.11 (dt,  $J$  = 12.3, 7.6 Hz, 1 H), 1.84 (ddd,  $J$  = 20.5, 10.8, 7.4 Hz, 1 H); HRMS (ESI)  $m/z$  calcd for C<sub>21</sub>H<sub>22</sub>ClF<sub>2</sub>N<sub>2</sub>O ([M+H]<sup>+</sup>) 391.1383, found 391.1374. The enantiomeric excess was >99% ee (SFC Chiralpak-IC (250 x 10 mm); 30% MeOH, 220 nm, 7 mL/min; retention time: 5.60 min).

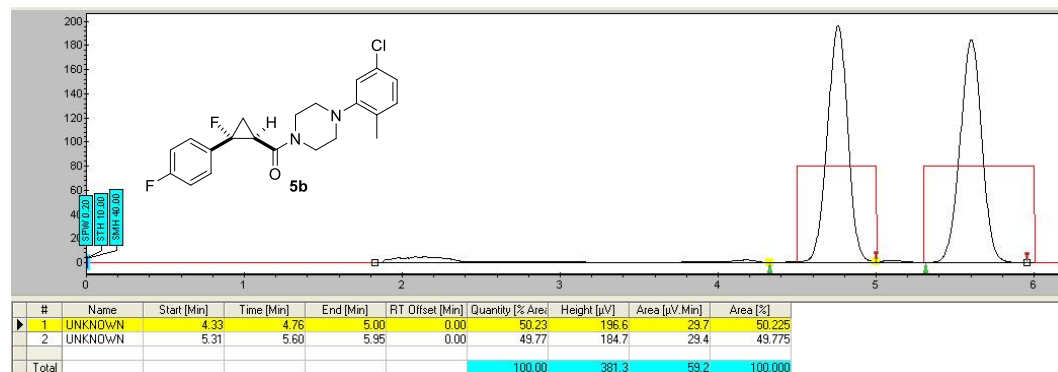


**Figure 22.** SFC chromatogram of racemic **5b**.

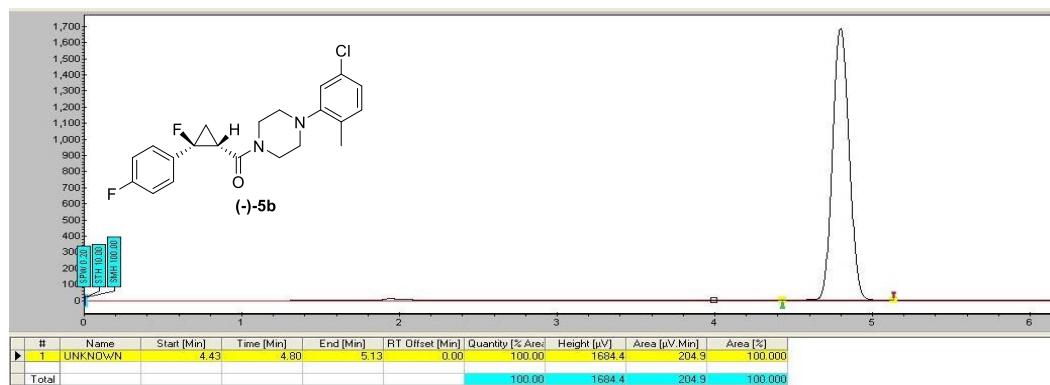


**Figure 23.** SFC resolution of (-)-5b.

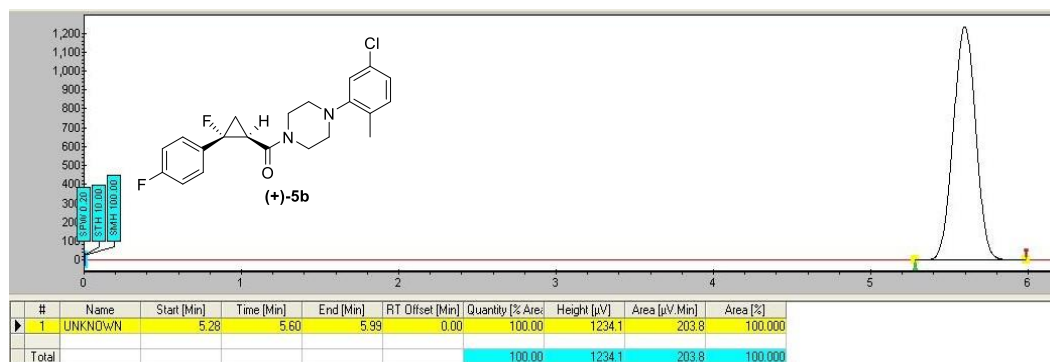
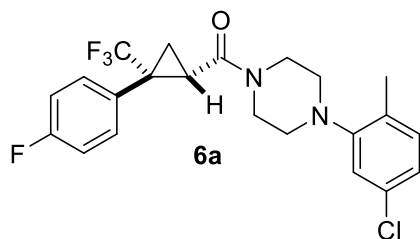


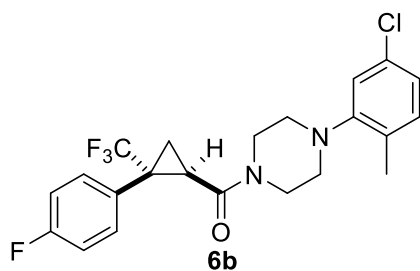
**Figure 24.** SFC resolution of (+)-5b.



*cis*-(4-(5-Chloro-2-methylphenyl)piperazin-1-yl)((1*SR*,2*RS*)-2-(4-fluorophenyl)-2-(trifluoromethyl)cyclopropyl)methanone (**6a**). A solution **4a** (0.100 g, 0.403 mmol) and 1-(5-chloro-2-methylphenyl)piperazine hydrochloride (0.120 g, 0.484 mmol) in distilled CH<sub>2</sub>Cl<sub>2</sub> (4 mL) was cooled to 0 °C and then added with triethylamine (0.168 mL, 1.21 mmol). The cooled solution was then treated with T3P (50wt.% solution in EtOAc), 0.43 mL, 0.604 mmol)

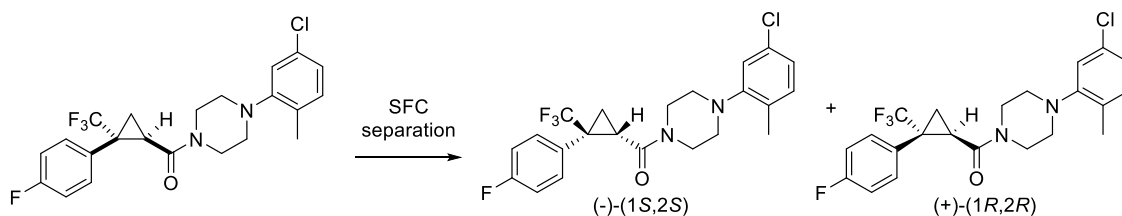


dropwise. The reaction mixture was stirred at 0 °C for 30 min and allowed to warm to room temperature and stirred for 18 h. After completion of the reaction by TLC analysis, the reaction was diluted with CH<sub>2</sub>Cl<sub>2</sub> (30 mL) and washed with 1 M HCl (30 mL), saturated NaHCO<sub>3</sub> solution (20 mL), dried (MgSO<sub>4</sub>), filtered and concentrated *in vacuo*. The brown crude oil residue was purified via chromatography on SiO<sub>2</sub> (100 hexanes - 40% EtOAc/hexanes gradient) to afford **6a** (108 mg, 0.245 mmol, 61%) as a colorless oil which foamed up upon drying: IR (CDCl<sub>3</sub>) 2917, 2825, 1651, 1593, 1513, 1435, 1227, 1159, 1137, 835, 727 cm<sup>-1</sup>; <sup>1</sup>H NMR (CDCl<sub>3</sub>, 500 MHz) δ 7.47 (dd, *J* = 8.7, 5.2 Hz, 2 H), 7.14-7.06 (m, 3 H), 7.00 (dd, *J* = 8.1, 2.1 Hz, 1 H), 6.97 (d, *J* = 2.1 Hz, 1 H), 3.99-3.87 (m, 3 H), 3.81-3.76 (m, 1 H), 3.01 (t, *J* = 5.0 Hz, 2 H), 2.94-2.86 (m, 2 H), 2.31 (s, 3 H), 2.22-2.17 (m, 2 H), 1.60-1.56 (m, 1 H); <sup>13</sup>C NMR (CDCl<sub>3</sub>, 125 MHz) δ 164.9, 162.9 (d, *J*<sub>C-F</sub> = 249 Hz), 152.0, 132.3, 132.0, 131.8 (d, *J*<sub>C-F</sub> = 8 Hz), 131.1, 125.6 (q, *J*<sub>C-F</sub> = 276 Hz), 123.9, 119.9, 116.0 (d, *J*<sub>C-F</sub> = 22 Hz), 51.7, 51.6, 46.3, 42.9, 35.1 (q, *J*<sub>C-F</sub> = 34 Hz), 28.1, 17.60, 14.55; <sup>19</sup>F NMR (CDCl<sub>3</sub>, 470 MHz) δ -64.7 (s, 3 F), -112.2 (s, 1 F); HRMS (ESI) *m/z* calcd for C<sub>22</sub>H<sub>22</sub>ClF<sub>4</sub>N<sub>2</sub>O ([M+H]<sup>+</sup>) 441.1351, found 441.1350.



***trans*-(4-(5-Chloro-2-methylphenyl)piperazin-1-yl)((1*RS*,2*RS*)-2-(4-fluorophenyl)-2-(trifluoromethyl)cyclopropyl)methanone (**6b**)**. A solution of **4b** (0.100 g, 0.403 mmol) and 1-(5-chloro-2-methylphenyl)piperazine hydrochloride (0.120 g, 0.484 mmol) in distilled CH<sub>2</sub>Cl<sub>2</sub> (4 mL) was cooled to 0 °C and then added with triethylamine (0.168 mL, 1.21 mmol). The cooled

solution was then treated with T3P (50wt.% solution in EtOAc), 0.43 mL, 0.604 mmol) dropwise. The reaction mixture was stirred at 0 °C for 30 min and allowed to warm to room temperature and stirred for 18 h. After completion of the reaction by TLC analysis, the reaction was diluted with CH<sub>2</sub>Cl<sub>2</sub> (30 mL) and washed with 1 M HCl (30 mL), saturated NaHCO<sub>3</sub> solution (20 mL), dried (MgSO<sub>4</sub>), filtered and concentrated *in vacuo*. The brown crude oil residue was purified via chromatography on SiO<sub>2</sub> (100 hexanes - 40% EtOAc/hexanes gradient) to afford **6b** (162 mg, 0.367 mmol, 91%) as a colorless oil which foamed up upon drying: IR (CDCl<sub>3</sub>) 2894, 2820, 1652, 1593, 1514, 1436, 1296, 1226, 1160, 1143, 830, 735; <sup>1</sup>H NMR (CDCl<sub>3</sub>, 500 MHz) δ 7.31 (dd, *J* = 8.6, 5.3 Hz, 2 H), 7.13 (d, *J* = 8.1 Hz, 1 H), 7.06-7.00 (m, 3 H), 6.96 (d, *J* = 2.0 Hz, 1 H), 3.99-3.86 (m, 2 H), 3.70-3.56 (m, 2 H), 3.07-2.99 (m, 2 H), 2.86-2.75 (m, 2 H), 2.59 (dd, *J* = 8.8, 6.2 Hz, 1 H), 2.30 (s, 3 H), 2.12-2.09 (m, 1 H), 1.70 (dd, *J* = 8.8, 5.3 Hz, 1 H); <sup>13</sup>C NMR (CDCl<sub>3</sub>, 100 MHz) δ 165.3, 162.9 (d, *J*<sub>C-F</sub> = 248 Hz), 151.8, 132.8 (d, *J*<sub>C-F</sub> = 8 Hz), 132.3, 132.1, 131.1, 127.1 (d, *J*<sub>C-F</sub> = 3 Hz), 125.4 (q, *J*<sub>C-F</sub> = 274 Hz), 124.0, 119.8, 115.8 (d, *J*<sub>C-F</sub> = 22 Hz), 52.1, 51.7, 46.2, 42.8, 34.9 (q, *J*<sub>C-F</sub> = 33 Hz), 22.8, 17.6, 13.9. <sup>19</sup>F NMR (CDCl<sub>3</sub>, 470 MHz) δ -69.6 (s, 3 F), -112.4 (s, 1 F); HRMS (ESI) *m/z* calcd for C<sub>22</sub>H<sub>22</sub>ClF<sub>4</sub>N<sub>2</sub>O ([M+H]<sup>+</sup>) 441.1351, found 441.1351.



Racemic *trans*-(4-(5-chloro-2-methylphenyl)piperazin-1-yl)((1*S*,2*S*)-2-(4-fluorophenyl)-2-(trifluoromethyl)cyclopropyl)methanone was separated on a SFC Chiralpak-IC semiprep (250 x 10 mm) column (13% MeOH, 7 mL/min, 220 nM, P=100) to afford (-)-(4-(5-chloro-2-

**methylphenyl)piperazin-1-yl)(2-(4-fluorophenyl)-2-**

**(trifluoromethyl)cyclopropyl)methanone** (retention time 6.01 min) as a colorless oil which foamed up upon drying (100% purity by ESLD):  $[\alpha]_{\text{D}}^{20}$  -179.6 (*c* 0.69, MeOH);  $^1\text{H}$  NMR ( $\text{CDCl}_3$ , 400 MHz)  $\delta$  7.31 (dd,  $J = 8.6, 5.3$  Hz, 2 H), 7.13 (d,  $J = 7.6$  Hz, 1 H), 7.07-7.00 (m, 3 H), 6.96 (d,  $J = 2.1$  Hz, 1 H), 3.99-3.85 (m, 2 H), 3.71-3.54 (m, 2 H), 3.08-2.98 (m, 2 H), 2.86-2.74 (m, 2 H), 2.59 (dd,  $J = 8.8, 6.1$  Hz, 1 H), 2.30 (s, 3 H), 2.13-2.08 (m, 1 H), 1.70 (dd,  $J = 8.8, 5.3$  Hz, 1 H); HRMS (ESI)  $m/z$  calcd for  $\text{C}_{22}\text{H}_{22}\text{ClF}_4\text{N}_2\text{O}$  ( $[\text{M}+\text{H}]^+$ ) 441.1344, found 441.1351. The enantiomeric excess was >99% ee (SFC Chiralpak-IC (250 x 10 mm); 10% MeOH, 220 nm, 7 mL/min; retention time: 6.01 min).

**(+)-(4-(5-Chloro-2-methylphenyl)piperazin-1-yl)(2-(4-fluorophenyl)-2-**

**(trifluoromethyl)cyclopropyl)methanone** (retention time 7.16 min) was obtained as a colorless oil which foamed up upon drying (100% purity by ESLD):  $[\alpha]_{\text{D}}^{20}$  -177.9 (*c* 0.67, MeOH);  $^1\text{H}$  NMR ( $\text{CDCl}_3$ , 400 MHz)  $\delta$  7.31 (dd,  $J = 8.6, 5.3$  Hz, 2 H), 7.13 (d,  $J = 8.1$  Hz, 1 H), 7.07-7.00 (m, 3 H), 6.96 (d,  $J = 2.1$  Hz, 1 H), 3.99-3.85 (m, 2 H), 3.71-3.54 (m, 2 H), 3.07-3.00 (m, 2 H), 2.87-2.74 (m, 2 H), 2.59 (dd,  $J = 8.9, 6.1$  Hz, 1 H), 2.30 (s, 3 H), 2.12-2.08 (m, 1 H), 1.70 (dd,  $J = 8.8, 5.3$  Hz, 1 H); HRMS (ESI)  $m/z$  calcd for  $\text{C}_{22}\text{H}_{22}\text{ClF}_4\text{N}_2\text{O}$  ( $[\text{M}+\text{H}]^+$ ) 441.1340, found 441.1351. The enantiomeric excess was >99% ee (SFC Chiralpak-IC (250 x 10 mm); 13% MeOH, 220 nm, 7 mL/min; retention time: 7.12 min).

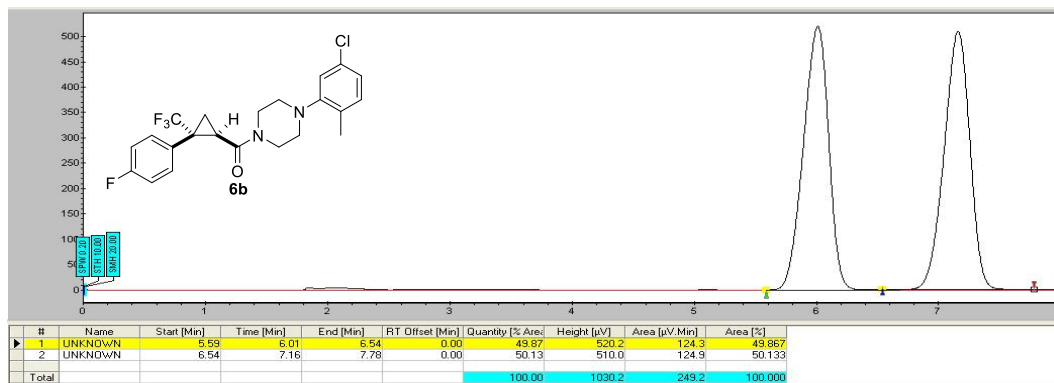


**Figure 25.** SFC chromatogram of racemic **6b**.

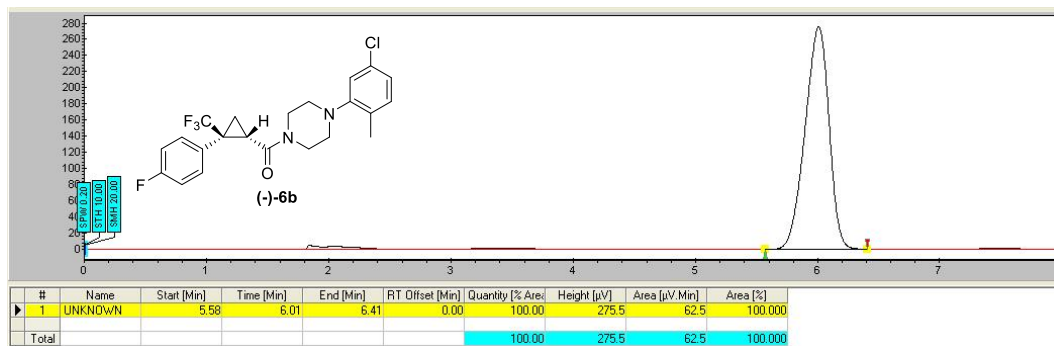


**Figure 26.** SFC resolution of **(-)-6b**.

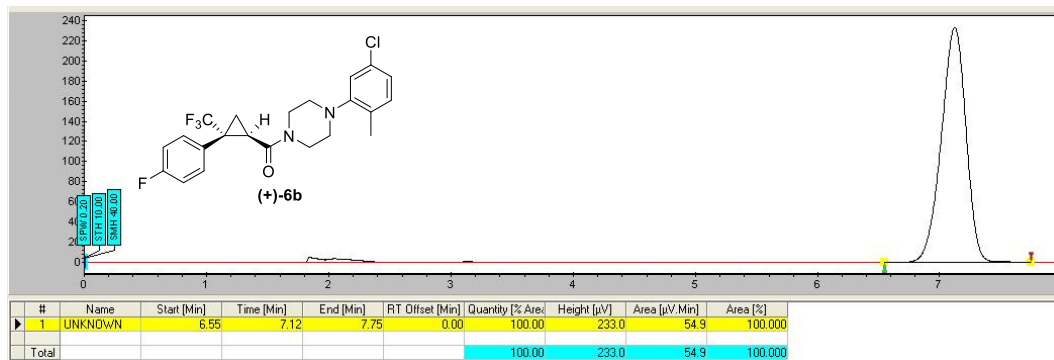
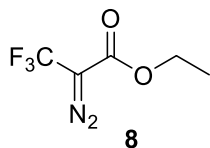
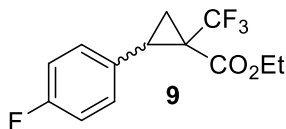


**Figure 27.** SFC resolution of **(+)-6b**.



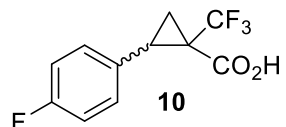
**Ethyl 2-diazo-3,3,3-trifluoropropanoate (8).**<sup>62,63</sup> To a stirred solution of p-toluenesulfonyl hydrazide (11.5 g, 60.5 mmol) in distilled CH<sub>2</sub>Cl<sub>2</sub> (65 mL) was added ethyl trifluoropyruvate (7.79 mL, 57.6 mmol). The reaction was stirred at room temperature for 18 h. Phosphorus oxychloride (7.05 mL, 74.9 mmol) was added dropwise followed by pyridine (6.11 mL, 74.9 mmol) (Note: when pyridine was added dropwise the reaction mixture warmed up to a self-sustaining gentle reflux). The reaction mixture was stirred at room temperature for another 18 h. The mixture was washed with water and the organic layer was separated. The aqueous layer was extracted with CH<sub>2</sub>Cl<sub>2</sub> (3 x 100 mL). The combined organic layers were washed with brine, dried (MgSO<sub>4</sub>), filtered and concentrated *in vacuo* to give **ethyl 3,3,3-trifluoro-2-(2-tosylhydrazineylidene)propanoate 7** as a yellow liquid which solidified to a white solid upon standing. The crude product was used in the next step without further purification. To a solution of **7** (18.3 g, 54.1 mmol) in anhydrous CH<sub>2</sub>Cl<sub>2</sub> (433 mL) was added triethylamine (15.2 mL, 0.108 mol) dropwise. The reaction mixture was stirred at room temperature for 2 days. The solution was carefully concentrated *in vacuo* and the crude product was purified via distillation. The distillate was washed with 1 M HCl (20 mL x 2) to remove the excess triethylamine. The organic layers collected were dried (MgSO<sub>4</sub>), filtered and carefully concentrated *in vacuo* to afford **8** (4.89 g, 26.9 mmol, 50 % over 2 steps) as a yellow oil: Bp lit: 60 - 62 °C (100 mmHg)<sup>4</sup>; <sup>1</sup>H NMR (CDCl<sub>3</sub>, 500 MHz) δ 4.32 (q, *J* = 7.1 Hz, 2 H), 1.32 (t, *J* = 7.1 Hz, 3 H); <sup>13</sup>C NMR (CDCl<sub>3</sub>, 125 MHz) δ 161.0, 122.8 (q, *J*<sub>C-F</sub> = 269 Hz), 62.3, 14.4 (C=N signal not observed).



***cis-* and *trans*-Ethyl 2-(4-fluorophenyl)-1-(trifluoromethyl)cyclopropane-1-carboxylate (**9**).**

To a flame-dried flask containing 4-fluorostyrene (3.3 mL, 27.5 mmol) and  $\text{Rh}_2(\text{OAc})_4$  (0.121 g, 0.275 mmol, 5 mol%) in distilled  $\text{CH}_2\text{Cl}_2$  (25 mL) was added **8** (1.00 g, 5.49 mmol) in distilled  $\text{CH}_2\text{Cl}_2$  (20 mL) via a syringe pump over 16 h at room temperature. After consumption of the diazo compound by TLC, the mixture was passed through a pad of  $\text{SiO}_2$  to remove the rhodium catalyst and washed with  $\text{CH}_2\text{Cl}_2$ . The solvent was removed in vacuo. The crude product was purified by chromatography on  $\text{SiO}_2$  (1:2  $\text{CH}_2\text{Cl}_2$ /hexanes) to give **9** (*cis/trans* ratio 1:1.6) as a yellow oil (*Note: The mixture also contained side product from the dimerization of the diazo compound*). *cis*-**9** (597 mg, 2.16 mmol, 34 % calcd yield):  $^1\text{H}$  NMR ( $\text{CDCl}_3$ , 500 MHz)  $\delta$  7.26 (m, 2 H), 7.00 (t,  $J = 8.7$  Hz, 2 H), 4.33-4.25 (m, 2 H), 3.04 (t,  $J = 8.9$  Hz, 1 H), 1.95 (ddq,  $J = 9.5, 5.4, 1.8$  Hz, 1 H), 1.88 (dd,  $J = 8.2, 5.3$  Hz, 1 H), 1.34 (t,  $J = 7.1$  Hz, 3 H);  $^{19}\text{F}$  NMR ( $\text{CDCl}_3$ , 470 MHz)  $\delta$  -61.1 (s, 3 F), -114.5 (s, 1 F);

*trans*-**9** (955 mg, 3.46 mmol, 54 % calcd yield):  $^1\text{H}$  NMR ( $\text{CDCl}_3$ , 500 MHz)  $\delta$  7.22 (dd,  $J = 8.2, 5.4$  Hz, 2 H), 6.98 (t,  $J = 8.7$  Hz, 2 H), 3.96-3.87 (m, 2 H), 2.90 (t,  $J = 9.0$  Hz, 1 H), 2.14-2.11 (m, 1 H), 1.78 (dd,  $J = 9.7, 5.7$  Hz, 1 H), 0.94 (t,  $J = 7.1$  Hz, 3 H);  $^{19}\text{F}$  NMR ( $\text{CDCl}_3$ , 470 MHz)  $\delta$  -66.8 (s, 3 F), -114.5 (s, 1 F).

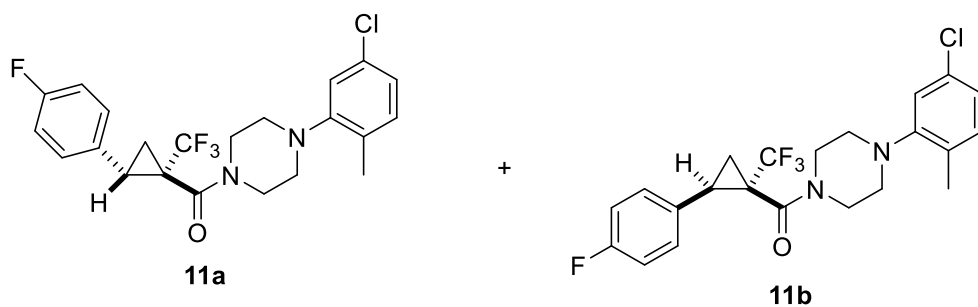


***cis-* and *trans*-2-(4-Fluorophenyl)-1-(trifluoromethyl)cyclopropane-1-carboxylic acid (**10**).**

To a solution of KOH (1.02 g, 18.1 mmol) in methanol (9 ml) was added **9** (0.500 g, 1.81 mmol)

dissolved in methanol (3.8 mL). The reaction mixture was heated to 55 °C and stirred at this temperature for 24 h. The mixture was cooled to room temperature and poured into water and extracted with CH<sub>2</sub>Cl<sub>2</sub> (25 mL). The organic layer was discarded and the aqueous layer acidified with 6 M HCl and extracted with CH<sub>2</sub>Cl<sub>2</sub> (2 x 25 mL). The combined organic layers were dried (Na<sub>2</sub>SO<sub>4</sub>) and concentrated under reduced pressure to give **10** as a pale yellow solid (*cis/trans* ratio 1:1.16) which was used in the next step without purification. *cis*-**10** (168 mg, 0.677 mmol, 37 % calcd yield): <sup>1</sup>H NMR (CDCl<sub>3</sub>, 500 MHz) δ 7.29-7.26 (m, 2 H), 7.02 (t, *J* = 8.6 Hz, 2 H), 3.16 (t, *J* = 9.0 Hz, 1 H), 2.04-1.97 (m, 2 H); <sup>19</sup>F NMR (CDCl<sub>3</sub>, 471 MHz) δ -61.5 (s, 3 F), -114.0 (s, 1 F);

*trans*-**10** (262 mg, 1.06 mmol, 58 % calcd yield): <sup>1</sup>H NMR (CDCl<sub>3</sub>, 500 MHz) δ 7.18 (dd, *J* = 8.4, 5.4 Hz, 2 H), 6.97 (t, *J* = 8.6 Hz, 2 H), 2.99 (t, *J* = 9.0 Hz, 1 H), 2.09 (t, *J* = 6.5 Hz, 1 H), 1.84 (dd, *J* = 9.7, 5.8 Hz, 1 H); <sup>19</sup>F NMR (CDCl<sub>3</sub>, 470 MHz) δ -66.9 (s, 3 F), -114.1 (s, 1 F).



*cis*- and *trans*-(4-(5-Chloro-2-methylphenyl)piperazin-1-yl)(2-(4-fluorophenyl)-1-(trifluoromethyl)cyclopropyl)methanone (**11a** and **11b**). To a suspension of **10** (0.250 g, 1.01 mmol) in distilled CH<sub>2</sub>Cl<sub>2</sub> (10 mL) cooled to 0 °C was added oxalyl chloride (0.18 mL, 2.01 mmol) followed by a catalytic amount of DMF and the reaction was gradually warmed to room temperature and stirred for another 2 h. The reaction was concentrated *in vacuo* (water bath 25°C) to afford the yellow crude acid chloride. The crude residue formed above was dissolved in

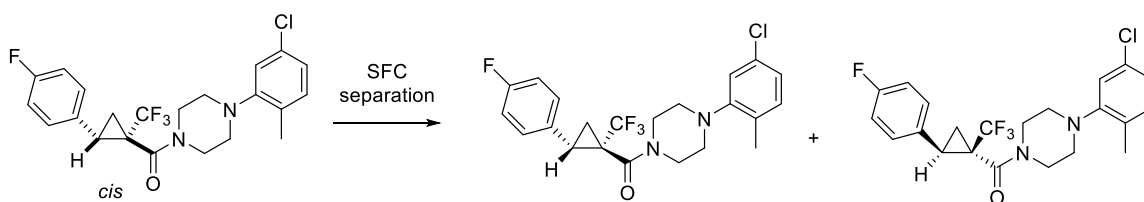
distilled CH<sub>2</sub>Cl<sub>2</sub> (10 mL) cooled to 0°C and added with 1-(5-chloro-2-methylphenyl)piperazine hydrochloride (0.349 g, 1.41 mmol) and Et<sub>3</sub>N (0.50 mL, 3.60 mmol) and the reaction was allowed to warm to room temperature and stirred for 20 h. LCMS and NMR analysis showed presence of starting material carboxylic acid (possibly due to hydrolysis of the acyl chloride). The reaction mixture was cooled to 0 °C and T3P (50wt.% in EtOAc, 0.85 mL, 1.21 mmol) was added to couple the remaining of the carboxylic acid to the piperazine. The mixture was stirred at room temperature for 3 days until no starting material was seen in LCMS. The reaction was diluted with CH<sub>2</sub>Cl<sub>2</sub> (30 mL) and washed with saturated NaHCO<sub>3</sub> (20 mL), dried (MgSO<sub>4</sub>), filtered and concentrated in vacuo. The crude oil residue was dissolved purified via chromatography on SiO<sub>2</sub> (1:2 Et<sub>2</sub>O/hexanes) to afford the **11a** and **11b** respectively as yellow oil.

**cis-11a** (107 mg, 0.244 mmol, 24%): IR (CDCl<sub>3</sub>) 2926, 1647, 1515, 1438, 1226, 1153, 1125, 842, 738 cm<sup>-1</sup>; <sup>1</sup>H NMR (CDCl<sub>3</sub>, 500 MHz) δ 7.32 (dd, *J* = 8.5, 5.4 Hz, 2 H), 7.12 (d, *J* = 8.1 Hz, 1 H), 7.05-7.00 (m, 3 H), 6.96 (d, *J* = 2.1 Hz, 1 H), 3.88 (br s, 4 H), 2.94 (br s, 4 H), 2.79 (t, *J* = 8.7 Hz, 1 H), 2.30 (s, 3 H), 1.98 (dd, *J* = 7.9, 6.2 Hz, 1 H), 1.73-1.69 (m, 1 H); <sup>13</sup>C NMR (CDCl<sub>3</sub>, 150 MHz) δ 164.6, 162.3 (d, *J* = 246 Hz), 151.8, 132.3, 132.1, 131.1, 130.7 (d, *J*<sub>C-F</sub> = 8 Hz), 129.3 (d, *J*<sub>C-F</sub> = 3 Hz), 124.7 (q, *J*<sub>C-F</sub> = 276 Hz), 124.0, 120.0, 115.5 (d, *J*<sub>C-F</sub> = 21 Hz), 51.8, 47.1, 43.4, 34.8 (q, *J*<sub>C-F</sub> = 32 Hz), 27.6, 17.6, 14.8; <sup>19</sup>F NMR (CDCl<sub>3</sub>, 470 MHz) δ -60.7 (s, 3 F), -114.8 (s, 1 F); HRMS (ESI) *m/z* calcd for C<sub>22</sub>H<sub>22</sub>ClF<sub>4</sub>N<sub>2</sub>O ([M+H]<sup>+</sup>) 441.1351, found 441.1352.

**trans-11b** (151 mg, 0.342 mmol, 34 %): IR (CDCl<sub>3</sub>) 2925, 2860, 1643, 1516, 1437, 1226, 1149, 1132, 845, 812, 733 cm<sup>-1</sup>; <sup>1</sup>H NMR (CDCl<sub>3</sub>, 500 MHz) δ 7.12-7.04 (m, 5 H), 6.95 (dd, *J* = 8.1, 2.1 Hz, 1 H), 6.65 (d, *J* = 1.7 Hz, 1 H), 3.77 (s, 1 H), 3.49-3.47 (m, 2 H), 3.03 (s, 1 H), 2.80 (dd, *J* = 9.8, 7.5 Hz, 1 H), 2.74-2.71 (m, 1 H), 2.53-2.42 (m, 2 H), 2.16 (s, 3 H), 1.87 (t, *J* = 7.0 Hz, 1



H), 1.79 (dd,  $J = 9.8, 6.6$  Hz, 1 H), 1.51 (s, 1 H);  $^{13}\text{C}$  NMR ( $\text{CDCl}_3$ , 100 MHz)  $\delta$  162.6 (d,  $J_{\text{C-F}} = 248$  Hz), 161.7, 151.7, 132.1, 132.0, 131.1, 130.9 (d,  $J_{\text{C-F}} = 3$  Hz), 128.8 (d,  $J_{\text{C-F}} = 8$  Hz), 124.6 (q,  $J_{\text{C-F}} = 272$  Hz), 123.9, 119.8, 116.0 (d,  $J_{\text{C-F}} = 22$  Hz), 51.3, 50.9, 46.8, 43.2, 36.8 (q,  $J_{\text{C-F}} = 33$  Hz), 27.3, 17.4, 15.5;  $^{19}\text{F}$  NMR ( $\text{CDCl}_3$ , 470 MHz)  $\delta$  -66.3 (s, 3 F), -114.0 (s, 1 F); HRMS (ESI)  $m/z$  calcd for  $\text{C}_{22}\text{H}_{22}\text{ClF}_4\text{N}_2\text{O}$  ( $[\text{M}+\text{H}]^+$ ) 441.1351, found 441.1349.



Racemic ***cis*-(4-(5-chloro-2-methylphenyl)piperazin-1-yl)((1*SR*,2*SR*)-2-(4-fluorophenyl)-1-(trifluoromethyl)cyclopropyl)methanone** was separated on a SFC Chiralpak-IC semiprep (250 x 10 mm) column (10% MeOH, 6 mL/min, 220 nM, P=100) to afford **(-)-(4-(5-chloro-2-methylphenyl)piperazin-1-yl)(-2-(4-fluorophenyl)-1-(trifluoromethyl)cyclopropyl)methanone** (retention time 14.46 min) as a colorless oil which foamed up upon drying (100% purity by ESLD):  $[\alpha]_{\text{D}}^{20} -57.3$  ( $c$  0.44, MeOH);  $^1\text{H}$  NMR ( $\text{CDCl}_3$ , 500 MHz)  $\delta$  7.32 (dd,  $J = 8.5, 5.4$  Hz, 2 H), 7.13 (d,  $J = 8.1$  Hz, 1 H), 7.05-7.00 (m, 3 H), 6.96 (d,  $J = 2.1$  Hz, 1 H), 3.89-3.88 (m, 4 H), 2.94 (s, 4 H), 2.79 (t,  $J = 8.7$  Hz, 1 H), 2.30 (s, 3 H), 1.98 (dd,  $J = 7.9, 6.2$  Hz, 1 H), 1.71 (ddq,  $J = 9.5, 6.0, 1.8$  Hz, 1 H). HRMS (ESI)  $m/z$  calcd for  $\text{C}_{22}\text{H}_{22}\text{ClF}_4\text{N}_2\text{O}$  ( $[\text{M}+\text{H}]^+$ ) 441.1348, found 441.1351. The enantiomeric excess was >99% ee (SFC Chiralpak-IC (250 x 10 mm); 10% MeOH, 220 nm, 6 mL/min; retention time: 14.55 min).

**(+)-(4-(5-Chloro-2-methylphenyl)piperazin-1-yl)(-2-(4-fluorophenyl)-1-(trifluoromethyl)cyclopropyl)methanone** (retention time 16.17 min) was obtained as a

colorless oil which foamed up upon drying (100% purity by ESLD):  $[\alpha]^{20}_{\text{D}} +58.4$  ( $c$  0.42, MeOH);  $^1\text{H}$  NMR ( $\text{CDCl}_3$ , 500 MHz)  $\delta$  7.32 (dd,  $J = 8.5, 5.3$  Hz, 2 H), 7.13 (d,  $J = 8.1$  Hz, 1 H), 7.05-7.00 (m, 3 H), 6.96 (d,  $J = 2.1$  Hz, 1 H), 3.89-3.88 (m, 4 H), 2.94 (s, 4 H), 2.79 (t,  $J = 8.7$  Hz, 1 H), 2.30 (s, 3 H), 1.98 (dd,  $J = 7.9, 6.2$  Hz, 1 H), 1.71 (ddq,  $J = 9.6, 6.0, 1.9$  Hz, 1 H); HRMS (ESI)  $m/z$ . calcd for  $\text{C}_{22}\text{H}_{22}\text{ClF}_4\text{N}_2\text{O}$  ( $[\text{M}+\text{H}]^+$ ) 441.1348, found 441.1351. The enantiomeric excess was >99% ee (SFC Chiralpak-IC (250 x 10 mm); 10% MeOH, 220 nm, 6 mL/min; retention time: 16.31 min).

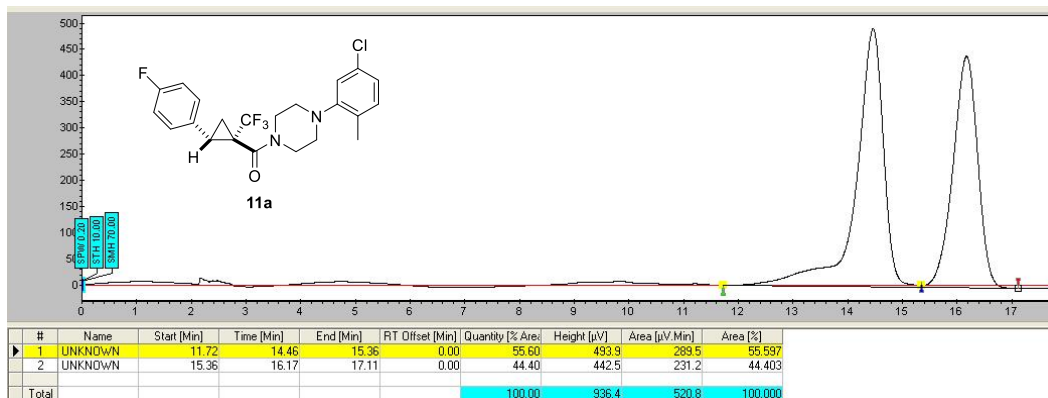


**Figure 28.** SFC resolution of **11a**.

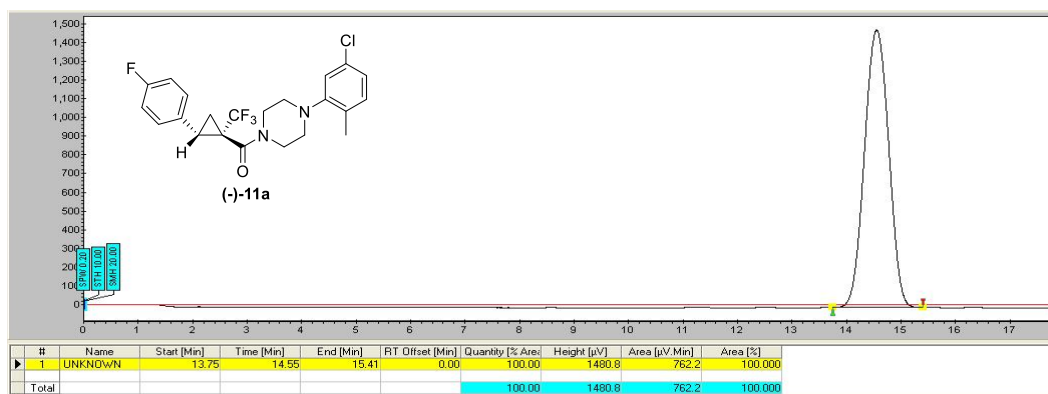


**Figure 29.** SFC resolution of **(-)-11a**.

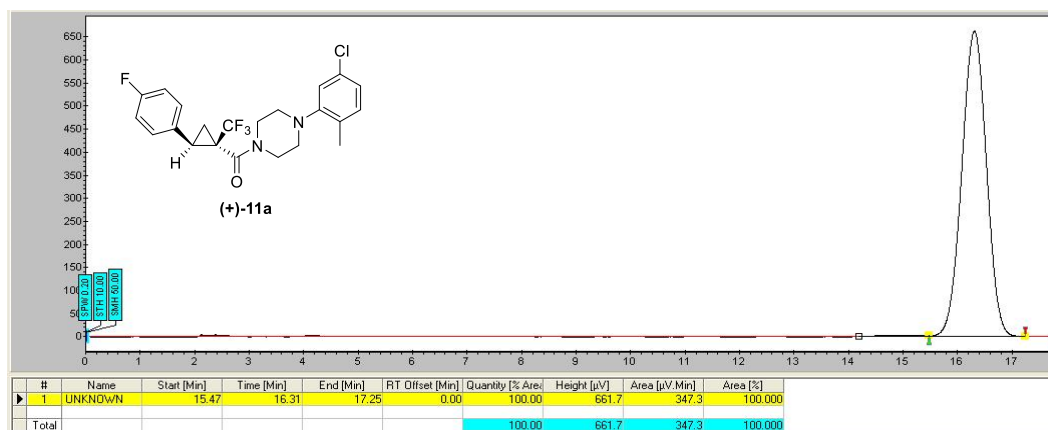
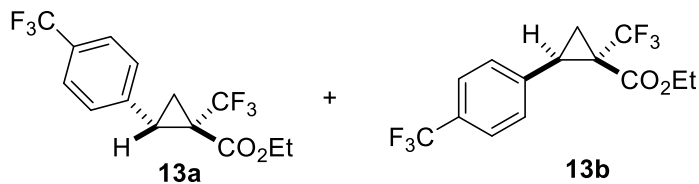


**Figure 30.** SFC resolution of **(+)-11a**.

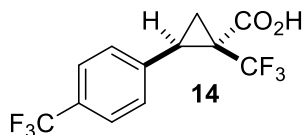


*cis*- and *trans*-Ethyl-1-(trifluoromethyl)-2-(4-(trifluoromethyl)phenyl)cyclopropane-1-carboxylate (**13a** and **13b**). To a flame-dried round-bottom flask was added  $\text{Rh}_2(\text{OAc})_4$  (64.2

mg, 0.145 mmol) and 4-(trifluoromethyl)styrene in distilled  $\text{CH}_2\text{Cl}_2$  (3 mL). A solution of **8** (0.793 g, 4.36 mmol) in distilled  $\text{CH}_2\text{Cl}_2$  (10 mL) was added via a syringe pump over 18 h. The mixture was stirred for another 2 h and then filtered through a plug of  $\text{SiO}_2$  and washed with  $\text{CH}_2\text{Cl}_2$ . The solution was concentrated under reduced pressure and the crude residue was purified via chromatography on  $\text{SiO}_2$  (1:2  $\text{CH}_2\text{Cl}_2$ /hexanes) to afford **13a** and **13b** respectively as

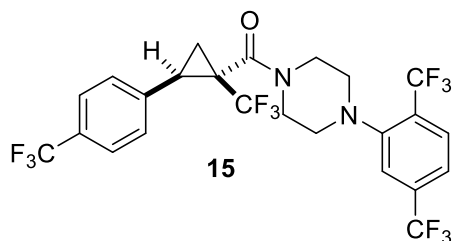
pale yellow oil. *cis*-**13a** (224 mg, 0.686 mmol, 24%):  $^1\text{H}$  NMR ( $\text{CDCl}_3$ , 500 MHz)  $\delta$  7.58 (d,  $J$  = 8.2 Hz, 2 H), 7.42 (d,  $J$  = 8.1 Hz, 2 H), 4.35-4.27 (m, 2 H), 3.11 (t,  $J$  = 8.9 Hz, 1 H), 1.99 (ddq,  $J$  = 9.5, 5.5, 1.8 Hz, 1 H), 1.94 (dd,  $J$  = 8.3, 5.4 Hz, 1 H), 1.35 (t,  $J$  = 7.1 Hz, 3 H);  $^{19}\text{F}$  NMR ( $\text{CDCl}_3$ , 470 MHz)  $\delta$  -61.1 (s, 3 F), -62.6 (s, 3 F).

*trans*-**13b** (435 mg, 1.33 mmol, 46%):  $^1\text{H}$  NMR ( $\text{CDCl}_3$ , 500 MHz)  $\delta$  7.56 (d,  $J$  = 8.1 Hz, 2 H), 7.37 (d,  $J$  = 8.6 Hz, 2 H), 3.91 (q,  $J$  = 7.1 Hz, 2 H), 2.97 (t,  $J$  = 8.9 Hz, 1 H), 2.18 (ddq,  $J$  = 8.0, 6.0, 2.0 Hz, 1 H), 1.84 (dd,  $J$  = 9.7, 5.8 Hz, 1 H), 0.91 (t,  $J$  = 7.1 Hz, 3 H);  $^{19}\text{F}$  NMR ( $\text{CDCl}_3$ , 470 MHz)  $\delta$  -62.6 (s, 3 F), -67.0 (s, 3 F). A fraction containing a mixture of both diastereomers was also obtained (157 mg, 0.481 mmol, 17%).



***cis*-1-(Trifluoromethyl)-2-(4-(trifluoromethyl)phenyl)cyclopropane-1-carboxylic acid (14).**

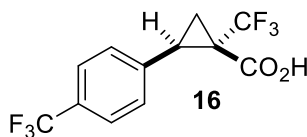
A solution of **13a** (0.220 g, 0.674 mmol) in methanol (1.4 mL) was added to KOH (0.378 g, 6.74 mmol) in methanol (3.4 mL). The reaction mixture was heated to 55 °C and stirred for 3 d. The mixture was cooled to room temperature and poured into water and extracted with CH<sub>2</sub>Cl<sub>2</sub> (15 mL). The organic layer was discarded and the aqueous layer acidified with 6 M HCl and extracted with CH<sub>2</sub>Cl<sub>2</sub> (2 x 15 mL). The combined organic layers were dried (Na<sub>2</sub>SO<sub>4</sub>) and concentrated under reduced pressure to give **14** (0.190 g, 0.636 mmol, 94%) as a white solid: <sup>1</sup>H NMR (CDCl<sub>3</sub>, 500 MHz) δ 7.60 (d, *J* = 8.2 Hz, 2 H), 7.44 (d, *J* = 8.2 Hz, 2 H), 3.24 (t, *J* = 9.1 Hz, 1 H), 2.10-2.04 (m, 2 H); <sup>13</sup>C NMR (CDCl<sub>3</sub>, 125 MHz) δ 173.7, 137.1, 130.4 (q, *J*<sub>C-F</sub> = 33 Hz), 130.0, 125.6 (q, *J*<sub>C-F</sub> = 4 Hz), 124.1 (q, *J*<sub>C-F</sub> = 272 Hz), 123.6 (q, *J*<sub>C-F</sub> = 275 Hz), 32.9 (q, *J*<sub>C-F</sub> = 34 Hz), 32.6, 17.0; <sup>19</sup>F NMR (CDCl<sub>3</sub>, 470 MHz) δ -61.6 (s, 3 F), -62.7 (s, 3 F).



***cis*-(4-(2,5-Bis(trifluoromethyl)phenyl)piperazin-1-yl)(1-(trifluoromethyl)-2-(4-**

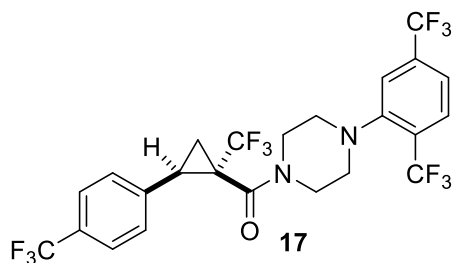
**(trifluoromethyl)phenyl)cyclopropyl)methanone (15).** A solution of **14** (50.0 mg, 0.168 mmol) and 1-(2,5-trifluoromethylphenyl)piperazine hydrochloride (73 mg, 0.218 mmol) in distilled CH<sub>2</sub>Cl<sub>2</sub> (0.85 mL) was cooled to 0 °C and then added with triethylamine (0.12 mL, 0.838 mmol). The cooled solution was treated with T3P (50wt.% solution in EtOAc, 0.14 mL,

0.201 mmol) dropwise. The reaction mixture was stirred at 0 °C for 30 min and allowed to warm to room temperature and stirred for 3 d. After completion of the reaction by TLC and LCMS analysis, the reaction mixture was diluted with CH<sub>2</sub>Cl<sub>2</sub> (10 mL) and washed with 1 M HCl (10 mL), saturated NaHCO<sub>3</sub> (10 mL), dried (MgSO<sub>4</sub>), filtered and concentrated *in vacuo*. The crude residue was purified via chromatography on SiO<sub>2</sub> (1:3 EtOAc/hexanes) to afford **15** as a white solid (77.6 mg, 0.134 mmol, 80%): Mp 128.4 – 131.7 °C; IR (CDCl<sub>3</sub>) 2925, 2833, 1648, 1425, 1326, 1313, 1122, 1085, 846, 736; <sup>1</sup>H NMR (CDCl<sub>3</sub>, 500 MHz) δ 7.81 (d, *J* = 8.1 Hz, 1 H), 7.60 (d, *J* = 8.2 Hz, 2 H), 7.56 (d, *J* = 8.3 Hz, 2 H), 7.48 (d, *J* = 8.1 Hz, 2 H), 3.91-3.87 (m, 4 H), 3.02 (t, *J* = 4.6 Hz, 4 H), 2.88 (t, *J* = 8.6 Hz, 1 H), 2.07 (t, *J* = 7.1 Hz, 1 H), 1.75 (t, *J* = 7.8 Hz, 1 H); <sup>13</sup>C NMR (CDCl<sub>3</sub>, 125 MHz) δ 164.2, 152.2, 137.8, 135.3 (q, *J*<sub>C-F</sub> = 33 Hz), 130.9 (q, *J*<sub>C-F</sub> = 29 Hz), 130.1 (t, *J*<sub>C-F</sub> = 33 Hz), 129.5, 128.5 (q, *J*<sub>C-F</sub> = 5 Hz), 125.5 (q, *J*<sub>C-F</sub> = 4 Hz), 124.5 (q, *J*<sub>C-F</sub> = 281 Hz), 124.2 (q, *J*<sub>C-F</sub> = 272 Hz), 123.4 (q, *J*<sub>C-F</sub> = 274 Hz), 123.2 (q, *J*<sub>C-F</sub> = 273 Hz), 122.6 (q, *J*<sub>C-F</sub> = 4 Hz), 121.2 (q, *J*<sub>C-F</sub> = 4 Hz), 53.3, 53.2, 46.9, 43.1, 35.1 (q, *J*<sub>C-F</sub> = 33 Hz), 27.9, 14.8 (d, *J*<sub>C-F</sub> = 2 Hz); <sup>19</sup>F NMR (CDCl<sub>3</sub>, 470 MHz) δ -60.9 (d, 6 F), -62.6 (s, 3 F), -63.2 (s, 3 F); HRMS (ESI) *m/z* calcd for C<sub>24</sub>H<sub>19</sub>F<sub>12</sub>N<sub>2</sub>O ([M+H]<sup>+</sup>) 579.1300, found 579.1298.



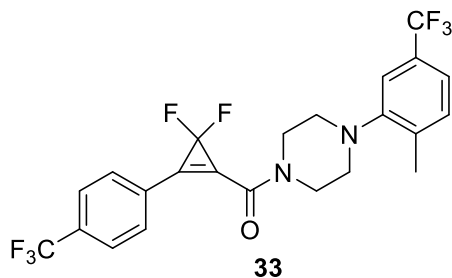
***trans*-1-(Trifluoromethyl)-2-(4-(trifluoromethyl)phenyl)cyclopropane-1-carboxylic acid (16).** A solution of **13b** (0.200 g, 0.613 mmol) in methanol (1.3 mL) was added to KOH (0.344 g, 6.13 mmol) in methanol (3 mL). The reaction mixture was heated to 55 °C and stirred for 3 d. The mixture was cooled to room temperature and poured into water and extracted with CH<sub>2</sub>Cl<sub>2</sub> (15 mL). The organic layer was discarded and the aqueous layer acidified with 6 M HCl and

extracted with CH<sub>2</sub>Cl<sub>2</sub> (2 x 15 mL). The combined organic layers were dried (Na<sub>2</sub>SO<sub>4</sub>) and concentrated under reduced pressure to give **16** (187 mg, 0.627 mmol, quant.) as a white solid: <sup>1</sup>H NMR (CDCl<sub>3</sub>, 500 MHz) δ 7.54 (d, *J* = 8.2 Hz, 2 H), 7.33 (d, *J* = 8.2 Hz, 2 H), 3.04 (t, *J* = 9.1 Hz, 1 H), 2.16-2.13 (m, 1 H), 1.89 (dd, *J* = 9.7, 5.9 Hz, 1 H); <sup>13</sup>C NMR (CDCl<sub>3</sub>, 125 MHz) δ 170.7, 137.1 (d, *J*<sub>C-F</sub> = 1 Hz), 130.3 (q, *J*<sub>C-F</sub> = 33 Hz), 129.6, 125.4 (q, *J*<sub>C-F</sub> = 4 Hz), 124.1 (q, *J*<sub>C-F</sub> = 272 Hz), 123.9 (q, *J*<sub>C-F</sub> = 274 Hz), 34.3 (q, *J*<sub>C-F</sub> = 34 Hz), 30.1 (d, *J*<sub>C-F</sub> = 1 Hz), 16.2; <sup>19</sup>F NMR (CDCl<sub>3</sub>, 470 MHz) δ -62.7 (s, 3 F), -67.1 (s, 3 F).



***trans*-(4-(2,5-bis(trifluoromethyl)phenyl)piperazin-1-yl)(1-(trifluoromethyl)-2-(4-(trifluoromethyl)phenyl)cyclopropyl)methanone (17)**. A solution of **16** (0.100 g, 0.335 mmol) and 1-(2,5-trifluoromethylphenyl)piperazine hydrochloride (0.146 g, 0.436 mmol) in distilled CH<sub>2</sub>Cl<sub>2</sub> (1.7 mL) was cooled to 0 °C and then added with triethylamine (0.24 mL, 1.68 mmol). The cooled solution was treated with T3P (50wt.% solution in EtOAc, 0.28 mL, 0.402 mmol) dropwise. The reaction mixture was stirred at 0 °C for 30 min and allowed to warm to room temperature and stirred for 4 d. After completion of the reaction by TLC and LCMS analysis, the reaction mixture was diluted with CH<sub>2</sub>Cl<sub>2</sub> (15 mL) and washed with 1 M HCl (15 mL), saturated NaHCO<sub>3</sub> (15 mL), dried (MgSO<sub>4</sub>), filtered and concentrated *in vacuo*. The crude residue was purified via chromatography on SiO<sub>2</sub> (1:3 EtOAc/hexanes) to afford **17** as colorless oil (51.5 mg, 0.0890 mmol, 27%): IR (CDCl<sub>3</sub>) 2925, 2833, 1643, 1510, 1424, 1310, 1115, 1070, 908, 851, 732

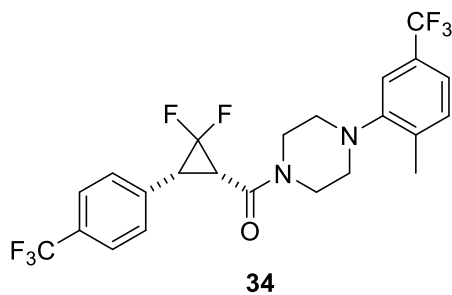
cm<sup>-1</sup>; <sup>1</sup>H NMR (CDCl<sub>3</sub>, 500 MHz) δ 7.71 (d, *J* = 8.2 Hz, 1 H), 7.63 (d, *J* = 8.2 Hz, 2 H), 7.48 (d, *J* = 8.2 Hz, 1 H), 7.27 (d, *J* = 8.0 Hz, 2 H), 7.14 (s, 1 H), 4.06-4.01 (m, 1 H), 3.44-3.29 (m, 2 H), 3.19-3.15 (m, 1 H), 2.86 (dd, *J* = 9.7, 7.5 Hz, 1 H), 2.82-2.80 (m, 1 H), 2.56-2.43 (m, 2 H), 1.98 (t, *J* = 7.0 Hz, 1 H), 1.86 (dd, *J* = 9.7, 6.7 Hz, 1 H), 1.20 (s, 1 H); <sup>13</sup>C NMR (CDCl<sub>3</sub>, 125 MHz) δ 161.4, 152.0, 139.6, 135.3 (q, *J*<sub>C-F</sub> = 33 Hz), 130.7 (q, *J*<sub>C-F</sub> = 29 Hz), 130.4 (q, *J*<sub>C-F</sub> = 33 Hz), 128.4 (q, *J*<sub>C-F</sub> = 5 Hz), 127.7, 125.8 (q, *J*<sub>C-F</sub> = 4 Hz), 124.5 (q, *J*<sub>C-F</sub> = 271 Hz), 123.9 (q, *J*<sub>C-F</sub> = 272 Hz), 123.2 (q, *J*<sub>C-F</sub> = 274 Hz), 123.1 (q, *J*<sub>C-F</sub> = 273 Hz), 122.4 (q, *J*<sub>C-F</sub> = 4 Hz), 120.6 (q, *J*<sub>C-F</sub> = 3 Hz), 52.7, 52.4, 46.7, 43.1, 37.4 (q, *J*<sub>C-F</sub> = 33 Hz), 27.5, 15.7; <sup>19</sup>F NMR (CDCl<sub>3</sub>, 470 MHz) δ -61.1 (s, 3 F), -62.8 (s, 3 F), -63.5 (s, 3 F), -66.2 (s, 3 F); HRMS (ESI) *m/z* calcd for C<sub>24</sub>H<sub>19</sub>F<sub>12</sub>N<sub>2</sub>O ([M+H]<sup>+</sup>) 579.1300, found 579.1299.



**(3,3-Difluoro-2-(4-(trifluoromethyl)phenyl)cycloprop-1-en-1-yl)(4-(2-methyl-5-(trifluoromethyl)phenyl)piperazin-1-yl)methanone (33).** Under an inert atmosphere, 1-(4-(2-methyl-5-(trifluoromethyl)phenyl)piperazin-1-yl)-3-(4-(trifluoromethyl)phenyl)prop-2-en-1-one (0.400 g, 0.908 mmol), TMSF<sub>2</sub>Br (0.28 mL, 1.82 mmol), *n*Bu<sub>4</sub>NBr (14.6 mg, 0.0454 mmol), and toluene (3.6 mL) were added into an oven-dried pressure tube at room temperature. After being heated at 110 °C for 20 h, The reaction mixture was cooled to room temperature and poured into saturated NaHCO<sub>3</sub> solution (15 mL) and extracted with EtOAc (2 x 20 mL). The combined organic layers were dried (Na<sub>2</sub>SO<sub>4</sub>), filtered, and concentrated under reduced pressure.

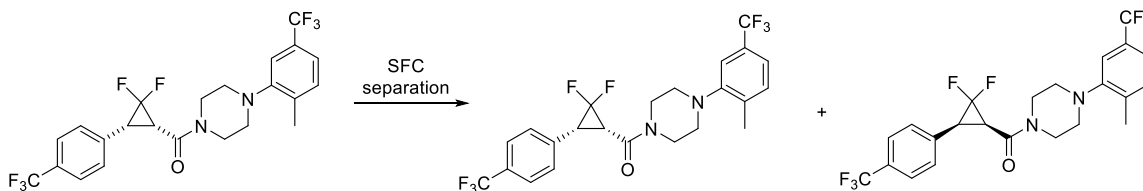


The crude product was subjected to chromatography on SiO<sub>2</sub> (1:9 EtOAc/hexanes). The fractions collected contained ~10% of impurities. The product was resubjected to chromatography on SiO<sub>2</sub> (1:2 CH<sub>2</sub>Cl<sub>2</sub>/hexanes) to afford **33** (0.325 g, 0.663 mmol, 73%) as a pale yellow oil that foamed up upon drying under vacuum: IR (CDCl<sub>3</sub>) 2925, 2825, 1776, 1643, 1442, 1303, 1120, 1061, 1031, 909, 850, 730 cm<sup>-1</sup>; <sup>1</sup>H NMR (CDCl<sub>3</sub>, 500 MHz) δ 8.13 (d, *J* = 8.0 Hz, 2 H), 7.79 (d, *J* = 8.1 Hz, 2 H), 7.31 (q, *J* = 8.7 Hz, 2 H), 7.22 (s, 1 H), 3.94 (t, *J* = 4.7 Hz, 2 H), 3.88 (t, *J* = 5.0 Hz, 2 H), 3.04 (dt, *J* = 25.5, 5.0 Hz, 4 H), 2.41 (s, 3 H); <sup>13</sup>C NMR (CDCl<sub>3</sub>, 125 MHz) δ 155.1, 150.9, 137.0, 135.5 (t, *J*<sub>C-F</sub> = 10 Hz), 134.4 (q, *J*<sub>C-F</sub> = 33 Hz), 132.6, 131.8, 129.4 (q, *J*<sub>C-F</sub> = 32 Hz), 126.3 (q, *J*<sub>C-F</sub> = 3.6 Hz), 126.0, 124.3 (q, *J*<sub>C-F</sub> = 272 Hz), 123.6 (q, *J*<sub>C-F</sub> = 273 Hz), 120.9 (q, *J*<sub>C-F</sub> = 3.9 Hz), 119.7 (t, *J*<sub>C-F</sub> = 13 Hz), 116.3 (q, *J*<sub>C-F</sub> = 3.6 Hz), 98.8 (t, *J*<sub>C-F</sub> = 278 Hz), 52.2, 51.5, 46.9, 42.6, 18.1; <sup>19</sup>F NMR (CDCl<sub>3</sub>, 470 MHz) δ -62.3 (s, 3 F), -63.2 (s, 3 F), -102.3 (s, 2 F) ; HRMS (ESI) *m/z* calcd for C<sub>23</sub>H<sub>19</sub>ON<sub>2</sub>F<sub>8</sub> ([M+H]<sup>+</sup>) 491.1364, found 491.1363.



***cis*-((1*SR*,3*RS*)-2,2-Difluoro-3-(4-(trifluoromethyl)phenyl)cyclopropyl)(4-(2-methyl-5-(trifluoromethyl)phenyl)piperazin-1-yl)methanone (34).** A solution of **33** (260 mg, 0.530 mmol) in EtOAc (4.6 mL) was added Pd/C (10% Pd on carbon, 56.4 mg, 10.0 mol%). The reaction vessel was placed in the parr hydrogenator (7 bar) and stirred for 24 h at room temperature. The mixture was filtered through celite and concentrated *in vacuo*. The crude oil was then passed through a plug of SiO<sub>2</sub> to remove baseline impurities. The crude residue (270

mg) contained a mixture of the desired *cis*-product and ring-opening side products which was inseparable by normal phase column chromatography.



The crude racemic **34** was purified and separated on a SFC Chiralpak-IC semiprep (250 x 10 mm) column (15% *i*PrOH, 6 mL/min, 220 nm, P=100) to afford the (-)-enantiomer (45.1 mg, 0.0916 mmol, 17%) and (+)-enantiomer (41.3 mg, 0.0839 mmol, 16%) respectively as a white solid: Mp 123.5 – 127.8 °C; IR (CDCl<sub>3</sub>) 2917, 2820, 1648, 1416, 1323, 1308, 1115, 1070, 986, 856, 731 cm<sup>-1</sup>.

**(-)-2,2-Difluoro-3-(4-(trifluoromethyl)phenyl)cyclopropyl(4-(2-methyl-5-(trifluoromethyl)phenyl)piperazin-1-yl)methanone** (retention time 7.52 min) was obtained as a white solid (99.5% purity by ESLD): [α]<sub>D</sub><sup>20</sup> -32.1 (*c* 1.03, *i*PrOH); <sup>1</sup>H NMR (CDCl<sub>3</sub>, 500 MHz) δ 7.60 (d, *J* = 8.3 Hz, 2 H), 7.44 (d, *J* = 8.1 Hz, 2 H), 7.28-7.24 (m, 4 H), 7.02 (s, 1 H), 3.80-3.77 (m, 1 H), 3.66-3.53 (m, 3 H), 3.13 (td, *J* = 12.6, 2.0 Hz, 1 H), 2.90 (td, *J* = 12.5, 2.4 Hz, 1 H), 2.83 (dtd, *J* = 11.5, 5.8, 3.4 Hz, 2 H), 2.61 (ddd, *J* = 11.2, 8.0, 3.0 Hz, 1 H), 2.39-2.33 (m, 1 H), 2.31 (s, 3 H); <sup>19</sup>F NMR (CDCl<sub>3</sub>, 470 MHz) δ -62.4 (s, 3 F), -62.8 (s, 3 F), -118.9 (d, *J*<sub>F-F</sub> = 161 Hz, 1 F), -147.2 (d, *J*<sub>F-F</sub> = 161 Hz, 1 F); HRMS (ESI) *m/z* calcd for C<sub>23</sub>H<sub>21</sub>ON<sub>2</sub>F<sub>8</sub> ([M+H]<sup>+</sup>) 493.1521, found 493.1522. The enantiomeric excess was >99% ee (SFC Chiralpak-IC (250 x 10 mm); 15% *i*PrOH, 220 nm, 6 mL/min; retention time: 7.54 min).

**(+)-2,2-Difluoro-3-(4-(trifluoromethyl)phenyl)cyclopropyl(4-(2-methyl-5-(trifluoromethyl)phenyl)piperazin-1-yl)methanone** (retention time 9.64 min) was obtained as

a white solid (99.5% purity by ESLD):  $[\alpha]_D^{20} +33.5$  ( $c$  0.60,  $i$ PrOH);  $^1\text{H}$  NMR ( $\text{CDCl}_3$ , 500 MHz)  $\delta$  7.60 (d,  $J$  = 8.2 Hz, 2 H), 7.44 (d,  $J$  = 8.1 Hz, 2 H), 7.28-7.24 (m, 5 H), 7.02 (s, 1 H), 3.81-3.76 (m, 1 H), 3.66-3.52 (m, 3 H), 3.13 (td,  $J$  = 12.6, 2.2 Hz, 1 H), 2.90 (td,  $J$  = 12.5, 2.6 Hz, 1 H), 2.83 (dtd,  $J$  = 11.5, 5.8, 3.3 Hz, 2 H), 2.61 (ddd,  $J$  = 11.4, 7.9, 3.0 Hz, 1 H), 2.39-2.33 (m, 1 H), 2.31 (s, 3 H);  $^{13}\text{C}$  NMR ( $\text{CDCl}_3$ , 125 MHz)  $\delta$  160.9, 150.9, 136.9, 135.0, 131.7, 130.1 (q,  $J_{\text{C-F}}$  = 32.8 Hz), 129.5 (d,  $J_{\text{C-F}}$  = 2.7 Hz), 129.3 (q,  $J_{\text{C-F}}$  = 34.0 Hz), 125.4 (q,  $J_{\text{C-F}}$  = 3.6 Hz), 124.2 (q,  $J_{\text{C-F}}$  = 272.0 Hz), 124.1 (q,  $J_{\text{C-F}}$  = 272.1 Hz), 120.7 (q,  $J_{\text{C-F}}$  = 3.7 Hz), 116.0 (q,  $J_{\text{C-F}}$  = 3.6 Hz), 111.0 (t,  $J_{\text{C-F}}$  = 289.7 Hz), 51.7, 51.5, 46.2, 42.1, 31.4 (dd,  $J_{\text{C-F}}$  = 12.9, 9.8 Hz), 30.3 (dd,  $J_{\text{C-F}}$  = 10.4, 8.9 Hz), 18.0;  $^{19}\text{F}$  NMR ( $\text{CDCl}_3$ , 470 MHz)  $\delta$  -62.4 (s, 3 F), -62.8 (s, 3 F), -118.9 (d,  $J_{\text{F-F}}$  = 161 Hz, 1 F), -147.2 (d,  $J_{\text{F-F}}$  = 161 Hz, 1 F). HRMS (ESI)  $m/z$  calcd for  $\text{C}_{23}\text{H}_{21}\text{ON}_2\text{F}_8$  ( $[\text{M}+\text{H}]^+$ ) 493.1521, found 493.1522. The enantiomeric excess was >99% ee (SFC Chiralpak-IC (250 x 10 mm); 15%  $i$ PrOH, 220 nm, 6 mL/min; retention time: 9.66 min).

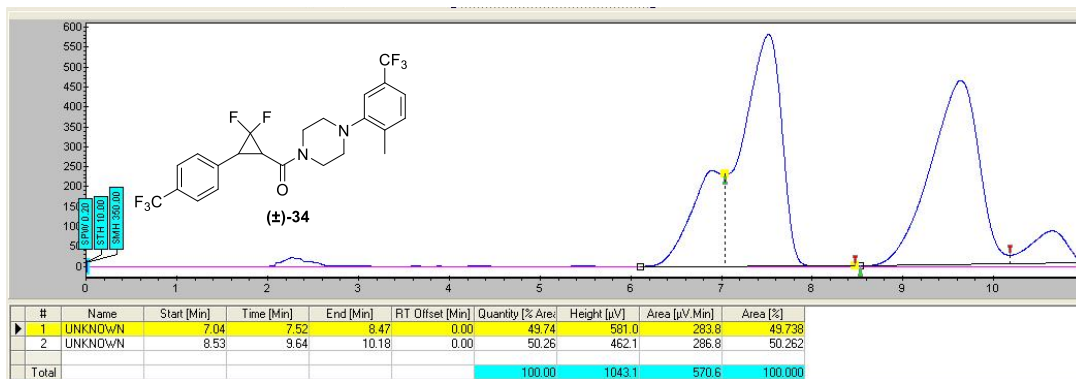


**Figure 31.** SFC chromatogram of crude racemic **34**.

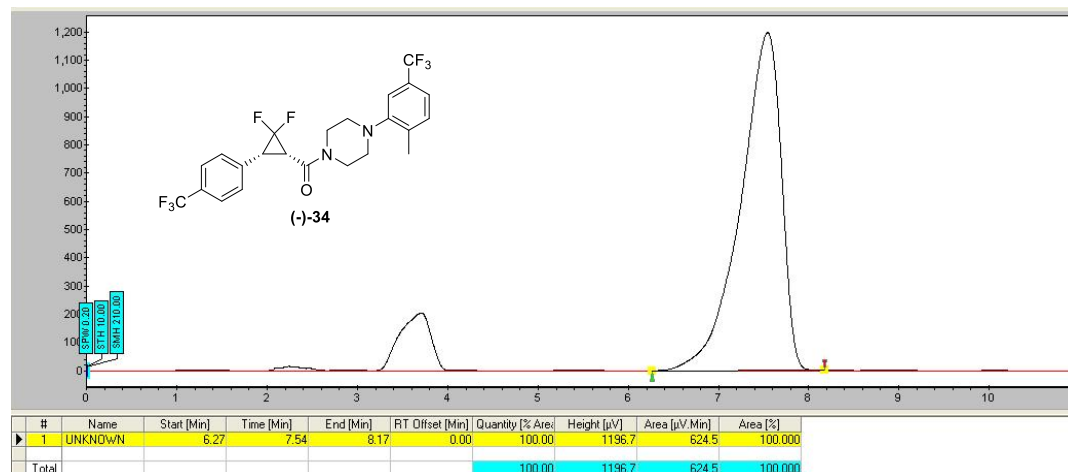


Figure 32. SFC resolution of (-)-34.

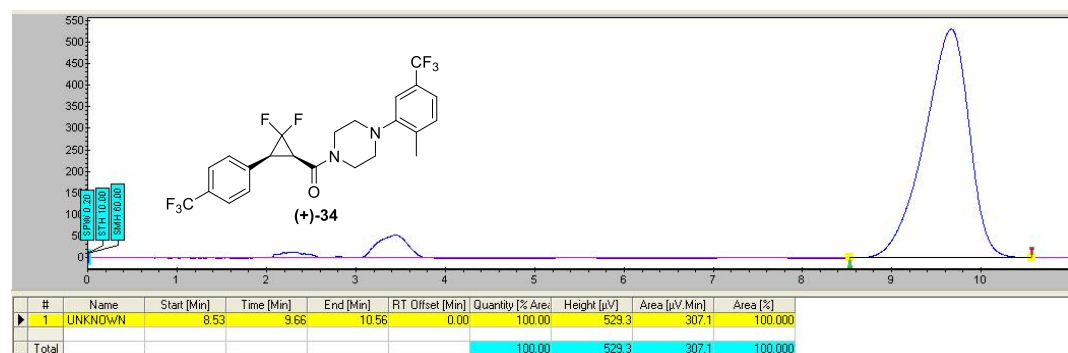
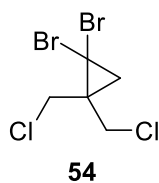


Figure 33. SFC resolution of (+)-34.



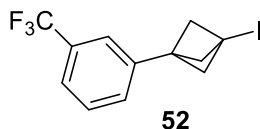
**1,1-Dibromo-2,2-bis(chloromethyl)cyclopropane (54).**<sup>88</sup> A solution of NaOH (50 w/w % in H<sub>2</sub>O, 102 mL, 10 eq) cooled to 0 °C was added to a 1 L 3-neck round-bottomed flask equipped with mechanical stirrer, internal thermometer, N<sub>2</sub> inlet, a vigorously stirred solution of 3-chloro-2-chloromethyl-1-propene (25.0 g, 0.198 mol) and phase-transfer catalyst aliquat 336 (1.00 mL, 2.19 mmol, 0.011 eq) in bromoform (44.6 mL, 0.495 mol). The reaction mixture was warmed to

an internal temperature of 40 °C using a sand bath. After completion of the reaction (84 h), the reaction mixture was then poured into a separating funnel and diluted with water (500 mL). The organic layer was separated and the aqueous layer extracted with dichloromethane (3 x 200 mL). The combined organic layers were dried (MgSO<sub>4</sub>), filtered, and concentrated under reduced pressure to afford the crude tetrahalide as a dark brown oil. The oil was distilled under vacuum at 55 °C to remove residual starting material alkene and bromoform and then at 105 °C to afford the tetrahalide. The tetrahalide obtained was recrystallized with pentane at -20°C to give the pure **54** (20.5 g, 69.1 mmol, 35 %) as white needles: <sup>1</sup>H NMR (CDCl<sub>3</sub>, 500 MHz) δ 4.01-3.94 (m, 4 H), 1.83 (s, 2 H); <sup>13</sup>C NMR (CDCl<sub>3</sub>, 125 MHz) δ 47.8, 35.4, 34.1, 32.2.

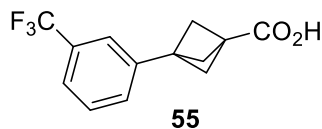


**39**

**Tricyclo[1.1.1.0<sup>1,3</sup>]pentane (39).**<sup>88,109</sup> To a solution of **54** (15.0 g, 50.5 mmol) in distilled Et<sub>2</sub>O (35 mL) under nitrogen at -40 °C (dry ice/acetonitrile) was added phenyllithium solution (1.9 M in dibutyl ether, 53.2 mL, 101 mmol) dropwise. The reaction mixture was stirred at -40 °C for another 5 min and then warmed to 0 °C and stirred at 0 °C for 2 h. The product was distilled via vacuum distillation (30 °C, 60 mmHg) with the catch flask cooled to -78 °C in dry ice/acetone bath to afford **39** as a clear, colorless solution in diethyl ether (0.86 M, 2.86 g, 85 %): <sup>1</sup>H NMR (CDCl<sub>3</sub>, 500 MHz) δ 1.94 (s, 6 H).

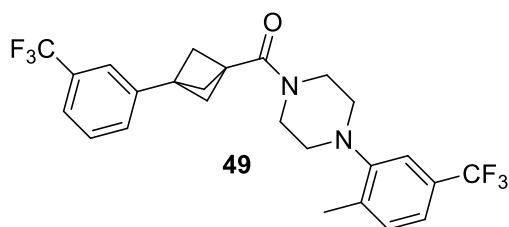


**1-Iodo-3-(3-(trifluoromethyl)phenyl)bicyclo[1.1.1]pentane (52).** To a solution of **39** (2.85 g, 50 mL, 0.86 M in diethyl ether solution) in pentane (340 mL) and diethyl ether (50 mL) was added 3-iodobenzotrifluoride (14.9 mL, 0.103 mol) in a quartz vessel. The reaction mixture was irradiated at 254 nm (vycor filter) with a 450-W mercury immersion lamp for 9 h and concentrated *in vacuo* to give an orange oil. The crude mixture was purified via chromatography on SiO<sub>2</sub> (hexanes) to afford **52** (1.53 g, 4.53 mmol, 11 %) as a pale yellow oil: IR (CDCl<sub>3</sub>) 2995, 2917, 2879, 1347, 1301, 1277, 1195, 1125, 1069, 848, 805, 700, 691 cm<sup>-1</sup>; <sup>1</sup>H NMR (CDCl<sub>3</sub>, 500 MHz) δ 7.50 (d, *J* = 7.7 Hz, 1 H), 7.43 (t, *J* = 7.7 Hz, 1 H), 7.35 (s, 1 H), 7.31 (d, *J* = 7.6 Hz, 1 H), 2.62 (s, 6 H); <sup>13</sup>C NMR (CDCl<sub>3</sub>, 125 MHz) δ 139.4, 131.0 (q, *J*<sub>C-F</sub> = 32.2 Hz), 129.6, 129.1, 124.1 (q, *J*<sub>C-F</sub> = 273 Hz), 124.0 (q, *J*<sub>C-F</sub> = 3.7 Hz), 123.0 (q, *J*<sub>C-F</sub> = 3.7 Hz), 61.9, 50.1, 6.0; <sup>19</sup>F NMR (CDCl<sub>3</sub>, 470 MHz) δ -62.7 (s, 3 F).



**3-(3-(Trifluoromethyl)phenyl)bicyclo[1.1.1]pentane-1-carboxylic acid (55).** A solution of **52** (0.250 g, 0.739 mmol) in distilled diethyl ether (3 mL) was treated with *tert*-butyllithium solution (1.7 M in pentane, 1.1 mL, 1.85 mmol) dropwise at -78 °C over 10 min. The mixture was stirred for another 15 min at -78 °C and CO<sub>2</sub> gas was bubbled through the mixture and the solution was gradually warmed to room temperature. The mixture was extracted with water (3 x 5 mL) and the combined aqueous layers were acidified with 6 M HCl, saturated with sodium chloride solution, and extracted with CH<sub>2</sub>Cl<sub>2</sub> (3 x 5 mL). The combined organic layers were

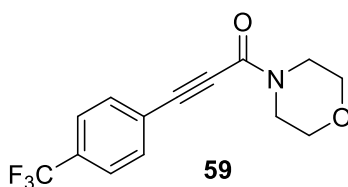
dried (MgSO<sub>4</sub>), filtered, and concentrated under reduced pressure to afford **55** (0.173 g, 0.676 mmol, 79 % corrected yield) as an off-white solid: <sup>1</sup>H NMR (CDCl<sub>3</sub>, 500 MHz) δ 11.38 (br s, 1 H), 7.51 (d, *J* = 7.5 Hz, 1 H), 7.46-7.39 (m, 3 H), 2.40 (s, 6 H); <sup>19</sup>F NMR (CDCl<sub>3</sub>, 470 MHz) δ -62.6 (s, 3 F). (*Note: The final product isolated also contains 23 mg (12 %) of pivalic acid based on NMR calculation.*)



**(4-(2-Methyl-5-(trifluoromethyl)phenyl)piperazin-1-yl)(3-(3-**

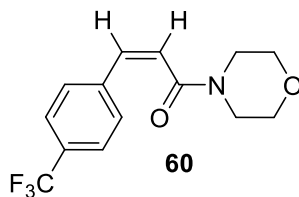
**(trifluoromethyl)phenyl)bicyclo[1.1.1]pentan-1-yl)methanone (49).** To a solution of **55** (100 mg, 0.336 mmol, 86% purity) in distilled CH<sub>2</sub>Cl<sub>2</sub> (4 mL) at 0 °C was added 1-(2-methyl-5-(trifluoromethyl)phenyl)piperazine monohydrochloride (132 mg, 0.470 mmol) and triethylamine (0.21 mL, 1.51 mmol). T3P (0.36 mL, 0.503 mmol) was added dropwise and the reaction mixture was stirred at 0 °C for 30 min and allowed to warm to room temperature. The reaction mixture was stirred for 18 h at room temperature, diluted with CH<sub>2</sub>Cl<sub>2</sub> (10 mL) and washed with 1 M HCl (10 mL). The aqueous phase was extracted with CH<sub>2</sub>Cl<sub>2</sub> (3 x 5 mL) and the combined organic layers were dried (MgSO<sub>4</sub>), filtered, and concentrated *in vacuo*. The crude material was purified by chromatography on SiO<sub>2</sub> (0-35 % EtOAc in hexanes gradient) to afford **49** (155 mg, 0.321 mmol, 96 %) as a colorless oil which foamed up upon drying under vacuum: IR (CDCl<sub>3</sub>) 2977, 2915, 2878, 2821, 1629, 1307, 1117, 1071, 731, 701 cm<sup>-1</sup>; <sup>1</sup>H NMR (CDCl<sub>3</sub>, 500 MHz) δ 7.51 (d, *J* = 7.4 Hz, 1 H), 7.46-7.41 (m, 3 H), 7.30 (m, 2 H), 7.21 (s, 1 H), 3.86-3.80 (m, 4 H), 2.94 (dt, *J* = 22.9, 4.8 Hz, 4 H), 2.47 (s, 6 H), 2.38 (s, 3 H); <sup>13</sup>C NMR (CDCl<sub>3</sub>, 125 MHz) δ

168.1, 151.3, 140.7, 137.0, 131.7, 130.9 (q,  $J_{C-F} = 32.1$  Hz), 129.6, 129.2 (q,  $J_{C-F} = 32.2$  Hz), 128.9, 124.3 (q,  $J_{C-F} = 272$  Hz), 124.2 (q,  $J_{C-F} = 272$  Hz), 123.9 (q,  $J_{C-F} = 3.7$  Hz), 123.0 (q,  $J_{C-F} = 3.7$  Hz), 120.6 (q,  $J_{C-F} = 3.9$  Hz), 116.2 (q,  $J_{C-F} = 3.8$  Hz), 54.8, 52.0, 51.8, 46.1, 42.7, 42.6, 39.3, 18.1;  $^{19}\text{F}$  NMR ( $\text{CDCl}_3$ , 470 MHz)  $\delta$  -62.3 (s, 1 F), -62.6 (s, 1 F). HRMS (ESI)  $m/z$  calcd for  $\text{C}_{25}\text{H}_{25}\text{ON}_2\text{F}_6$  ( $[\text{M}+\text{H}]^+$ ) 483.1866, found 483.1863.

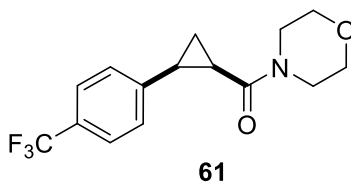


**1-Morpholino-3-(4-(trifluoromethyl)phenyl)prop-2-yn-1-one (59).** To a solution of 3-(4-(trifluoromethyl)phenyl)propionic acid (0.310 g, 1.45 mmol) in distilled  $\text{CH}_2\text{Cl}_2$  (14 mL) at 0 °C was added morpholine (0.17 mL, 1.88 mmol) and triethylamine (0.60 mL, 4.34 mmol). T3P (1.44 mL, 2.03 mmol) was added dropwise and the reaction was stirred at 0 °C for 30 min, allowed to warm to room temperature, and stirred for another 18 h. The reaction mixture was diluted with  $\text{CH}_2\text{Cl}_2$  (30 mL) and washed with 1 M HCl (30 mL). The aqueous phase was extracted with  $\text{CH}_2\text{Cl}_2$  (3 x 20 mL) and the combined organic layers were dried ( $\text{MgSO}_4$ ), filtered, and concentrated *in vacuo*. The crude material was purified by chromatography on  $\text{SiO}_2$  (1:3 EtOAc/hexanes) to afford **59** (0.397 g, 1.40 mmol, 97 %) as a white solid:  $^1\text{H}$  NMR ( $\text{CDCl}_3$ , 500 MHz)  $\delta$  7.67-7.62 (m, 4 H), 3.84-3.75 (m, 4 H), 3.71 (s, 4 H);  $^{13}\text{C}$  NMR ( $\text{CDCl}_3$ , 125 MHz)  $\delta$  152.8, 132.7, 132.0 (q,  $J_{C-F} = 32.7$  Hz), 125.7, 124.2, 123.7 (q,  $J_{C-F} = 272.5$  Hz), 89.3, 82.6, 67.0, 66.6, 47.5, 42.2.  $^{19}\text{F}$  NMR ( $\text{CDCl}_3$ , 470 MHz)  $\delta$  -63.1 (s, 3 F). HRMS (ESI)  $m/z$  calcd for  $\text{C}_{14}\text{H}_{13}\text{O}_2\text{NF}_3$  ( $[\text{M}+\text{H}]^+$ ) 284.0893, found 284.0890.



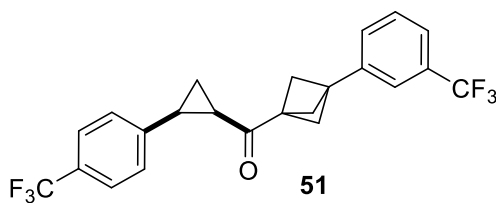


**(Z)-1-Morpholino-3-(4-(trifluoromethyl)phenyl)prop-2-en-1-one (60).** A solution of **59** (0.780 g, 2.75 mmol) in EtOAc (13.6 mL) at room temperature was treated with quinoline (1.63 mL, 13.8 mmol) and 5% Pd/BaSO<sub>4</sub> (87.9 mg, 0.0413 mmol, 1.5 mol% based on Pd) and the reaction was stirred under an atmosphere of H<sub>2</sub> (3 x backfill cycles) and checked by TLC analysis every 20 min (50 % EtOAc in hexanes) until all starting material had been mostly consumed (~2 h) to avoid over reduction. The reaction was filtered through celite (eluting with EtOAc), and the filtrate was washed with 1 M HCl (3 x 25 mL), dried (MgSO<sub>4</sub>), filtered and concentrated *in vacuo*. The crude residue was purified via chromatography on SiO<sub>2</sub> (0-70 % ethyl acetate in hexanes gradient) to afford **60** (0.739 g, 2.59 mmol, 94 %) as a colorless oil: <sup>1</sup>H NMR (CDCl<sub>3</sub>, 500 MHz) δ 7.60 (d, *J* = 8.2 Hz, 2 H), 7.49 (d, *J* = 8.2 Hz, 2 H), 6.73 (d, *J* = 12.6 Hz, 1 H), 6.16 (d, *J* = 12.6 Hz, 1 H), 3.67-3.61 (m, 4 H), 3.32 (s, 4 H); <sup>19</sup>F NMR (CDCl<sub>3</sub>, 470 MHz) δ -62.7 (s, 3 F). HRMS (ESI) *m/z* calcd for C<sub>14</sub>H<sub>15</sub>O<sub>2</sub>NF<sub>3</sub> ([M+H]<sup>+</sup>) 286.1049, found 286.1048.



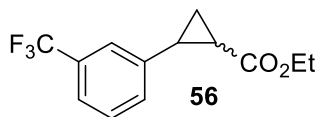
***cis*-Morpholino((1*R*,2*S*)-2-(4-(trifluoromethyl)phenyl)cyclopropyl)methanone (61).** To a flame-dried microwave vial containing anhydrous CrCl<sub>2</sub> (1.08 g, 8.76 mmol) was added a solution of **60** (0.500 g, 1.75 mmol) in anhydrous THF (17.5 mL) and CH<sub>2</sub>ICl (0.77 mL, 10.5

mmol) at room temperature and under inert atmosphere. The reaction mixture was sealed and stirred for 20 h at 75 °C. The reaction was cooled to room temperature, quenched with 1 M HCl, and extracted with diethyl ether (3 x 30 mL). The combined organic layers were washed with saturated NH<sub>4</sub>Cl solution (50 mL), water (50 mL), dried (MgSO<sub>4</sub>), and concentrated *in vacuo*. The crude residue was purified via chromatography on SiO<sub>2</sub> (2:1 EtOAc/hexanes) and the isolated product was filtered through basic alumina to afford **61** (0.556 g, 1.86 mmol, 88 %) as a pale yellow solid: <sup>1</sup>H NMR (CDCl<sub>3</sub>, 500 MHz) δ 7.51 (d, *J* = 8.3 Hz, 2 H), 7.25 (d, *J* = 8.9 Hz, 3 H), 3.65-3.56 (m, 3 H), 3.50 (t, *J* = 4.8 Hz, 2 H), 3.21 (ddd, *J* = 12.7, 8.8, 3.4 Hz, 1 H), 3.09 (ddd, *J* = 11.1, 8.4, 2.6 Hz, 1 H), 2.95 (dt, *J* = 11.3, 5.6 Hz, 1 H), 2.49 (q, *J* = 8.0 Hz, 1 H), 2.20 (td, *J* = 8.8, 6.0 Hz, 1 H), 1.90 (q, *J* = 6.1 Hz, 1 H), 1.40 (td, *J* = 8.4, 5.6 Hz, 1 H); <sup>13</sup>C NMR (CDCl<sub>3</sub>, 125 MHz) δ 166.9, 141.8, 128.9 (q, *J*<sub>C-F</sub> = 30.8 Hz), 128.0, 125.2 (q, *J*<sub>C-F</sub> = 3.7 Hz), 124.3 (q, *J*<sub>C-F</sub> = 271.7 Hz), 66.9, 66.9, 45.7, 42.3, 24.3, 24.1, 11.1; <sup>19</sup>F NMR (CDCl<sub>3</sub>, 470 MHz) δ -62.4 (s, 3 F). HRMS (ESI) *m/z* calcd for C<sub>15</sub>H<sub>17</sub>O<sub>2</sub>NF<sub>3</sub> ([M+H]<sup>+</sup>) 300.1206, found 300.1206.



*cis*-(3-(3-(Trifluoromethyl)phenyl)bicyclo[1.1.1]pentan-1-yl)((1*R*,2*S*)-2-(4-(trifluoromethyl)phenyl)cyclopropyl)methanone (**51**). A solution of **52** (0.207 g, 0.612 mmol) in distilled diethyl ether (2.5 mL) was added *tert*-butyllithium solution (1.7 M in pentane, 0.30 mL, 0.51 mmol) at -78 °C dropwise. The mixture was stirred at -78 °C for 30 min. A solution of **61** (0.168 g, 0.561 mmol) in distilled THF (1.5 mL) was added dropwise and the reaction mixture was stirred for 1 h at -78 °C and then left to reach room temperature. The reaction

mixture was quenched with saturated NH<sub>4</sub>Cl solution (5 mL) and extracted with diethyl ether (3 x 10 mL). The combined organic layers were washed with water, dried (Na<sub>2</sub>SO<sub>4</sub>), concentrated under reduced pressure and purified via chromatography on SiO<sub>2</sub> (1:4 EtOAc in hexanes) to afford **51** (37.4 mg, 0.0872 mmol, 17 %) as an off-white solid: Mp 82.4 – 84.5 °C; IR (CDCl<sub>3</sub>) 2977, 2916, 2878, 1688, 1322, 1309, 1114, 1068, 864, 701 cm<sup>-1</sup>; <sup>1</sup>H NMR (CDCl<sub>3</sub>, 500 MHz) δ 7.50 (t, *J* = 8.0 Hz, 3 H), 7.42 (t, *J* = 7.7 Hz, 2 H), 7.36 (d, *J* = 7.3 Hz, 1 H), 7.30 (d, *J* = 8.4 Hz, 2 H), 2.78 (q, *J* = 8.4 Hz, 1 H), 2.71 (ddd, *J* = 9.3, 7.5, 5.9 Hz, 1 H), 2.25-2.20 (m, 6 H), 1.97-1.94 (m, 1 H), 1.43 (ddd, *J* = 8.4, 7.5, 5.0 Hz, 1 H); <sup>13</sup>C NMR (CDCl<sub>3</sub>, 125 MHz) δ 202.5, 140.7, 140.0, 130.7 (q, *J*<sub>C-F</sub> = 32.1 Hz), 129.5, 129.3, 128.8, 124.9 (q, *J*<sub>C-F</sub> = 3.7 Hz), 124.2 (q, *J*<sub>C-F</sub> = 271.7 Hz), 124.1 (q, *J*<sub>C-F</sub> = 272.3 Hz), 123.8 (q, *J* = 3.8 Hz), 122.9 (q, *J*<sub>C-F</sub> = 3.8 Hz), 52.7, 43.9, 41.0, 28.8, 26.8, 11.8. <sup>19</sup>F NMR (CDCl<sub>3</sub>, 470 MHz) δ -62.4 (s, 3 F), -62.6 (s, 3 F). HRMS (ESI) *m/z* calcd for C<sub>23</sub>H<sub>19</sub>OF<sub>6</sub> ([M+H]<sup>+</sup>) 425.1335, found 425.1334.

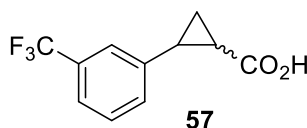


***cis*- and *trans*-Ethyl 2-(3-(trifluoromethyl)phenyl)cyclopropane-1-carboxylate (56).**

Rhodium acetate (0.126 g, 0.285 mmol) and 3-(trifluoromethyl)styrene (1.00 g, 0.86 mL, 5.69 mmol) were added into a flame-dried round-bottomed flask. Distilled CH<sub>2</sub>Cl<sub>2</sub> (6 mL) was added and the mixture was stirred. Ethyl diazoacetate (1.00 mL, 8.54 mmol) in distilled CH<sub>2</sub>Cl<sub>2</sub> (17 mL) was added via a syringe pump over 16 h. The mixture was stirred for another 2 h and then filtered through a SiO<sub>2</sub> plug and washed with CH<sub>2</sub>Cl<sub>2</sub>. The solution was concentrated under reduced pressure and purified via chromatography on SiO<sub>2</sub> (40% CH<sub>2</sub>Cl<sub>2</sub> in hexanes) to afford the 1:16 *cis/trans* mixture **56** (1.39 g, 95 %) as a colorless oil. *cis*-**56**: <sup>1</sup>H NMR (CDCl<sub>3</sub>, 500

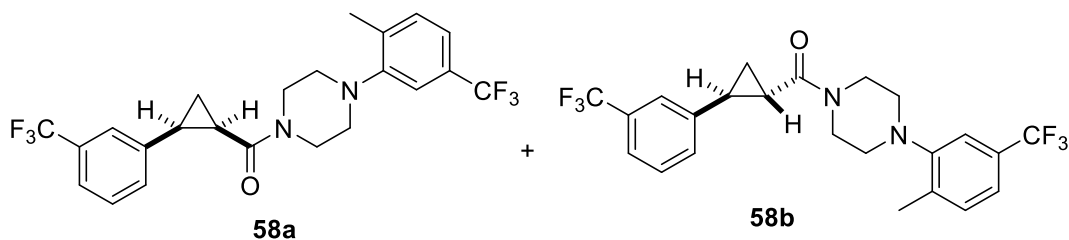
MHz)  $\delta$  7.53 (s, 1 H), 7.47-7.37 (m, 3 H), 3.93-3.83 (m, 2 H), 2.63-2.57 (m, 2 H), 2.13 (ddd,  $J = 9.2, 7.9, 5.7$  Hz, 1 H), 1.73 (dt,  $J = 7.4, 5.4$  Hz, 1 H), 1.39 (ddd,  $J = 8.6, 7.9, 5.2$  Hz, 1 H), 0.98 (t,  $J = 7.1$  Hz, 3 H);  $^{19}\text{F}$  NMR ( $\text{CDCl}_3$ , 470 MHz)  $\delta$  -62.6 (s, 3 F).

**trans-56:**  $^1\text{H}$  NMR ( $\text{CDCl}_3$ , 500 MHz)  $\delta$  7.47-7.36 (m, 2 H), 7.34 (s, 1 H), 7.29-7.28 (m, 1 H), 4.18 (qd,  $J = 7.1, 0.6$  Hz, 2 H), 2.62-2.57 (m, 1 H), 1.93 (ddd,  $J = 8.5, 5.4, 4.2$  Hz, 1 H), 1.65 (ddd,  $J = 9.2, 5.3, 4.8$  Hz, 1 H), 1.34 (ddd,  $J = 8.5, 6.4, 4.7$  Hz, 1 H), 1.29 (d,  $J = 14.3$  Hz, 3 H);  $^{19}\text{F}$  NMR ( $\text{CDCl}_3$ , 470 MHz)  $\delta$  -62.7 (s, 3 F).



**cis- and trans-2-(3-(Trifluoromethyl)phenyl)cyclopropane-1-carboxylic acid (57).** A solution of **56** (1.35 g, 5.23 mmol) in methanol (4 mL) was added to NaOH (1.46 g, 36.6 mmol) in methanol (9 mL). The reaction mixture was heated at 55 °C for 5 h. The mixture was cooled to room temperature and poured into water and extracted with  $\text{CH}_2\text{Cl}_2$  (50 mL). The organic layer was discarded and the aqueous layer acidified with 6 M HCl and extracted with  $\text{CH}_2\text{Cl}_2$  (3 x 50 mL). The combined organic layers were dried ( $\text{Na}_2\text{SO}_4$ ) and concentrated under reduced pressure to give the mixture of *cis/trans* acid **57** (1.31 g, 5.69 mmol, quant) as a pale-yellow oil which was used without further purification. **cis-57:**  $^1\text{H}$  NMR ( $\text{CDCl}_3$ , 500 MHz)  $\delta$  7.52 (s, 1 H), 7.48-7.36 (m, 3H), 2.68 (q,  $J = 8.5$  Hz, 1 H), 2.14 (ddd,  $J = 9.2, 7.8, 5.6$  Hz, 1 H), 1.74 (dt,  $J = 7.7, 5.4$  Hz, 1 H), 1.47 (ddd,  $J = 8.7, 7.9, 5.2$  Hz, 1 H);  $^{19}\text{F}$  NMR ( $\text{CDCl}_3$ , 470 MHz)  $\delta$  -62.6 (s, 3 F).

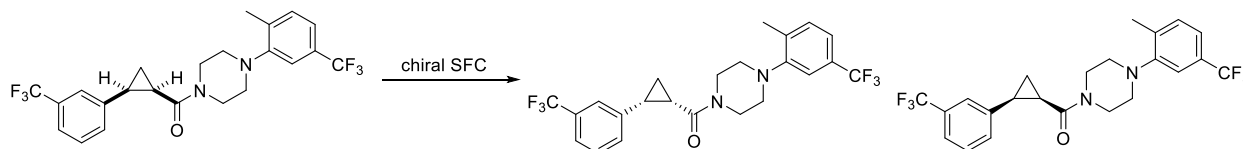
**trans-57:**  $^1\text{H}$  NMR ( $\text{CDCl}_3$ , 500 MHz)  $\delta$  7.48-7.36 (m, 2 H), 7.35 (s, 1 H), 7.28 (m, 1 H), 2.63 (ddd,  $J = 9.3, 6.6, 4.1$  Hz, 1 H), 1.91 (ddd,  $J = 8.5, 5.3, 4.1$  Hz, 1 H), 1.69 (dt,  $J = 9.3, 5.0$  Hz, 1 H), 1.42 (ddd,  $J = 8.5, 6.6, 4.8$  Hz, 1 H);  $^{19}\text{F}$  NMR ( $\text{CDCl}_3$ , 470 MHz)  $\delta$  -62.7 (s, 3 F).



*cis*- and *trans*-(4-(2-Methyl-5-(trifluoromethyl)phenyl)piperazin-1-yl)(2-(3-(trifluoromethyl)phenyl)cyclopropyl)methanone (**58a** and **58b**). To a solution of **57** (0.300 g, 1.30 mmol) and 1-(2-methyl-5-(trifluoromethyl)phenyl)piperazine monohydrochloride (0.476 g, 1.69 mmol) in distilled CH<sub>2</sub>Cl<sub>2</sub> (13 mL) was added Et<sub>3</sub>N (0.55 mL, 3.91 mmol) at 0 °C. T3P (1.4 mL, 1.96 mmol) was added dropwise and the reaction was stirred at 0 °C for 30 min and allowed to warm to room temperature and stirred for 18 h. The reaction was diluted with CH<sub>2</sub>Cl<sub>2</sub> (20 mL) and washed with 1 M HCl (30 mL). The aqueous phase was extracted with CH<sub>2</sub>Cl<sub>2</sub> (2 x 30 mL) and combined organic phase was dried (MgSO<sub>4</sub>), filtered, and concentrated *in vacuo*. The crude residue was purified by chromatography on SiO<sub>2</sub> (30% EtOAc in hexanes) to afford the *trans*-isomer as colorless oil followed by the *cis*-isomer as white solid. *cis*-**58a** (0.208 g, 0.456 mmol, 35 %): IR (CDCl<sub>3</sub>) 2917, 2822, 1638, 1417, 1326, 1307, 1161, 1115, 1074, 806, 729, 700 cm<sup>-1</sup>; <sup>1</sup>H NMR (CDCl<sub>3</sub>, 500 MHz) δ 7.48-7.46 (m, 2 H), 7.40 (t, *J* = 7.6 Hz, 1 H), 7.34-7.32 (m, 1 H), 7.25-7.21 (m, 2 H), 6.92 (s, 1 H), 3.96-3.94 (br m, 1 H), 3.80-3.78 (br m, 1 H), 3.60-3.55 (br m, 1 H), 3.25-3.21 (br m, 1 H), 2.79-2.73 (br m, 2 H), 2.53 (q, *J* = 8.0 Hz, 1 H), 2.29 (s, 3 H), 2.26 (m, 1 H), 2.19 (br m, 1 H), 2.08-2.04 (m, 1 H), 1.92 (q, *J* = 6.2 Hz, 1 H), 1.42 (td, *J* = 8.4, 5.6 Hz, 1 H); <sup>13</sup>C NMR (CDCl<sub>3</sub>, 125 MHz) δ 166.9, 151.3, 138.9, 137.0, 131.5, 130.8 (q, *J*<sub>C-F</sub> = 32.2 Hz), 130.7, 129.2 (q, *J*<sub>C-F</sub> = 31.9 Hz), 128.8, 125.2 (q, *J*<sub>C-F</sub> = 3.6 Hz), 124.3 (q, *J*<sub>C-F</sub> = 272.0 Hz), 124.2 (q, *J*<sub>C-F</sub> = 272.2 Hz), 123.4 (q, *J*<sub>C-F</sub> = 3.8 Hz), 120.5 (q, *J*<sub>C-F</sub> = 3.9 Hz), 116.2 (q, *J*<sub>C-F</sub> = 3.6 Hz), 51.9, 51.8, 45.7, 42.4, 24.3, 24.1, 17.9, 11.0; <sup>19</sup>F NMR (CDCl<sub>3</sub>, 470 MHz) δ -62.4 (s,

3 F), -62.6 (s, 3 F); HRMS (ESI)  $m/z$  calcd for  $C_{23}H_{23}F_6N_2O$  ( $[M+H]^+$ ) 457.1709, found 457.1708.

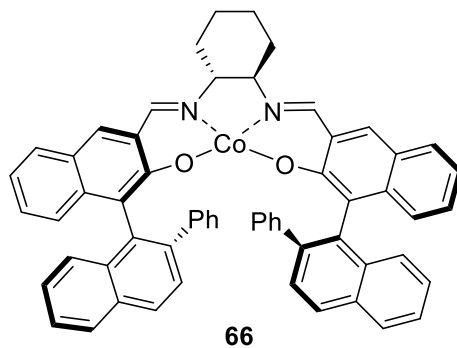
**trans-58b** (0.312 g, 0.684 mmol, 53 %): IR (CDCl<sub>3</sub>) 2917, 2823, 1635, 1418, 1328, 1308, 1162, 1115, 1074, 944, 798, 730, 700 cm<sup>-1</sup>; <sup>1</sup>H NMR (CDCl<sub>3</sub>, 500 MHz) δ 7.47-7.46 (br m, 1 H), 7.41 (t,  $J = 7.6$  Hz, 1 H), 7.35-7.33 (br m, 2 H), 7.30-7.25 (m, 2 H), 7.20 (s, 1 H), 3.87-3.77 (m, 4 H), 2.97-2.91 (m, 4 H), 2.62 (ddd,  $J = 9.0, 6.1, 4.2$  Hz, 1 H), 2.37 (s, 3 H), 2.05 (ddd,  $J = 8.4, 5.3, 4.3$  Hz, 1 H), 1.74 (ddd,  $J = 9.0, 5.2, 4.6$  Hz, 1 H), 1.36 (ddd,  $J = 8.4, 6.2, 4.5$  Hz, 1 H). ; <sup>13</sup>C NMR (CDCl<sub>3</sub>, 125 MHz) δ 170.2, 151.3, 142.1, 137.0, 131.7, 131.1 (q,  $J = 32.1$  Hz), 129.9, 129.3 (q,  $J_{C-F} = 32.2$  Hz), 129.1, 124.3 (q,  $J_{C-F} = 272.1$  Hz), 124.2 (q,  $J_{C-F} = 272.3$  Hz), 123.3 (q,  $J_{C-F} = 3.9$  Hz), 122.7 (q,  $J_{C-F} = 3.8$  Hz), 120.5 (q,  $J_{C-F} = 3.8$  Hz), 116.2 (q,  $J_{C-F} = 3.7$  Hz), 52.1, 51.7, 46.2, 42.8, 25.2, 23.4, 18.1, 16.5; <sup>19</sup>F NMR (CDCl<sub>3</sub>, 470 MHz) δ -62.3 (s, 3 F), -62.6 (s, 3 F); HRMS (ESI)  $m/z$  calcd for  $C_{23}H_{23}F_6N_2O$  ( $[M+H]^+$ ) 457.1709, found 457.1706.



Racemic **58a** was separated on a SFC Chiralpak-IC semiprep (250 x 10 mm) column (15% MeOH, 6.5 mL/min, 220 nM, P=100) to afford (-)-**58a** (retention time 5.73 min) as a colorless oil which foamed up upon drying (100% purity by ESLD):  $[\alpha]_D^{20} -123.8$  ( $c$  0.53, MeOH); <sup>1</sup>H NMR (CDCl<sub>3</sub>, 500 MHz) δ 7.48-7.47 (m, 2 H), 7.41 (t,  $J = 7.6$  Hz, 1 H), 7.34-7.32 (m, 1 H), 7.24-7.22 (m, 2 H), 6.92 (s, 1 H), 3.96-3.93 (br m, 1 H), 3.80-3.78 (br m, 1 H), 3.60-3.55 (br m, 1 H), 3.26-3.21 (br m, 1 H), 2.80-2.73 (br m, 2 H), 2.53 (td,  $J = 9.0, 7.0$  Hz, 1 H), 2.29 (s, 3 H), 2.28-2.24 (m, 1 H), 2.22-2.18 (br m, 1 H), 2.09-2.04 (br m, 1 H), 1.92 (q,  $J = 6.2$  Hz, 1 H), 1.42 (td,  $J = 8.4, 5.6$  Hz, 1 H). HRMS (ESI)  $m/z$  calcd for  $C_{23}H_{23}F_6N_2O$  ( $[M+H]^+$ ) 457.1709, found

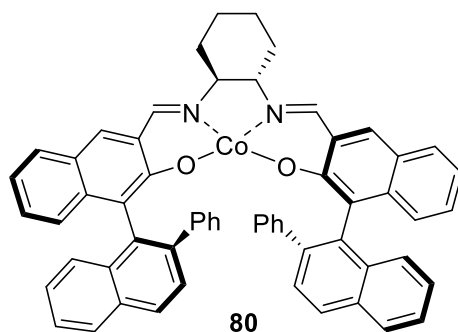
457.1709. The enantiomeric excess was >99% ee (SFC Chiralpak-IC (250 x 10 mm); 15% MeOH, 220 nm, 6.5 mL/min; retention time: 6.05 min).

(+)-**58** (retention time 6.41 min) was obtained as a colorless oil which foamed up upon drying (100% purity by ESLD):  $[\alpha]_D^{20} +119.4$  ( $c$  0.55, MeOH);  $^1\text{H NMR}$  ( $\text{CDCl}_3$ , 500 MHz)  $\delta$  7.48-7.47 (m, 2 H), 7.41 (t,  $J = 7.6$  Hz, 1 H), 7.34-7.32 (m, 1 H), 7.24-7.22 (m, 1 H), 6.92 (s, 1 H), 3.96-3.92 (br m, 1 H), 3.80-3.77 (br m, 1 H), 3.60-3.55 (br m, 1 H), 3.26-3.21 (br m, 1 H), 2.80-2.73 (br m, 2 H), 2.53 (td,  $J = 8.9, 7.0$  Hz, 1 H), 2.29 (s, 3 H), 2.28-2.24 (m, 1 H), 2.22-2.16 (br m, 1 H), 2.09-2.04 (br m, 1 H), 1.92 (q,  $J = 6.2$  Hz, 1 H), 1.42 (td,  $J = 8.4, 5.6$  Hz, 1 H).; HRMS (ESI)  $m/z$  calcd for  $\text{C}_{23}\text{H}_{23}\text{F}_6\text{N}_2\text{O}$  ( $[\text{M}+\text{H}]^+$ ) 457.1709, found 457.1704. The enantiomeric excess was >99% ee (SFC Chiralpak-IC (250 x 10 mm); 15% MeOH, 220 nm, 6.5 mL/min; retention time: 6.81 min).



**Co(II)-salen complex (66).**<sup>101,107</sup> To a solution of (1*R*,2*R*)-1,2-cyclohexanediamine (30.0 mg, 0.260 mmol) in EtOH (8 mL) was added (*R*)-3-formyl-2-hydroxy-2'-phenyl-1,1'-binaphthyl<sup>103,104</sup> (195 mg, 0.520 mmol) and stirred at room temperature for 18 h. The resulting light-yellow precipitate was filtered and dried under vacuum. This precipitate was added to a solution of  $\text{Co}(\text{OAc})_2$  (46.0 mg, 0.260 mmol) in degassed ethanol (8 mL) under nitrogen. The mixture was heated to reflux for 9 h, and cooled to room temperature. The resulting brown precipitate was

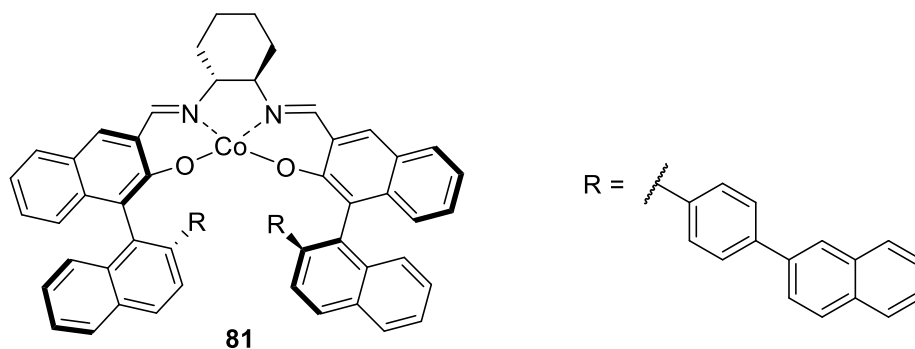
filtered, washed with degassed ethanol under a nitrogen atmosphere, and dried under vacuum to give the corresponding Co(II)-salen complex **66** (153 mg, 0.173 mmol, 67 %) as a dark-brown solid: IR (CH<sub>2</sub>Cl<sub>2</sub>) 3050, 2934, 2859, 1592, 1545, 1424, 1329, 1295, 1145, 1124, 952, 865, 817, 759, 697 cm<sup>-1</sup>; HRMS (ESI) *m/z* calcd for C<sub>60</sub>H<sub>44</sub>CoN<sub>2</sub>O<sub>2</sub> [M<sup>+</sup>] 883.2729, found 883.2728. (Note: Co(OAc)<sub>2</sub> was prepared by heating Co(OAc)<sub>2</sub>·4H<sub>2</sub>O at 80 °C under vacuum for 3 h. The color of the solid turned from pink to purple).



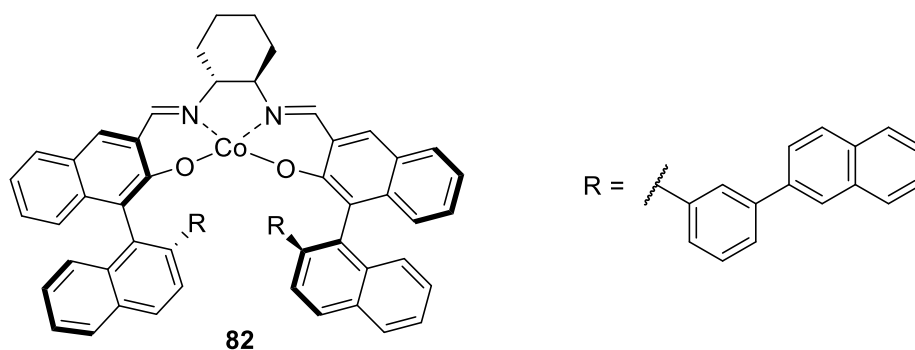
**Co(II)-salen complex (80).** To a solution of (1*S*,2*S*)-(+)-1,2-Cyclohexanediamine (0.180 g, 1.56 mmol) in EtOH (48 mL) was added (*S*)-3-formyl-2-hydroxy-2'-phenyl-1,1'-binaphthyl (1.17 g, 3.12 mmol) and stirred at room temperature for 18 h. The resulting light-yellow precipitate was filtered and dried under vacuum. This precipitate was added to a solution of Co(OAc)<sub>2</sub> (0.276 g, 1.56 mmol) in degassed ethanol (48 mL) under nitrogen. The mixture was heated to reflux for 12 h, and cooled to room temperature. The resulting brown precipitate was filtered, washed with degassed ethanol under a nitrogen atmosphere, and dried under vacuum to give the corresponding Co(II)-salen complex **80** (1.07 g, 1.21 mmol, 78%) as a dark-brown solid: IR (CH<sub>2</sub>Cl<sub>2</sub>) 3051, 2935, 2860, 1591, 1546, 1425, 1330, 1297, 1146, 952, 759, 743cm<sup>-1</sup>; HRMS (ESI) *m/z* calcd for C<sub>60</sub>H<sub>44</sub>CoN<sub>2</sub>O<sub>2</sub> [M<sup>+</sup>] 883.2729, found 883.2733. (Note: Co(OAc)<sub>2</sub> was



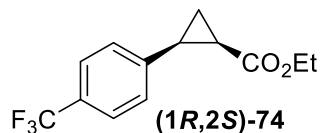
prepared by heating  $\text{Co}(\text{OAc})_2 \cdot 4\text{H}_2\text{O}$  at  $80\text{ }^\circ\text{C}$  under vacuum for 3 h. The color of the solid turned from pink to purple).



**Co(II)-salen complex (81).** In a microwave vial, a solution of (1*R*,2*R*)-1,2-cyclohexanediamine (30.0 mg, 0.260 mmol) in EtOH (8 mL) was added (*R*)-3-formyl-2-hydroxy-2'-(4-(naphthyl)phenyl)-1,1'-binaphthyl (260 mg, 0.520 mmol). The vial was sealed and the mixture was heated at  $110\text{ }^\circ\text{C}$  for 12 h. The resulting light-yellow precipitate was filtered and dried under vacuum. This precipitate was added to a solution of  $\text{Co}(\text{OAc})_2$  (46.0 mg, 0.260 mmol) in degassed ethanol (8 mL) under nitrogen. The mixture was heated at  $110\text{ }^\circ\text{C}$  for 18 h in a sealed microwave vial. After cooling to room temperature, the resulting brown precipitate was filtered, washed with degassed ethanol under a nitrogen atmosphere, and dried under vacuum to give the corresponding Co(II)-salen complex **81** (222 mg, 0.195 mmol, 72%) as a dark-brown solid: IR ( $\text{CH}_2\text{Cl}_2$ ) 3052, 2933, 2859, 1630, 1563, 1535, 1442, 1384, 1337, 1263, 942, 811, 734  $\text{cm}^{-1}$ ; HRMS (ESI)  $m/z$  calcd for  $\text{C}_{80}\text{H}_{56}\text{CoN}_2\text{O}_2$  [ $\text{M}^+$ ] 1135.3668, found 1135.3667. (Note:  $\text{Co}(\text{OAc})_2$  was prepared by heating  $\text{Co}(\text{OAc})_2 \cdot 4\text{H}_2\text{O}$  at  $80\text{ }^\circ\text{C}$  under vacuum for 3 h. The color of the solid turned from pink to purple).

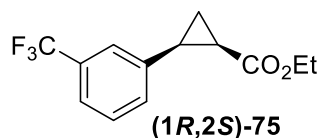


**Co(II)-salen complex (82).** In a microwave vial, a solution of (1*R*,2*R*)-1,2-cyclohexanediamine (30.0 mg, 0.260 mmol) in EtOH (8 mL) was added (*R*)-3-formyl-2-hydroxy-2'-(3-(naphthyl)phenyl)-1,1'-binaphthyl (260 mg, 0.520 mmol). The vial was sealed and the mixture was heated at 110 °C for 12 h. The resulting light-yellow precipitate was filtered and dried under vacuum. This precipitate was added to a solution of Co(OAc)<sub>2</sub> (46.0 mg, 0.260 mmol) in degassed ethanol (8 mL) under nitrogen. The mixture was heated at 100 °C for 12 h in a sealed microwave vial. After cooling to room temperature, the resulting brown precipitate was filtered, washed with degassed ethanol under a nitrogen atmosphere, and dried under vacuum to give the corresponding Co(II)-salen complex **82** (254 mg, 0.223 mmol, 86%) as a dark-brown solid: IR (CH<sub>2</sub>Cl<sub>2</sub>) 3051, 2933, 2859, 1628, 1595, 1332, 1319, 1263, 1145, 947, 819, 795, 736 cm<sup>-1</sup>; HRMS (ESI) *m/z* calcd for C<sub>80</sub>H<sub>56</sub>CoN<sub>2</sub>O<sub>2</sub> [M<sup>+</sup>] 1135.3668, found 1135.3667. (*Note: Co(OAc)<sub>2</sub> was prepared by heating Co(OAc)<sub>2</sub>·4H<sub>2</sub>O at 80 °C under vacuum for 3 h. The color of the solid turned from pink to purple.*)



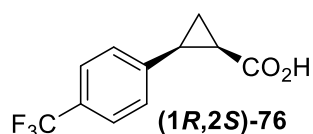
**Ethyl (1*R*,2*S*)-2-(4-(trifluoromethyl)phenyl)cyclopropane-1-carboxylate (74).** To a THF solution (4.2 mL) of Co(II)-Salen catalyst **66** (37.1 mg, 0.0419 mmol) was added a THF solution

of *N*-methylimidazole (0.17 mL, 0.5 M, 0.0839 mmol) and the mixture was stirred for 2 min. 4-(Trifluoromethyl)styrene (0.722 g, 0.62 mL, 4.19 mmol) was added to this solution and the mixture was stirred for another 3 min before being treated with ethyl diazoacetate (0.1 mL, 0.839 mmol). The reaction mixture was stirred for 24 h at room temperature and then concentrated *in vacuo*. The crude residue was purified by chromatography on SiO<sub>2</sub> (1:9, EtOAc/hexanes) to give the desired *cis*-product **74** (0.199 g, 0.771 mmol, 92 %) as a colorless oil: <sup>1</sup>H NMR (CDCl<sub>3</sub>, 500 MHz) δ 7.52 (d, *J* = 8.1 Hz, 2 H), 7.38 (d, *J* = 8.6 Hz, 2 H), 3.94-3.85 (m, 2 H), 2.59 (q, *J* = 8.4 Hz, 1 H), 2.14 (ddd, *J* = 9.3, 7.9, 5.7 Hz, 1 H), 1.74 (dt, *J* = 7.5, 5.4 Hz, 1 H), 1.39 (ddd, *J* = 8.6, 7.9, 5.2 Hz, 1 H), 0.99 (t, *J* = 7.1 Hz, 3 H); <sup>13</sup>C NMR (CDCl<sub>3</sub>, 125 MHz) δ 170.7, 141.0, 129.8, 129.1 (q, *J*<sub>C-F</sub> = 32.3 Hz), 125.0 (q, *J*<sub>C-F</sub> = 3.7 Hz), 124.4 (q, *J*<sub>C-F</sub> = 271.7 Hz), 60.5, 25.2, 22.2, 14.1, 11.5; <sup>19</sup>F NMR (CDCl<sub>3</sub>, 470 MHz) δ -62.4 (s, 3 F). The *cis:trans* diastereomic ratio is >99:1 based on NMR integration.

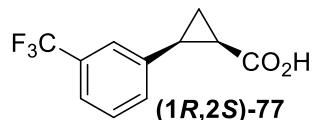


**Ethyl (1R,2S)-2-(3-(trifluoromethyl)phenyl)cyclopropane-1-carboxylate (75).** To a THF solution (4.2 mL) of Co(II)-Salen catalyst **66** (47.2 mg, 0.0534 mmol) was added a THF solution of *N*-methylimidazole (0.21 mL, 0.5 M, 0.107 mmol) and the mixture was stirred for 2 min. 3-(trifluoromethyl)styrene (0.81 mL, 5.34 mmol) was added to this solution and the mixture was stirred for another 3 min before being treated with ethyl diazoacetate (0.13 mL, 0.808 mmol). The reaction mixture was stirred for 24 h at room temperature and then concentrated *in vacuo*. The crude residue was purified by chromatography on SiO<sub>2</sub> (1:9, EtOAc/hexanes) to give **75** (0.265 g, 1.03 mmol, 96 %) as a colorless oil: <sup>1</sup>H NMR (CDCl<sub>3</sub>, 400 MHz) δ 7.52 (s, 1 H), 7.47-

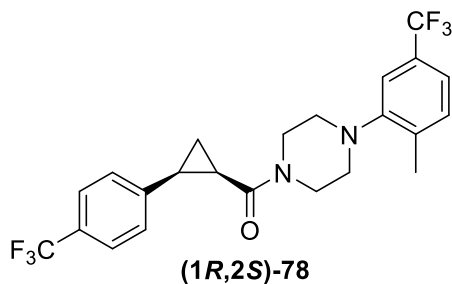
7.36 (m, 3 H), 3.94-3.82 (m, 2 H), 2.60 (q,  $J = 8.4$  Hz, 1 H), 2.13 (ddd,  $J = 9.2, 7.9, 5.7$  Hz, 1 H), 1.73 (dt,  $J = 7.4, 5.4$  Hz, 1 H), 1.39 (ddd,  $J = 8.6, 8.0, 5.2$  Hz, 1 H), 0.97 (d,  $J = 14.3$  Hz, 3 H);  $^{13}\text{C}$  NMR ( $\text{CDCl}_3$ , 125 MHz)  $\delta$  170.7, 137.9, 132.8, 130.5 (q,  $J_{\text{C-F}} = 32.0$  Hz), 128.5, 126.4 (q,  $J_{\text{C-F}} = 3.8$  Hz), 124.3 (q,  $J_{\text{C-F}} = 272.3$  Hz), 123.6 (q,  $J_{\text{C-F}} = 3.9$  Hz), 60.5, 25.1, 22.0, 14.1, 11.4;  $^{19}\text{F}$  NMR ( $\text{CDCl}_3$ , 375 MHz)  $\delta$  -62.6 (s, 3 F). The *cis:trans* diastereomic ratio is >99:1 based on NMR integration.



**(1*R*,2*S*)-2-(4-(Trifluoromethyl)phenyl)cyclopropane-1-carboxylic acid (76)**. A solution of **74** (0.165 g, 0.639 mmol) in methanol (0.6 mL) was added to NaOH (0.179 g, 4.47 mmol) in methanol (1.4 mL). The reaction mixture was heated at 55 °C for 5 h. The mixture was cooled to room temperature and poured into water and extracted with  $\text{CH}_2\text{Cl}_2$  (10 mL). The organic layer was discarded and the aqueous layer acidified with 6 M HCl and extracted with  $\text{CH}_2\text{Cl}_2$  (3 x 10 mL). The combined organic layers were dried ( $\text{Na}_2\text{SO}_4$ ) and concentrated under reduced pressure to give the acid **76** (0.150 g, 0.652 mmol, quant) as a pale-yellow oil which was used without further purification:  $^1\text{H}$  NMR ( $\text{CDCl}_3$ , 500 MHz)  $\delta$  7.50 (d,  $J = 8.1$  Hz, 2 H), 7.33 (d,  $J = 8.3$  Hz, 2 H), 2.64 (q,  $J = 8.5$  Hz, 1 H), 2.11 (ddd,  $J = 9.0, 8.0, 5.7$  Hz, 1 H), 1.70 (dt,  $J = 7.7, 5.4$  Hz, 1 H), 1.43 (ddd,  $J = 8.6, 7.9, 5.2$  Hz, 1 H);  $^{19}\text{F}$  NMR ( $\text{CDCl}_3$ , 470 MHz)  $\delta$  -62.5 (s, 3 F).



**(1R,2S)-2-(3-(Trifluoromethyl)phenyl)cyclopropane-1-carboxylic acid (77).** A solution of **75** (0.25 g, 0.968 mmol) in methanol (1 mL) was added to NaOH (0.232 g, 5.81 mmol) in methanol (1.5 ml). The reaction mixture was heated at 55 °C for 5 h. The mixture was cooled to room temperature and poured into water and extracted with CH<sub>2</sub>Cl<sub>2</sub> (10 mL). The organic layer was discarded and the aqueous layer acidified with 6M HCl and extracted with CH<sub>2</sub>Cl<sub>2</sub> (3 x 10 mL). The combined organic layers were dried (Na<sub>2</sub>SO<sub>4</sub>) and concentrated under reduced pressure to give the acid **77** (0.230 g, 0.999 mmol, quant) as a colorless oil which solidified upon standing. The product was used without further purification: <sup>1</sup>H NMR (CDCl<sub>3</sub>, 500 MHz) δ 7.48 (s, 1 H), 7.47-7.45 (m, 1 H), 7.40-7.33 (m, 2 H), 2.64 (q, *J* = 8.5 Hz, 1 H), 2.08 (ddd, *J* = 9.1, 7.8, 5.6 Hz, 1 H), 1.68 (dt, *J* = 7.7, 5.4 Hz, 1 H), 1.43 (ddd, *J* = 8.6, 7.9, 5.2 Hz, 1 H); <sup>19</sup>F NMR (CDCl<sub>3</sub>, 470 MHz) δ -62.7 (s, 3 F).



**(4-(2-Methyl-5-(trifluoromethyl)phenyl)piperazin-1-yl)((1R,2S)-2-(4-(trifluoromethyl)phenyl)cyclopropyl)methanone (78).** To a solution of **76** (0.14 g, 0.608 mmol) and 1-(2-methyl-5-(trifluoromethyl)phenyl)piperazine monohydrochloride (0.222 g, 0.791 mmol) in distilled CH<sub>2</sub>Cl<sub>2</sub> (6 mL) was added Et<sub>3</sub>N (0.26 mL, 1.83 mmol) at 0 °C. T3P (0.65 mL, 0.912 mmol) was added dropwise and the reaction was stirred at 0 °C for 30 min and

allowed to warm to room temperature for 16 h. The reaction was diluted with CH<sub>2</sub>Cl<sub>2</sub> (15 mL) and washed with 1 M HCl (15 mL). The aqueous phase was extracted with CH<sub>2</sub>Cl<sub>2</sub> (2 x 15 mL) and combined organic phase was dried (MgSO<sub>4</sub>), filtered, and concentrated in vacuo. The crude residue was purified by chromatography on SiO<sub>2</sub> (1:1 EtOAc/hexanes) to afford **78** (0.242 g, 0.530 mmol, 87 %) as a viscous oil that foamed up upon drying under vacuum:  $[\alpha]_D^{20} +124.1$  (*c* 0.75, MeOH); <sup>1</sup>H NMR (CDCl<sub>3</sub>, 500 MHz) δ 7.53 (d, *J* = 8.1 Hz, 2 H), 7.29 (d, *J* = 8.2 Hz, 2 H), 7.25-7.21 (m, 2 H), 6.93 (s, 1 H), 3.85-3.83 (m, 1 H), 3.71-3.60 (m, 2 H), 3.36-3.32 (m, 1 H), 2.82-2.74 (m, 2 H), 2.52 (q, *J* = 8.0 Hz, 1 H), 2.30-2.25 (m, 5 H), 2.16-2.12 (m, 1 H), 1.92 (q, *J* = 6.2 Hz, 1 H), 1.43 (td, *J* = 8.4, 5.6 Hz, 1 H); <sup>13</sup>C NMR (CDCl<sub>3</sub>, 125 MHz) δ 166.9, 151.2, 142.0, 136.9, 131.6, 129.3 (q, *J* = 32 Hz), 129.1 (q, *J* = 34 Hz), 128.1, 125.2 (q, *J* = 4 Hz), 124.3 (q, *J* = 272 Hz), 124.3 (q, *J* = 272 Hz), 120.6 (q, *J* = 4 Hz), 116.0 (q, *J* = 4 Hz), 52.0, 51.8, 45.7, 42.4, 24.7, 24.2, 18.0, 11.3; <sup>19</sup>F NMR (CDCl<sub>3</sub>, 470 MHz) δ -62.5 (s, 3 F), -62.5 (s, 3 F); HRMS (ESI) *m/z* calcd for C<sub>23</sub>H<sub>23</sub>F<sub>6</sub>N<sub>2</sub>O ([M+H]<sup>+</sup>) 457.1709, found 457.1708. The enantiomeric excess was 93.6% *ee* (SFC Chiralpak-IC (250 x 10 mm); 30% MeOH, 220 nm, 7.0 mL/min; retention time: 3.66 min).

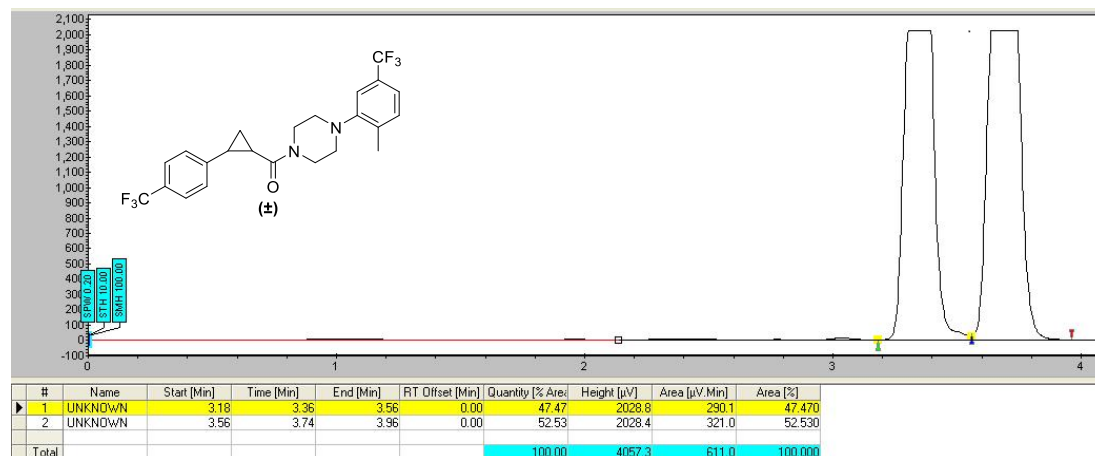
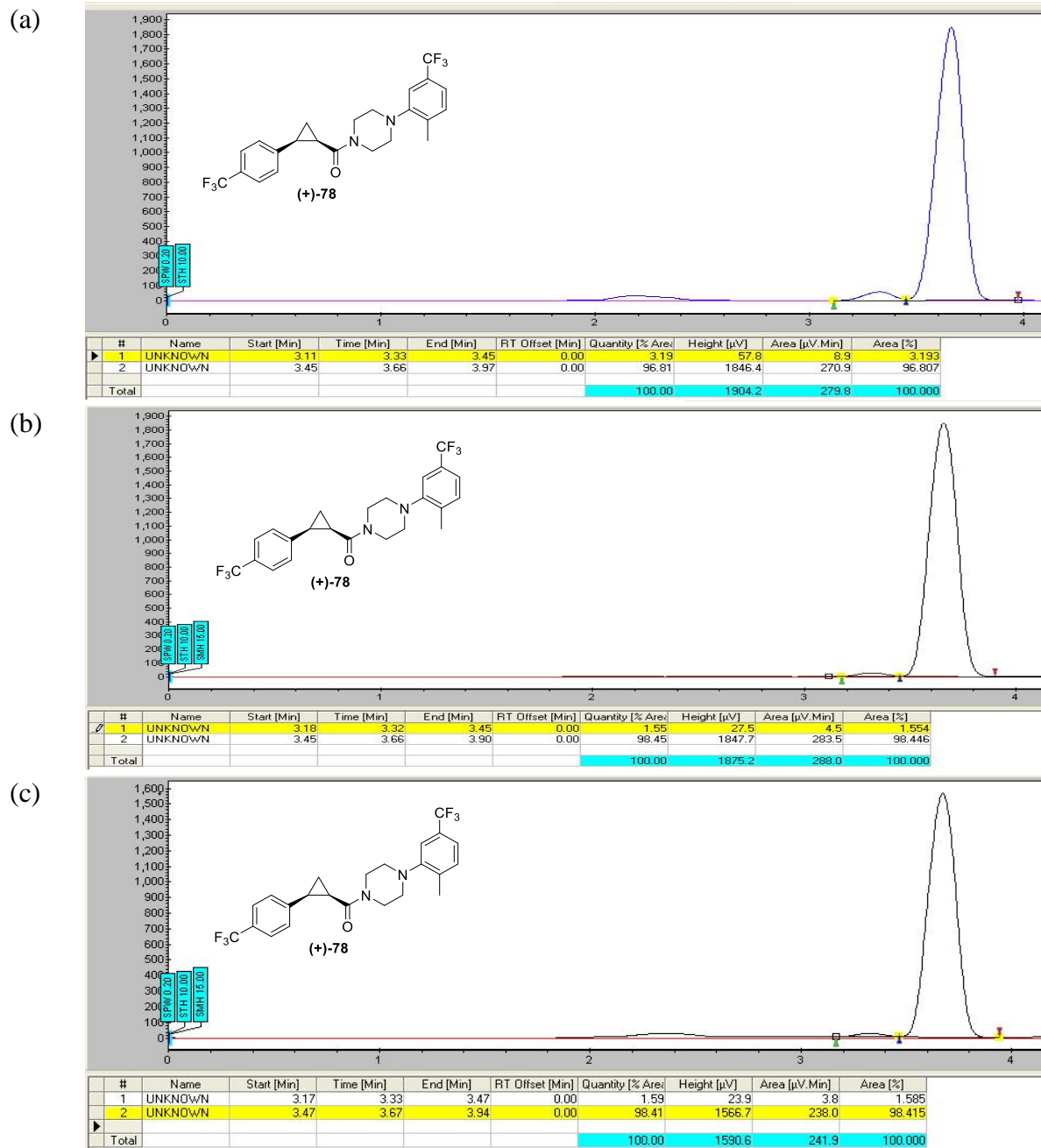
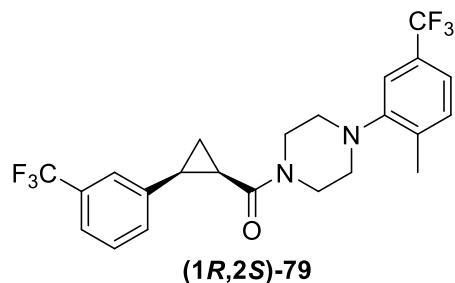


Figure 34. SFC chromatogram of racemic sample **78**.



**Figure 35.** Enantiomeric excess of (1*R*,2*S*)-78. (a) Co(II)-salen complex **66**, (b) Co(II)-salen complex **81**, (c) Co(II)-salen complex **82**.



**(4-(2-Methyl-5-(trifluoromethyl)phenyl)piperazin-1-yl)((1R,2S)-2-(3-**

**(trifluoromethyl)phenyl)cyclopropyl)methanone (79).** To a solution of **77** (0.100 g, 0.434 mmol) and 1-(2-methyl-5-(trifluoromethyl)phenyl)piperazine monohydrochloride (0.171 g, 0.608 mmol) in distilled CH<sub>2</sub>Cl<sub>2</sub> (4.3 mL) was added Et<sub>3</sub>N (0.18 mL, 1.30 mmol) at 0 °C. T3P (0.46 mL, 0.652 mmol) was added dropwise and the reaction was stirred at 0 °C for 30 min and allowed to warm to room temperature for 16 h. The reaction was diluted with CH<sub>2</sub>Cl<sub>2</sub> (15 mL) and washed with 1 M HCl (15 mL). The aqueous phase was extracted with CH<sub>2</sub>Cl<sub>2</sub> (2 x 15 mL) and combined organic phase was dried (MgSO<sub>4</sub>), filtered, and concentrated *in vacuo*. The crude residue was purified by chromatography on SiO<sub>2</sub> (1:1 EtOAc/hexanes) to afford the desired compound (+)-**79** (0.179 g, 0.391 mmol, 90 %) as a viscous oil: [α]<sub>D</sub><sup>20</sup> +120.8 (*c* 0.71, MeOH); <sup>1</sup>H NMR (CDCl<sub>3</sub>, 300 MHz) δ 7.48-7.46 (m, 2 H), 7.40 (t, *J* = 7.9 Hz, 1 H), 7.34-7.32 (m, 1 H), 7.24-7.20 (m, 2 H), 6.92 (s, 1 H), 3.97-3.92 (br m, 1 H), 3.81-3.76 (br m, 1 H), 3.62-3.54 (br m, 1 H), 3.28-3.19 (br m, 1 H), 2.81-2.72 (br m, 2 H), 2.53 (td, *J* = 8.9, 7.0 Hz, 1 H), 2.31-2.16 (m, 5 H), 2.11-2.03 (br m, 1 H), 1.92 (q, *J* = 6.2 Hz, 1 H), 1.42 (td, *J* = 8.4, 5.6 Hz, 1 H); HRMS (ESI) *m/z* calcd for C<sub>23</sub>H<sub>23</sub>F<sub>6</sub>N<sub>2</sub>O ([M+H]<sup>+</sup>) 457.1709, found 457.1702. The enantiomeric excess was 94.4% *ee* (SFC Chiralpak-IC (250 x 10 mm); 15% MeOH, 220 nm, 6.5 mL/min; retention time: 6.75 min).



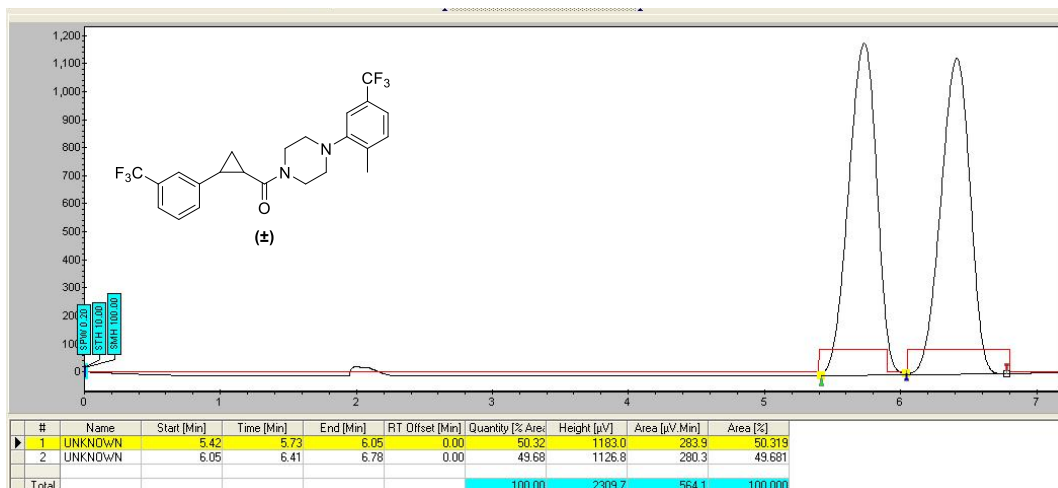


Figure 36. SFC chromatogram of racemic sample of **79**.

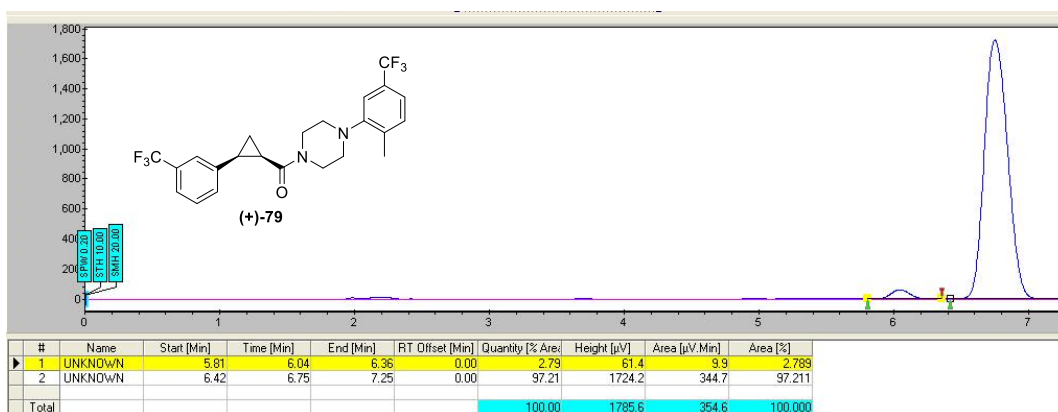
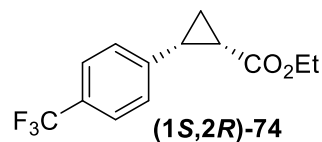
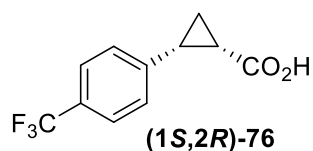


Figure 37. Enantiomeric excess of **(1*R*,2*S*)-79**.

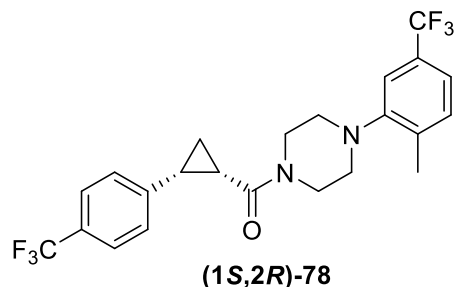


**Ethyl (1*S*,2*R*)-2-(4-(trifluoromethyl)phenyl)cyclopropane-1-carboxylate (74).** To a THF solution (4.2 mL) of Co(II)-Salen catalyst **80** (37.1 mg, 0.0419 mmol) was added a THF solution of *N*-methylimidazole (0.17 mL, 0.5 M, 0.0839 mmol) and the mixture was stirred for 2 min. 4-(trifluoromethyl)styrene (0.722 g, 0.62 mL, 4.19 mmol) was added to this solution and the

mixture was stirred for another 3 min before being treated with ethyl diazoacetate (0.1 mL, 0.839 mmol). The reaction mixture was stirred for 24 h at room temperature and then concentrated *in vacuo*. The crude residue was purified by chromatography on SiO<sub>2</sub> (1:9, EtOAc/hexanes) to give the desired *cis*-product **(1*S*,2*R*)-74** (0.181 g, 0.701 mmol, 84 %) as a colorless oil: <sup>1</sup>H NMR (CDCl<sub>3</sub>, 500 MHz) δ 7.52 (d, *J* = 7.6 Hz, 2 H), 7.38 (d, *J* = 7.8 Hz, 2 H), 3.93-3.84 (m, 2 H), 2.59 (q, *J* = 8.5 Hz, 1 H), 2.14 (q, *J* = 7.6 Hz, 1 H), 1.74 (q, *J* = 5.9 Hz, 1 H), 1.40 (q, *J* = 7.1 Hz, 1 H), 0.99 (t, *J* = 6.9 Hz, 3 H); <sup>19</sup>F NMR (CDCl<sub>3</sub>, 470 MHz) δ -62.4 (s, 3 F). The *cis:trans* diastereomeric ratio is *ca.* 95:5 based on NMR integration.



**(1*S*,2*R*)-2-(4-(Trifluoromethyl)phenyl)cyclopropane-1-carboxylic acid (76).** A solution of **(1*S*,2*R*)-74** (0.180 g, 0.697 mmol) in methanol (0.5 mL) was added to NaOH (0.139 g, 3.49 mmol) in methanol (1.2 mL). The reaction mixture was heated at 55 °C for 5 h. The mixture was cooled to room temperature and poured into water and extracted with CH<sub>2</sub>Cl<sub>2</sub> (10 mL). The organic layer was discarded and the aqueous layer acidified with 6 M HCl and extracted with CH<sub>2</sub>Cl<sub>2</sub> (3 x 10 mL). The combined organic layers were dried (Na<sub>2</sub>SO<sub>4</sub>), and concentrated under reduced pressure to give the acid **(1*S*,2*R*)-76** (0.176 g, 0.765 mmol, quant) as a pale-yellow oil which was used without further purification: <sup>1</sup>H NMR (CDCl<sub>3</sub>, 500 MHz) δ 7.50 (d, *J* = 7.8 Hz, 2 H), 7.34 (d, *J* = 7.7 Hz, 2 H), 2.64 (q, *J* = 8.6 Hz, 1 H), 2.11 (q, *J* = 7.6 Hz, 1 H), 1.70 (q, *J* = 6.1 Hz, 1 H), 1.44 (q, *J* = 7.3 Hz, 1 H).



**(4-(2-Methyl-5-(trifluoromethyl)phenyl)piperazin-1-yl)((1S,2R)-2-(4-(trifluoromethyl)phenyl)cyclopropyl)methanone (78).** To a solution of **(1S,2R)-76** (0.170 g, 0.739 mmol) and 1-(2-methyl-5-(trifluoromethyl)phenyl)piperazine monohydrochloride (0.290 g, 1.034 mmol) in distilled CH<sub>2</sub>Cl<sub>2</sub> (7.4 mL) was added Et<sub>3</sub>N (0.31 mL, 2.22 mmol) at 0 °C. T3P (0.78 mL, 1.11 mmol) was added dropwise and the reaction was stirred at 0 °C for 30 min and allowed to warm to room temperature for 16 h. The reaction was diluted with CH<sub>2</sub>Cl<sub>2</sub> (15 mL) and washed with 1 M HCl (15 mL). The aqueous phase was extracted with CH<sub>2</sub>Cl<sub>2</sub> (2 x 15 mL) and combined organic phase was dried (MgSO<sub>4</sub>), filtered, and concentrated *in vacuo*. The crude material was purified by chromatography on SiO<sub>2</sub> (1:1 EtOAc/hexanes) to afford the desired compound **(1S,2R)-78** (0.249 g, 0.546 mmol, 74%) as a pale yellow oil: [α]<sub>D</sub><sup>20</sup> -123.5 (*c* 0.78, MeOH); <sup>1</sup>H NMR (CDCl<sub>3</sub>, 500 MHz) δ 7.48-7.46 (m, 2 H), 7.40 (t, *J* = 7.9 Hz, 1 H), 7.34-7.32 (m, 1 H), 7.24-7.20 (m, 2 H), 6.92 (s, 1 H), 3.97-3.92 (br m, 1 H), 3.81-3.76 (br m, 1 H), 3.62-3.54 (br m, 1 H), 3.28-3.19 (br m, 1 H), 2.81-2.72 (br m, 2 H), 2.53 (td, *J* = 8.9, 7.0 Hz, 1 H), 2.31-2.16 (m, 5 H), 2.11-2.03 (br m, 1 H), 1.92 (q, *J* = 6.2 Hz, 1 H), 1.42 (td, *J* = 8.4, 5.6 Hz, 1 H); <sup>19</sup>F NMR (CDCl<sub>3</sub>, 470 MHz) δ -62.5 (s, 3 F), -62.5 (s, 3 F); HRMS (ESI) *m/z* calcd for C<sub>23</sub>H<sub>23</sub>F<sub>6</sub>N<sub>2</sub>O ([M+H]<sup>+</sup>) 457.1709, found 457.1711. The enantiomeric excess was 93.4% *ee* (SFC Chiralpak-IC (250 x 10 mm); 15% MeOH, 220 nm, 6.5 mL/min; retention time: 6.15 min).

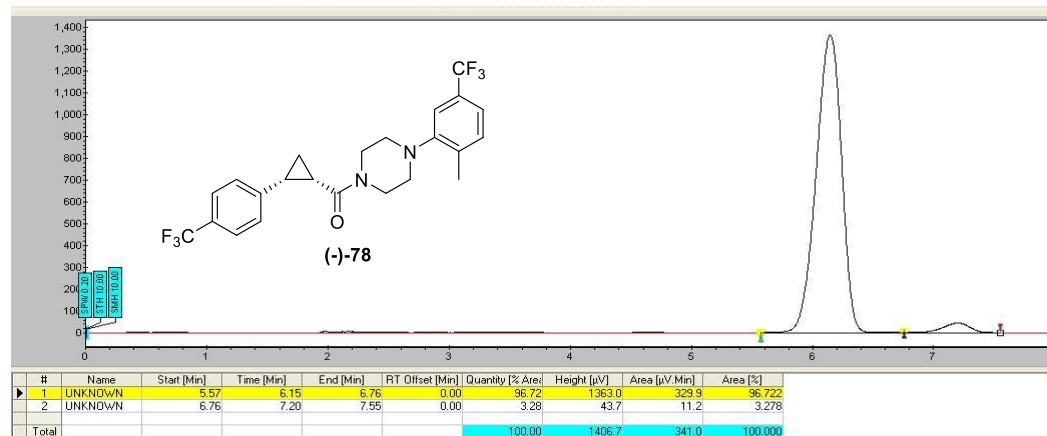
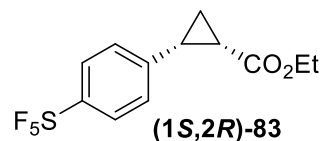
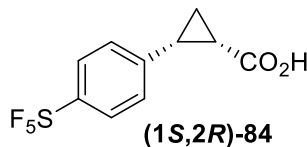


**Figure 38.** Enantiomeric excess of **(1S,2R)-78**.

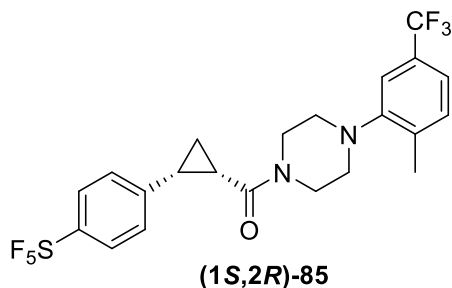


**Ethyl (1S,2R)-2-(4-(pentafluorosulfanyl)phenyl)cyclopropane-1-carboxylate (83).** To a THF solution (5.7 mL) of Co(II)-Salen catalyst **80** (167 mg, 0.189 mmol) was added a THF solution of *N*-methylimidazole (0.75 mL, 0.5 M, 0.377 mmol) and the mixture was stirred for 2 min. 4-(pentafluorosulfanyl)styrene (1.30 g, 5.66 mmol) was added to this solution and the mixture was stirred for another 3 min before being treated with ethyl diazoacetate (0.45 mL, 3.77 mmol, 87 wt% in CH<sub>2</sub>Cl<sub>2</sub>). The reaction mixture was stirred for 24 h at room temperature and then concentrated *in vacuo*. The residue was precipitated with hexanes and filtered to recover the catalyst. The hexanes filtrate was concentrated and purified by chromatography on SiO<sub>2</sub> (1:9, EtOAc/hexanes) to give the desired *cis*-product **(1S,2R)-74** (1.10 g, 3.47 mmol, 92%) as a colorless oil: <sup>1</sup>H NMR (CDCl<sub>3</sub>, 500 MHz) δ 7.64 (d, *J* = 8.8 Hz, 2 H), 7.35 (d, *J* = 8.2 Hz, 2 H), 3.96-3.86 (m, 2 H), 2.56 (q, *J* = 8.4 Hz, 1 H), 2.15 (ddd, *J* = 9.2, 8.0, 5.7 Hz, 1 H), 1.73 (dt, *J* = 7.5, 5.5 Hz, 1 H), 1.41 (td, *J* = 8.3, 5.2 Hz, 1 H), 1.00 (t, *J* = 7.1 Hz, 3 H); <sup>19</sup>F NMR (CDCl<sub>3</sub>, 470

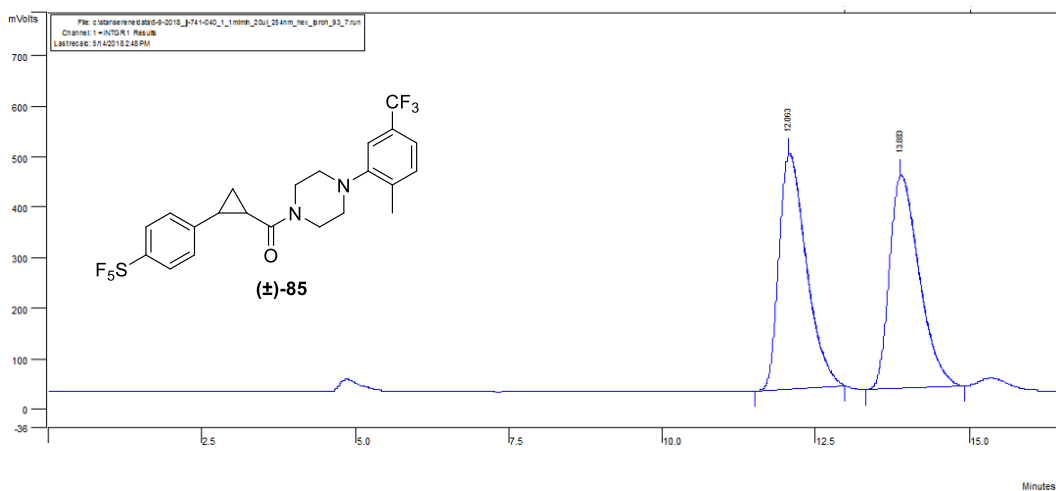
MHz)  $\delta$  84.9 (quintet,  $J = 150$  Hz, 1 F), 63.1 (d,  $J = 150$  Hz, 4 F). The *cis:trans* diastereomeric ratio is >95:5 based on NMR integration.



**(1S,2R)-2-(4-(Pentafluorosulfanyl)phenyl)cyclopropane-1-carboxylic acid (76).** A solution of **(1S,2R)-83** (0.180 g, 0.697 mmol) in methanol (0.5 mL) was added to NaOH (0.139 g, 3.49 mmol) in methanol (1.2 mL). The reaction mixture was heated at 55 °C for 5 h. The mixture was cooled to room temperature and poured into water and extracted with CH<sub>2</sub>Cl<sub>2</sub> (10 mL). The organic layer was discarded and the aqueous layer acidified with 6 M HCl and extracted with CH<sub>2</sub>Cl<sub>2</sub> (3 x 10 mL). The combined organic layers were dried (Na<sub>2</sub>SO<sub>4</sub>), and concentrated under reduced pressure to give the acid **(1S,2R)-84** (0.176 g, 0.765 mmol, quant) as a pale-yellow oil which solidified upon standing: <sup>1</sup>H NMR (CDCl<sub>3</sub>, 500 MHz)  $\delta$  7.62 (d,  $J = 8.8$  Hz, 2 H), 7.31 (d,  $J = 8.5$  Hz, 2 H), 2.62 (q,  $J = 8.5$  Hz, 1 H), 2.12 (td,  $J = 8.5, 5.7$  Hz, 1 H), 1.69 (dt,  $J = 7.7, 5.5$  Hz, 1 H), 1.45 (td,  $J = 8.2, 5.3$  Hz, 1 H); <sup>19</sup>F NMR (CDCl<sub>3</sub>, 470 MHz)  $\delta$  84.9 (quintet,  $J = 150$  Hz, 1 F), 63.0 (d,  $J = 150$  Hz, 4 F).

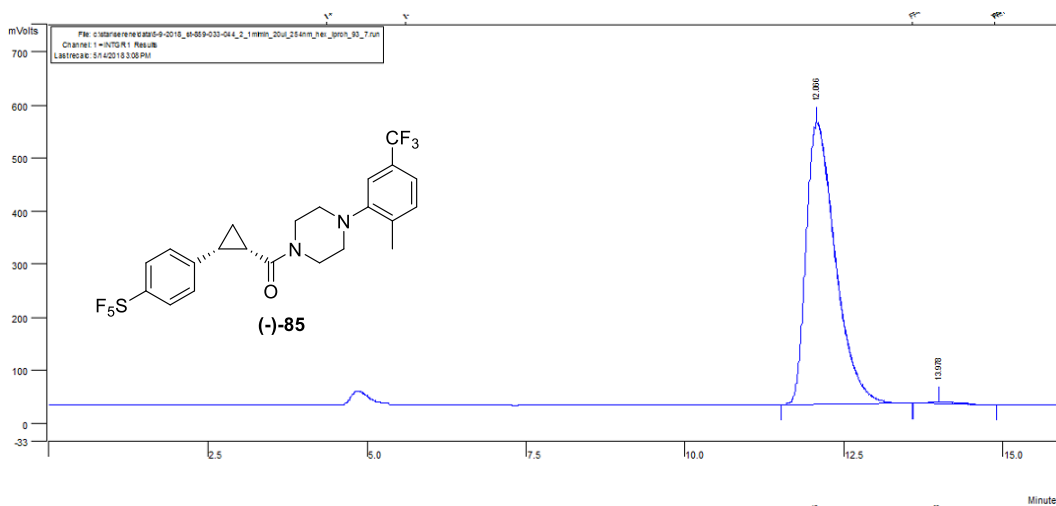


**(4-(2-Methyl-5-(trifluoromethyl)phenyl)piperazin-1-yl)((1S,2R)-2-(4-(pentafluorosulfanyl)phenyl)cyclopropyl)methanone (85).** To a solution of **(1S,2R)-84** (0.550 g, 1.77 mmol) and 1-(2-methyl-5-(trifluoromethyl)phenyl)piperazine monohydrochloride (0.734 g, 2.48 mmol) in distilled CH<sub>2</sub>Cl<sub>2</sub> (18 mL) was added Et<sub>3</sub>N (0.75 mL, 5.32 mmol) at 0 °C. T3P (1.88 mL, 2.66 mmol, 50 wt% in ethyl acetate) was added dropwise and the reaction was stirred at 0 °C for 30 min and allowed to warm to room temperature for 16 h. The reaction was diluted with CH<sub>2</sub>Cl<sub>2</sub> (30 mL) and washed with 1 M HCl (30 mL). The aqueous phase was extracted with CH<sub>2</sub>Cl<sub>2</sub> (2 x 30 mL) and combined organic phase was dried (MgSO<sub>4</sub>), filtered, and concentrated *in vacuo*. The crude material was purified by chromatography on SiO<sub>2</sub> (1:1 EtOAc/hexanes) to afford the desired compound **(1S,2R)-85** (0.838 g, 1.63 mmol, 92%) as a white solid: Mp 127.3 – 128.9 °C; IR (CHCl<sub>3</sub>) 3005, 2912, 2821, 1636, 1439, 1417, 1338, 1308, 1121, 826, 748 cm<sup>-1</sup>; <sup>1</sup>H NMR (CDCl<sub>3</sub>, 500 MHz) δ 7.65 (d, *J* = 8.8 Hz, 2 H), 7.26 – 7.22 (m, 4 H), 6.97 (s, 1 H), 3.86 – 3.81 (br m, 1 H), 3.71-3.61 (br m, 2 H), 3.38 – 3.34 (br m, 1 H), 2.85 – 2.76 (br m, 2 H), 2.50 (q, *J* = 8.0 Hz, 1 H), 2.33-2.27 (m, 5 H), 2.18 – 2.15 (br m, 1 H), 1.92 (q, *J* = 6.2 Hz, 1 H), 1.44 (td, *J* = 8.4, 5.6 Hz, 1 H); <sup>13</sup>C NMR (CDCl<sub>3</sub>, 125 MHz) δ 166.7, 152.5 (t, *J* = 17 Hz), 151.2, 142.0, 136.9, 131.6, 129.4 (q, *J* = 33 Hz), 127.9, 125.8 (t, *J* = 5 Hz), 124.3 (q, *J* = 272 Hz), 120.6 (q, *J* = 4 Hz), 116.0 (q, *J* = 4 Hz), 52.1, 51.7, 45.7, 42.4, 24.7, 23.9, 18.0, 11.5; <sup>19</sup>F NMR (CDCl<sub>3</sub>, 470 MHz) δ 84.6 (quintet, *J* = 150 Hz, 1F), 63.1 (d, *J* = 150 Hz, 4 F), -62.5 (s, 3 F); HRMS (ESI) *m/z* calcd for C<sub>22</sub>H<sub>23</sub>F<sub>8</sub>N<sub>2</sub>OS ([M+H]<sup>+</sup>) 515.1398, found 515.1398. The enantiomeric excess was enriched to 98.6% *ee* after recrystallization from CH<sub>2</sub>Cl<sub>2</sub>/hexanes (HPLC Chiralpak AD-H (4.6 x 250 mm, 5 μm); IPA:hexanes (7:93), 254 nm, 1.0 mL/min; inj. vol.: 20 μL; retention time: 12.07 min).



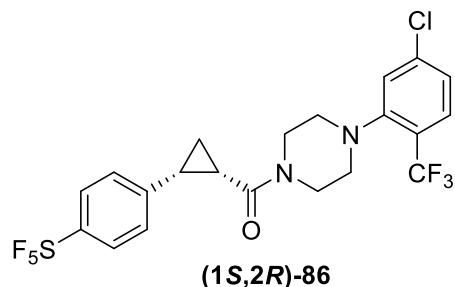
Peak	Retention time (min)	Area	% Area
1	12.06	14638727	50.5
2	13.88	14355130	49.5

**Figure 39.** HPLC chromatogram of racemic sample **85**.



Peak	Retention time (min)	Area	% Area
1	12.07	16997416	99.3
2	13.98	126266	0.7

**Figure 40.** Enantiomeric excess of **(1*R*,2*S*)-85**.

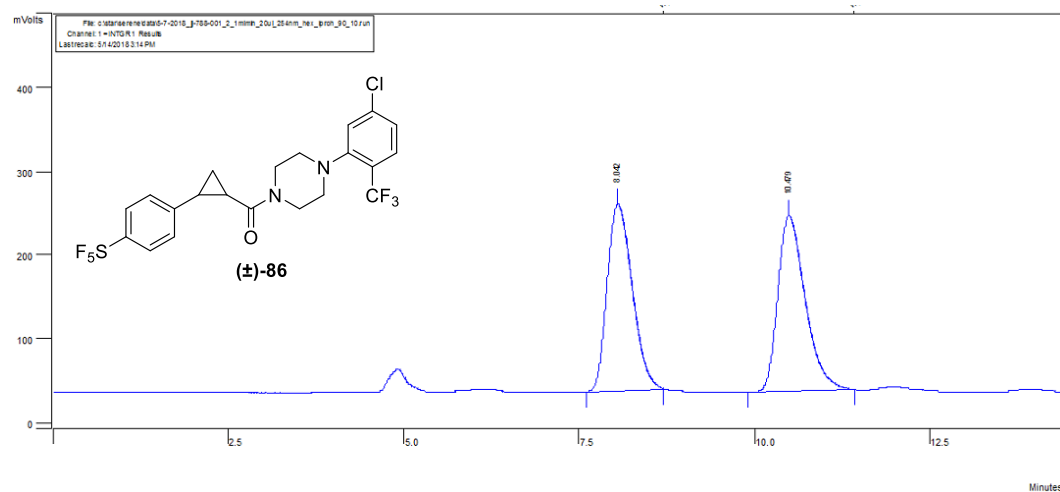


**(4-(5-Chloro-2-(trifluoromethyl)phenyl)piperazin-1-yl)((1S,2R)-2-(4-**

**(pentafluorosulfonyl)phenyl)cyclopropyl)methanone (86).** To a solution of **(1S,2R)-84** (1.32 g, 4.26 mmol) and 1-(5-chloro-2-(trifluoromethyl)phenyl)piperazine monohydrochloride (1.67 g, 5.54 mmol) in distilled CH<sub>2</sub>Cl<sub>2</sub> (43 mL) was added Et<sub>3</sub>N (1.80 mL, 12.8 mmol) at 0 °C. T3P (4.50 mL, 6.39 mmol, 50 wt% in ethyl acetate) was added dropwise and the reaction was stirred at 0 °C for 30 min and allowed to warm to room temperature for 16 h. The reaction was diluted with CH<sub>2</sub>Cl<sub>2</sub> (50 mL) and washed with 1 M HCl (50 mL). The aqueous phase was extracted with CH<sub>2</sub>Cl<sub>2</sub> (2 x 50 mL) and combined organic phase was dried (MgSO<sub>4</sub>), filtered, and concentrated *in vacuo*. The crude material was purified by chromatography on SiO<sub>2</sub> (1:1 EtOAc/hexanes) to afford the desired compound **(1S,2R)-86** (1.98 g, 3.70 mmol, 87%) as a white solid: Mp 125.8 – 127.7 °C; <sup>1</sup>H NMR (CDCl<sub>3</sub>, 500 MHz) δ 7.68 (d, *J* = 8.8 Hz, 2 H), 7.52 (d, *J* = 8.5 Hz, 1 H), 7.27-7.25 (m, 2 H), 7.20 (d, *J* = 8.5 Hz, 1 H), 6.93 (s, 1 H), 3.99 – 3.96 (br m, 1 H), 3.74 – 3.71 (br m, 1 H), 3.56 – 3.52 (br m, 1 H), 3.23 – 3.19 (br m, 1 H), 2.79 – 2.74 (br m, 2 H), 2.49 (q, *J* = 8.0 Hz, 1 H), 2.29 – 2.22 (m, 2 H), 1.98 – 1.94 (br m, 1 H), 1.91 (q, *J* = 6.2 Hz, 1 H), 1.45 (td, *J* = 8.4, 5.7 Hz, 1 H); <sup>13</sup>C NMR (CDCl<sub>3</sub>, 125 MHz) δ 166.6, 152.8, 152.5 (t, *J* = 18 Hz), 142.2, 139.2, 128.6 (q, *J* = 5 Hz), 127.9, 125.9 (q, *J* = 29 Hz), 125.9 (t, *J* = 5 Hz), 125.8, 124.5, 123.7 (q, *J* = 273 Hz), 54.0, 53.0, 45.7, 42.3, 25.0, 23.9, 11.6; <sup>19</sup>F NMR (CDCl<sub>3</sub>, 470 MHz) δ 84.8 (quintet, *J* = 150 Hz, 1 F), 63.3 (d, *J* = 150 Hz, 4 F), -60.4 (s, 3 F); HRMS (ESI) *m/z* calcd for C<sub>21</sub>H<sub>20</sub>ClF<sub>8</sub>N<sub>2</sub>OS ([M+H]<sup>+</sup>) 535.0852, found 535.0852. The enantiomeric excess was enriched to

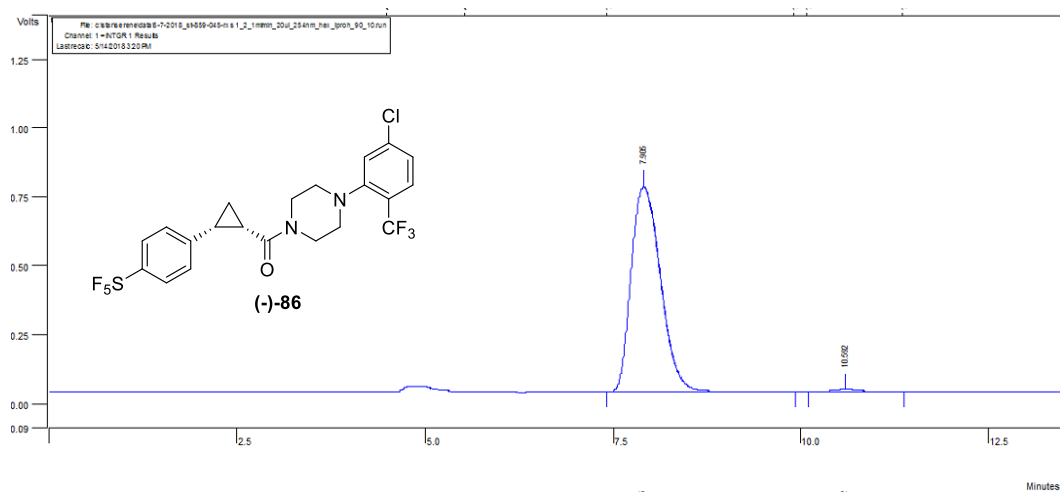


97.6% *ee* after recrystallization from CH<sub>2</sub>Cl<sub>2</sub>/hexanes (HPLC Chiralpak AD-H (4.6 x 250 mm, 5 μm); IPA:hexanes (1:9), 254 nm, 1.0 mL/min; inj. vol.: 20 μL; retention time: 12.07 min).



Peak	Retention time (min)	Area	% Area
1	8.04	5589901	49.3
2	10.48	5756253	50.7

**Figure 41.** HPLC chromatogram of racemic sample **86**.



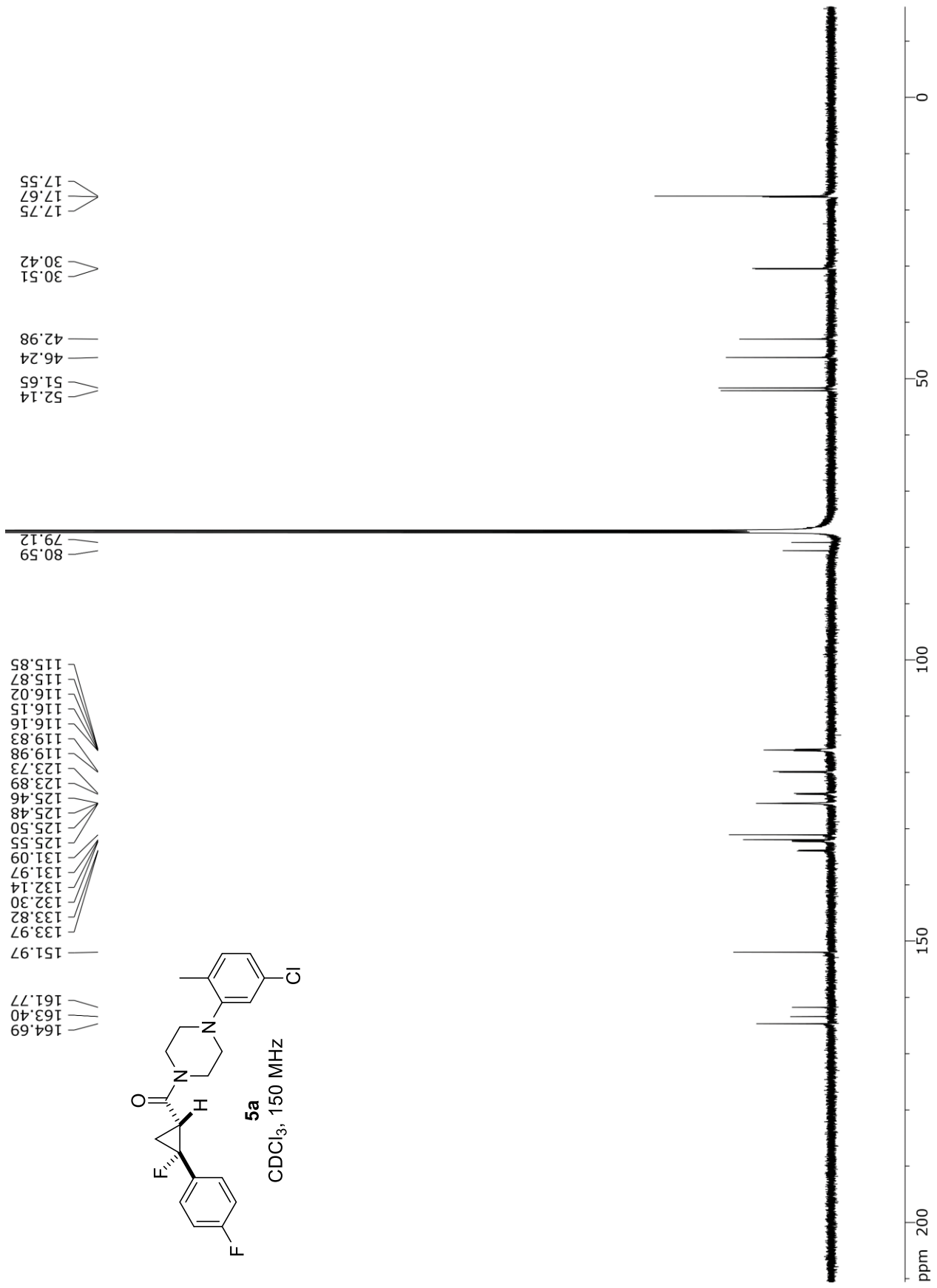
Peak	Retention time (min)	Area	% Area
1	7.91	20342400	98.8
2	10.59	252606	1.2

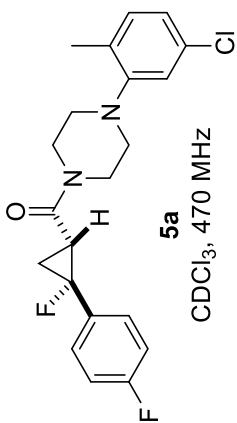
**Figure 42.** Enantiomeric excess of (**1*R*,2*S***)-**86**.

## **APPENDIX A**

### **SELECTED NMR SPECTRA**





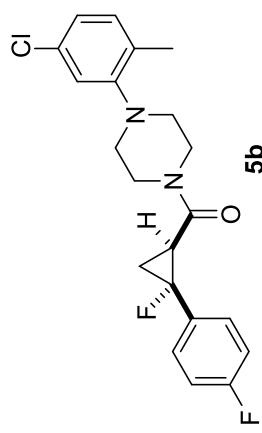


— -188.55

— -113.88

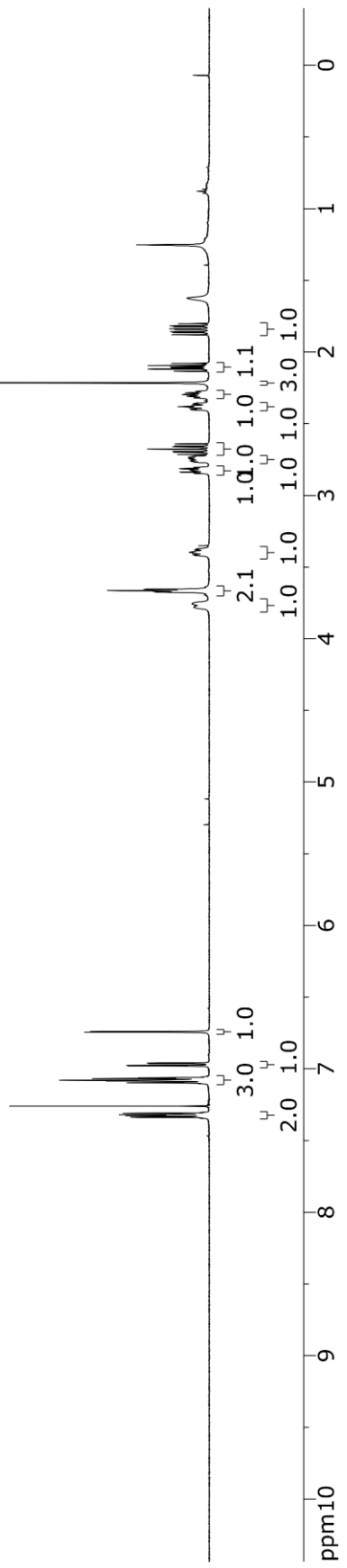
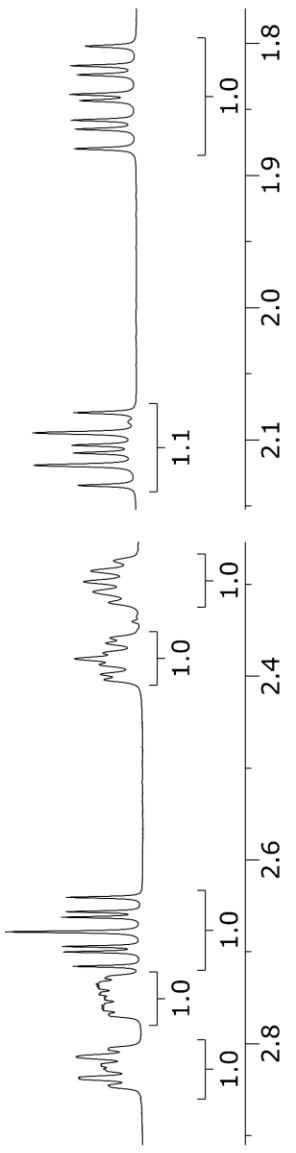


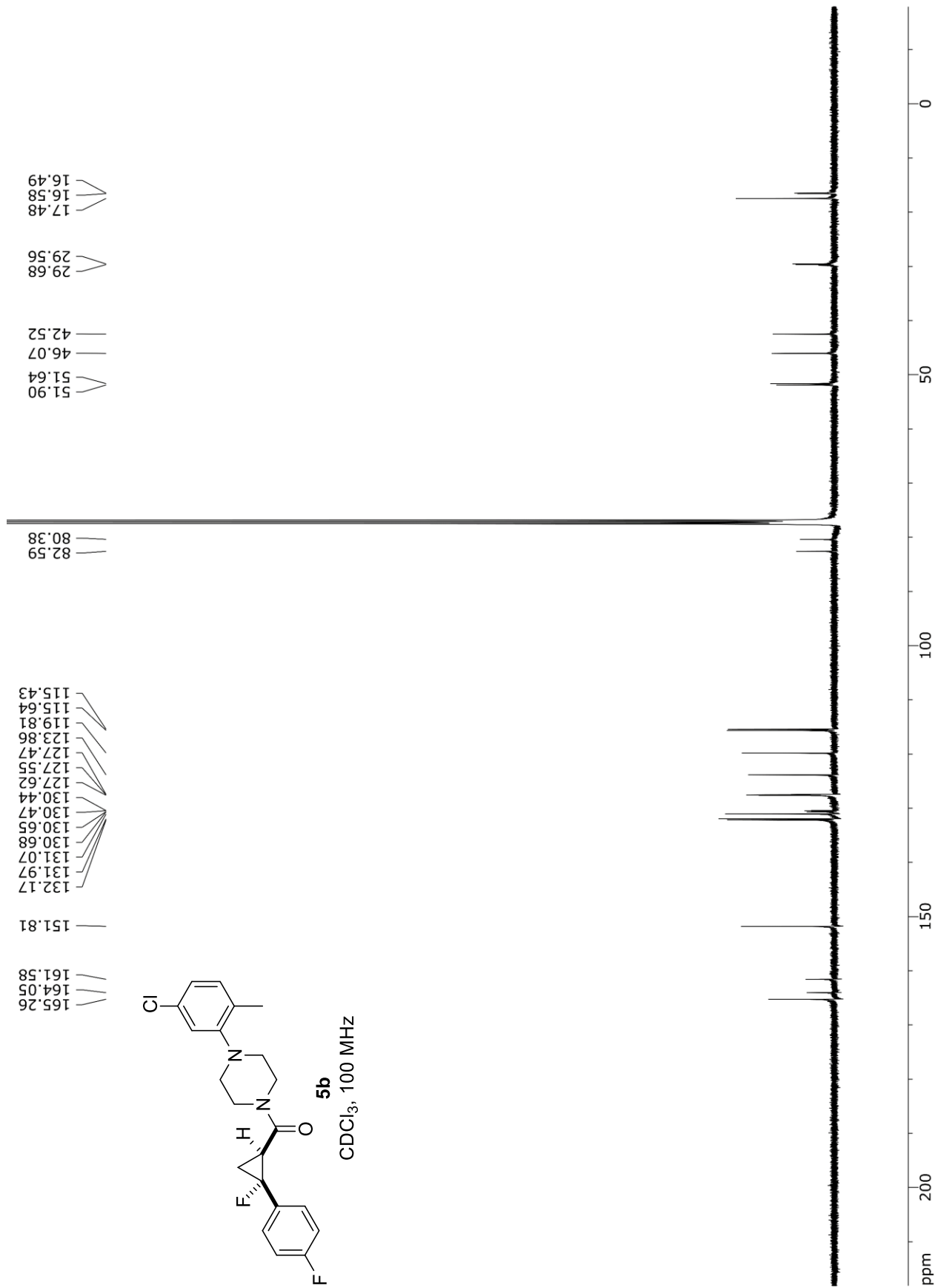
7.34  
7.332  
7.33  
7.32  
7.31  
7.10  
7.10  
7.10  
7.08  
7.08  
7.07  
7.06  
6.98  
6.98  
6.96  
6.96  
6.96  
6.74  
6.74  
3.78  
3.76  
3.66  
3.66  
3.66  
3.42  
3.40  
3.37  
2.85  
2.81  
2.77  
2.73  
2.72  
2.70  
2.69  
2.68  
2.66  
2.66  
2.64  
2.40  
2.40  
2.39  
2.38  
2.37  
2.36  
2.36  
2.32  
2.31  
2.30  
2.29  
2.27  
2.22  
2.13  
2.12  
2.11  
2.10  
2.09  
2.08  
1.88  
1.86  
1.86  
1.84  
1.84  
1.82  
1.82  
1.80

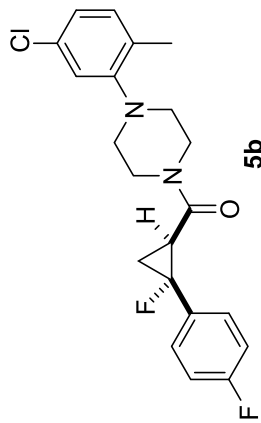


CDCl<sub>3</sub>, 500 MHz

2.85  
2.81  
2.77  
2.73  
2.72  
2.70  
2.69  
2.68  
2.66  
2.66  
2.64  
2.40  
2.40  
2.39  
2.38  
2.37  
2.36  
2.36  
2.32  
2.31  
2.30  
2.29  
2.27  
2.13  
2.12  
2.11  
2.10  
2.09  
2.08  
1.88  
1.86  
1.86  
1.84  
1.84  
1.82  
1.82  
1.80







CDCl<sub>3</sub>, 470 MHz

-164.01

-113.19

ppm

-0

-50

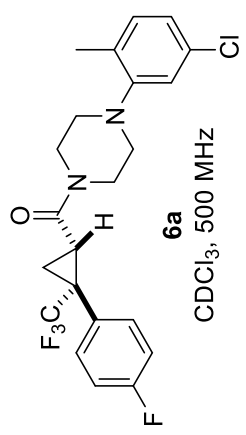
-100

-150

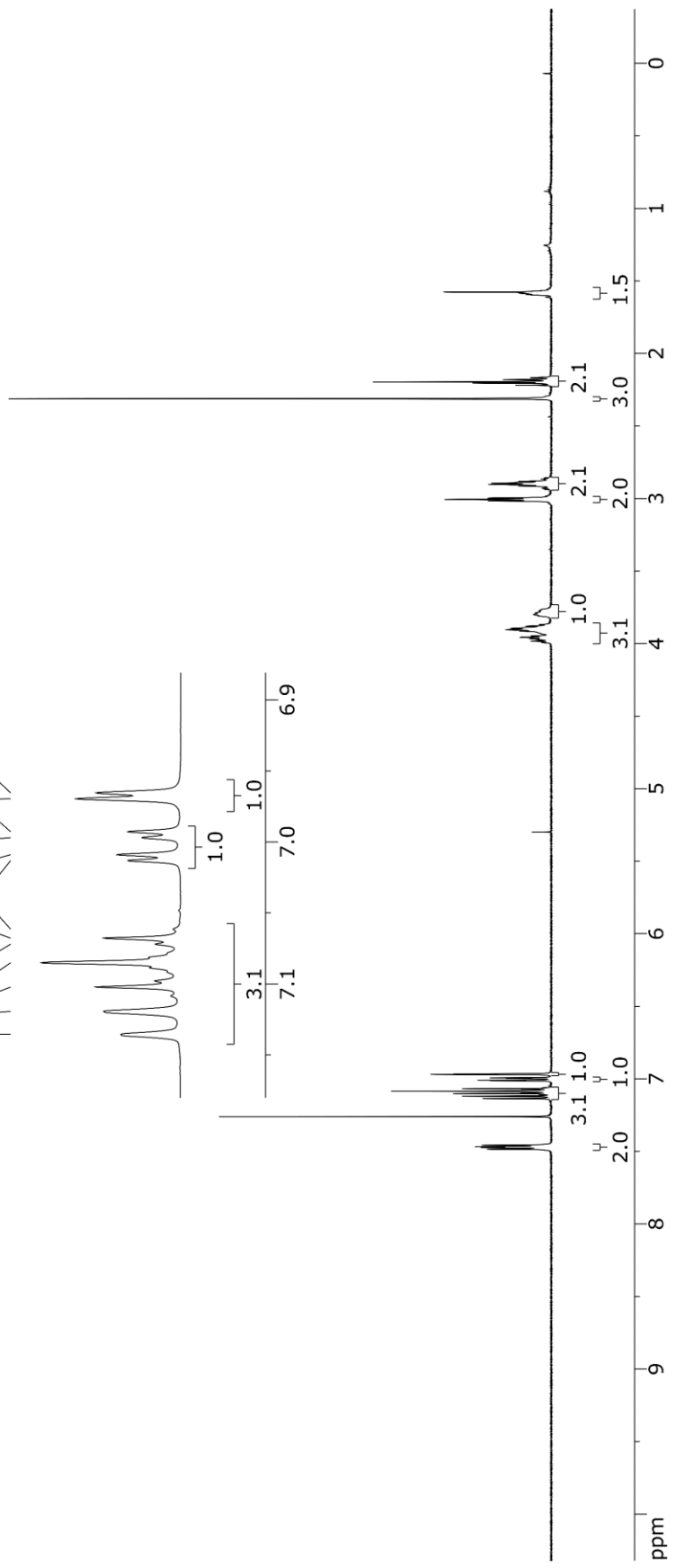
-200

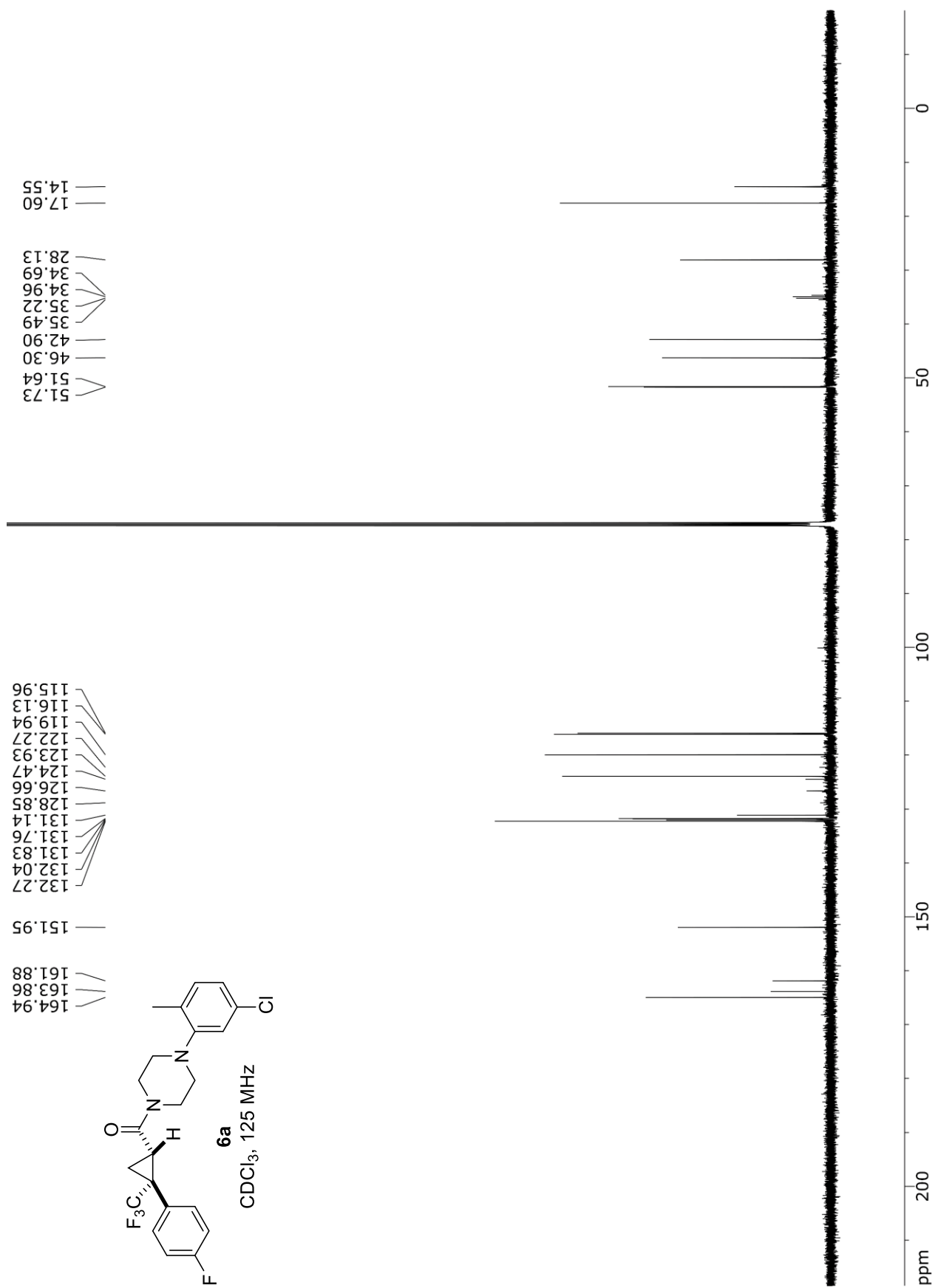


7.48  
7.47  
7.47  
7.46  
7.14  
7.12  
7.10  
7.09  
7.07  
7.07  
7.06  
7.01  
7.01  
7.00  
6.99  
6.97  
6.97  
3.99  
3.96  
3.95  
3.93  
3.90  
3.88  
3.87  
3.81  
3.76  
3.02  
3.01  
3.00  
2.94  
2.93  
2.91  
2.90  
2.89  
2.88  
2.87  
2.86  
2.31  
2.22  
2.22  
2.20  
2.18  
2.17  
1.61  
1.58  
1.56



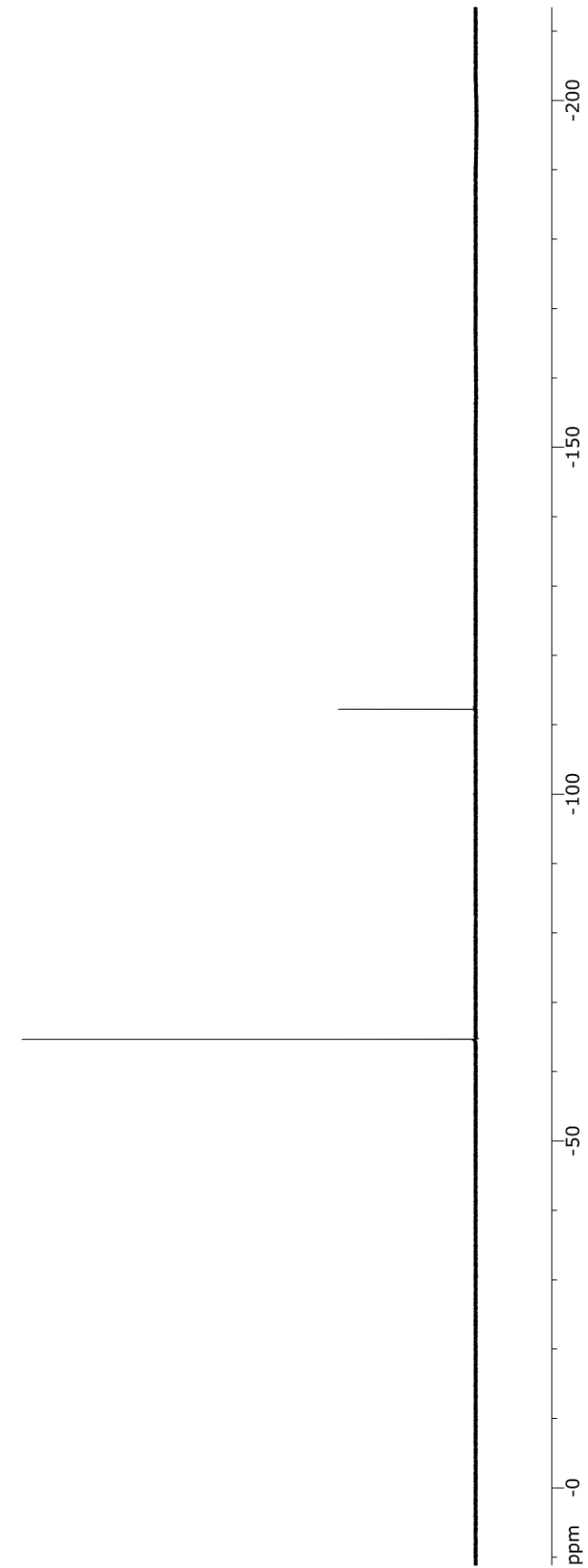
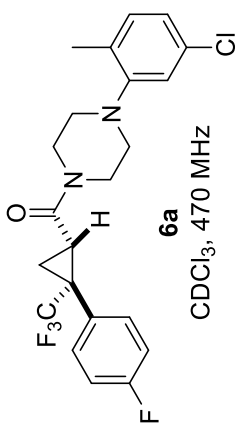
7.14  
7.12  
7.10  
7.09  
7.07  
7.07  
7.06  
7.01  
7.01  
7.00  
6.99  
6.97  
6.97



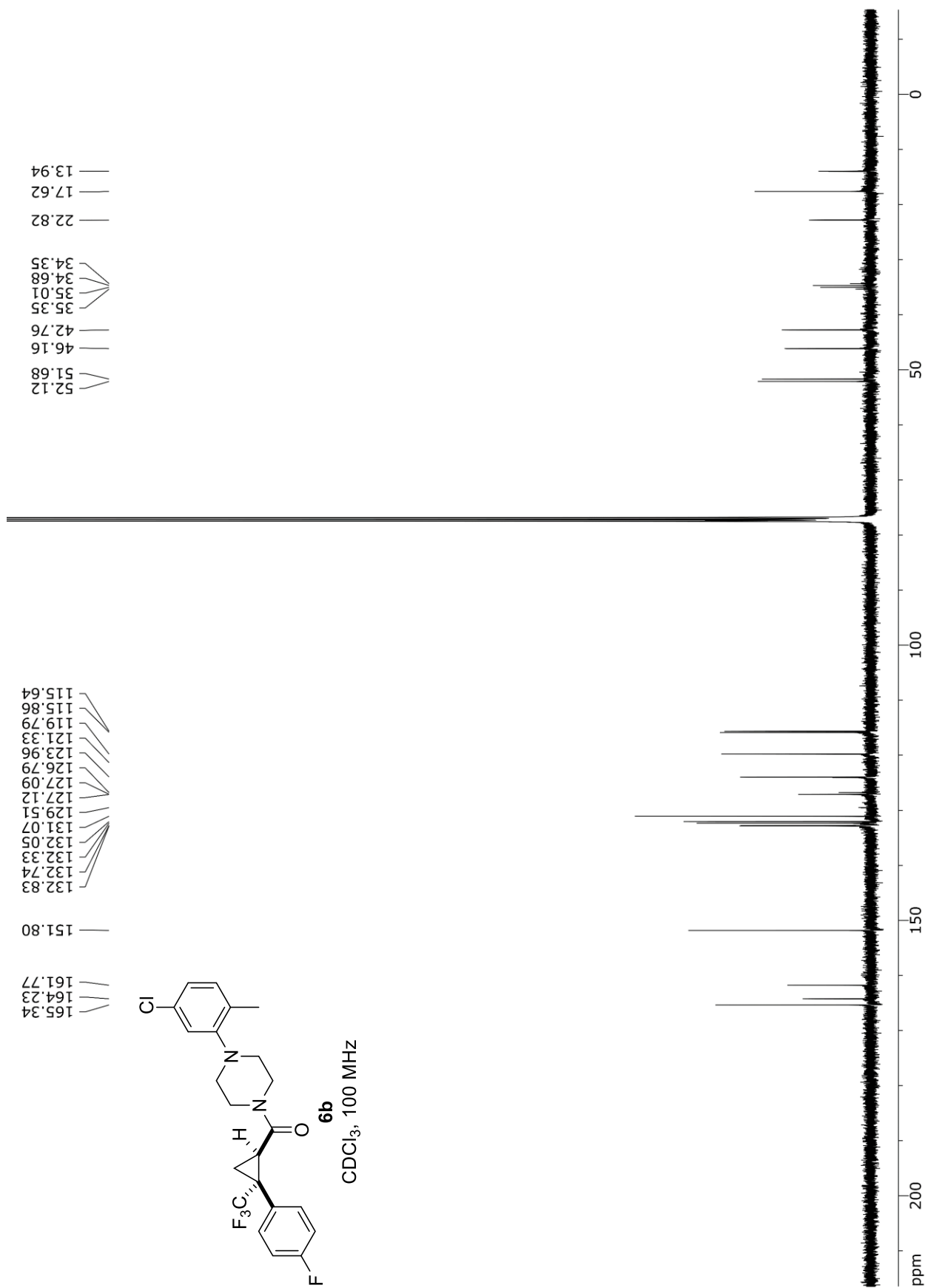


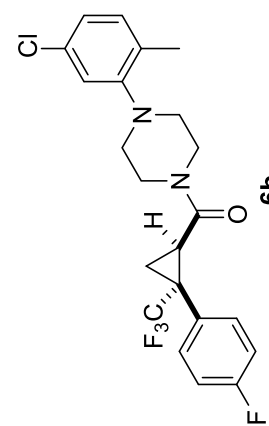
-112.22

-64.66





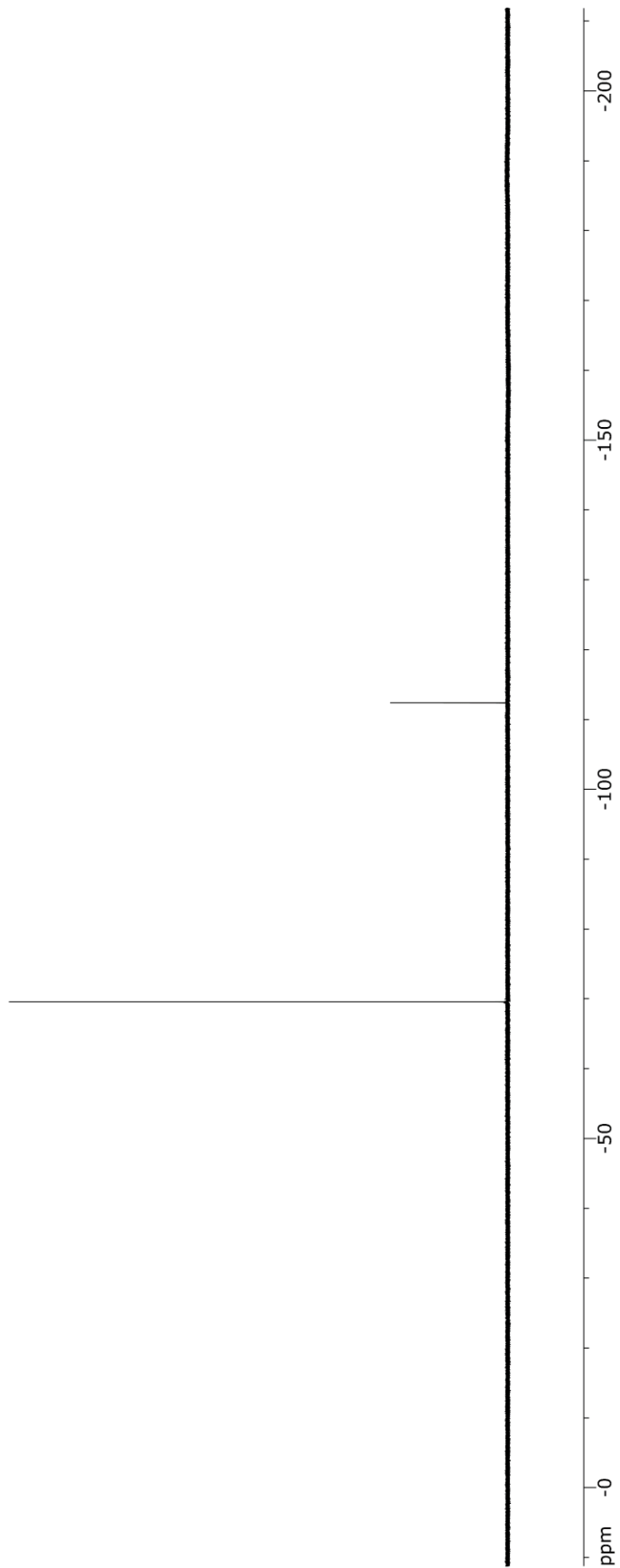


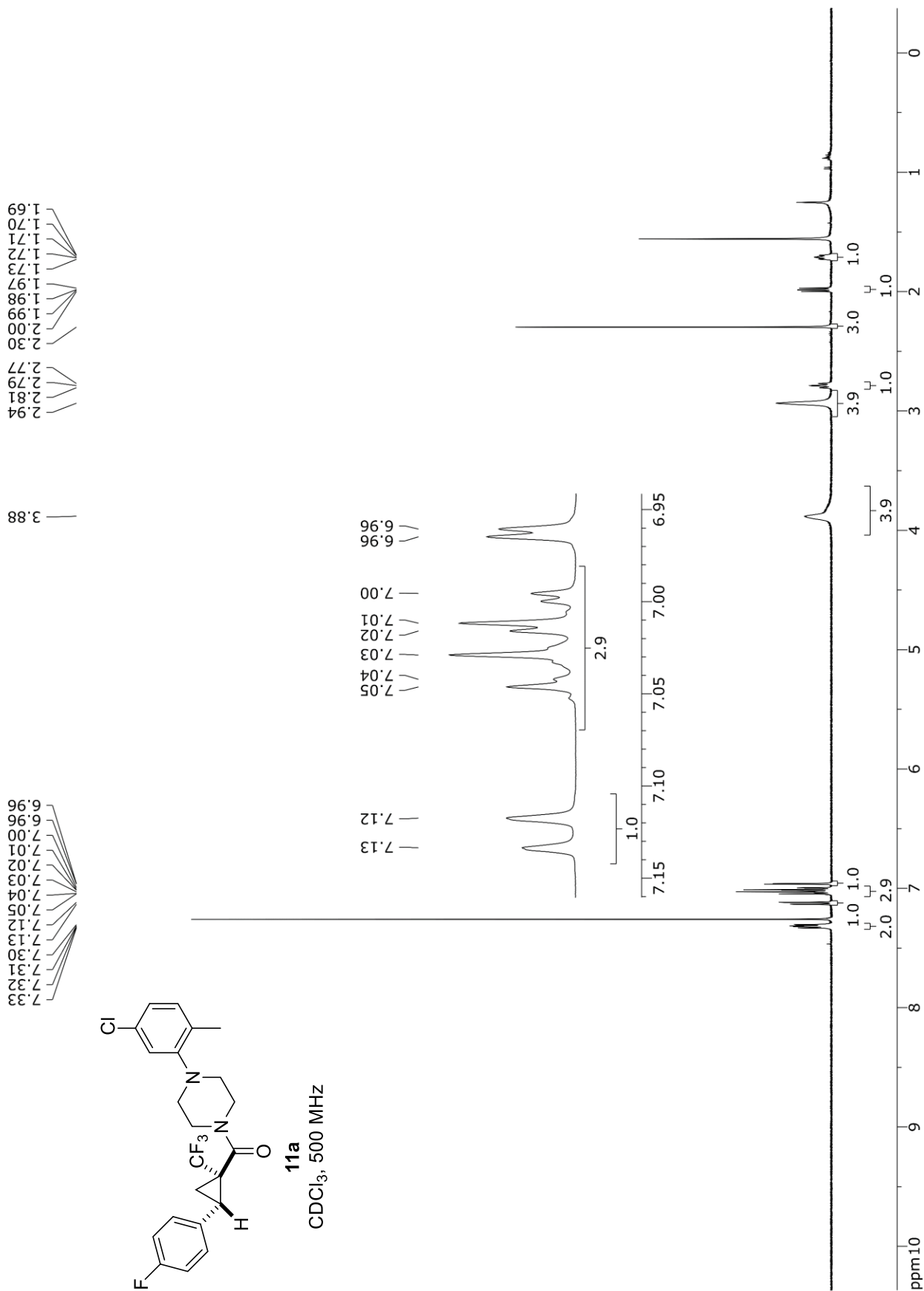


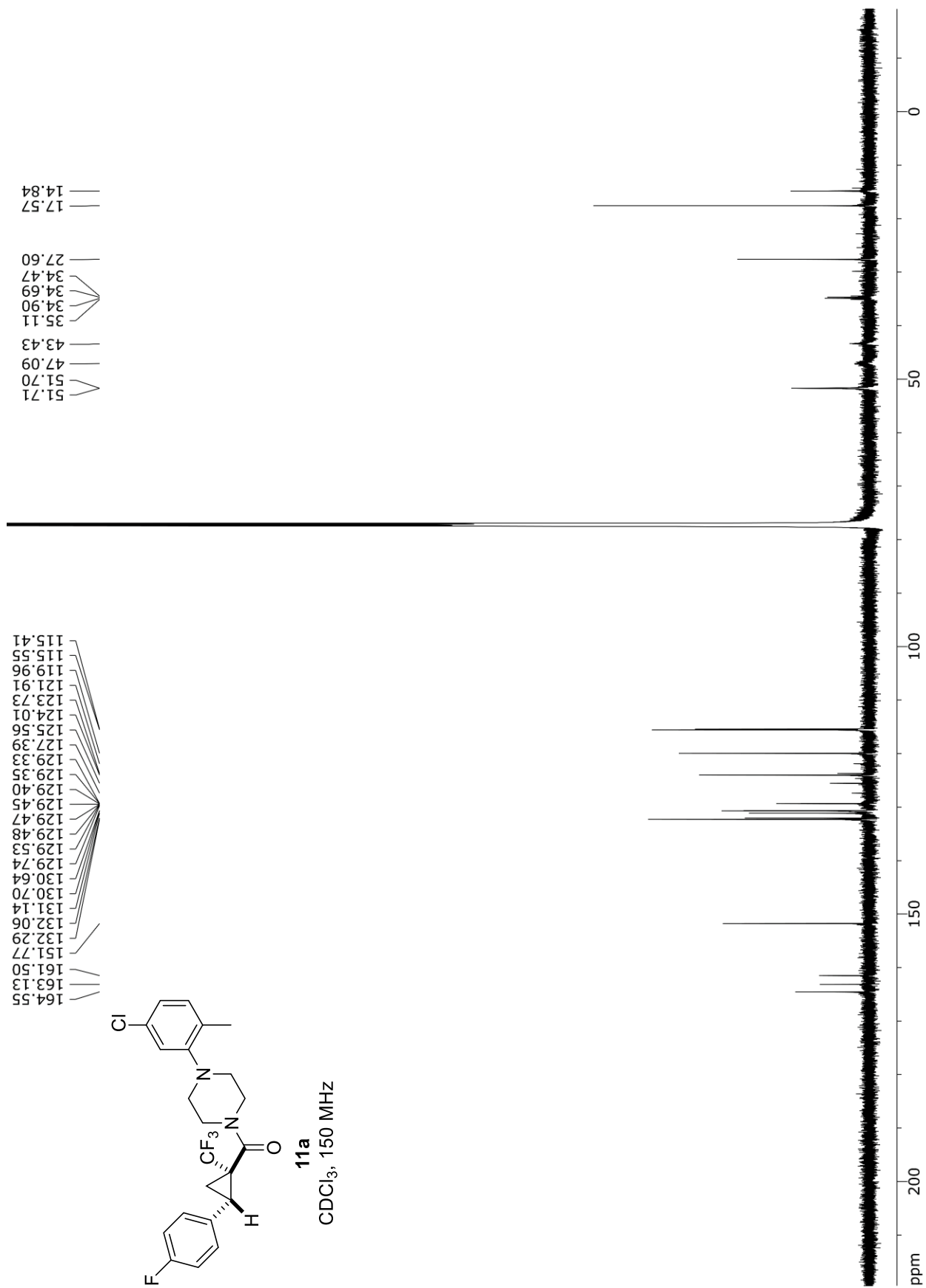
**6b**  
CDCl<sub>3</sub>, 470 MHz

— -112.37

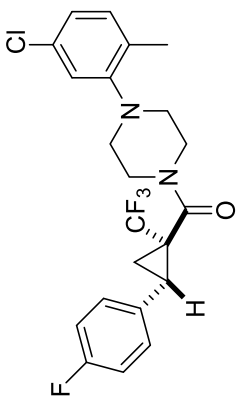
— -69.56



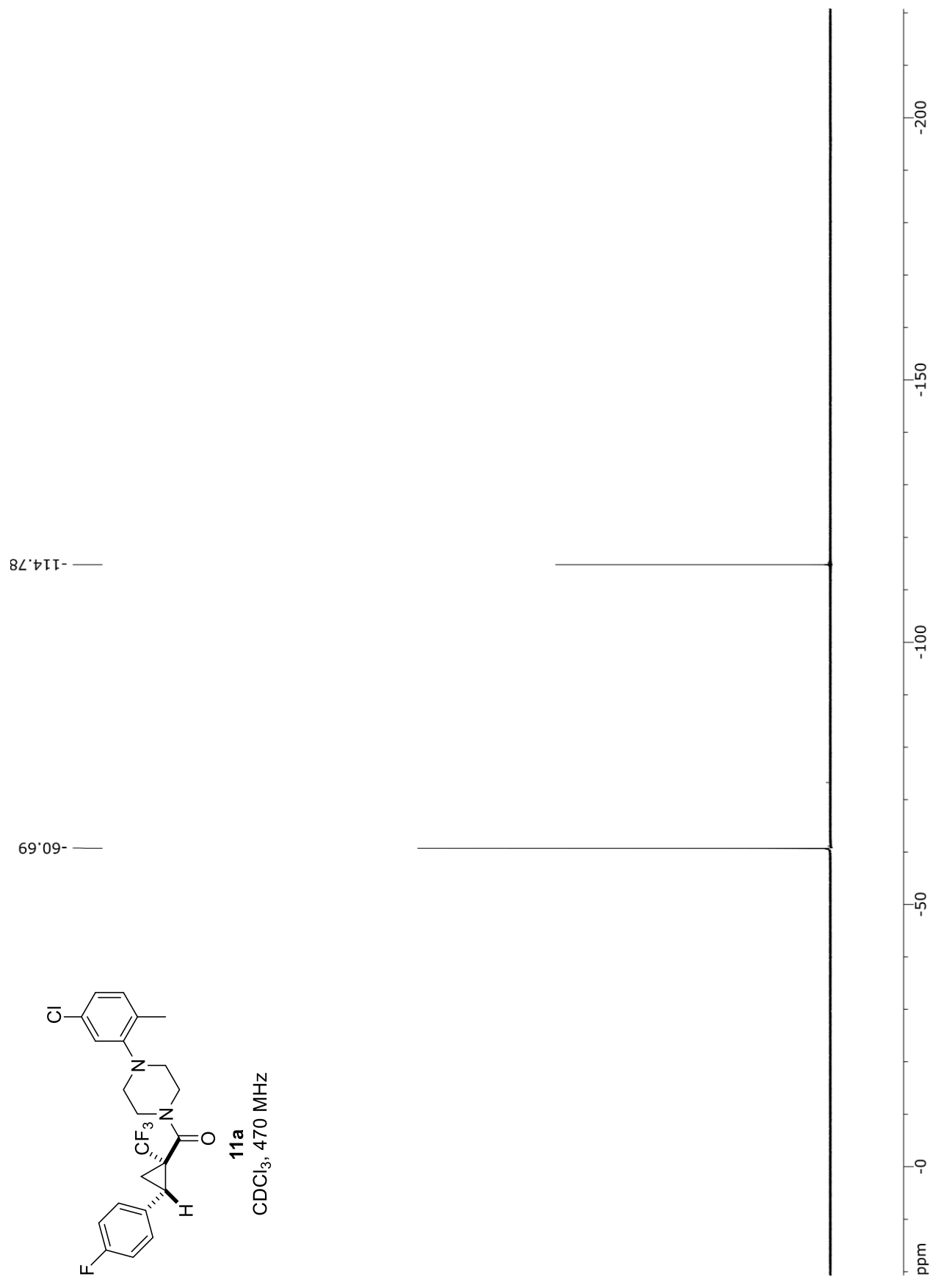




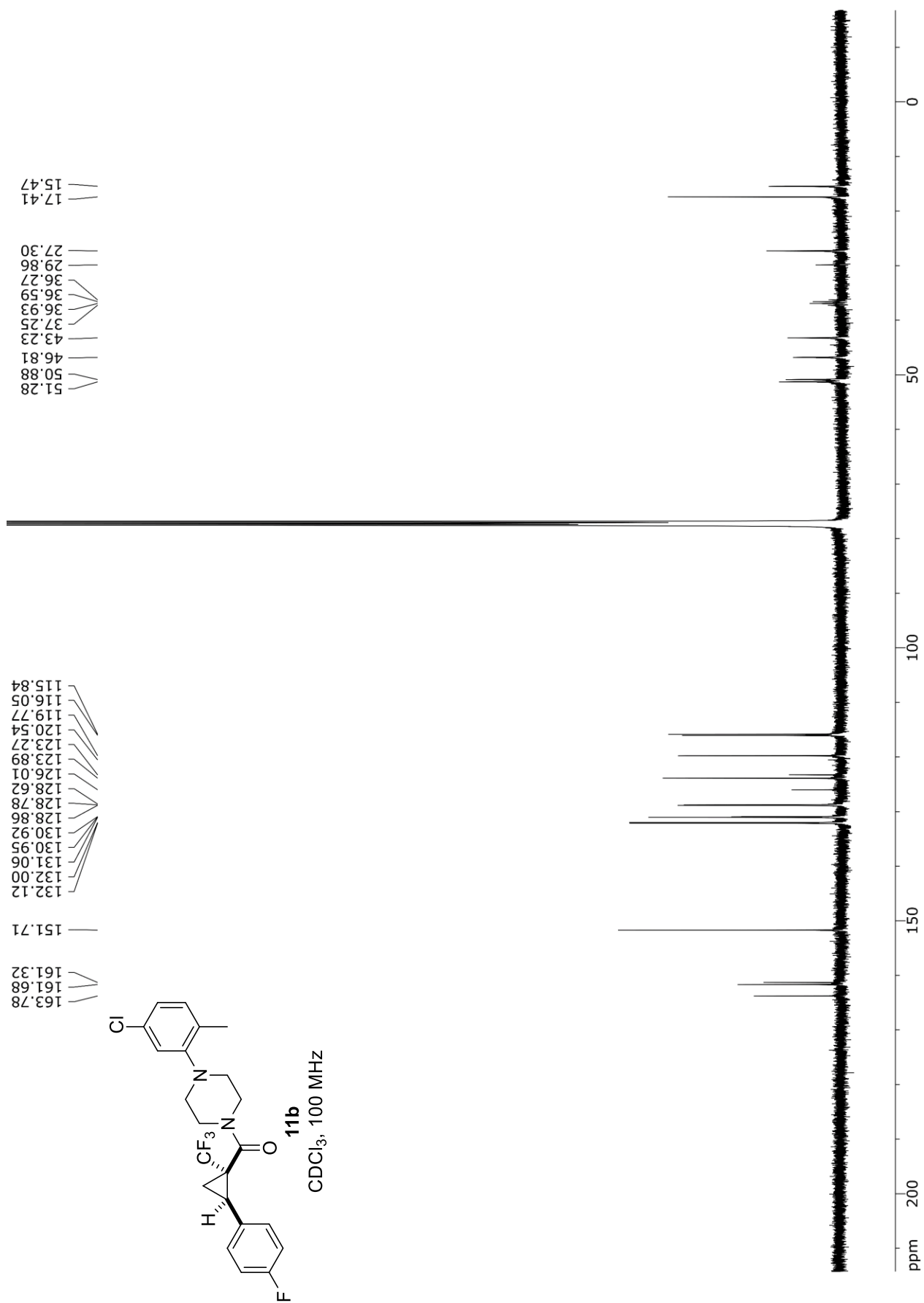


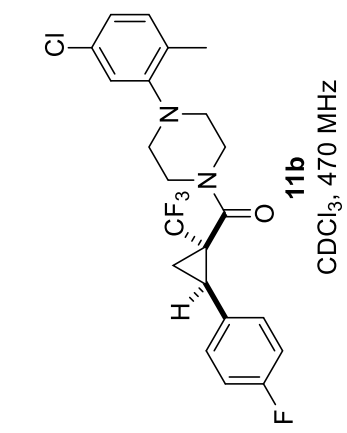


**11a**  
CDCl<sub>3</sub>, 470 MHz









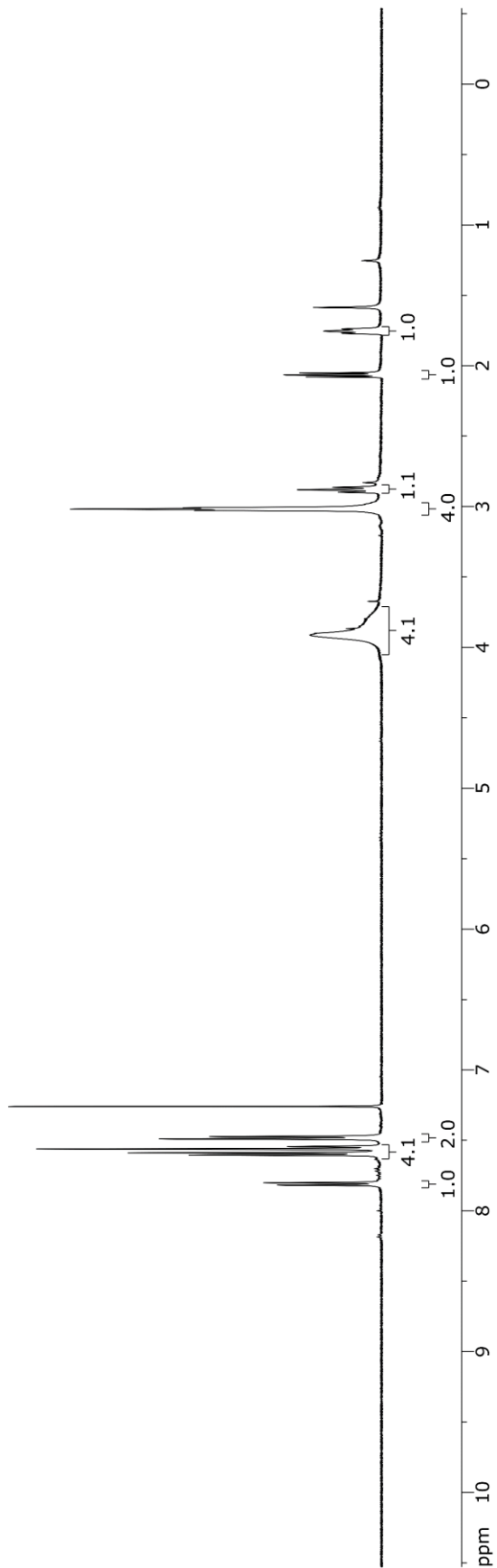
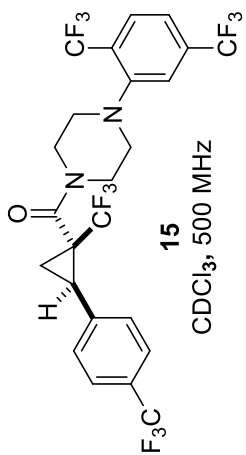
-114.00

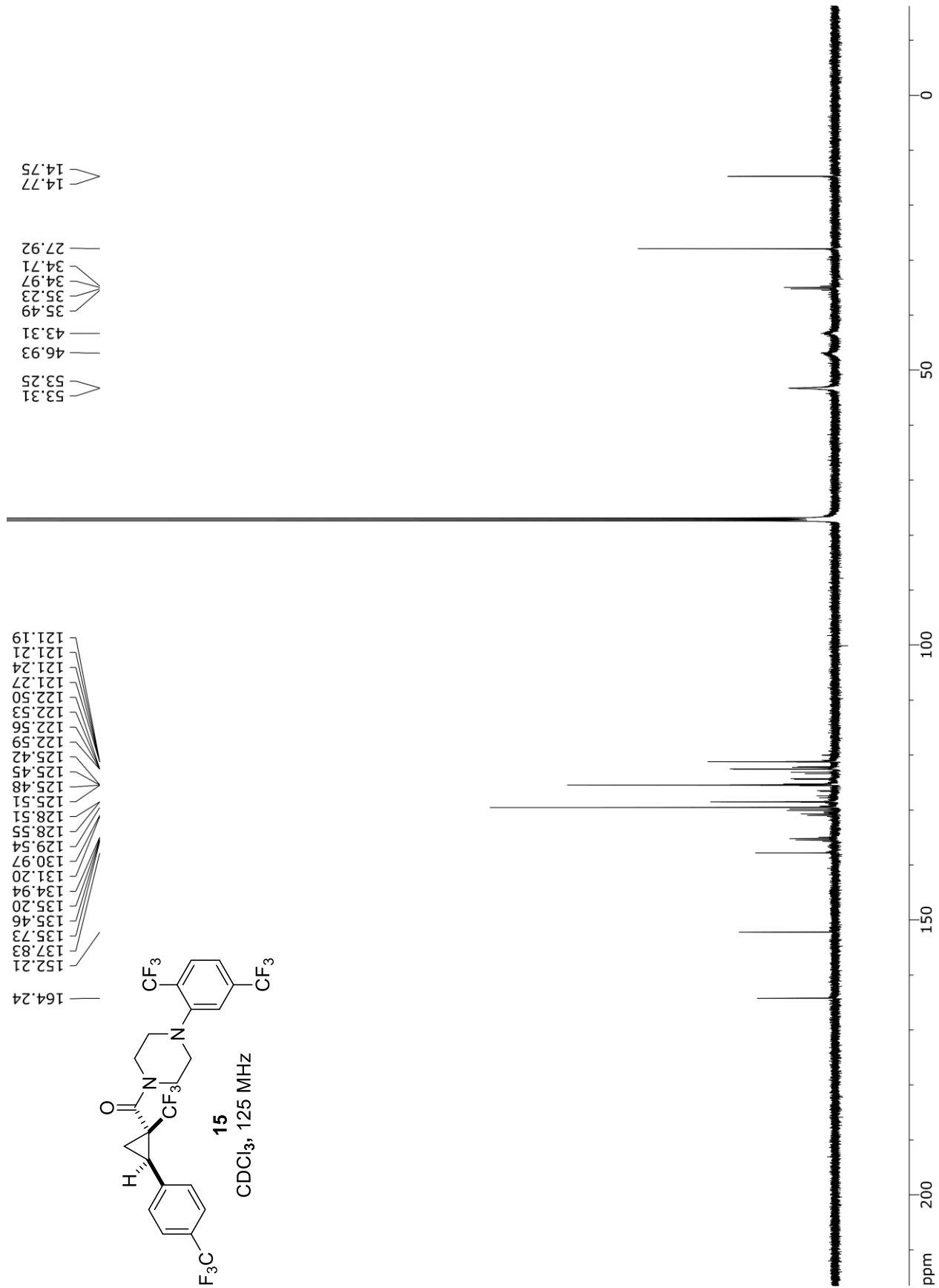
-66.27

ppm -0 -50 -100 -150 -200

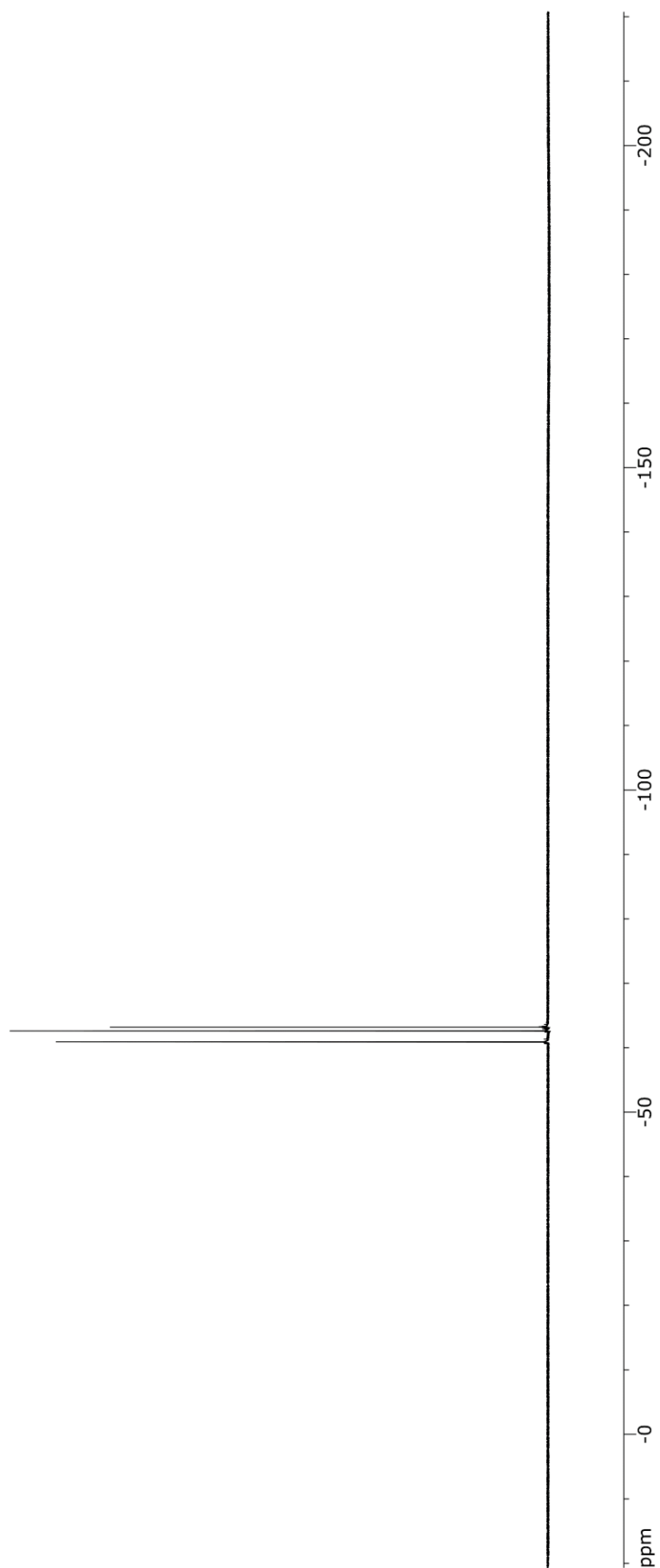
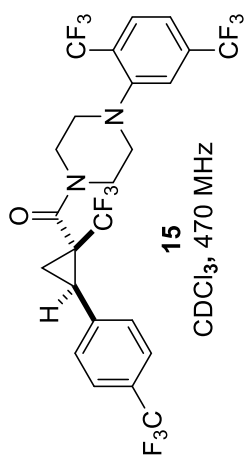
1.74  
 1.75  
 1.77  
 2.05  
 2.06  
 2.08  
 2.86  
 2.88  
 2.90  
 3.01  
 3.02  
 3.03  
 3.91

7.26  
 7.47  
 7.49  
 7.54  
 7.56  
 7.59  
 7.60  
 7.80  
 7.82



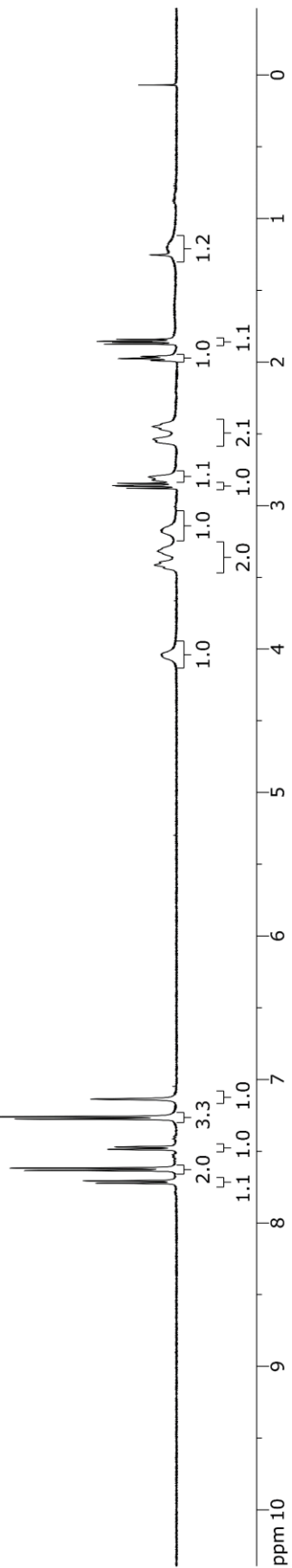
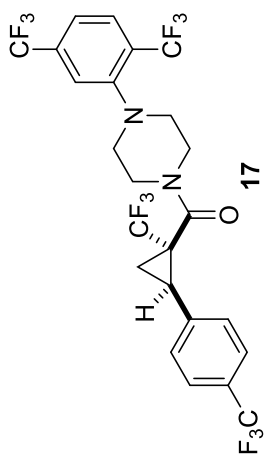


63.19  
62.59  
60.89  
60.88

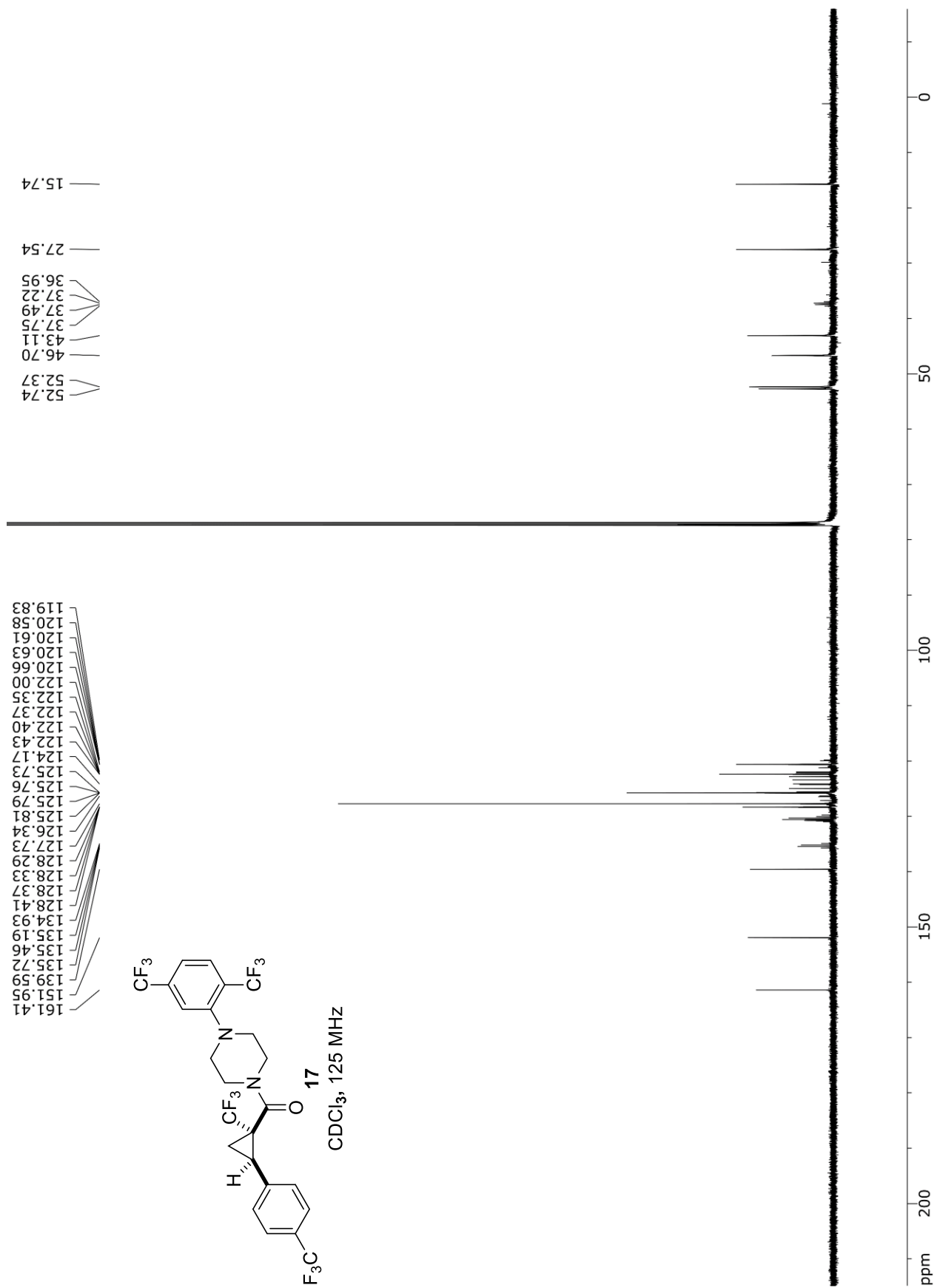


4.06  
 4.01  
 3.41  
 3.32  
 3.18  
 3.14  
 2.88  
 2.87  
 2.86  
 2.85  
 2.82  
 2.81  
 2.80  
 2.56  
 2.54  
 2.47  
 2.45  
 2.42  
 1.99  
 1.98  
 1.96  
 1.87  
 1.86  
 1.86  
 1.84  
 1.20

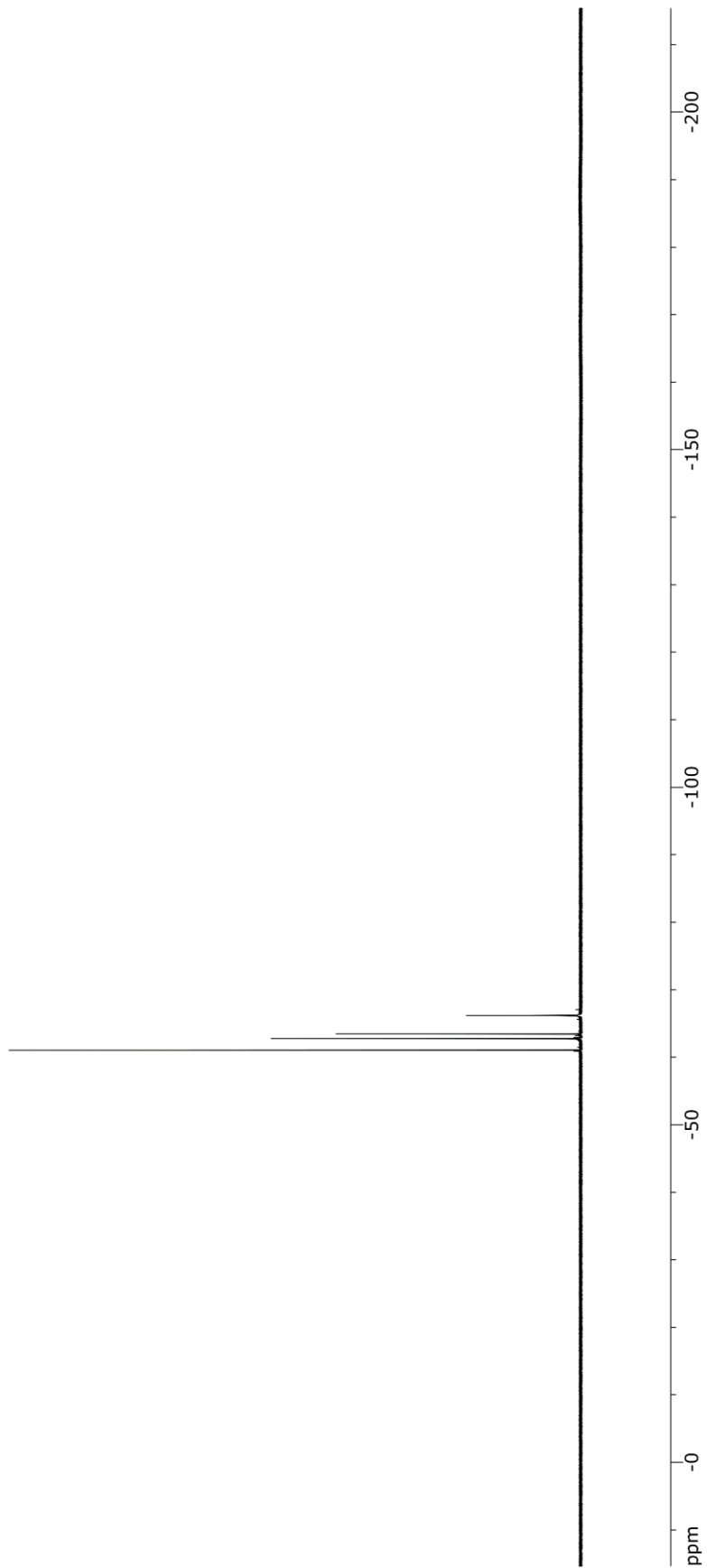
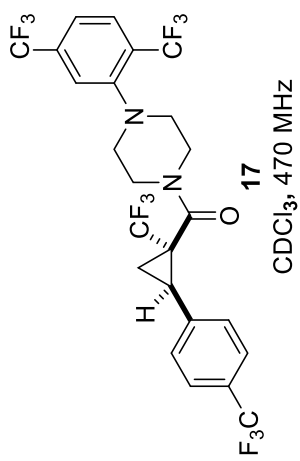
7.72  
 7.71  
 7.63  
 7.62  
 7.49  
 7.47  
 7.28  
 7.26  
 7.14

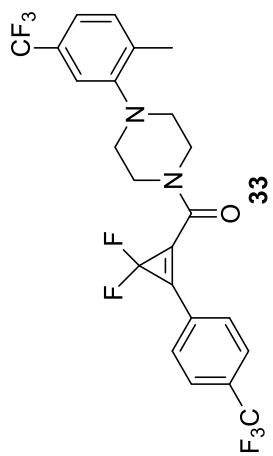






66.18  
63.45  
62.76  
61.05

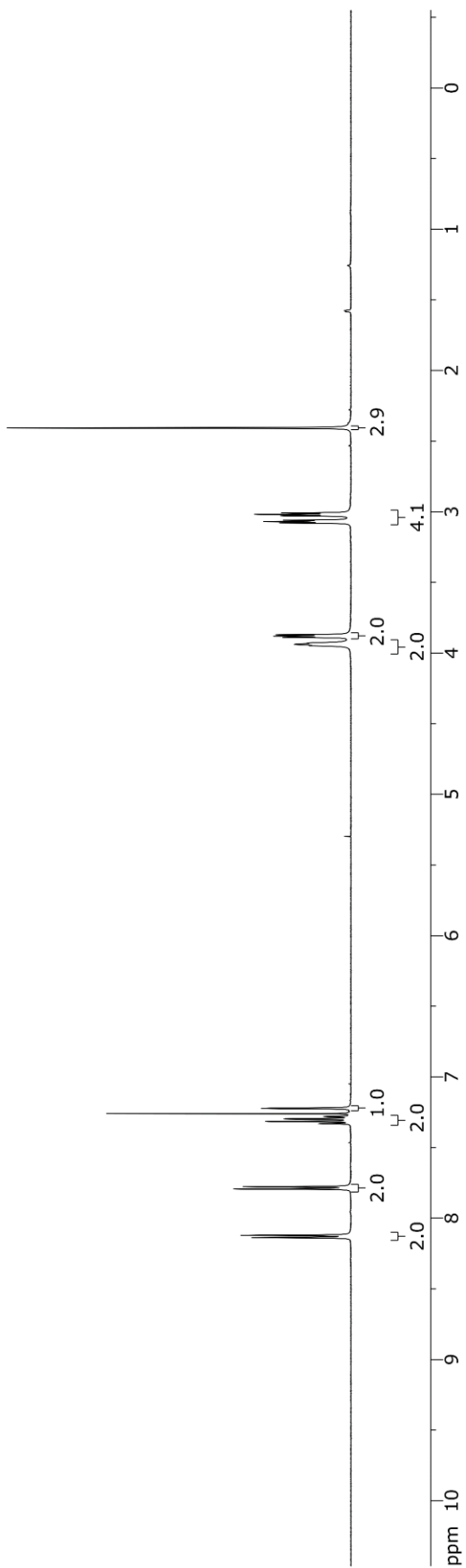


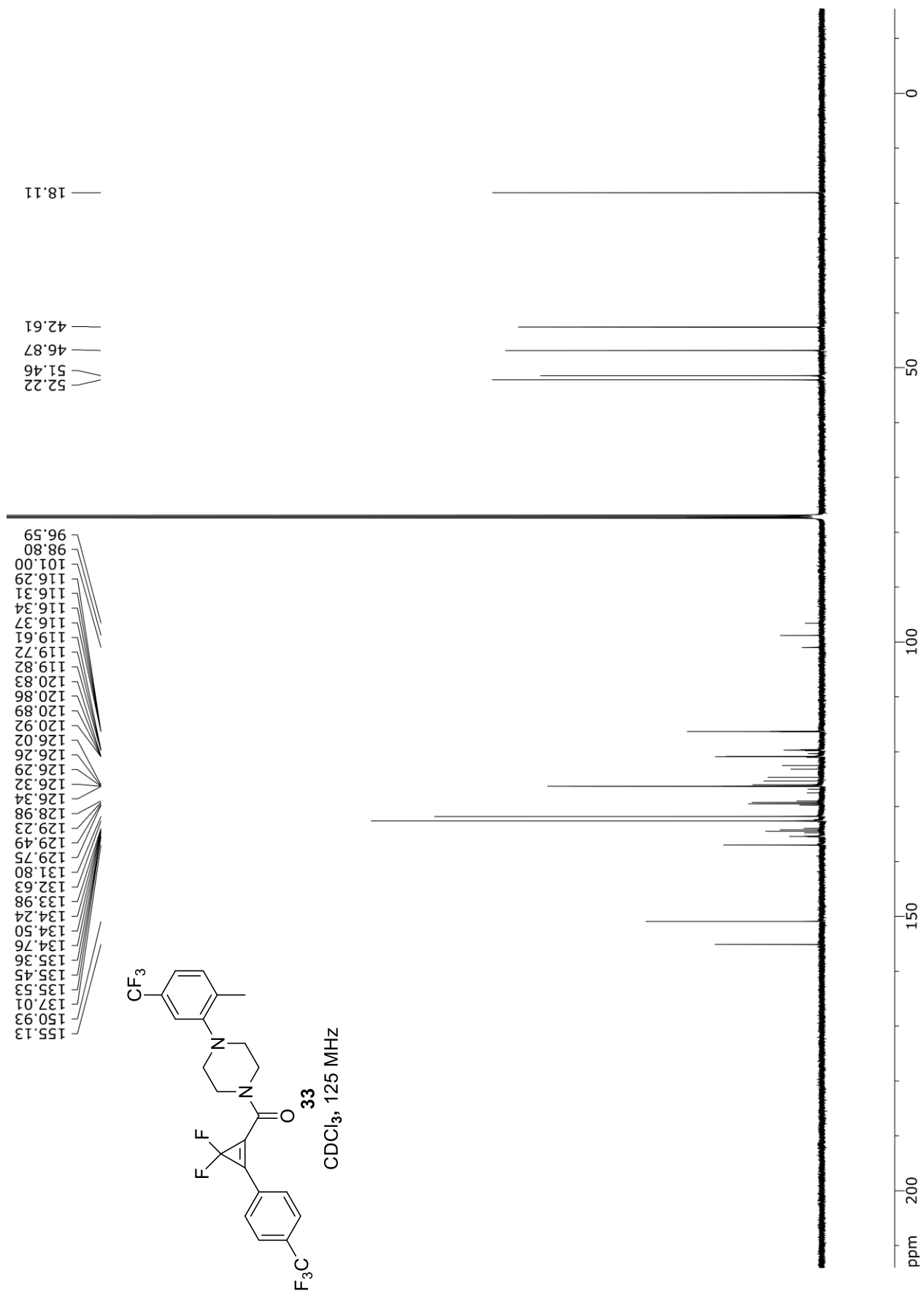


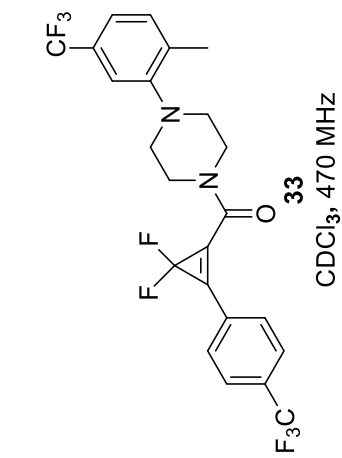
CDCl<sub>3</sub>, 500 MHz

3.95  
 3.94  
 3.93  
 3.89  
 3.88  
 3.87  
 3.08  
 3.07  
 3.06  
 3.03  
 3.02  
 3.01  
 2.41

8.14  
 8.12  
 7.79  
 7.78  
 7.33  
 7.32  
 7.30  
 7.28  
 7.22

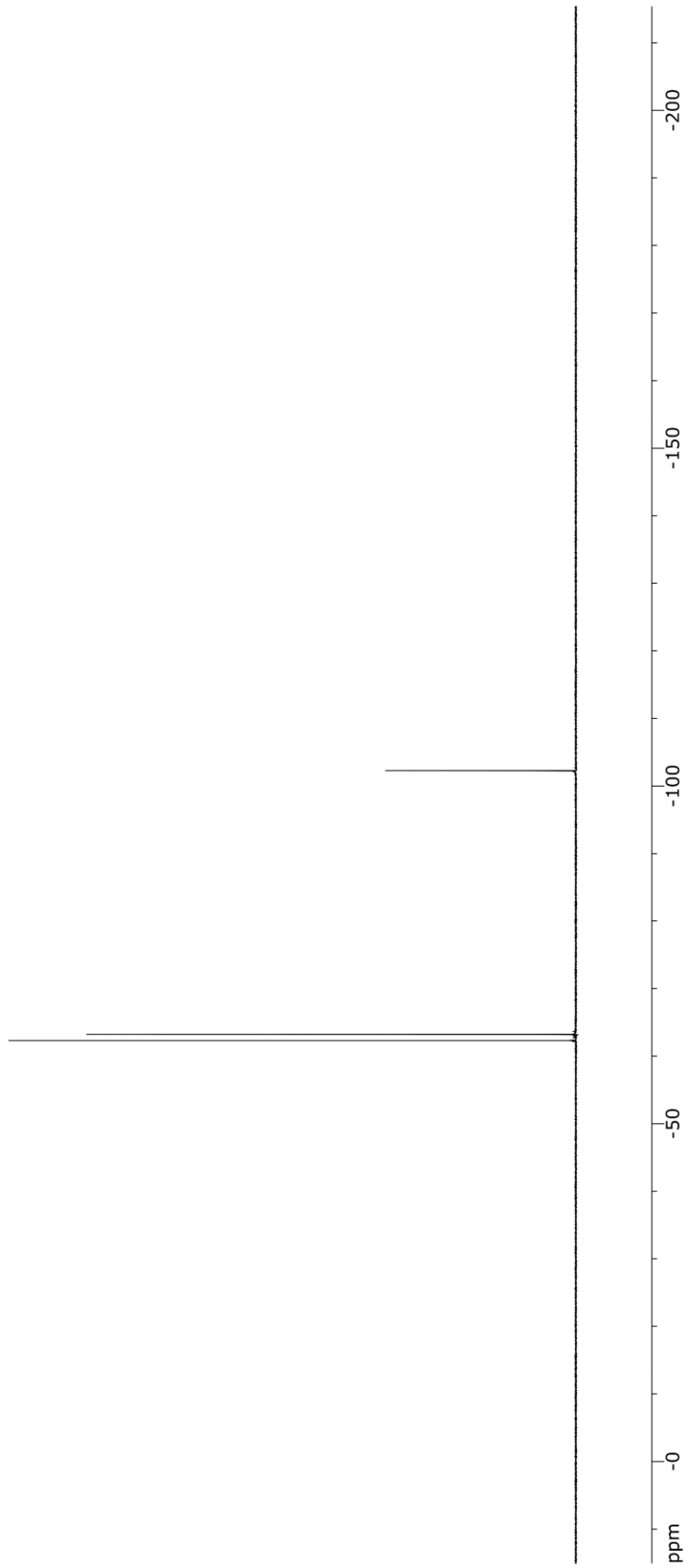


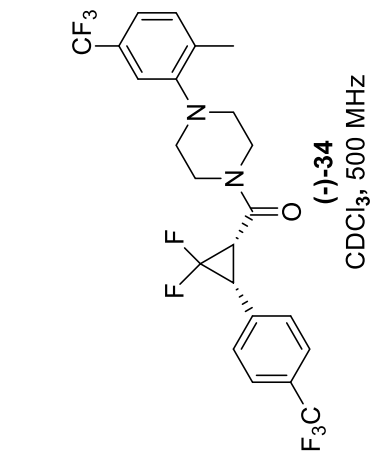




-62.30  
-63.22

-102.26





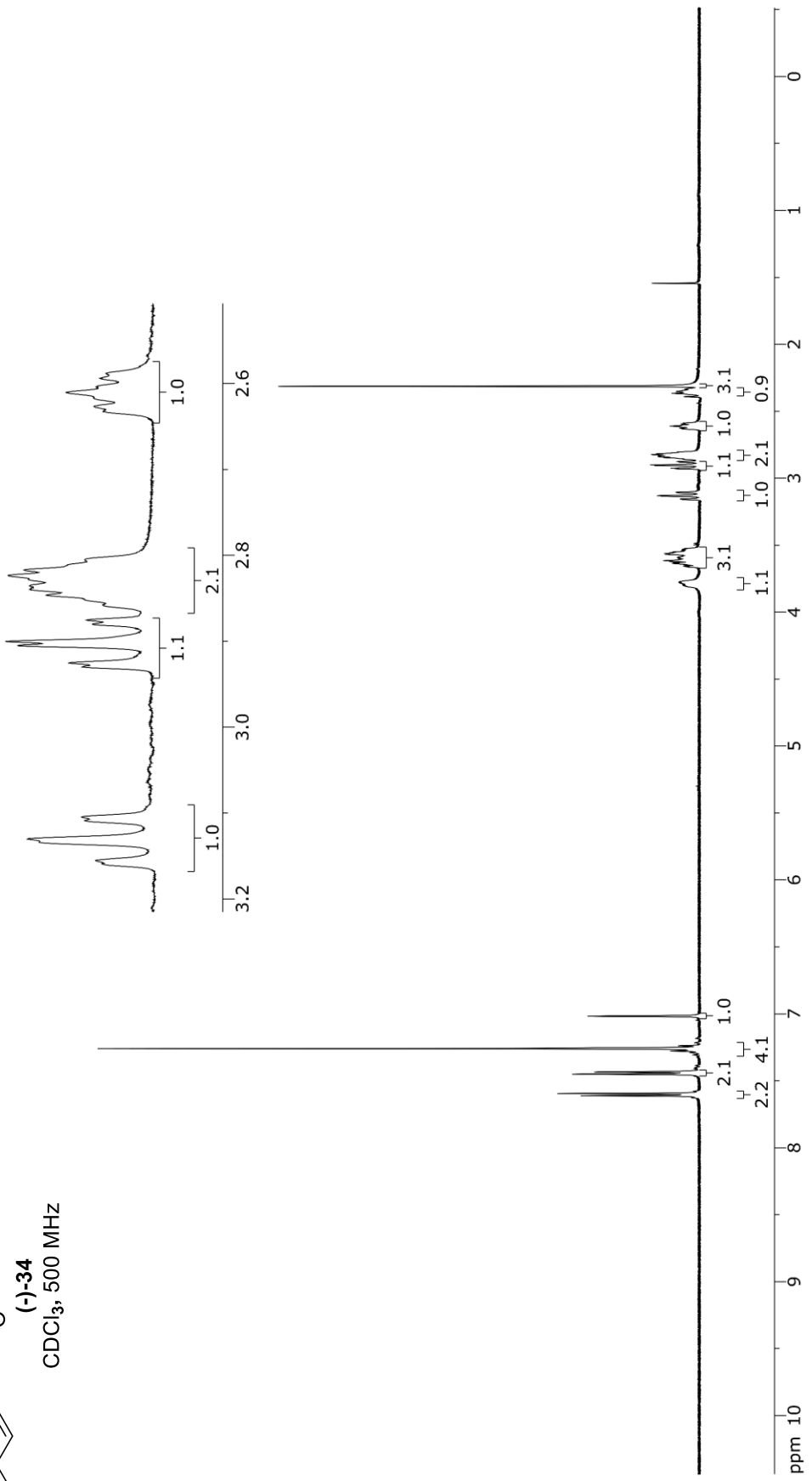
7.61  
 7.60  
 7.45  
 7.43  
 7.28  
 7.26  
 7.24  
 7.02

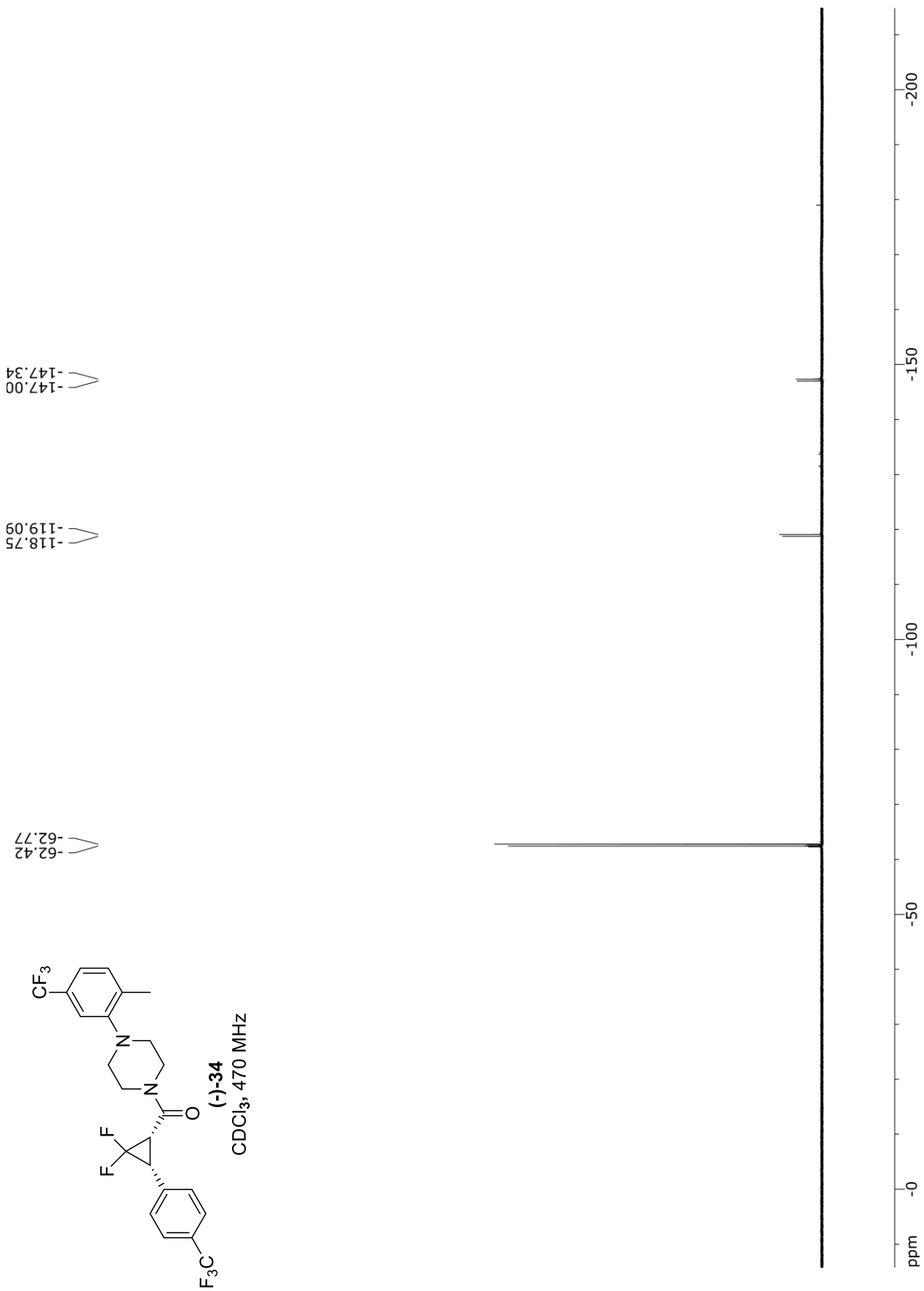
3.80  
 3.77  
 3.66  
 3.62  
 3.57  
 3.53  
 3.16  
 3.13  
 3.10

2.93  
 2.93  
 2.91  
 2.90  
 2.88  
 2.88  
 2.86  
 2.82  
 2.81

2.59  
 2.59  
 2.56  
 2.61  
 2.62  
 2.60  
 2.63  
 2.63  
 2.81  
 2.82  
 2.86  
 2.88  
 2.90  
 2.91  
 2.93  
 2.93

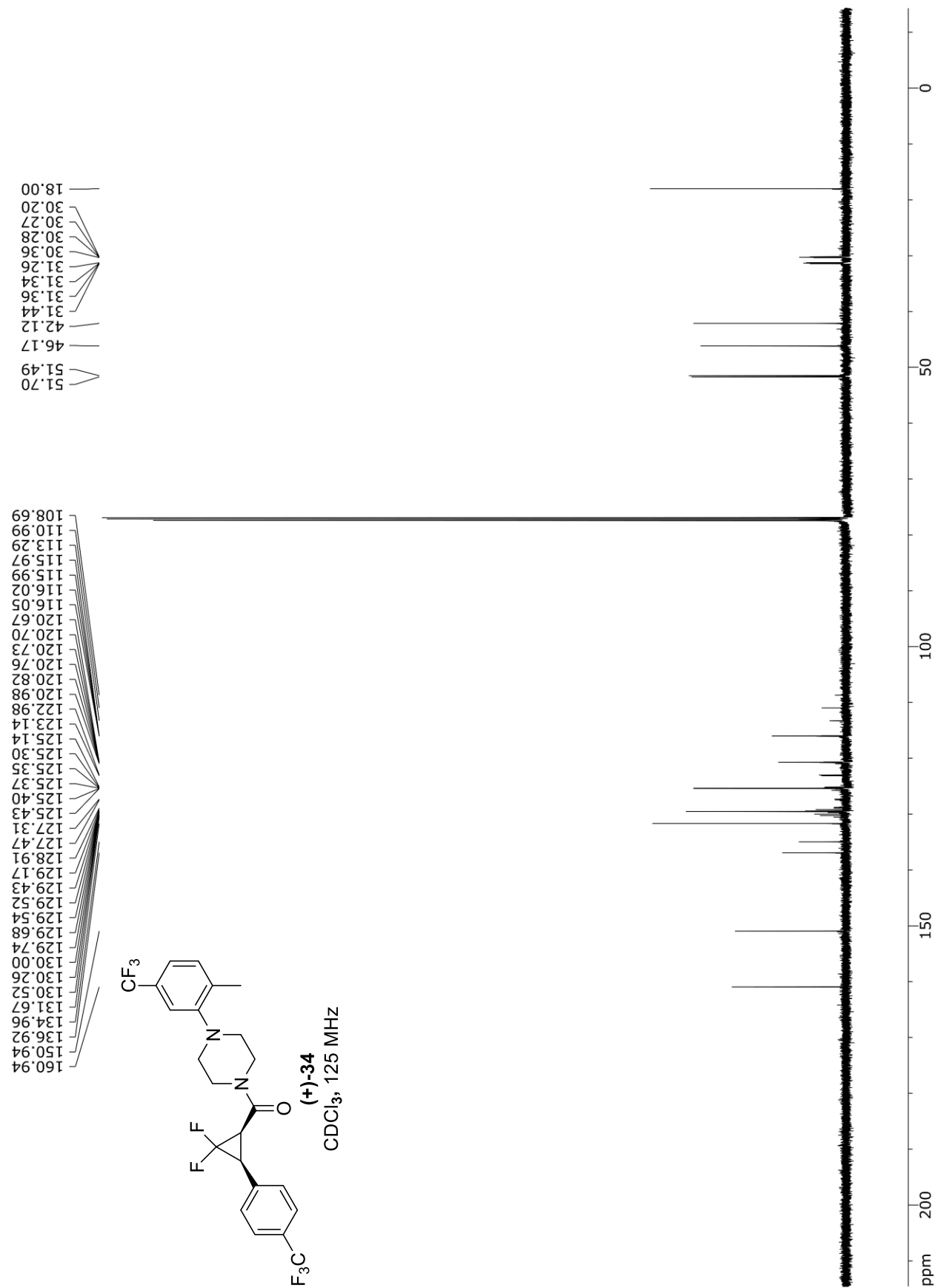
2.59  
 2.59  
 2.56  
 2.61  
 2.62  
 2.60  
 2.63  
 2.63  
 2.81  
 2.82  
 2.86  
 2.88  
 2.90  
 2.91  
 2.93  
 2.93

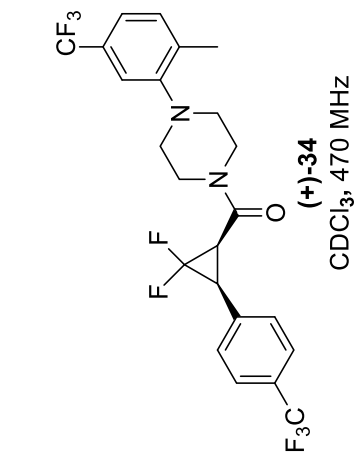








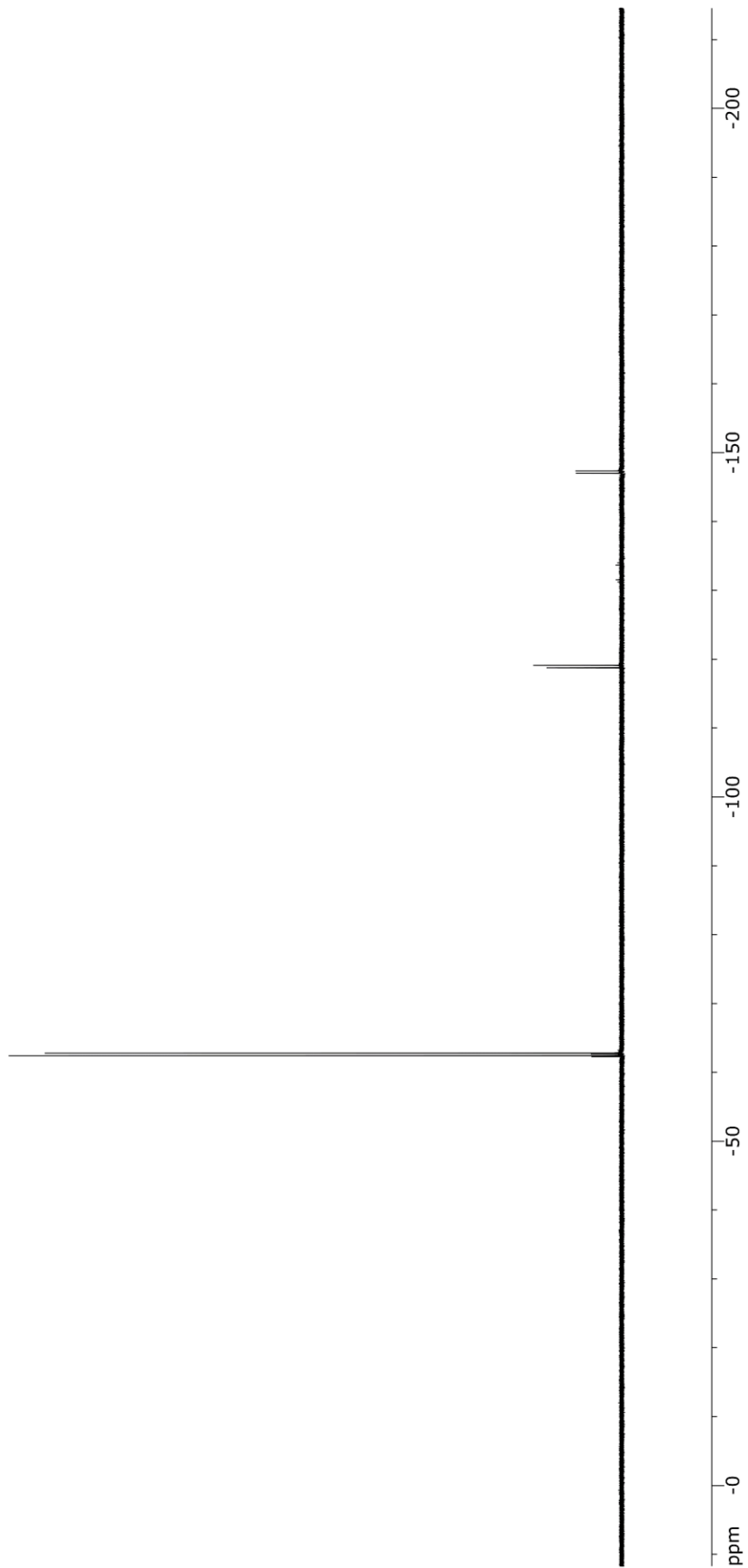




-62.42  
 -62.77

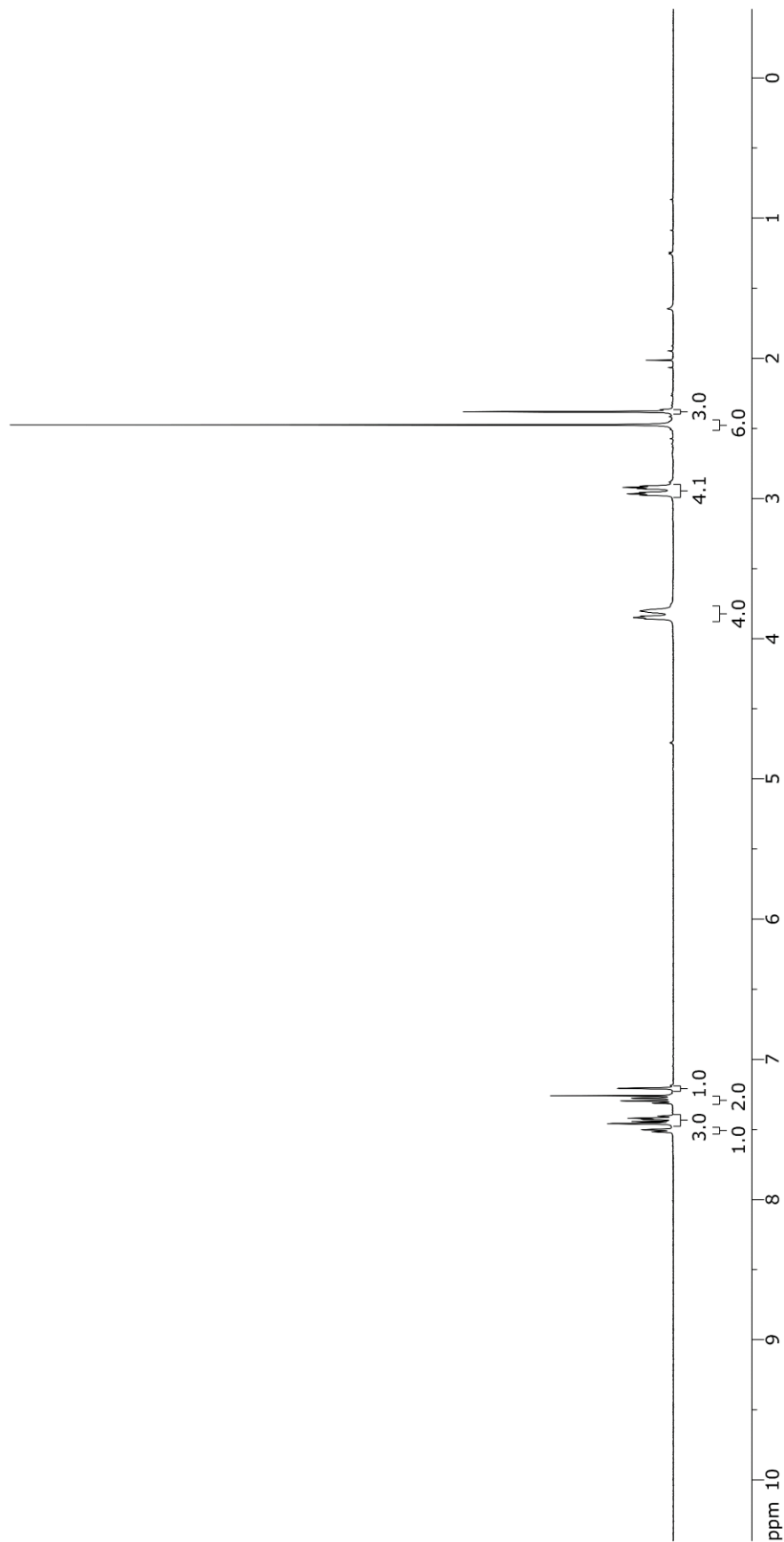
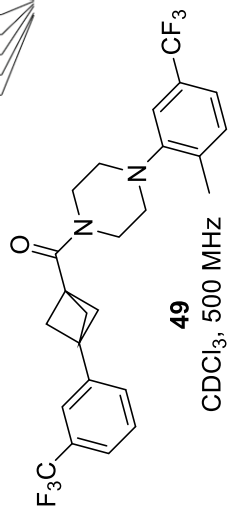
-118.75  
 -119.09

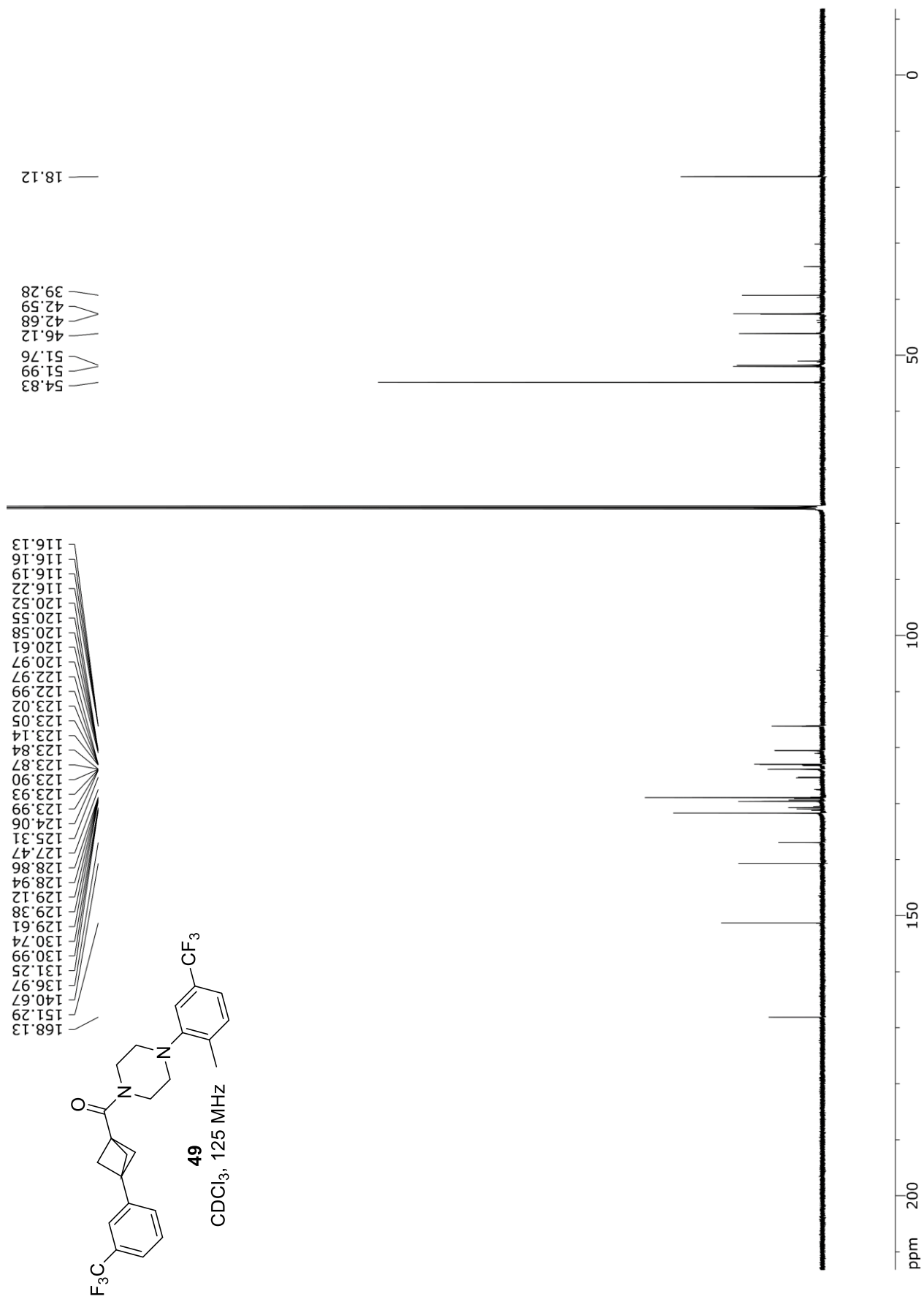
-147.00  
 -147.34



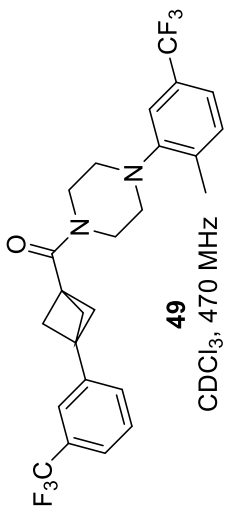
7.52  
7.50  
7.46  
7.44  
7.43  
7.42  
7.41  
7.31  
7.30  
7.28  
7.21

3.86  
3.85  
3.84  
3.80  
2.98  
2.97  
2.96  
2.93  
2.92  
2.91  
2.47  
2.38



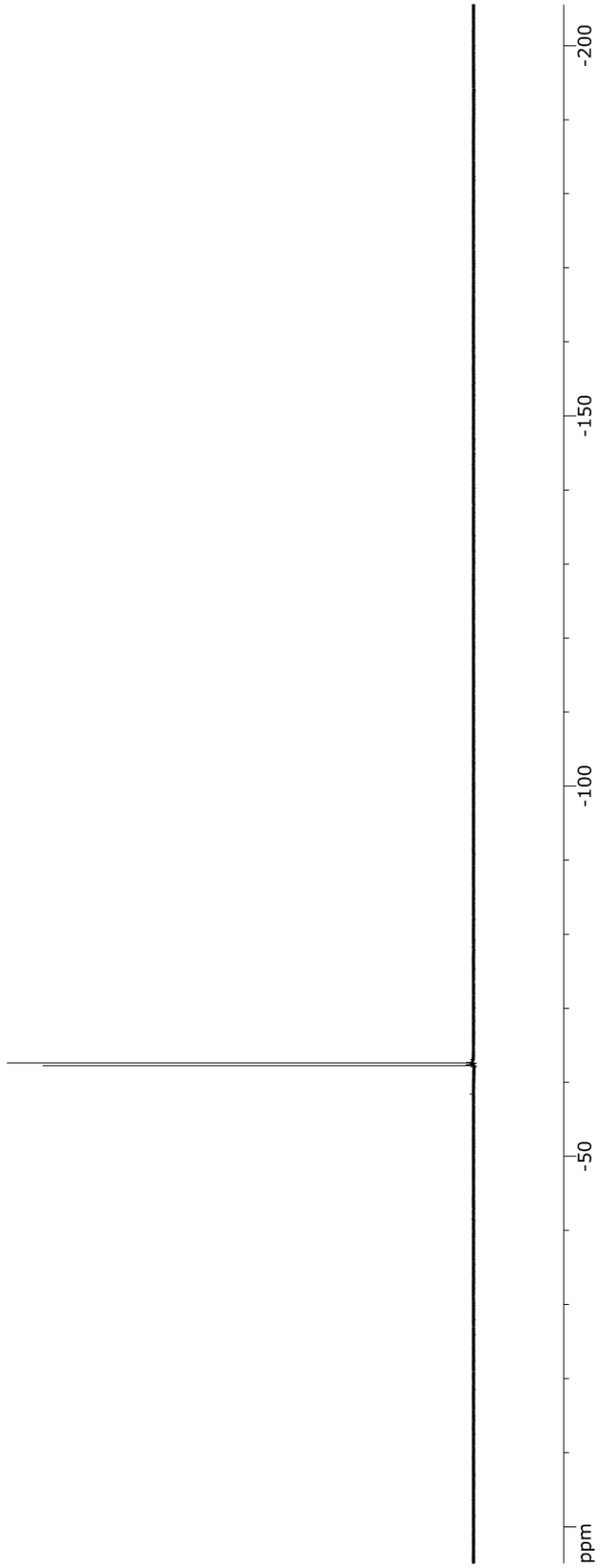


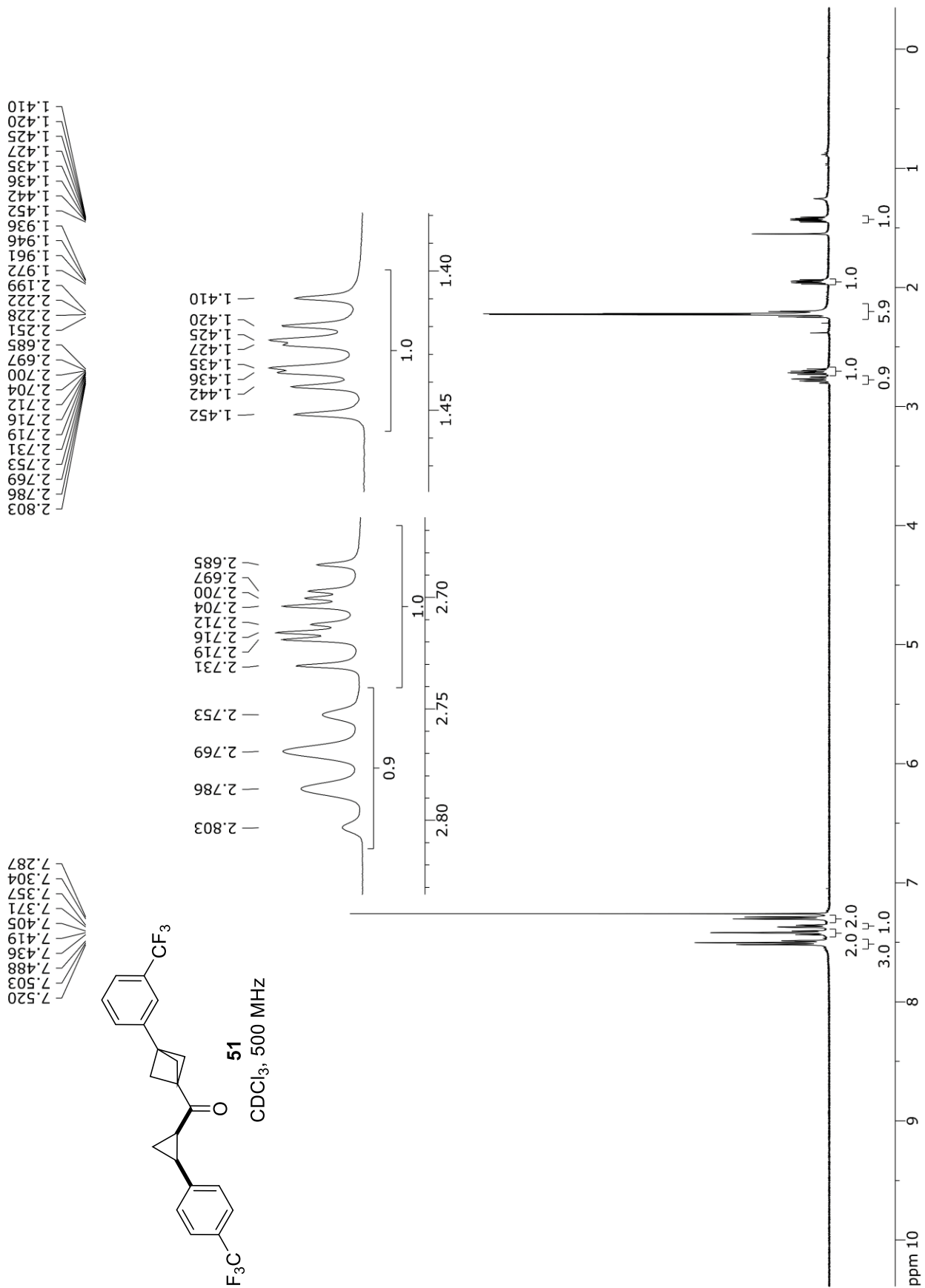
-62.25  
-62.62

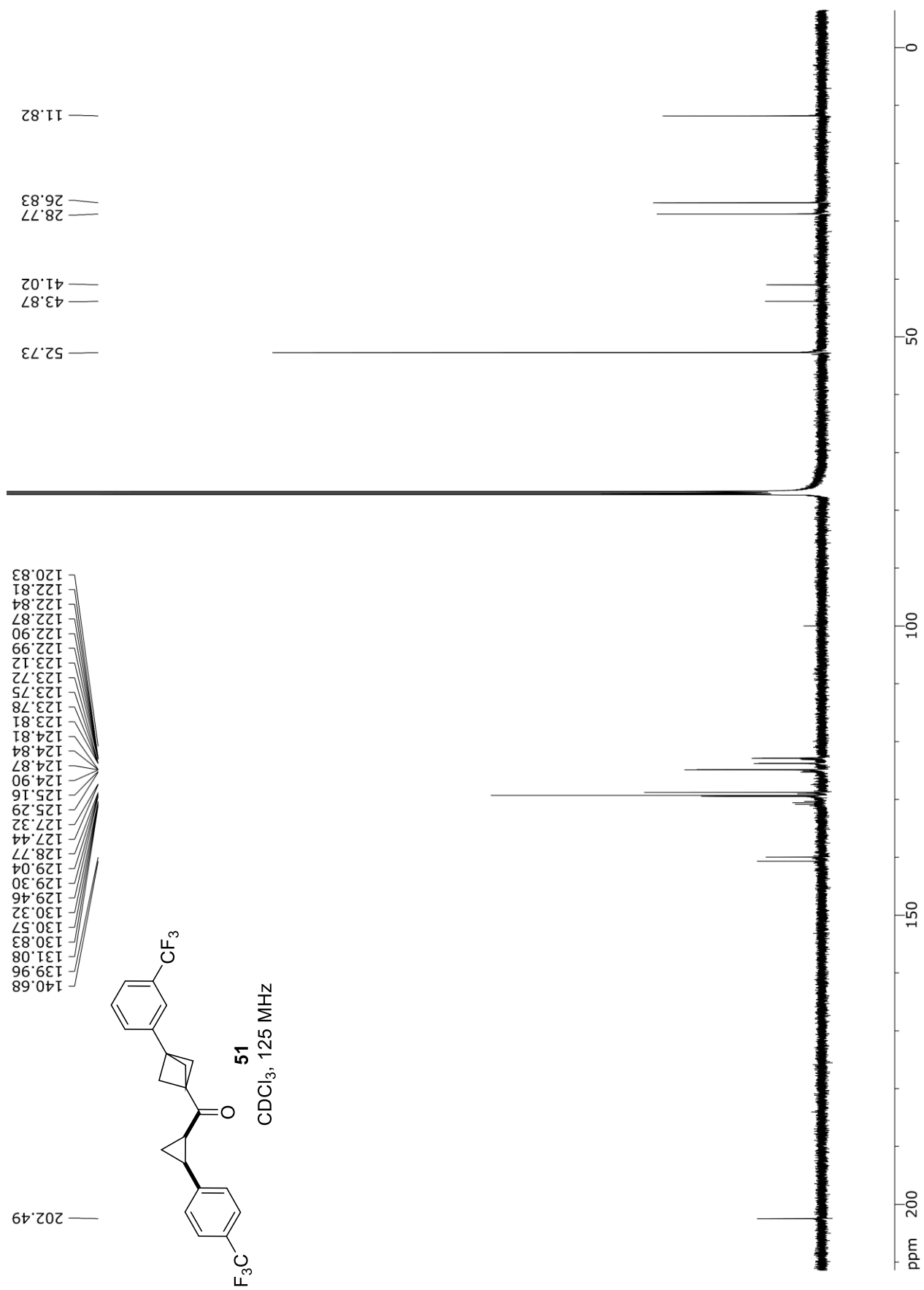


49

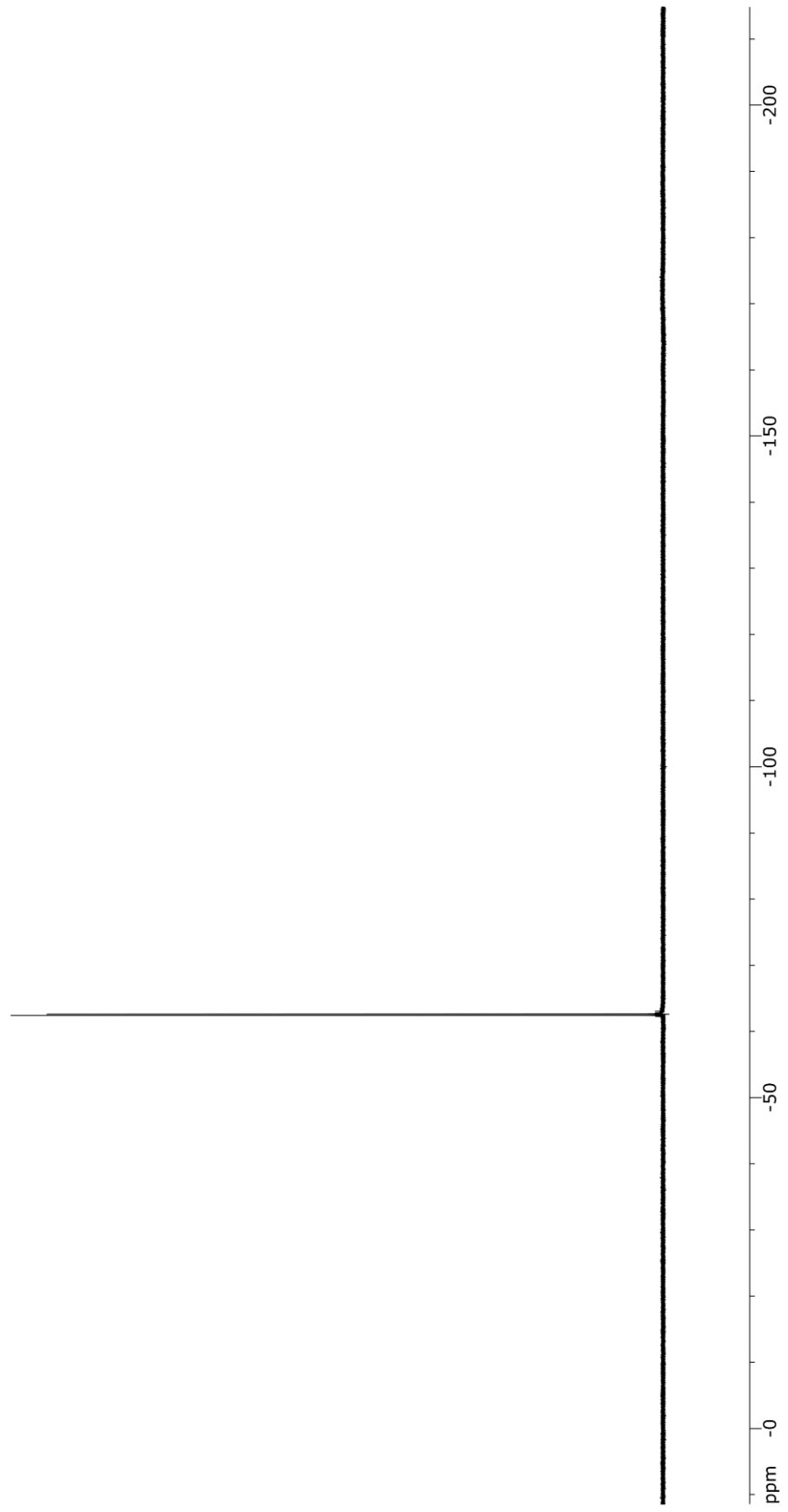
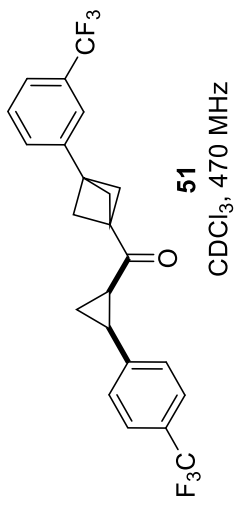
CDCl<sub>3</sub>, 470 MHz





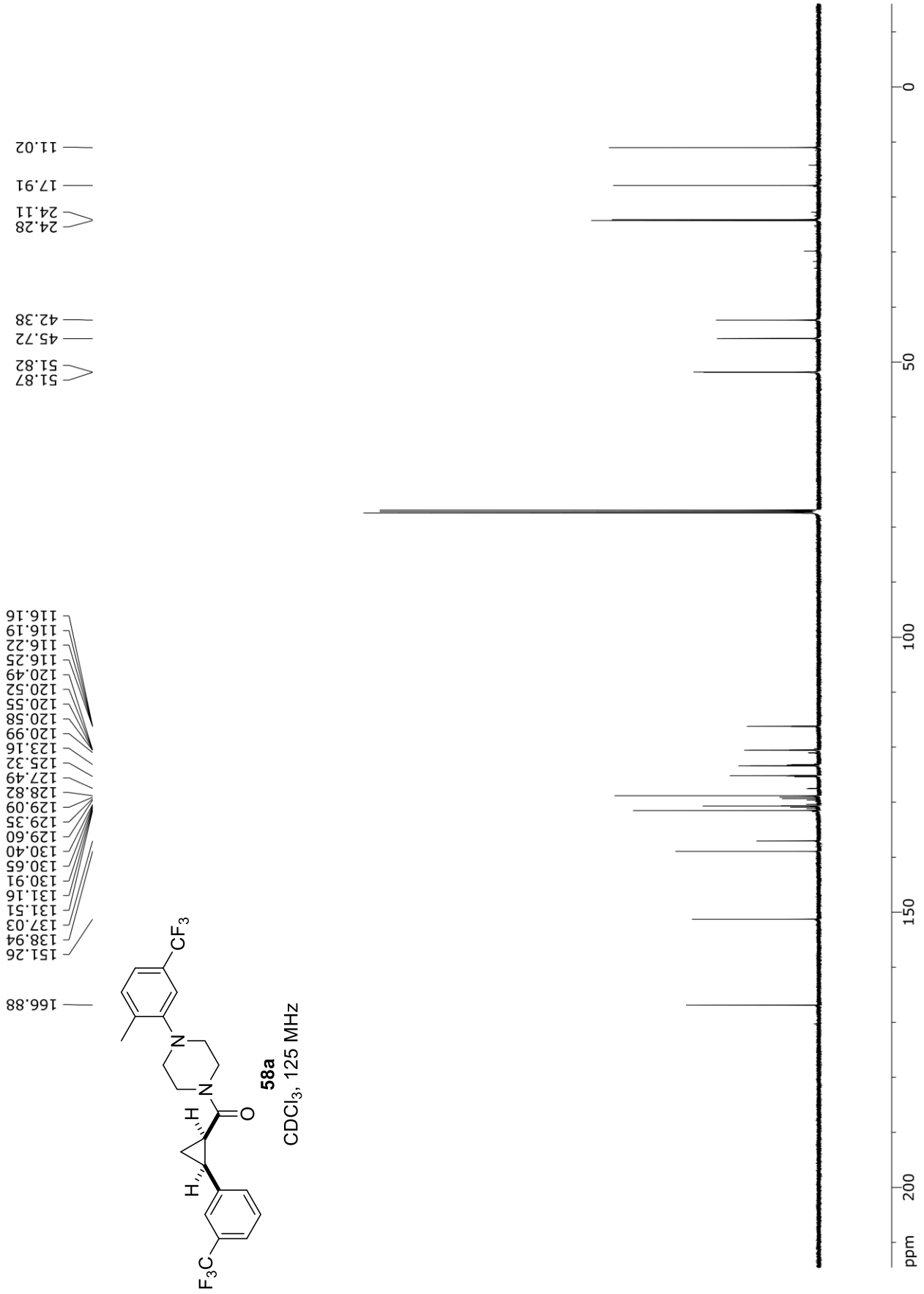


-62.63  
-62.41

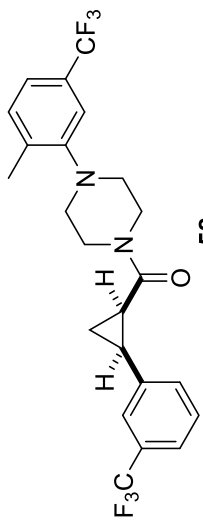








-62.60  
-62.41



**58a**

$\text{CDCl}_3$ , 470 MHz



ppm

-0

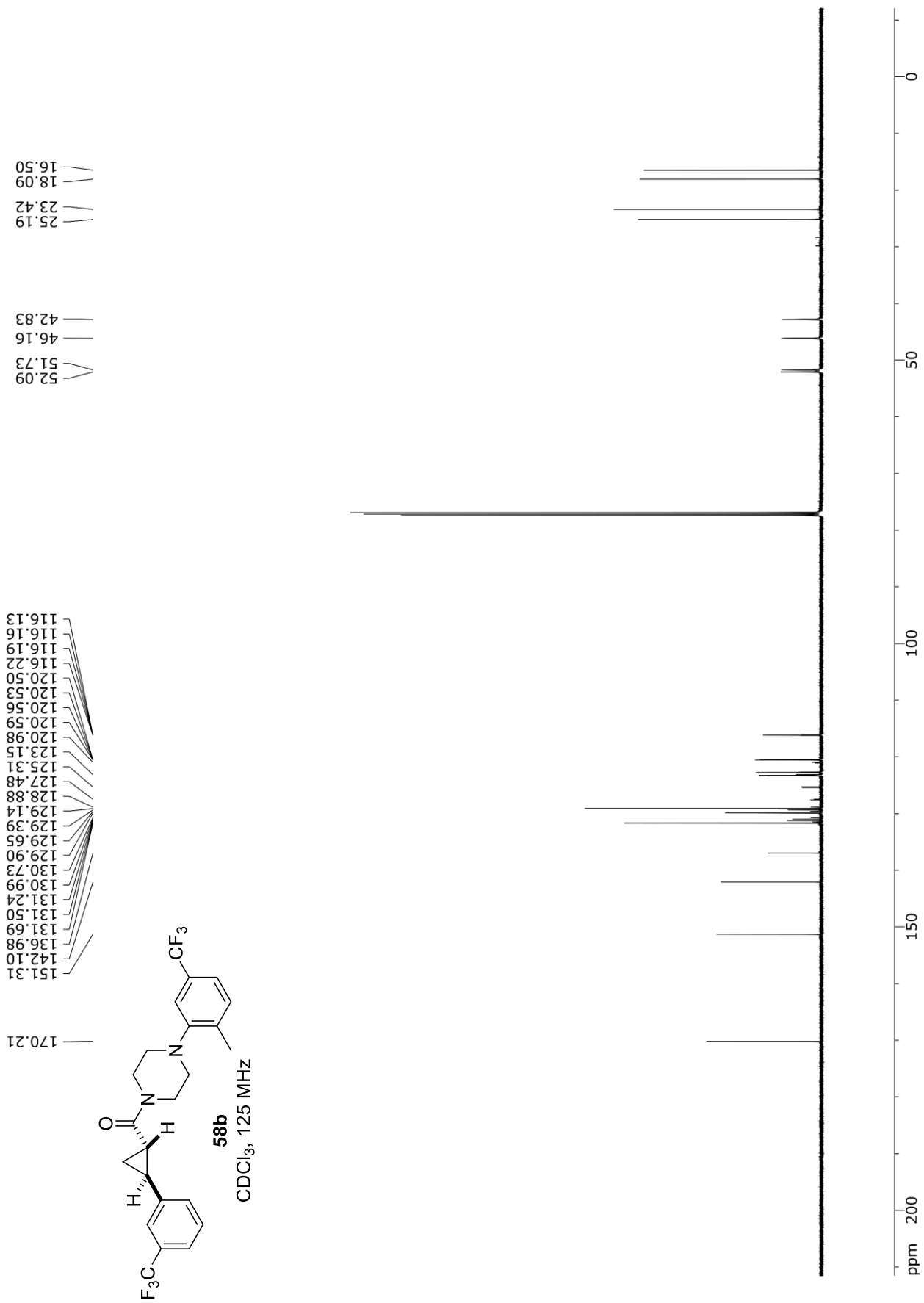
-50

-100

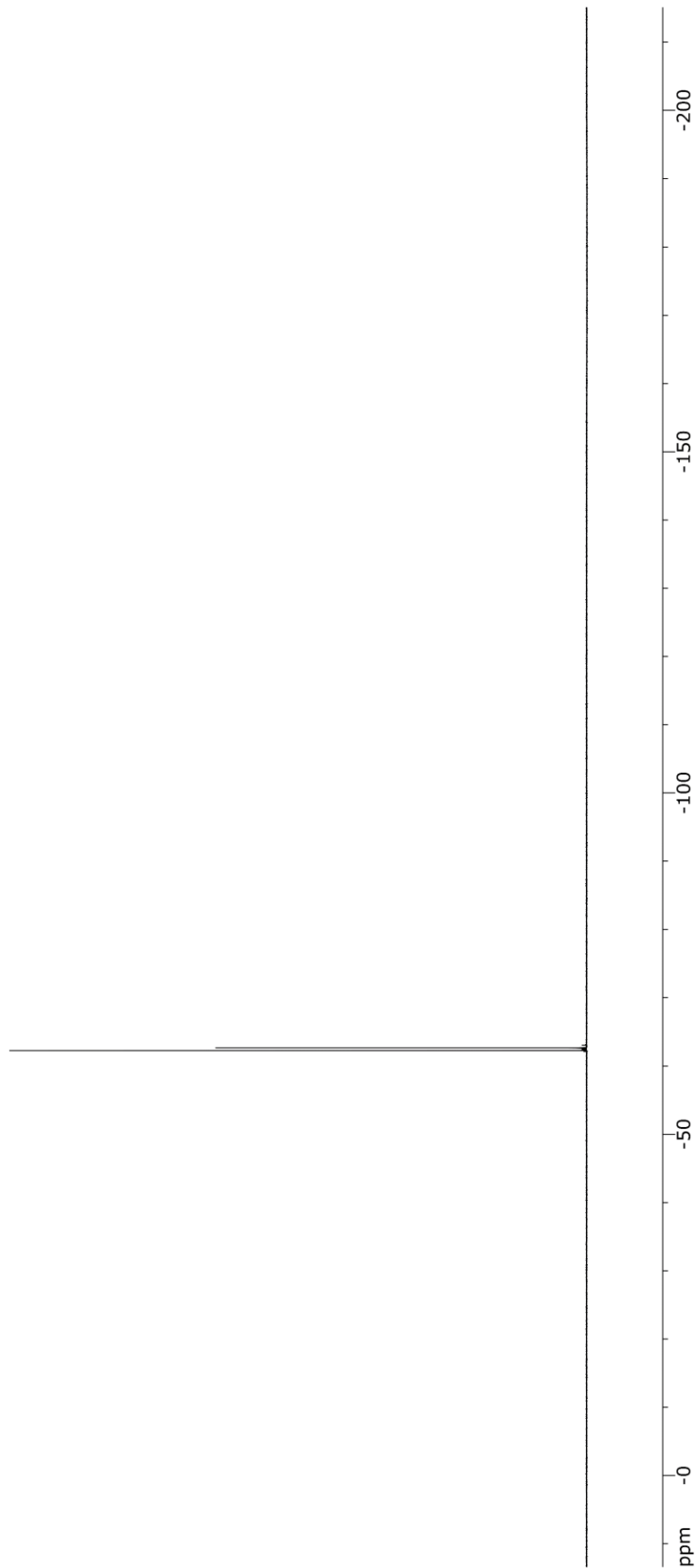
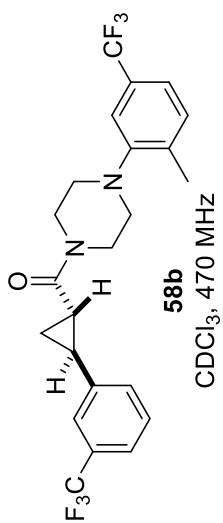
-150

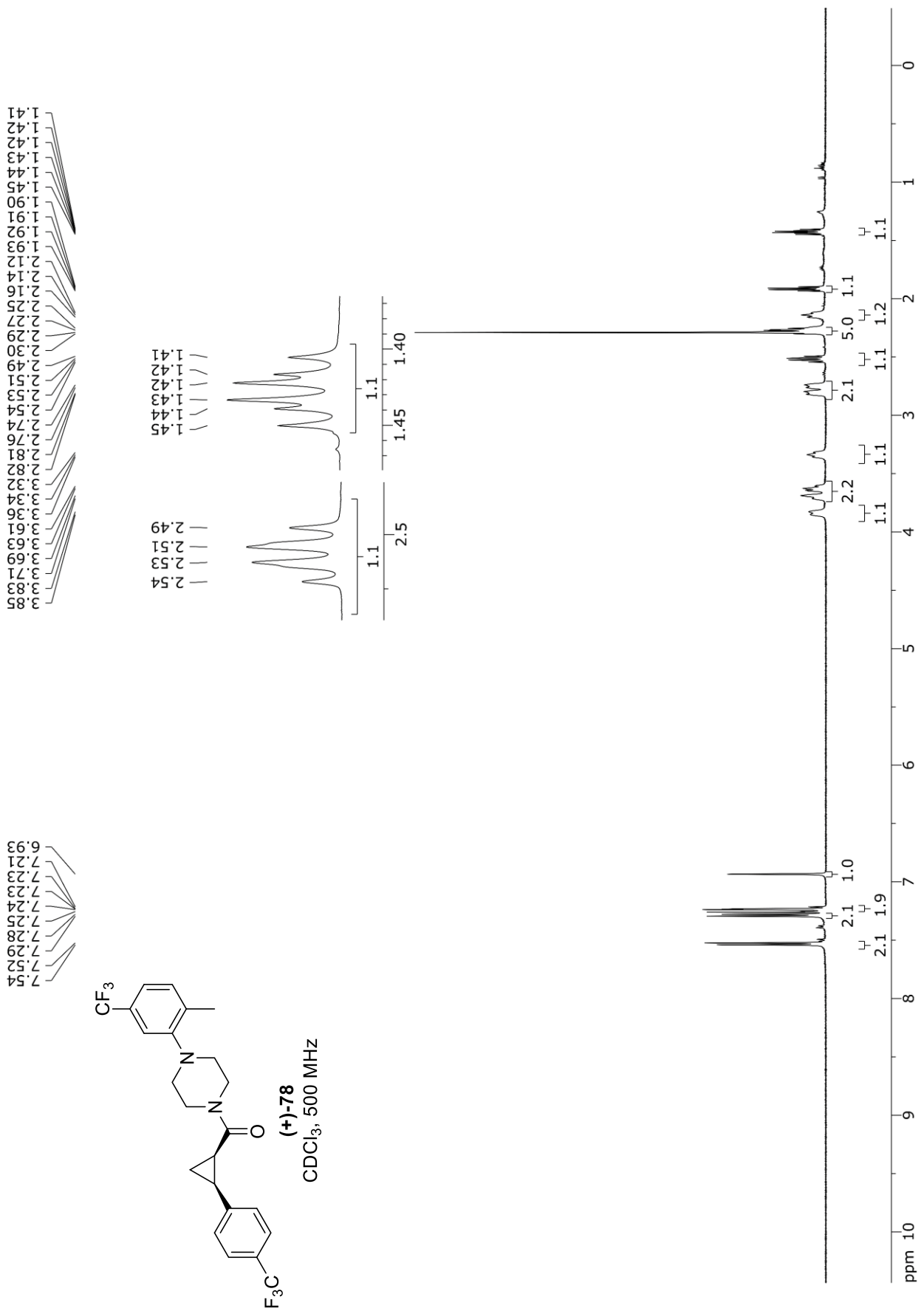
-200

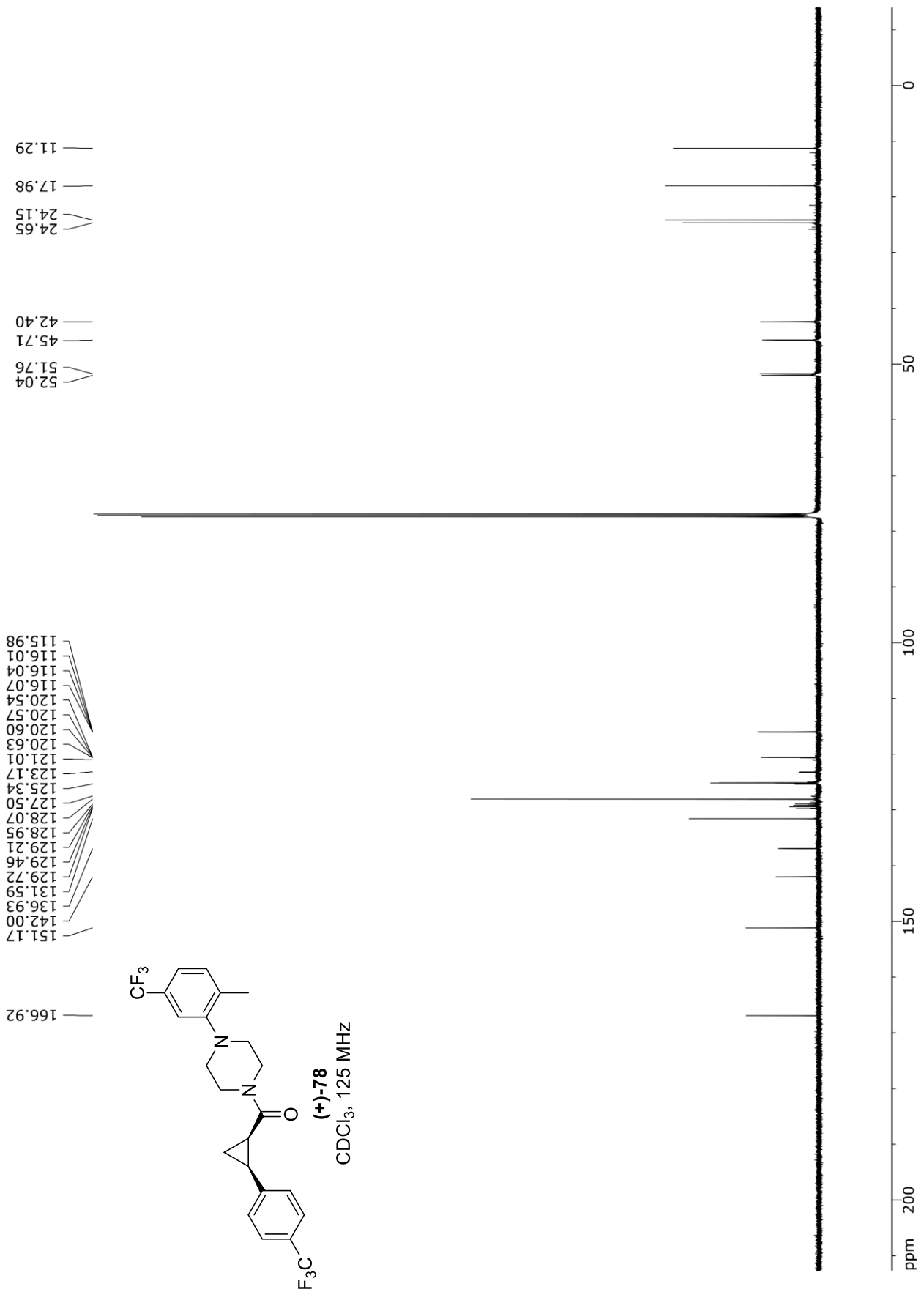




-62.27  
-62.64

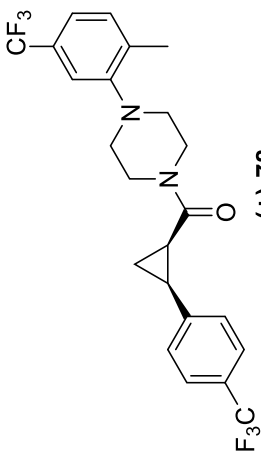




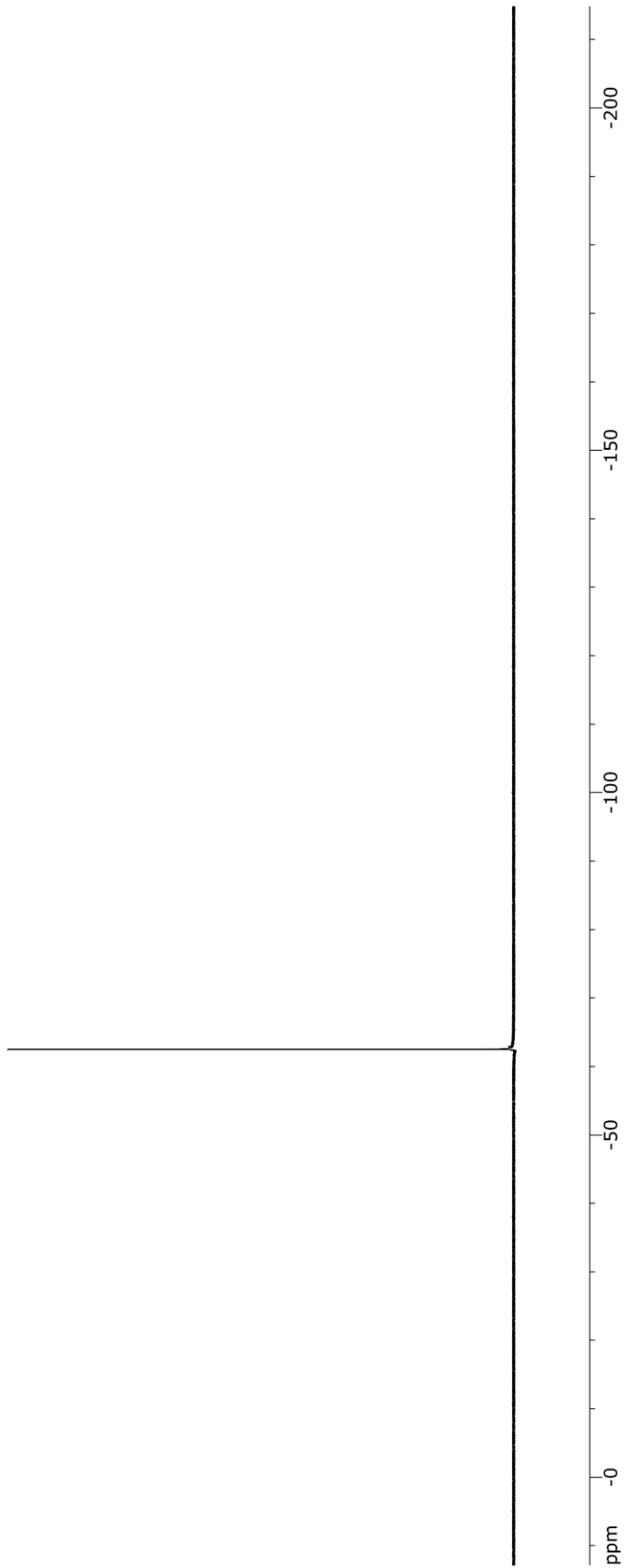




-62.47  
-62.53

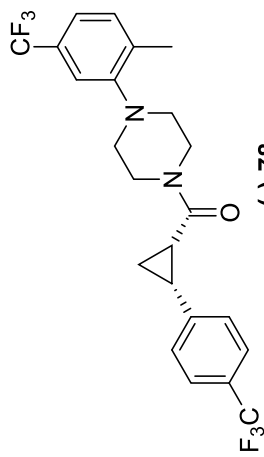


(+)-78  
CDCl<sub>3</sub>, 470 MHz

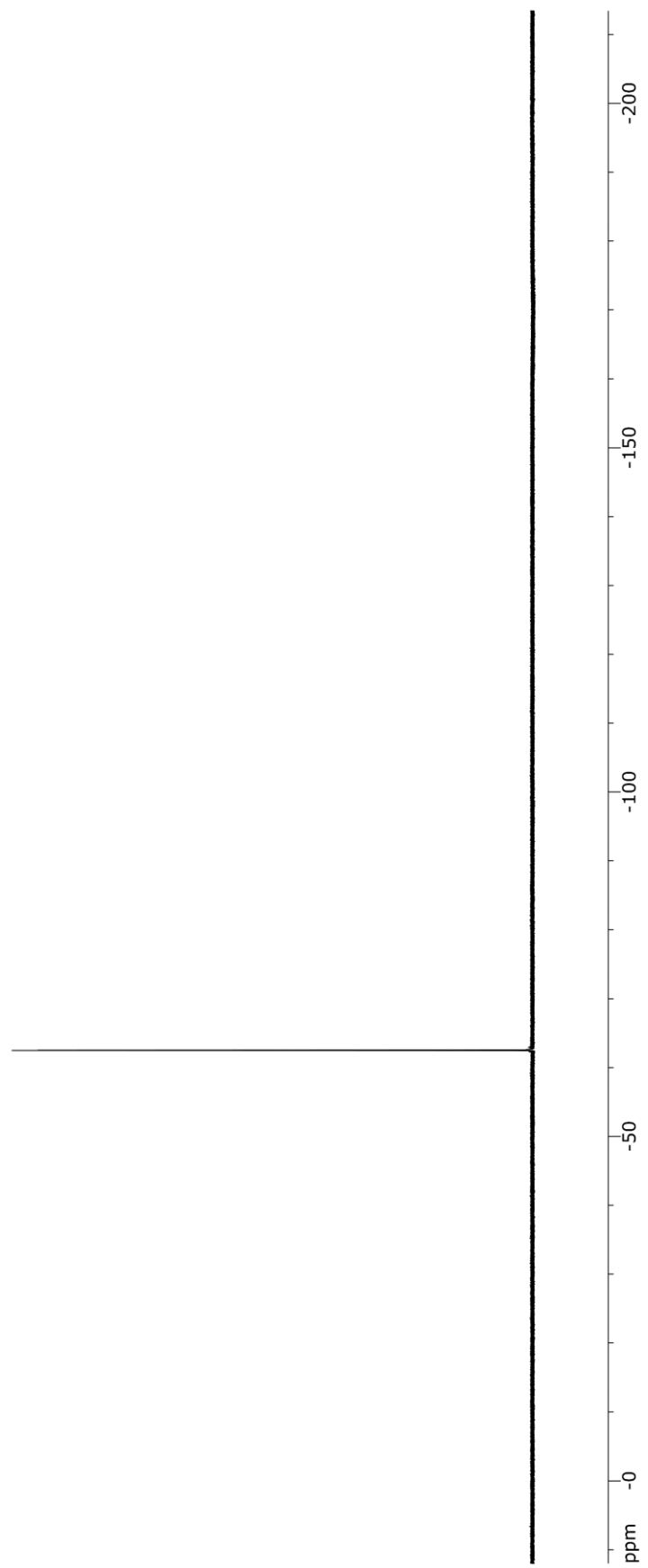


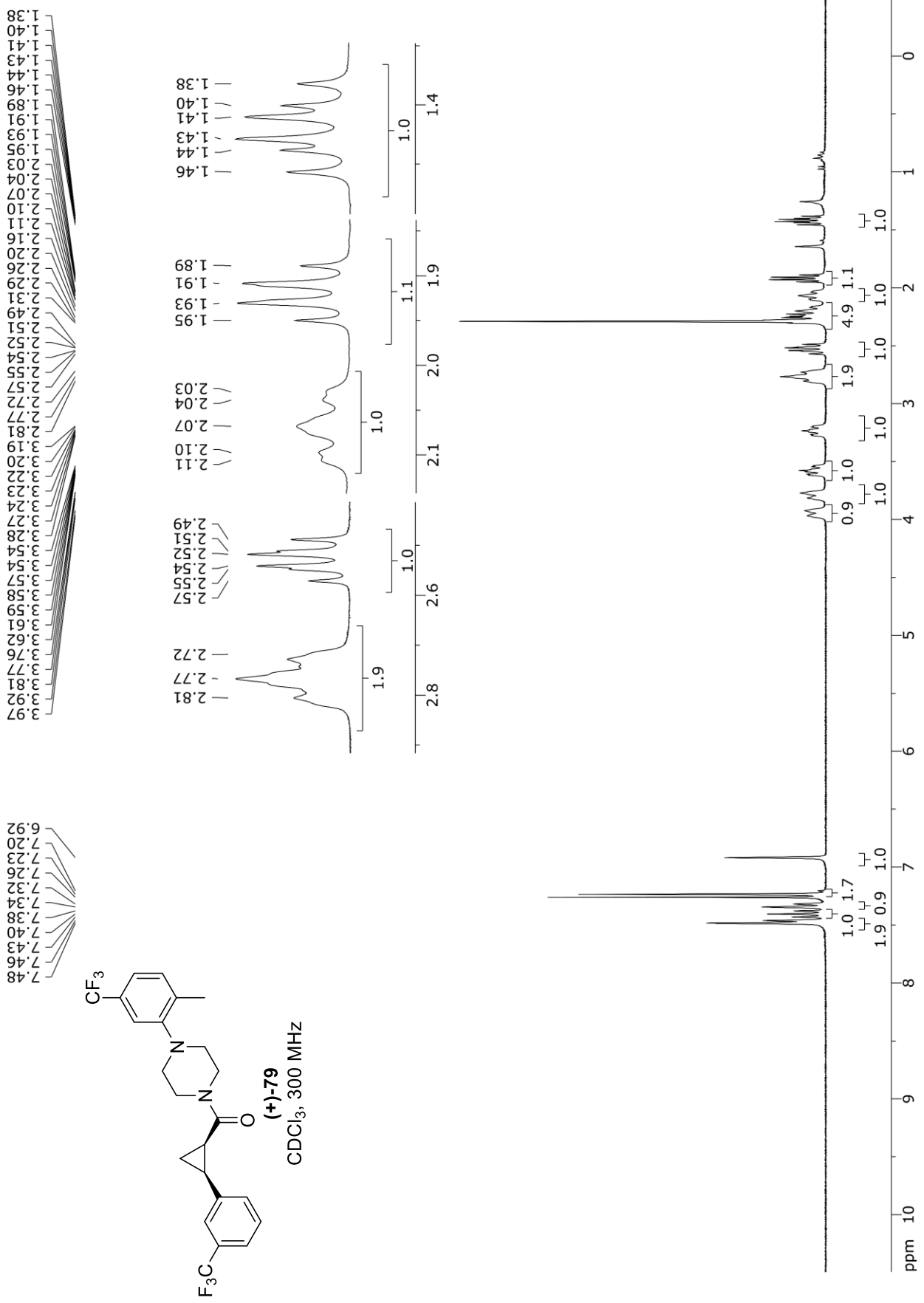


-62.54  
-62.47

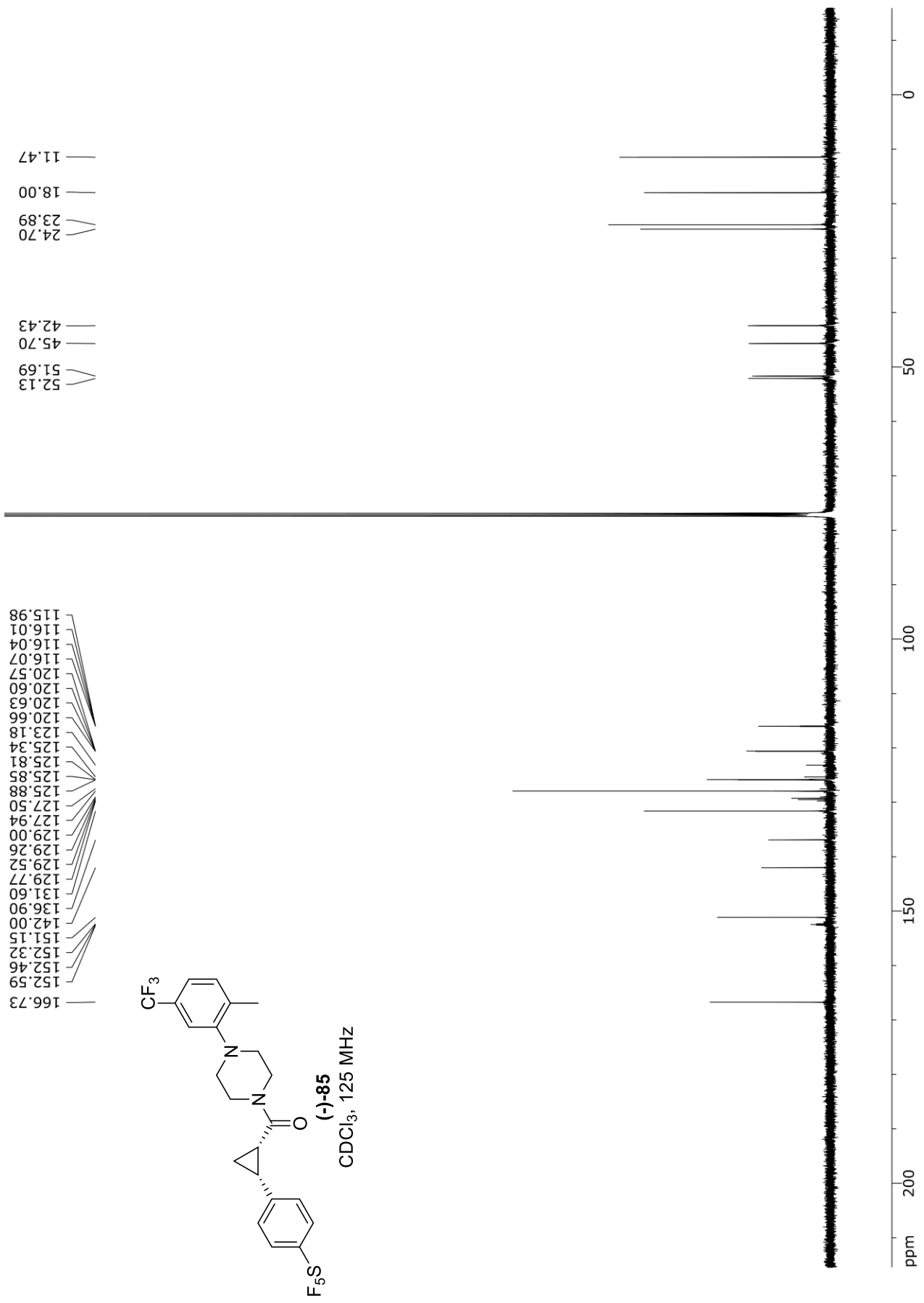


(-)-78  
CDCl<sub>3</sub>, 470 MHz

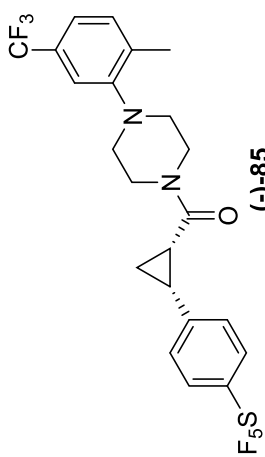




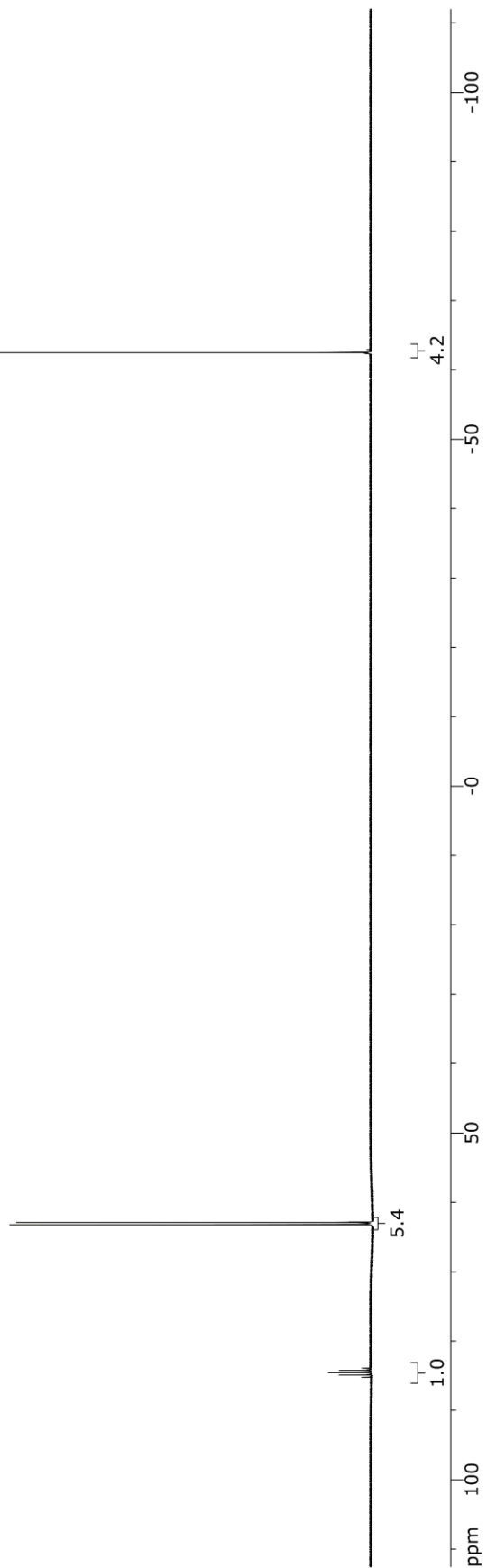




85.20  
84.88  
84.57  
84.25  
83.93  
63.20  
62.89

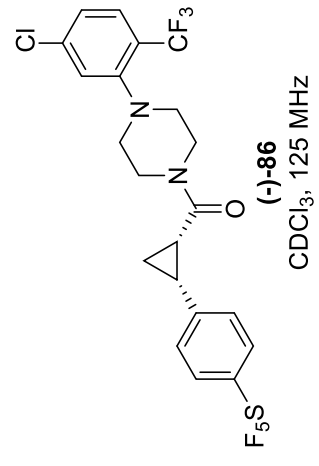
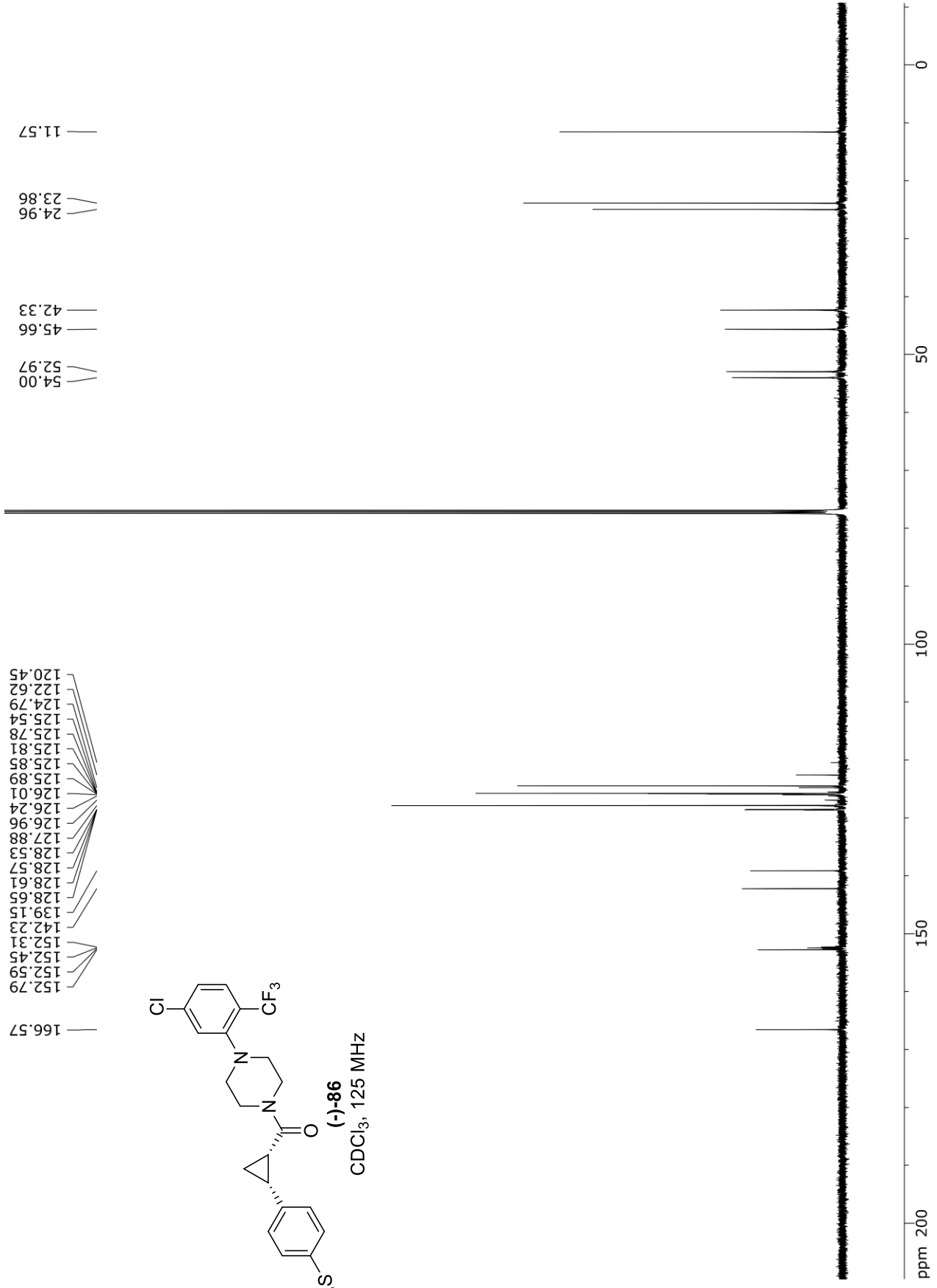


-62.47

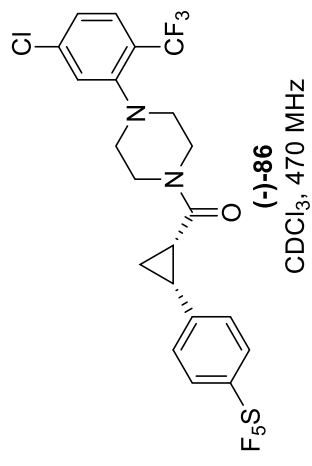








85.43  
85.11  
84.79  
84.47  
84.15  
63.50  
63.18

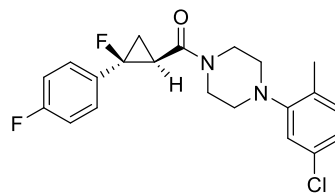
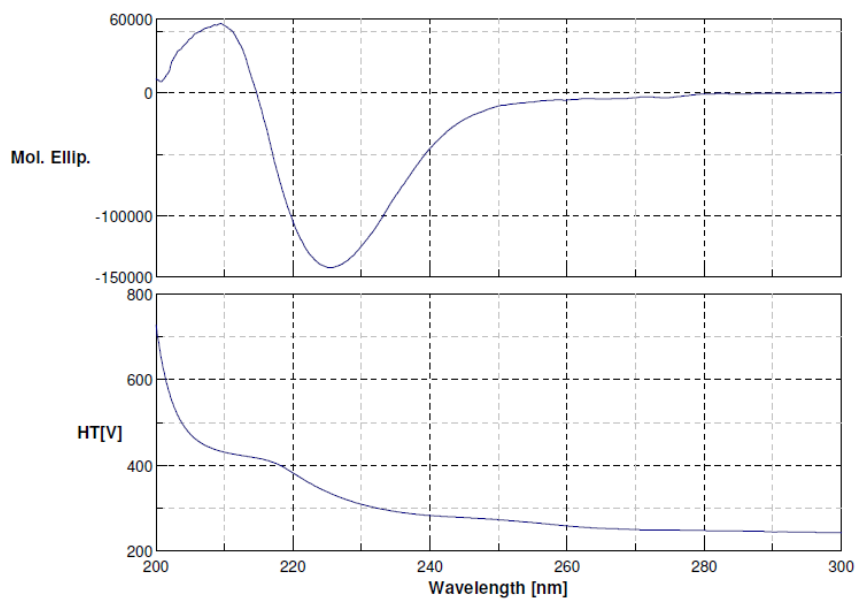


-60.36



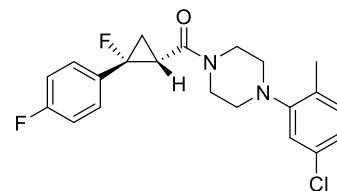
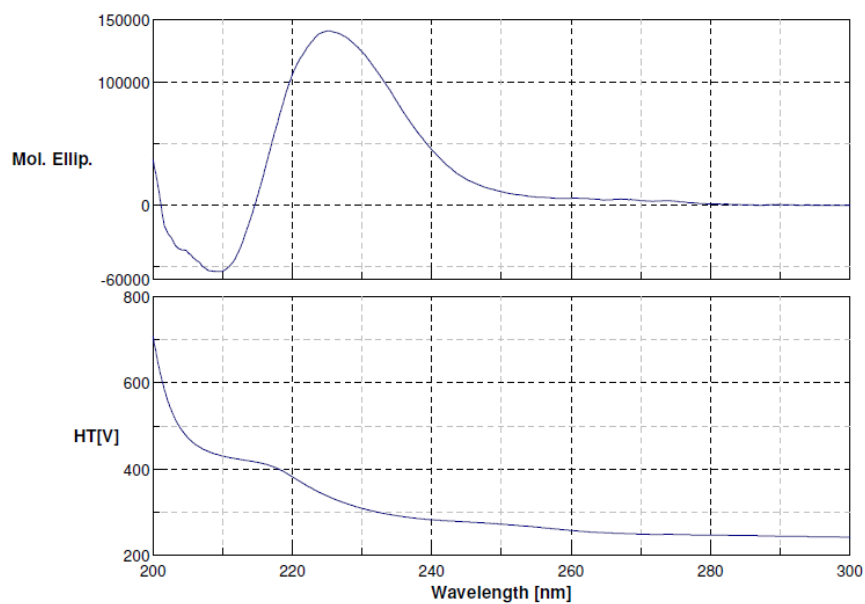
## **APPENDIX B**

### **CIRCULAR DICHROISM SPECTRA**



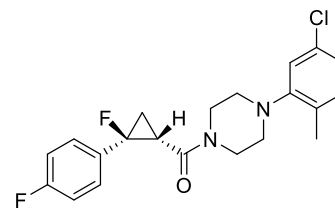
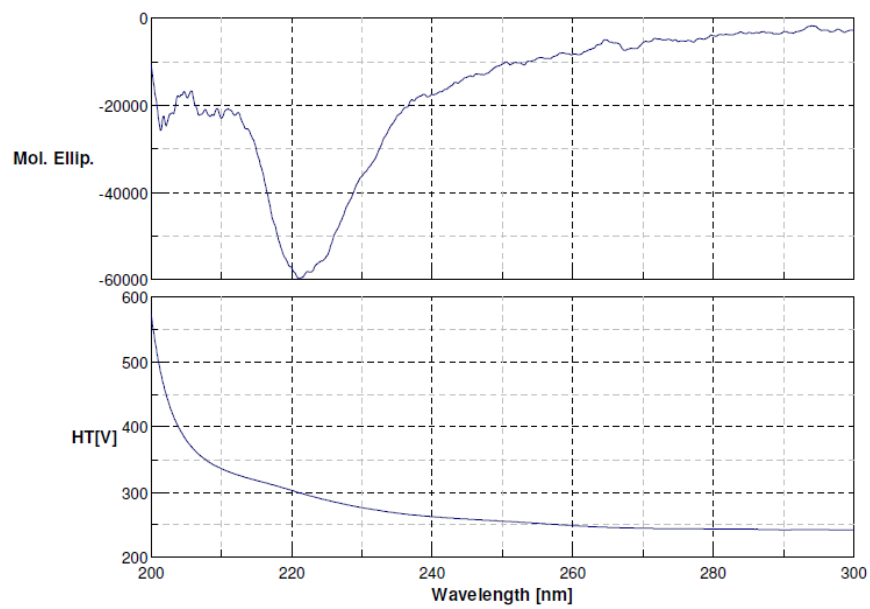
$c = 2.97 \times 10^{-5} \text{ M (MeOH)}$   
 $\lambda_{\text{max}} = 225.4 \text{ nm}$   
 $\theta = -144129 \text{ deg} \cdot \text{cm}^2/\text{dmol}$

**Figure 43.** CD spectra for (-)-5a.



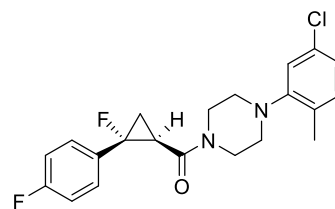
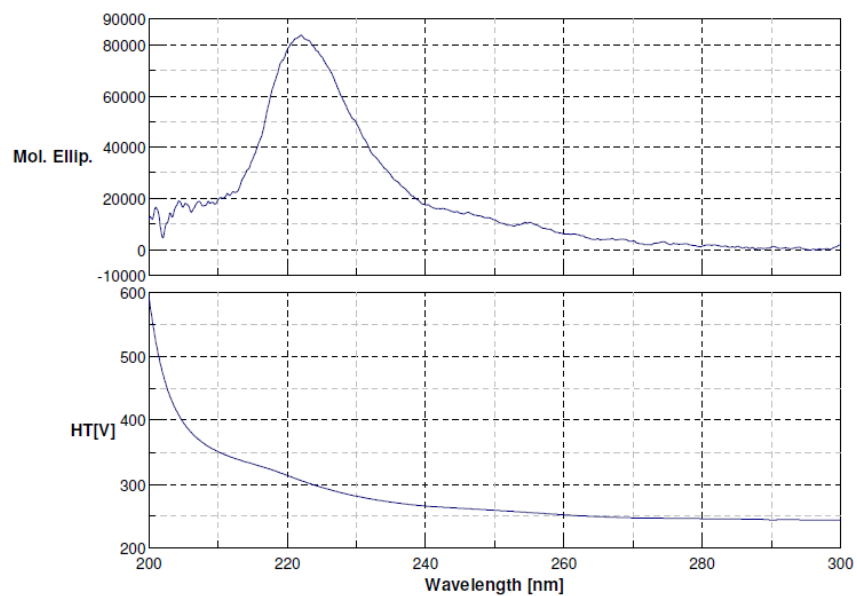
$c = 2.97 \times 10^{-5} \text{ M (MeOH)}$   
 $\lambda_{\text{max}} = 225.4 \text{ nm}$   
 $\theta = +142885 \text{ deg} \cdot \text{cm}^2/\text{dmol}$

**Figure 44.** CD spectra for (+)-5a.



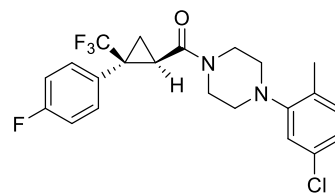
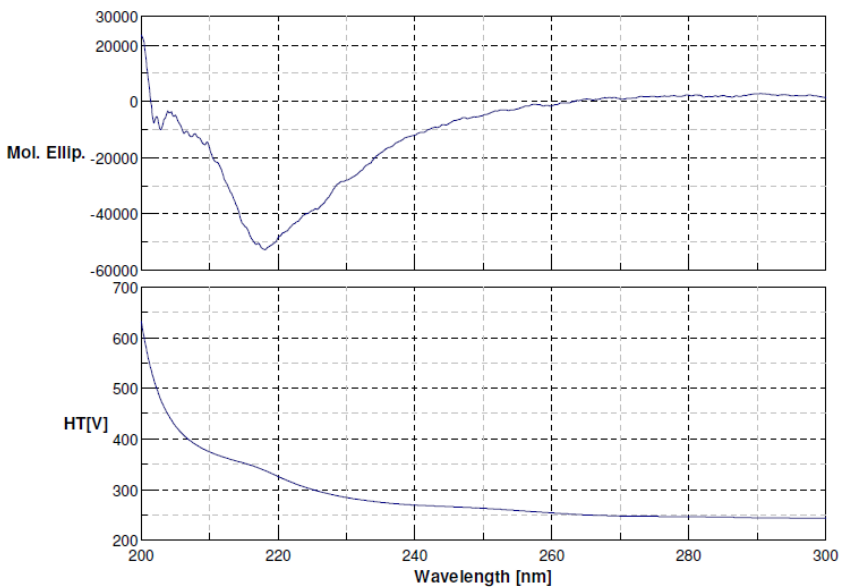
$c = 7.26 \times 10^{-6} \text{ M (MeOH)}$   
 $\lambda_{\text{max}} = 221.1 \text{ nm}$   
 $\theta = -60136 \text{ deg}^{\circ}\text{cm}^2/\text{dmol}$

**Figure 45.** CD spectra for (-)-**5b**.



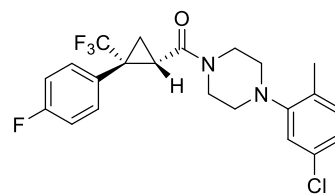
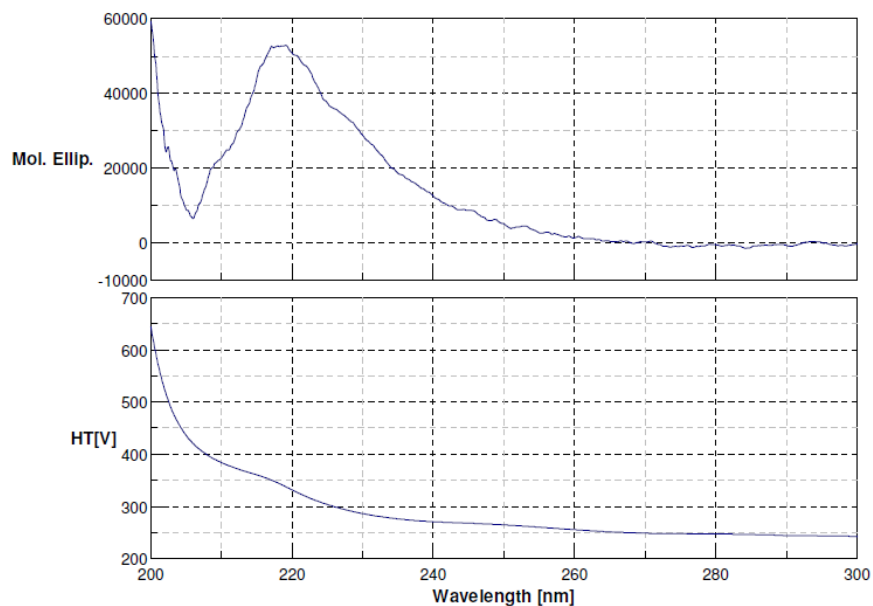
$c = 6.96 \times 10^{-6} \text{ M (MeOH)}$   
 $\lambda_{\text{max}} = 222.0 \text{ nm}$   
 $\theta = +84327 \text{ deg}^{\circ}\text{cm}^2/\text{dmol}$

**Figure 46.** CD spectra for (+)-**5b**.



$c = 1.29 \times 10^{-5} \text{ M (MeOH)}$   
 $\lambda_{\text{max}} = 218.1 \text{ nm}$   
 $\theta = -52992 \text{ deg} \cdot \text{cm}^2/\text{dmol}$

**Figure 47.** CD spectra for (-)-**6a**.



$c = 1.42 \times 10^{-5} \text{ M (MeOH)}$   
 $\lambda_{\text{max}} = 219.1 \text{ nm}$   
 $\theta = +52344 \text{ deg} \cdot \text{cm}^2/\text{dmol}$

**Figure 48.** CD spectra for (+)-**6a**.

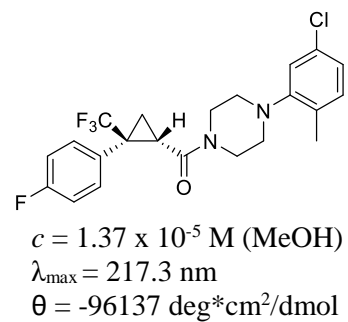
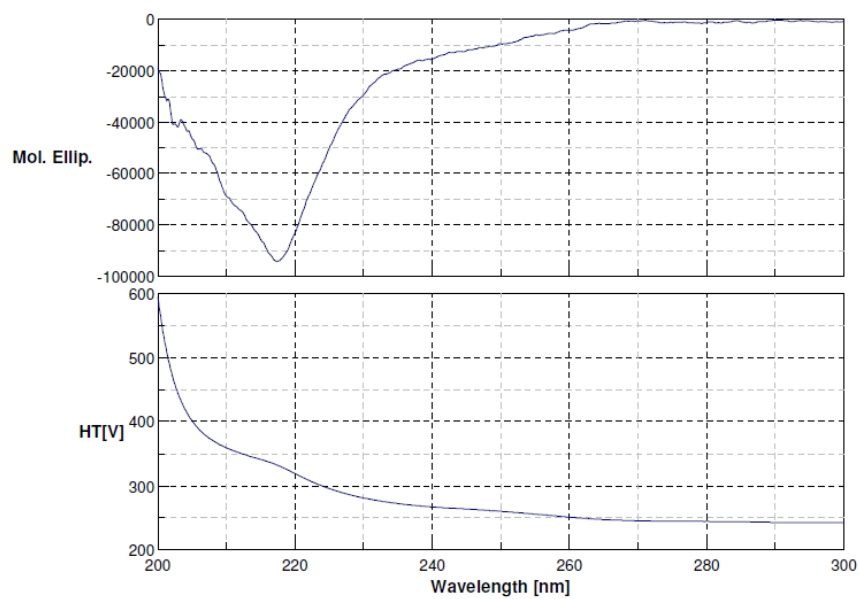


**Figure 49.** CD spectra for (-)-**6b**.

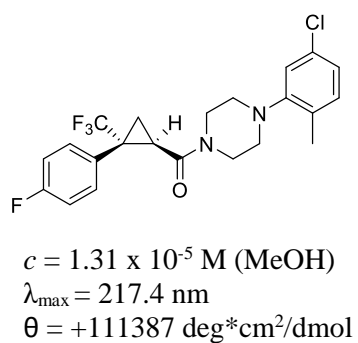
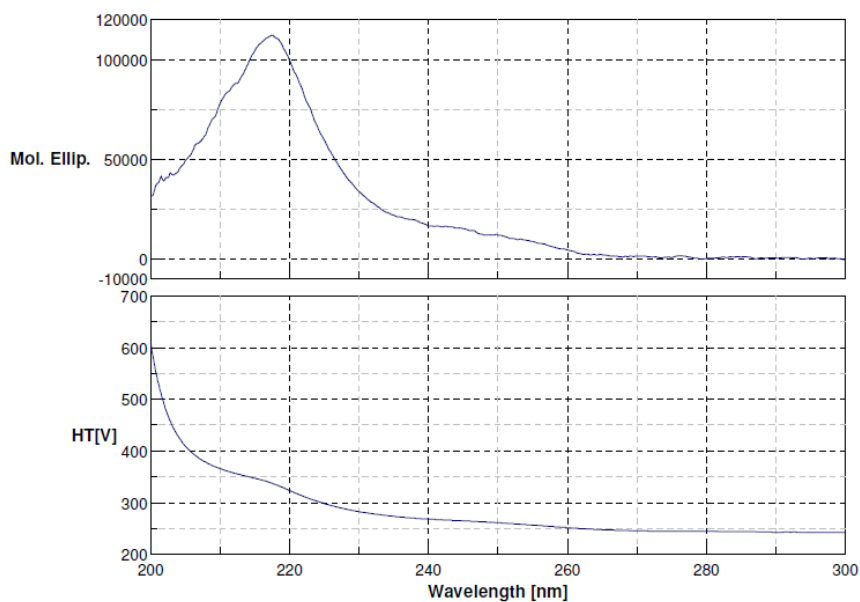
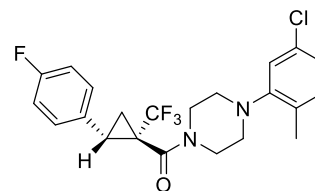
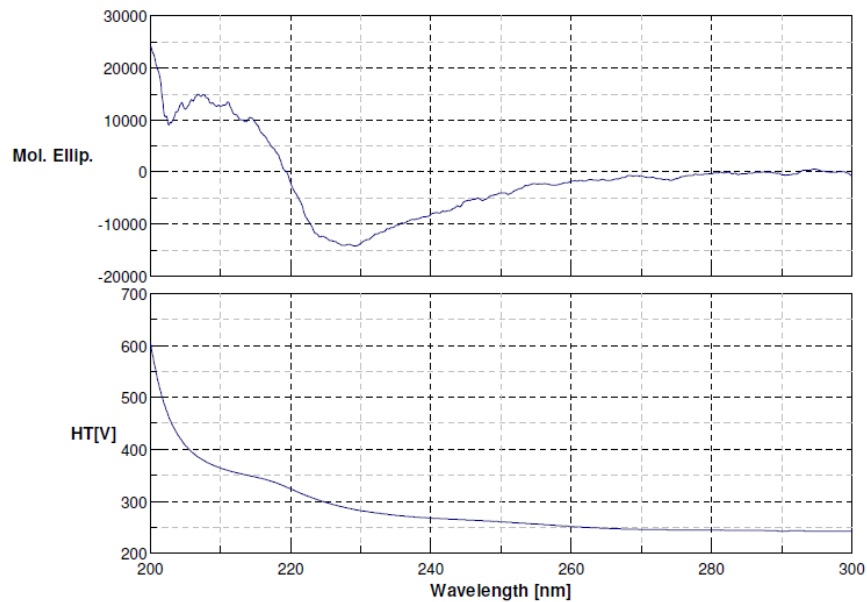
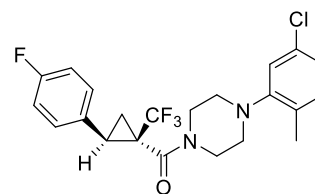
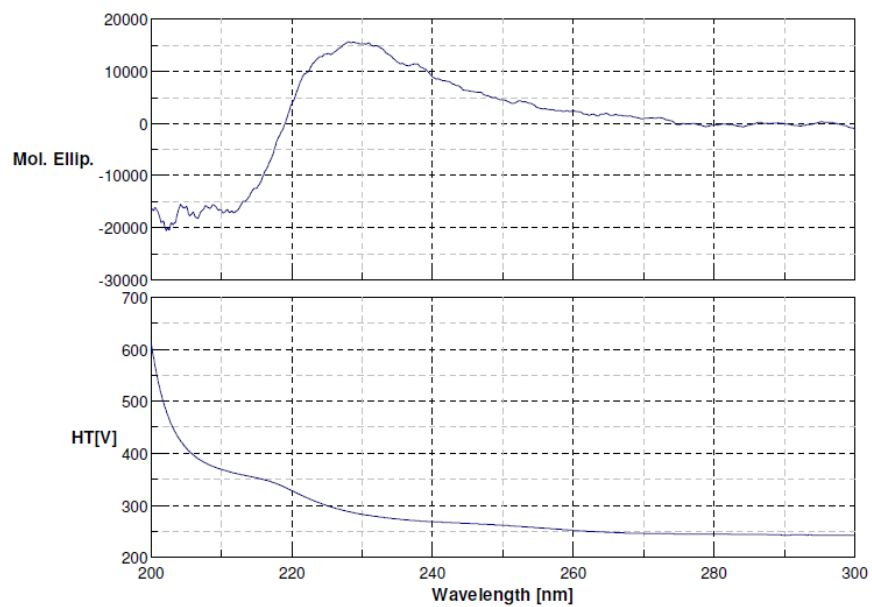


**Figure 50.** CD spectra for (+)-**6b**.



$c = 1.37 \times 10^{-5} \text{ M (MeOH)}$   
 $\lambda_{\text{max}} = 229.0 \text{ nm}$   
 $\theta = -14456 \text{ deg} \cdot \text{cm}^2/\text{dmol}$

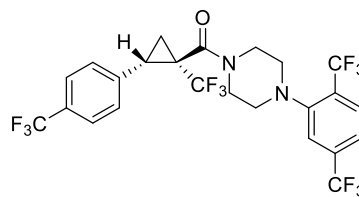
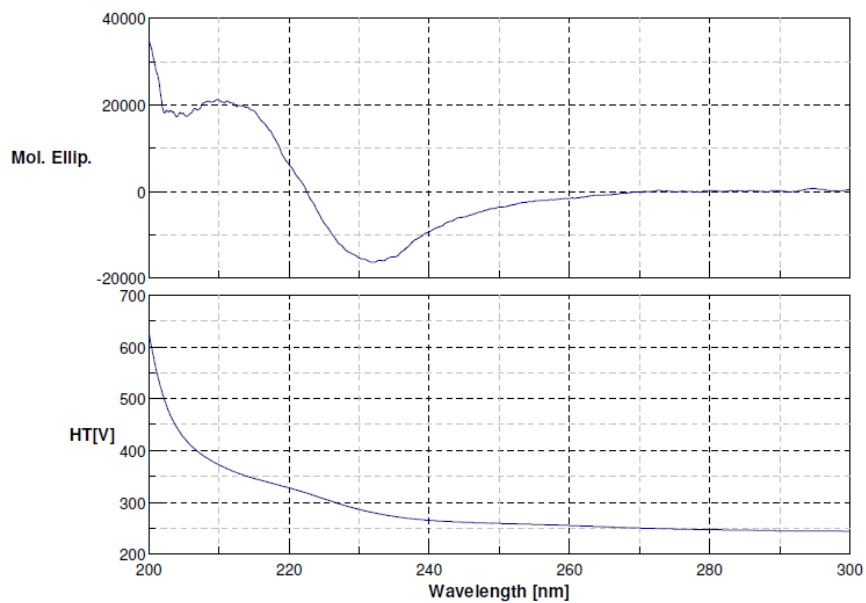
**Figure 51.** CD spectra for (-)-11a.



$c = 1.36 \times 10^{-5} \text{ M (MeOH)}$   
 $\lambda_{\text{max}} = 228.0 \text{ nm}$   
 $\theta = +16193 \text{ deg} \cdot \text{cm}^2/\text{dmol}$

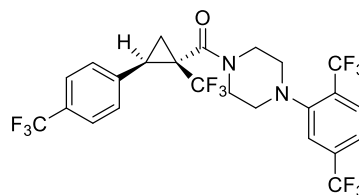
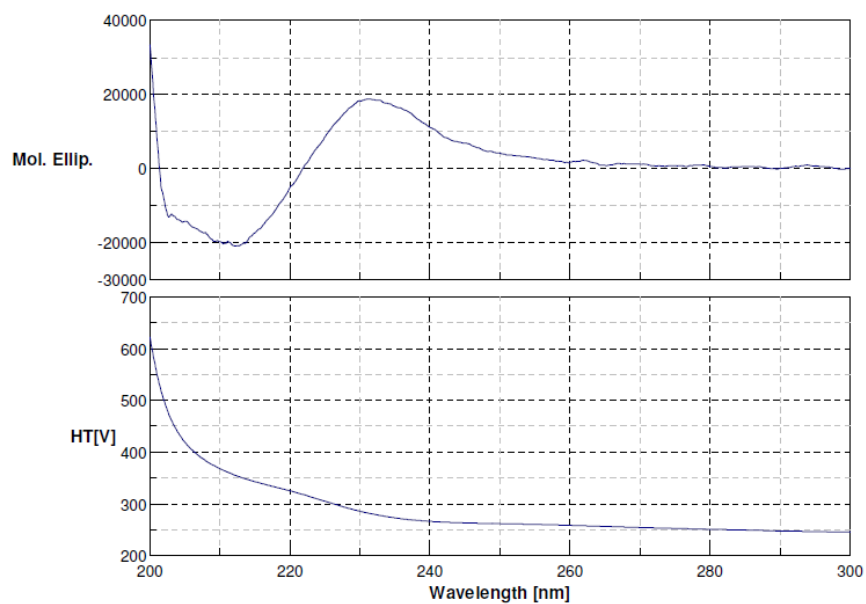
**Figure 52.** CD spectra for (+)-11a.





$c = 2.28 \times 10^{-5} \text{ M (MeOH)}$   
 $\lambda_{\text{max}} = 231.8 \text{ nm}$   
 $\theta = -16512 \text{ deg} \cdot \text{cm}^2 / \text{dmol}$

**Figure 53.** CD spectra for (-)-15.



$c = 1.94 \times 10^{-5} \text{ M (MeOH)}$   
 $\lambda_{\text{max}} = 231.3 \text{ nm}$   
 $\theta = +18537 \text{ deg} \cdot \text{cm}^2 / \text{dmol}$

**Figure 54.** CD spectra for (+)-15.

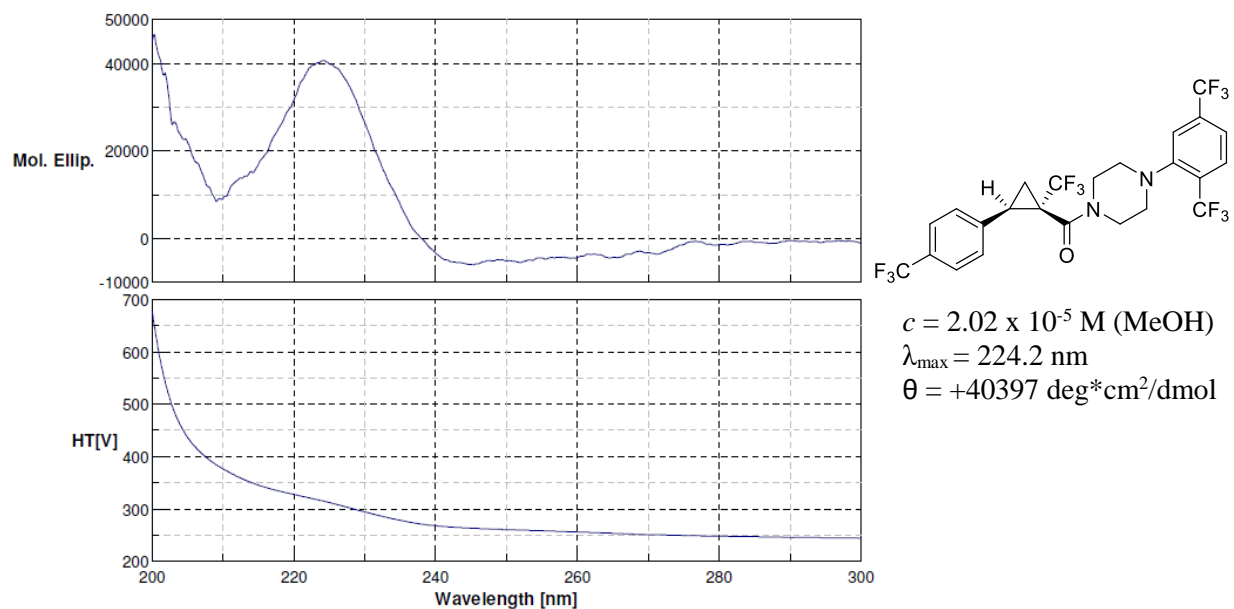


Figure 55. CD spectra for (-)-17.

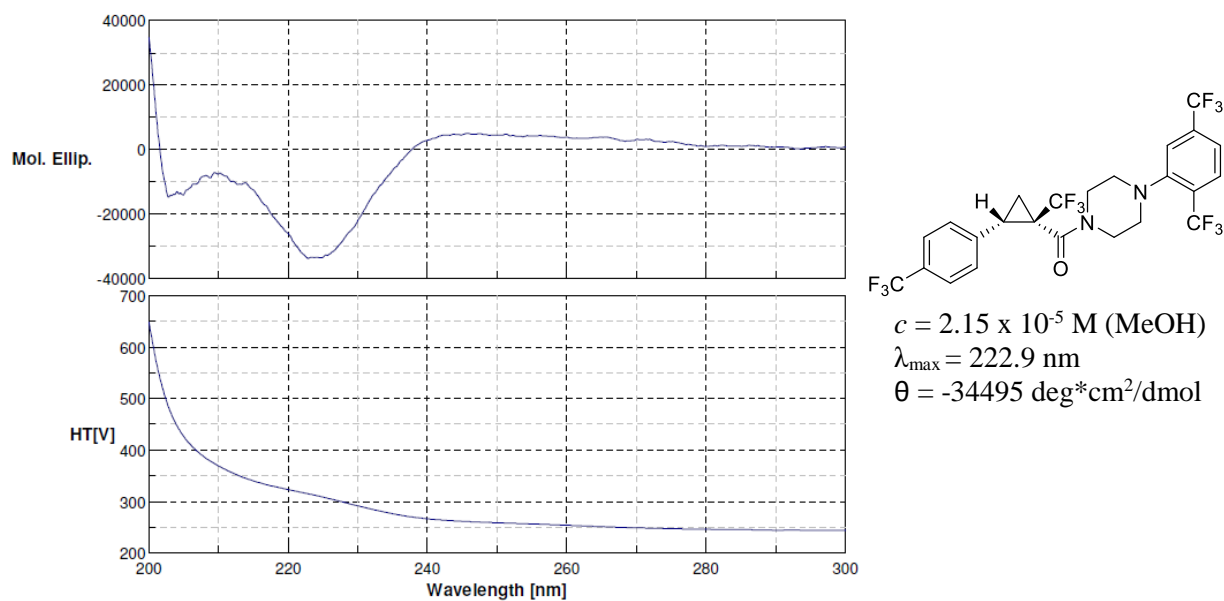
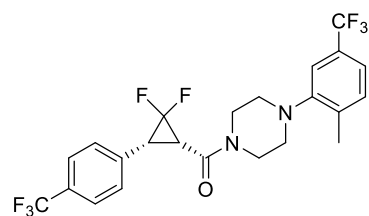
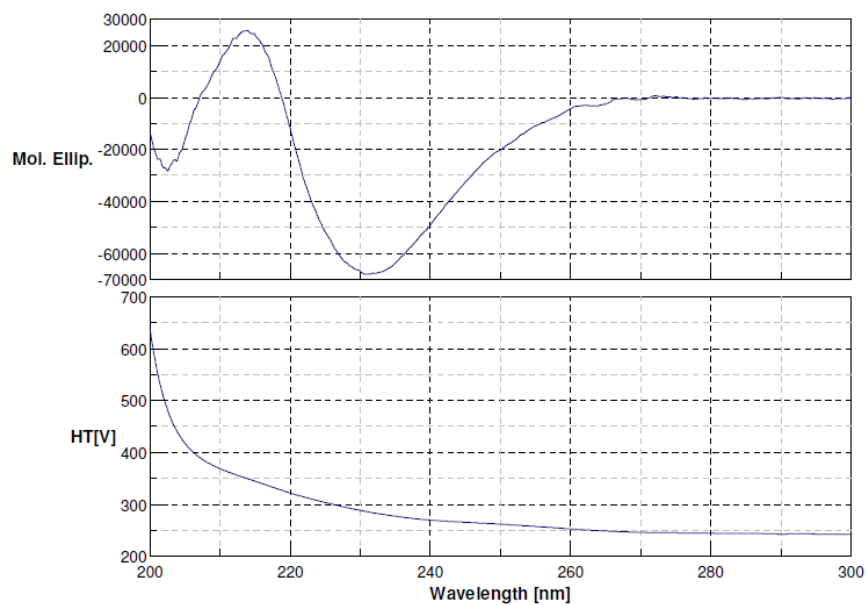
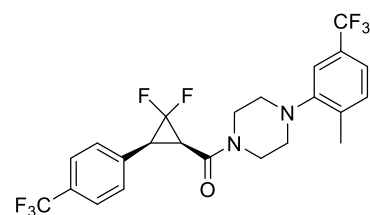
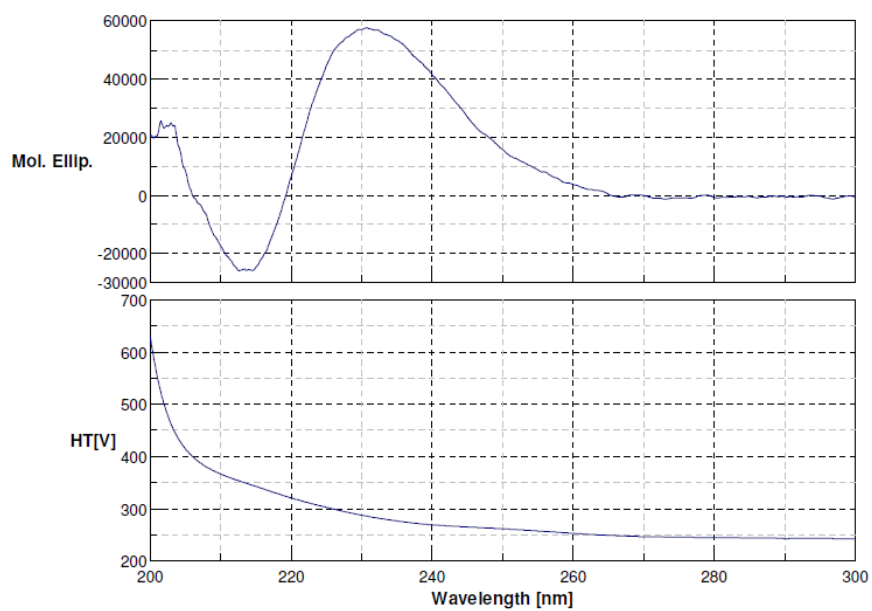


Figure 56. CD spectra for (+)-17.



$c = 1.18 \times 10^{-5} \text{ M (MeOH)}$   
 $\lambda_{\text{max}} = 231.2 \text{ nm}$   
 $\theta = -69315 \text{ deg} \cdot \text{cm}^2/\text{dmol}$

**Figure 57.** CD spectra for (-)-34.



$c = 1.29 \times 10^{-5} \text{ M (MeOH)}$   
 $\lambda_{\text{max}} = 230.7 \text{ nm}$   
 $\theta = +58061 \text{ deg} \cdot \text{cm}^2/\text{dmol}$

**Figure 58.** CD spectra for (+)-34.

## **APPENDIX C**

### **X-RAY CRYSTALLOGRAPHY DATA**

X-ray structural information for *trans*-cyclopropyl carboxylic acid **3b**:

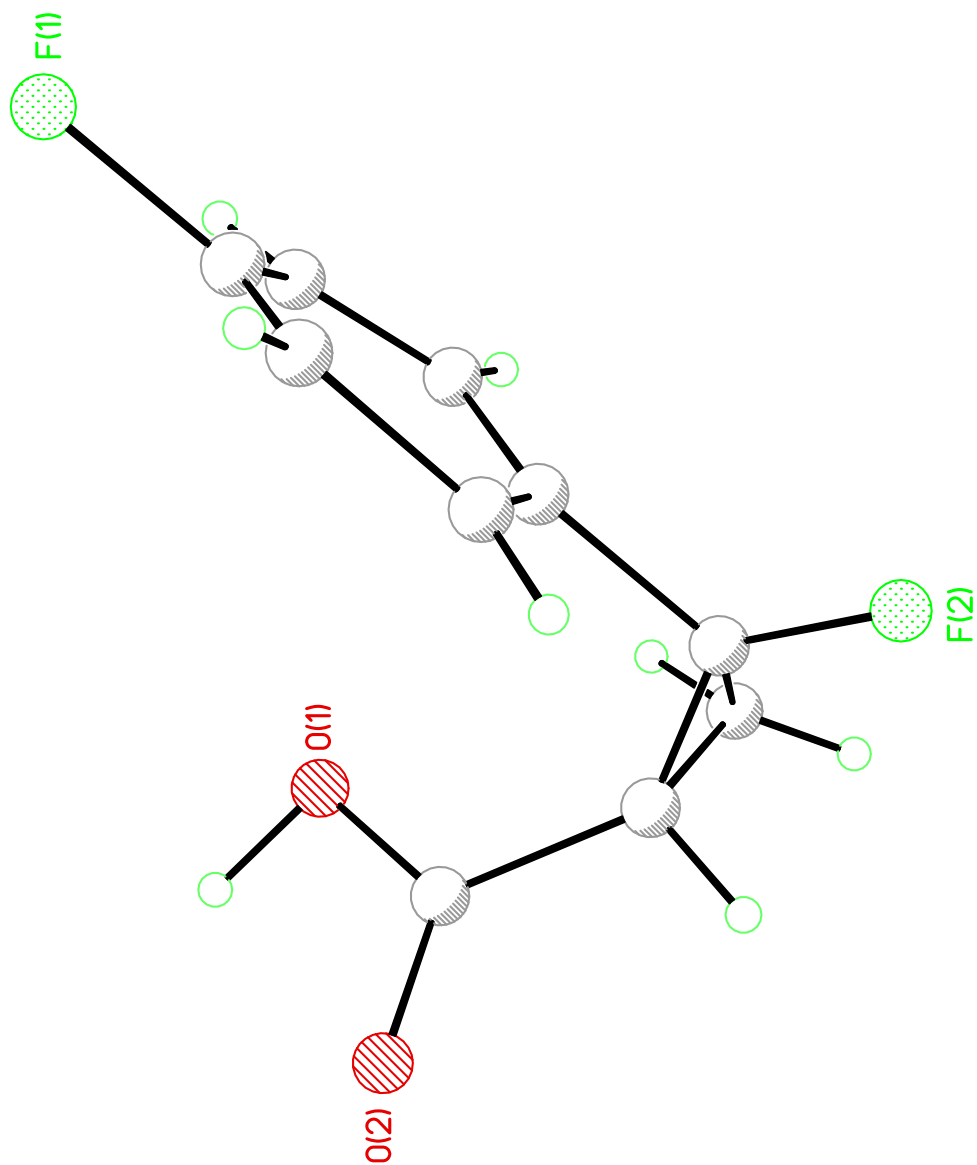


**Table 9.** Crystal Data for **3b**.

<b>Chemical formula</b>	C <sub>10</sub> H <sub>8</sub> F <sub>2</sub> O <sub>2</sub>	
<b>Formula weight</b>	198.16 g/mol	
<b>Temperature</b>	230(2) K	
<b>Wavelength</b>	1.54184 Å	
<b>Crystal system</b>	monoclinic	
<b>Space group</b>	P 1 21/c 1	
<b>Unit cell dimensions</b>	a = 12.4315(14) Å	α = 90°
	b = 5.6124(7) Å	β = 109.803(7)°
	c = 13.6208(13) Å	γ = 90°
<b>Volume</b>	894.13(18) Å <sup>3</sup>	
<b>Z</b>	4	
<b>Density (calculated)</b>	1.472 g/cm <sup>3</sup>	
<b>Absorption coefficient</b>	1.122 mm <sup>-1</sup>	
<b>F(000)</b>	408	

**Table 10.** Data collection and structure refinement for **3b**.

<b>Diffractometer</b>	Bruker X8 Prospector Ultra with Apex II CCD	
<b>Radiation source</b>	IMuS, Cu Kα	
<b>Theta range for data collection</b>	3.78 to 83.53°	
<b>Index ranges</b>	-16<=h<=16, -6<=k<=6, -14<=l<=13	
<b>Reflections collected</b>	3550	
<b>Independent reflections</b>	1500 [R(int) = 0.0775]	
<b>Coverage of independent reflections</b>	75.1%	
<b>Absorption correction</b>	Multi-Scan	
<b>Structure solution technique</b>	direct methods	
<b>Structure solution program</b>	XT, VERSION 2014/5	
<b>Refinement method</b>	Full-matrix least-squares on F <sup>2</sup>	
<b>Refinement program</b>	SHELXL-2014/7 (Sheldrick, 2014)	
<b>Function minimized</b>	Σ w(F <sub>o</sub> <sup>2</sup> - F <sub>c</sub> <sup>2</sup> ) <sup>2</sup>	
<b>Data / restraints / parameters</b>	1500 / 0 / 131	
<b>Goodness-of-fit on F<sup>2</sup></b>	4.676	
<b>Δ/σ<sub>max</sub></b>	0.475	
<b>Final R indices</b>	807 data; I>2σ(I)	R1 = 0.4436, wR2 = 0.7232
	all data	R1 = 0.4807, wR2 = 0.7683

<b>Weighting scheme</b>	$w=1/[\sigma^2(F_o^2)+(0.0680P)^2]$ ; where $P=(F_o^2+2F_c^2)/3$
<b>Largest diff. peak and hole</b>	1.899 and -1.197 eÅ <sup>-3</sup>
<b>R.M.S. deviation from mean</b>	0.302 eÅ <sup>-3</sup>

**Table 11.** Atomic coordinates and equivalent isotropic atomic displacement parameters (Å<sup>2</sup>) for **3b**.

U(eq) is defined as one third of the trace of the orthogonalized U<sub>ij</sub> tensor.

	<b>x/a</b>	<b>y/b</b>	<b>z/c</b>	<b>U(eq)</b>
C1	0.212(3)	0.532(4)	0.3626(14)	0.123(13)
F1	0.0116(18)	0.257(3)	0.4719(12)	0.131(6)
O1	0.3930(17)	0.031(3)	0.3826(13)	0.116(7)
C2	0.134(3)	0.501(6)	0.428(2)	0.142(15)
F2	0.2614(16)	0.624(3)	0.1640(12)	0.130(7)
O2	0.535(2)	0.275(3)	0.4399(13)	0.112(7)
C3	0.0884(16)	0.306(5)	0.4077(15)	0.079(7)
C4	0.092(3)	0.119(4)	0.3353(16)	0.121(13)
C5	0.143(2)	0.158(5)	0.2682(19)	0.106(10)
C6	0.207(2)	0.363(4)	0.2871(13)	0.083(8)
C7	0.290(2)	0.423(4)	0.2189(13)	0.074(7)
C8	0.339(2)	0.226(4)	0.1642(16)	0.095(8)
C9	0.3873(16)	0.355(3)	0.2660(16)	0.075(7)
C10	0.4462(16)	0.208(4)	0.3678(16)	0.071(7)

**Table 12.** Bond lengths (Å) for **3b**.

C1-C6	1.38(3)	C1-C2	1.53(5)
C1-H1A	0.94	F1-C3	1.52(3)
O1-C10	1.25(3)	O1-H1O	1.07(9)
C2-C3	1.22(4)	C2-H2A	0.94
F2-C7	1.33(2)	O2-C10	1.26(2)
C3-C4	1.45(4)	C4-C5	1.30(4)
C4-H4A	0.94	C5-C6	1.37(4)
C5-H5A	0.94	C6-C7	1.64(3)
C7-C9	1.22(3)	C7-C8	1.57(4)
C8-C9	1.50(3)	C8-H8A	0.98
C8-H8B	0.98	C9-C10	1.57(3)

C9-H9A 0.99

**Table 13.** Bond angles (°) for **3b**.

C6-C1-C2	118.(2)	C6-C1-H1A	121.0
C2-C1-H1A	120.8	C10-O1-H1O	100.(6)
C3-C2-C1	108.(2)	C3-C2-H2A	125.9
C1-C2-H2A	126.0	C2-C3-C4	133.(3)
C2-C3-F1	112.(2)	C4-C3-F1	115.(2)
C5-C4-C3	119.(2)	C5-C4-H4A	120.2
C3-C4-H4A	120.4	C4-C5-C6	113.(2)
C4-C5-H5A	123.3	C6-C5-H5A	123.3
C5-C6-C1	127.(3)	C5-C6-C7	120.(2)
C1-C6-C7	114.(2)	C9-C7-F2	126.(2)
C9-C7-C6	110.0(16)	F2-C7-C6	113.(2)
C9-C7-C8	63.5(18)	F2-C7-C8	113.7(17)
C6-C7-C8	123.2(19)	C9-C8-C7	46.9(12)
C9-C8-H8A	118.9	C7-C8-H8A	119.0
C9-C8-H8B	118.9	C7-C8-H8B	118.9
H8A-C8-H8B	116.4	C7-C9-C8	69.6(16)
C7-C9-C10	135.(2)	C8-C9-C10	119.0(17)
C7-C9-H9A	108.6	C8-C9-H9A	108.7
C10-C9-H9A	108.7	O2-C10-O1	119.(2)
O2-C10-C9	123.8(19)	O1-C10-C9	116.7(15)

**Table 14.** Anisotropic atomic displacement parameters (Å<sup>2</sup>) for **3b**.

The anisotropic atomic displacement factor exponent takes the form:  $-2\pi^2 [ h^2 a^{*2} U_{11} + \dots + 2 h k a^* b^* U_{12} ]$

	<b>U<sub>11</sub></b>	<b>U<sub>22</sub></b>	<b>U<sub>33</sub></b>	<b>U<sub>23</sub></b>	<b>U<sub>13</sub></b>	<b>U<sub>12</sub></b>
C1	0.25(3)	0.063(14)	0.049(11)	-0.020(9)	0.045(15)	-0.077(18)
F1	0.198(17)	0.107(12)	0.143(12)	-0.013(9)	0.130(11)	-0.011(11)
O1	0.173(18)	0.057(10)	0.132(14)	0.008(9)	0.069(13)	0.011(12)
C2	0.18(3)	0.12(2)	0.12(2)	-0.086(18)	0.04(2)	-0.08(2)
F2	0.213(16)	0.086(11)	0.139(12)	0.052(8)	0.119(10)	0.051(10)
O2	0.190(19)	0.067(11)	0.109(12)	0.015(8)	0.090(13)	0.037(12)
C3	0.048(11)	0.14(2)	0.059(11)	0.013(12)	0.031(9)	0.012(13)



	<b>U<sub>11</sub></b>	<b>U<sub>22</sub></b>	<b>U<sub>33</sub></b>	<b>U<sub>23</sub></b>	<b>U<sub>13</sub></b>	<b>U<sub>12</sub></b>
C4	0.26(4)	0.065(15)	0.054(12)	-0.015(9)	0.069(17)	-0.045(18)
C5	0.16(3)	0.085(19)	0.074(15)	-0.033(12)	0.034(16)	-0.037(18)
C6	0.128(19)	0.066(13)	0.041(9)	-0.008(7)	0.013(11)	-0.033(12)
C7	0.107(18)	0.076(14)	0.039(10)	-0.003(8)	0.023(10)	-0.009(12)
C8	0.16(2)	0.060(14)	0.080(13)	-0.016(10)	0.060(14)	-0.029(14)
C9	0.069(12)	0.047(11)	0.087(14)	-0.023(9)	-0.001(11)	-0.038(9)
C10	0.050(10)	0.075(14)	0.070(12)	-0.036(10)	-0.002(9)	-0.016(9)

**Table 15.** Hydrogen atomic coordinates and isotropic atomic displacement parameters ( $\text{\AA}^2$ ) for **3b**.

	<b>x/a</b>	<b>y/b</b>	<b>z/c</b>	<b>U(eq)</b>
H1A	0.2622	0.6629	0.3735	0.147
H2A	0.1240	0.6124	0.4755	0.171
H4A	0.0567	-0.0285	0.3368	0.145
H5A	0.1376	0.0554	0.2121	0.128
H8A	0.3134	0.0609	0.1644	0.114
H8B	0.3646	0.2715	0.1061	0.114
H9A	0.4416	0.4778	0.2592	0.089
H1O	0.459(8)	-0.057(17)	0.443(7)	0.00(2)

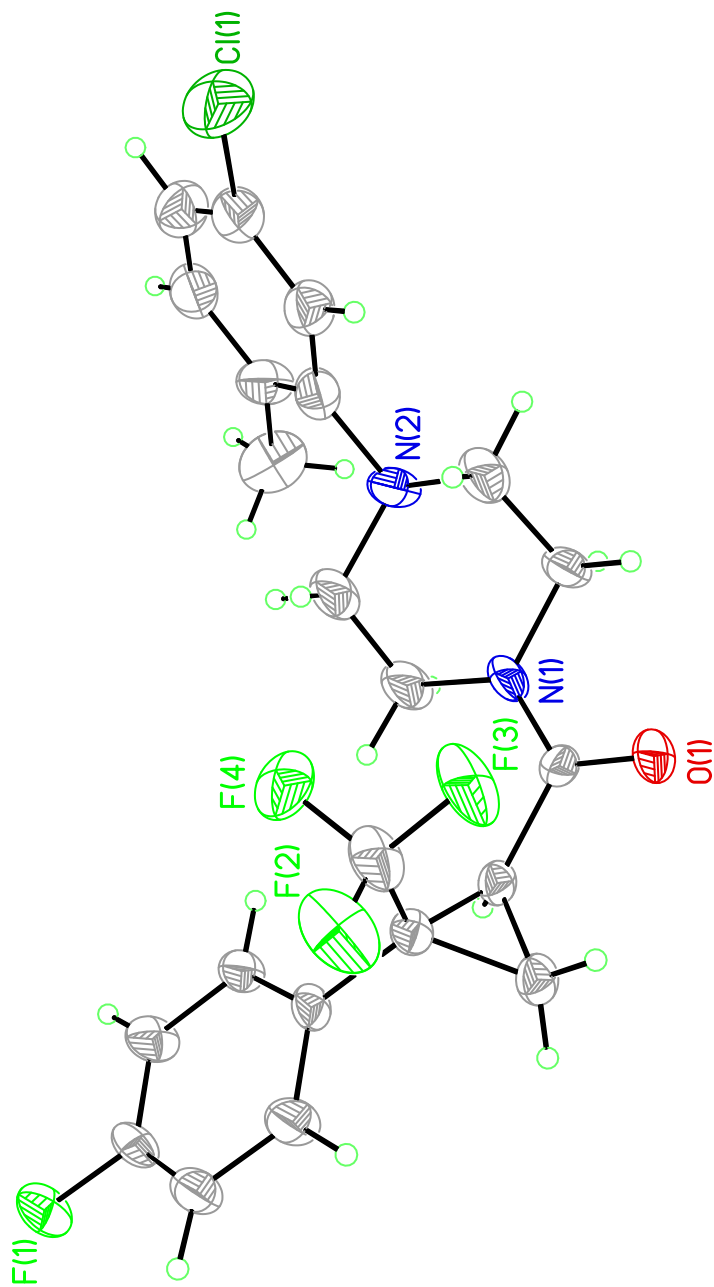


**Figure 59.** X-ray structural information for *rac*-6a.

**Table 16.** Crystal data for **6a**.

<b>Chemical formula</b>	C <sub>22</sub> H <sub>21</sub> ClF <sub>4</sub> N <sub>2</sub> O	
<b>Formula weight</b>	440.86 g/mol	
<b>Temperature</b>	230(2) K	
<b>Wavelength</b>	1.54178 Å	
<b>Crystal system</b>	triclinic	
<b>Space group</b>	P -1	
<b>Unit cell dimensions</b>	a = 7.5803(4) Å	α = 77.301(3)°
	b = 8.3837(4) Å	β = 86.162(3)°
	c = 17.4921(8) Å	γ = 73.979(3)°
<b>Volume</b>	1042.30(9) Å <sup>3</sup>	
<b>Z</b>	2	
<b>Density (calculated)</b>	1.405 g/cm <sup>3</sup>	
<b>Absorption coefficient</b>	2.086 mm <sup>-1</sup>	
<b>F(000)</b>	456	

**Table 17.** Data collection and structure refinement for **6a**.

<b>Diffractometer</b>	Bruker Apex II CCD	
<b>Radiation source</b>	Bruker X8 Prospector Ultra, IMuS Cu K/a	
<b>Theta range for data collection</b>	2.59 to 68.34°	
<b>Index ranges</b>	-9 ≤ h ≤ 9, -10 ≤ k ≤ 10, -21 ≤ l ≤ 20	
<b>Reflections collected</b>	15778	
<b>Independent reflections</b>	3736 [R(int) = 0.1862]	
<b>Absorption correction</b>	multi-scan	
<b>Structure solution technique</b>	direct methods	
<b>Structure solution program</b>	SHELXT 2014/4 (Sheldrick, 2014)	
<b>Refinement method</b>	Full-matrix least-squares on F <sup>2</sup>	
<b>Refinement program</b>	SHELXL-2016/6 (Sheldrick, 2016)	
<b>Function minimized</b>	Σ w(F <sub>o</sub> <sup>2</sup> - F <sub>c</sub> <sup>2</sup> ) <sup>2</sup>	
<b>Data / restraints / parameters</b>	3736 / 0 / 271	
<b>Goodness-of-fit on F<sup>2</sup></b>	3.374	
<b>Δ/σ<sub>max</sub></b>	0.006	
<b>Final R indices</b>	2740 data; I > 2σ(I)	R1 = 0.1853, wR2 = 0.4655
	all data	R1 = 0.2076, wR2 = 0.4848

<b>Weighting scheme</b>	$w=1/[\sigma^2(F_o^2)+(0.0680P)^2]$ ; where $P=(F_o^2+2F_c^2)/3$
<b>Largest diff. peak and hole</b>	3.223 and -0.725 eÅ <sup>-3</sup>
<b>R.M.S. deviation from mean</b>	0.176 eÅ <sup>-3</sup>

**Table 18.** Atomic coordinates and equivalent isotropic atomic displacement parameters (Å<sup>2</sup>) for **6a**.

U(eq) is defined as one third of the trace of the orthogonalized U<sub>ij</sub> tensor.

	<b>x/a</b>	<b>y/b</b>	<b>z/c</b>	<b>U(eq)</b>
C1	0.4716(10)	0.5561(9)	0.8607(5)	0.0434(18)
C2	0.5876(10)	0.3899(10)	0.8748(5)	0.051(2)
C3	0.5185(10)	0.2667(9)	0.9198(5)	0.0420(18)
C4	0.3499(12)	0.2910(10)	0.9495(5)	0.053(2)
C5	0.2371(12)	0.4582(11)	0.9370(6)	0.060(3)
C6	0.2966(9)	0.5906(9)	0.8899(4)	0.0378(16)
C7	0.1651(9)	0.7660(9)	0.8741(4)	0.0369(16)
C8	0.0853(10)	0.8472(9)	0.9418(5)	0.0433(18)
C9	0.2242(9)	0.9135(9)	0.8900(4)	0.0385(17)
C10	0.0423(12)	0.7919(11)	0.8063(6)	0.061(2)
C11	0.1592(10)	0.0962(9)	0.8426(4)	0.0394(17)
C12	0.2220(14)	0.3223(11)	0.7389(5)	0.071(3)
C13	0.2467(13)	0.3241(12)	0.6548(6)	0.065(3)
C14	0.4539(15)	0.0418(12)	0.7623(7)	0.081(4)
C15	0.4721(15)	0.0562(11)	0.6803(6)	0.075(3)
C16	0.4751(13)	0.2509(11)	0.5547(5)	0.055(2)
C17	0.3405(13)	0.3078(11)	0.4968(5)	0.060(2)
C18	0.3879(15)	0.3287(13)	0.4181(6)	0.072(3)
C19	0.5678(15)	0.2996(13)	0.3960(6)	0.070(3)
C20	0.7037(16)	0.2477(12)	0.4517(6)	0.068(3)
C21	0.6597(12)	0.2290(13)	0.5343(6)	0.063(3)
C22	0.8160(17)	0.1725(18)	0.5937(7)	0.092(4)
Cl1	0.2140(5)	0.3842(5)	0.34800(19)	0.1125(14)
F1	0.6287(6)	0.1010(5)	0.9314(3)	0.0591(14)
F2	0.9397(8)	0.6803(8)	0.8182(4)	0.090(2)
F3	0.9231(8)	0.9460(7)	0.7900(4)	0.0835(19)
F4	0.1328(9)	0.7732(8)	0.7412(3)	0.0819(18)
N1	0.2695(10)	0.1435(8)	0.7832(4)	0.0548(19)

	<b>x/a</b>	<b>y/b</b>	<b>z/c</b>	<b>U(eq)</b>
N2	0.4346(9)	0.2365(9)	0.6383(4)	0.058(2)
O1	0.0194(7)	0.1923(7)	0.8599(3)	0.0509(15)

**Table 19.** Bond lengths (Å) for **6a**.

C1-C6	1.366(10)	C1-C2	1.406(10)
C1-H1A	0.94	C2-C3	1.359(11)
C2-H2A	0.94	C3-C4	1.326(12)
C3-F1	1.388(8)	C4-C5	1.405(11)
C4-H4A	0.94	C5-C6	1.392(11)
C5-H5A	0.94	C6-C7	1.510(9)
C7-C10	1.497(11)	C7-C8	1.504(10)
C7-C9	1.510(10)	C8-C9	1.487(10)
C8-H8A	0.98	C8-H8B	0.98
C9-C11	1.535(9)	C9-H9A	0.99
C10-F4	1.307(12)	C10-F2	1.348(11)
C10-F3	1.340(9)	C11-O1	1.207(9)
C11-N1	1.349(9)	C12-C13	1.468(14)
C12-N1	1.486(10)	C12-H12A	0.98
C12-H12B	0.98	C13-N2	1.453(11)
C13-H13A	0.98	C13-H13B	0.98
C14-C15	1.414(16)	C14-N1	1.491(11)
C14-H14A	0.98	C14-H14B	0.98
C15-N2	1.486(11)	C15-H15A	0.98
C15-H15B	0.98	C16-C17	1.396(13)
C16-C21	1.393(12)	C16-N2	1.460(11)
C17-C18	1.386(13)	C17-H17A	0.94
C18-C19	1.362(15)	C18-Cl1	1.756(11)
C19-C20	1.378(16)	C19-H19A	0.94
C20-C21	1.446(14)	C20-H20A	0.94
C21-C22	1.531(15)	C22-H22A	0.97
C22-H22B	0.97	C22-H22C	0.97

**Table 20.** Bond angles (°) for **6a**.

C6-C1-C2	121.2(7)	C6-C1-H1A	119.4
C2-C1-H1A	119.4	C3-C2-C1	116.9(7)
C3-C2-H2A	121.6	C1-C2-H2A	121.6
C2-C3-C4	125.0(7)	C2-C3-F1	117.5(7)
C4-C3-F1	117.4(6)	C3-C4-C5	117.6(7)
C3-C4-H4A	121.2	C5-C4-H4A	121.2
C4-C5-C6	120.6(7)	C4-C5-H5A	119.7
C6-C5-H5A	119.7	C1-C6-C5	118.5(7)
C1-C6-C7	123.1(6)	C5-C6-C7	118.4(6)
C10-C7-C6	111.7(6)	C10-C7-C8	117.8(7)
C6-C7-C8	119.5(6)	C10-C7-C9	120.0(6)
C6-C7-C9	119.5(6)	C8-C7-C9	59.1(5)
C9-C8-C7	60.6(5)	C9-C8-H8A	117.7
C7-C8-H8A	117.7	C9-C8-H8B	117.7
C7-C8-H8B	117.7	H8A-C8-H8B	114.8
C8-C9-C7	60.3(5)	C8-C9-C11	116.5(6)
C7-C9-C11	124.1(6)	C8-C9-H9A	114.9
C7-C9-H9A	114.9	C11-C9-H9A	114.9
F4-C10-F2	105.6(8)	F4-C10-F3	105.6(8)
F2-C10-F3	105.8(7)	F4-C10-C7	112.9(7)
F2-C10-C7	112.4(7)	F3-C10-C7	113.9(8)
O1-C11-N1	122.7(7)	O1-C11-C9	120.9(6)
N1-C11-C9	116.4(6)	C13-C12-N1	109.0(8)
C13-C12-H12A	109.9	N1-C12-H12A	109.9
C13-C12-H12B	109.9	N1-C12-H12B	109.9
H12A-C12-H12B	108.3	C12-C13-N2	110.4(8)
C12-C13-H13A	109.6	N2-C13-H13A	109.6
C12-C13-H13B	109.6	N2-C13-H13B	109.6
H13A-C13-H13B	108.1	C15-C14-N1	110.9(9)
C15-C14-H14A	109.5	N1-C14-H14A	109.5
C15-C14-H14B	109.5	N1-C14-H14B	109.5
H14A-C14-H14B	108.1	C14-C15-N2	111.5(9)
C14-C15-H15A	109.3	N2-C15-H15A	109.3
C14-C15-H15B	109.3	N2-C15-H15B	109.3
H15A-C15-H15B	108.0	C17-C16-C21	120.5(9)
C17-C16-N2	123.7(8)	C21-C16-N2	115.1(8)
C18-C17-C16	120.9(9)	C18-C17-H17A	119.5

C16-C17-H17A	119.5	C19-C18-C17	120.1(10)
C19-C18-C11	120.8(8)	C17-C18-C11	119.1(8)
C18-C19-C20	120.3(10)	C18-C19-H19A	119.9
C20-C19-H19A	119.9	C19-C20-C21	121.3(10)
C19-C20-H20A	119.3	C21-C20-H20A	119.3
C16-C21-C20	116.5(9)	C16-C21-C22	124.1(9)
C20-C21-C22	119.2(9)	C21-C22-H22A	109.5
C21-C22-H22B	109.5	H22A-C22-H22B	109.5
C21-C22-H22C	109.5	H22A-C22-H22C	109.5
H22B-C22-H22C	109.5	C11-N1-C12	119.1(7)
C11-N1-C14	127.0(6)	C12-N1-C14	113.2(7)
C16-N2-C13	113.3(7)	C16-N2-C15	111.5(7)
C13-N2-C15	108.7(6)		

**Table 21.** Anisotropic atomic displacement parameters ( $\text{\AA}^2$ ) for **6a**.

The anisotropic atomic displacement factor exponent takes the form:  $-2\pi^2[ h^2 a^{*2}U_{11} + \dots + 2 h k a^* b^* U_{12} ]$

	<b>U<sub>11</sub></b>	<b>U<sub>22</sub></b>	<b>U<sub>33</sub></b>	<b>U<sub>23</sub></b>	<b>U<sub>13</sub></b>	<b>U<sub>12</sub></b>
C1	0.034(4)	0.037(4)	0.050(4)	-0.001(3)	0.009(3)	-0.001(3)
C2	0.032(3)	0.044(4)	0.059(5)	0.004(4)	-0.004(3)	0.007(3)
C3	0.039(4)	0.026(3)	0.052(4)	0.001(3)	-0.015(3)	0.003(3)
C4	0.053(5)	0.035(4)	0.063(5)	-0.001(4)	0.009(4)	-0.007(4)
C5	0.047(4)	0.043(5)	0.074(6)	0.001(4)	0.030(4)	-0.005(4)
C6	0.032(3)	0.033(3)	0.042(4)	-0.010(3)	-0.004(3)	0.005(3)
C7	0.030(3)	0.038(4)	0.038(4)	-0.008(3)	-0.007(3)	0.001(3)
C8	0.033(3)	0.043(4)	0.051(5)	-0.015(3)	0.006(3)	-0.004(3)
C9	0.033(3)	0.039(4)	0.037(4)	-0.010(3)	0.002(3)	0.003(3)
C10	0.048(5)	0.050(5)	0.075(6)	-0.015(5)	-0.028(4)	0.013(4)
C11	0.038(4)	0.041(4)	0.033(4)	-0.007(3)	0.006(3)	-0.002(3)
C12	0.074(6)	0.041(5)	0.063(6)	0.014(4)	0.032(5)	0.015(4)
C13	0.054(5)	0.052(5)	0.075(6)	-0.009(4)	0.002(4)	0.007(4)
C14	0.076(7)	0.047(5)	0.084(7)	0.007(5)	0.038(6)	0.018(5)
C15	0.071(6)	0.043(5)	0.084(7)	0.000(5)	0.039(5)	0.010(4)
C16	0.059(5)	0.047(4)	0.060(5)	-0.017(4)	0.000(4)	-0.010(4)
C17	0.056(5)	0.060(5)	0.063(6)	-0.017(4)	0.001(4)	-0.007(4)
C18	0.079(7)	0.062(6)	0.066(6)	-0.017(5)	-0.011(5)	-0.001(5)

	<b>U<sub>11</sub></b>	<b>U<sub>22</sub></b>	<b>U<sub>33</sub></b>	<b>U<sub>23</sub></b>	<b>U<sub>13</sub></b>	<b>U<sub>12</sub></b>
C19	0.077(7)	0.070(6)	0.064(6)	-0.018(5)	0.016(5)	-0.025(6)
C20	0.074(6)	0.054(5)	0.075(7)	-0.017(5)	0.011(5)	-0.014(5)
C21	0.042(4)	0.067(6)	0.060(6)	0.007(4)	0.008(4)	0.000(4)
C22	0.078(8)	0.122(11)	0.085(8)	-0.018(7)	0.000(6)	-0.045(8)
Cl1	0.107(3)	0.135(3)	0.075(2)	-0.031(2)	-0.0352(17)	0.016(2)
F1	0.045(2)	0.037(2)	0.077(3)	0.000(2)	-0.012(2)	0.0113(19)
F2	0.066(4)	0.074(4)	0.132(6)	-0.018(4)	-0.050(4)	-0.014(3)
F3	0.061(3)	0.058(3)	0.118(5)	-0.029(3)	-0.055(3)	0.028(3)
F4	0.084(4)	0.100(4)	0.048(3)	-0.026(3)	-0.025(3)	0.013(3)
N1	0.054(4)	0.030(3)	0.061(4)	-0.002(3)	0.014(3)	0.012(3)
N2	0.042(4)	0.050(4)	0.056(4)	0.013(3)	0.018(3)	0.007(3)
O1	0.032(3)	0.046(3)	0.062(4)	-0.011(3)	0.010(2)	0.008(2)

**Table 22.** Hydrogen atomic coordinates and isotropic atomic displacement parameters ( $\text{\AA}^2$ ) for **6a**.

	<b>x/a</b>	<b>y/b</b>	<b>z/c</b>	<b>U(eq)</b>
H1A	0.5154	-0.3549	0.8307	0.052
H2A	0.7073	-0.6349	0.8540	0.061
H4A	0.3075	-0.8003	0.9780	0.064
H5A	0.1203	-0.5190	0.9606	0.072
H8A	-0.0422	-0.0831	0.9377	0.052
H8B	0.1233	-0.2168	0.9947	0.052
H9A	0.3478	-0.1170	0.9131	0.046
H12A	0.0943	0.3791	0.7498	0.085
H12B	0.3013	0.3832	0.7552	0.085
H13A	0.2179	0.4418	0.6252	0.078
H13B	0.1623	0.2686	0.6382	0.078
H14A	0.5493	0.0818	0.7813	0.097
H14B	0.4708	-0.0776	0.7880	0.097
H15A	0.3864	0.0037	0.6624	0.09
H15B	0.5969	-0.0051	0.6678	0.09
H17A	0.2159	0.3323	0.5115	0.072
H19A	0.5995	0.3151	0.3425	0.084
H20A	0.8273	0.2240	0.4356	0.082
H22A	0.9322	0.1660	0.5661	0.138



	<b>x/a</b>	<b>y/b</b>	<b>z/c</b>	<b>U(eq)</b>
H22B	0.7979	0.2539	0.6272	0.138
H22C	0.8169	0.0618	0.6255	0.138

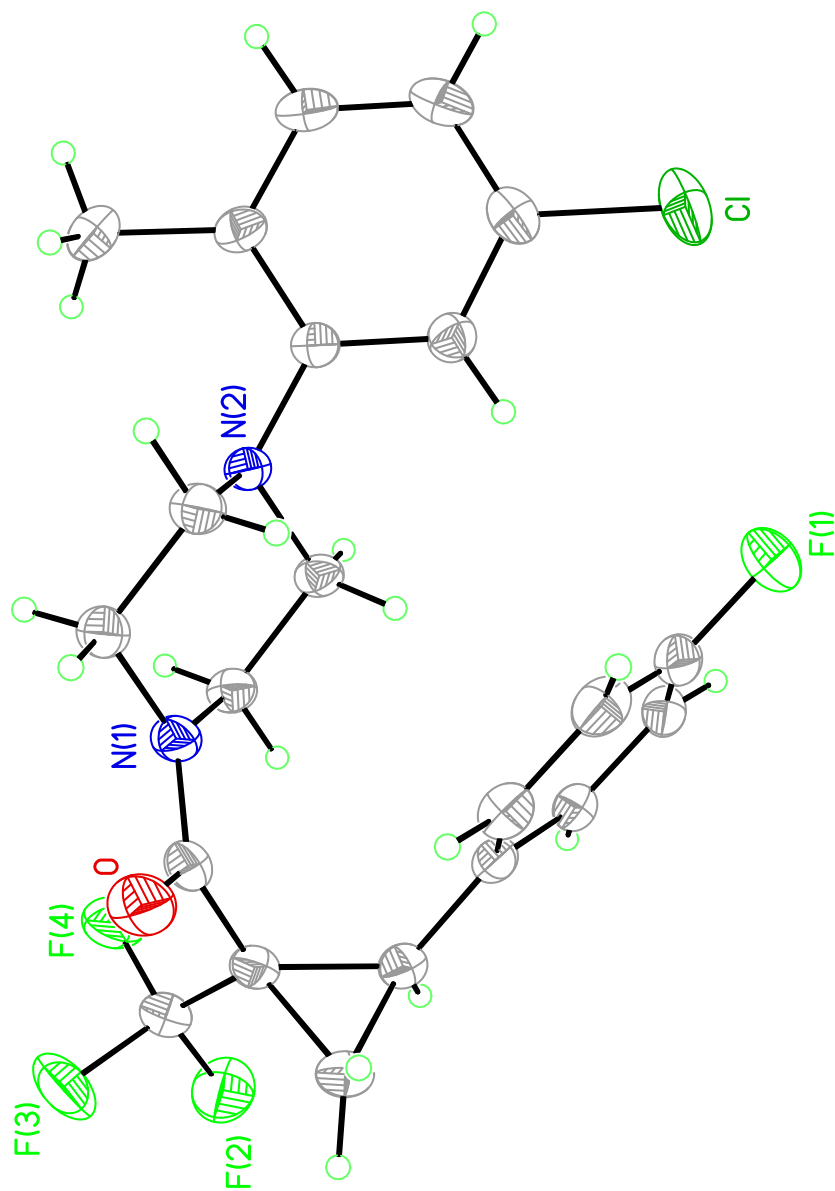


**Figure 60.** X-ray structural information for *rac*-11a.

**Table 23.** Crystal data for **11a**.

<b>Chemical formula</b>	C <sub>22</sub> H <sub>21</sub> ClF <sub>4</sub> N <sub>2</sub> O	
<b>Formula weight</b>	440.86 g/mol	
<b>Temperature</b>	230(2) K	
<b>Wavelength</b>	1.54178 Å	
<b>Crystal size</b>	0.180 x 0.150 x 0.110 mm	
<b>Crystal system</b>	monoclinic	
<b>Space group</b>	P 1 21/c 1	
<b>Unit cell dimensions</b>	a = 10.0445(3) Å	α = 90°
	b = 19.2372(6) Å	β = 96.4030(16)°
	c = 10.7617(3) Å	γ = 90°
<b>Volume</b>	2066.49(11) Å <sup>3</sup>	
<b>Z</b>	4	
<b>Density (calculated)</b>	1.417 g/cm <sup>3</sup>	
<b>Absorption coefficient</b>	2.105 mm <sup>-1</sup>	
<b>F(000)</b>	912	

**Table 24.** Data collection and structure refinement for **11a**.

<b>Diffractometer</b>	Bruker Apex II CCD	
<b>Radiation source</b>	Bruker X8 Prospector Ultra, IMuS Cu K/α	
<b>Theta range for data collection</b>	4.43 to 68.61°	
<b>Index ranges</b>	-12 ≤ h ≤ 12, -23 ≤ k ≤ 23, -12 ≤ l ≤ 12	
<b>Reflections collected</b>	21368	
<b>Independent reflections</b>	3771 [R(int) = 0.0335]	
<b>Absorption correction</b>	multi-scan	
<b>Max. and min. transmission</b>	0.9800 and 0.9500	
<b>Refinement method</b>	Full-matrix least-squares on F <sup>2</sup>	
<b>Refinement program</b>	SHELXL-2016/6 (Sheldrick, 2016)	
<b>Function minimized</b>	Σ w(F <sub>o</sub> <sup>2</sup> - F <sub>c</sub> <sup>2</sup> ) <sup>2</sup>	
<b>Data / restraints / parameters</b>	3771 / 0 / 344	
<b>Goodness-of-fit on F<sup>2</sup></b>	1.508	
<b>Final R indices</b>	3360 data; I > 2σ(I)	R1 = 0.0387, wR2 = 0.1264
	all data	R1 = 0.0429, wR2 = 0.1301
<b>Weighting scheme</b>	w = 1/[σ <sup>2</sup> (F <sub>o</sub> <sup>2</sup> ) + (0.0680P) <sup>2</sup> ]; where P = (F <sub>o</sub> <sup>2</sup> + 2F <sub>c</sub> <sup>2</sup> )/3	

**Largest diff. peak and hole**      0.246 and -0.411 eÅ<sup>-3</sup>  
**R.M.S. deviation from mean**      0.046 eÅ<sup>-3</sup>

**Table 25.** Atomic coordinates and equivalent isotropic atomic displacement parameters (Å<sup>2</sup>) for **11a**.

U(eq) is defined as one third of the trace of the orthogonalized U<sub>ij</sub> tensor.

	<b>x/a</b>	<b>y/b</b>	<b>z/c</b>	<b>U(eq)</b>
Cl	0.59290(7)	0.04930(3)	0.41410(5)	0.0813(2)
O	0.13357(13)	0.24498(6)	0.74991(13)	0.0568(3)
F1	0.23430(13)	0.03012(7)	0.27604(10)	0.0709(4)
N1	0.32362(13)	0.18220(6)	0.78810(12)	0.0393(3)
C1	0.19640(16)	0.04025(9)	0.15272(14)	0.0455(4)
N2	0.54194(12)	0.16345(6)	0.97698(11)	0.0343(3)
F2	0.08444(15)	0.05829(7)	0.50384(11)	0.0769(4)
C2	0.20732(15)	0.98568(8)	0.07215(15)	0.0417(3)
C3	0.16829(14)	0.99612(7)	0.94620(14)	0.0349(3)
F3	0.09894(15)	0.16797(7)	0.47993(11)	0.0772(4)
F4	0.27416(11)	0.10957(7)	0.53875(9)	0.0627(3)
C4	0.11827(13)	0.05969(7)	0.90068(13)	0.0338(3)
C5	0.10833(16)	0.11353(8)	0.98583(16)	0.0412(3)
C6	0.14727(17)	0.10404(9)	0.11240(16)	0.0477(4)
C7	0.07645(14)	0.06591(8)	0.76383(14)	0.0385(3)
C8	0.97496(16)	0.11847(10)	0.71051(18)	0.0487(4)
C9	0.11840(14)	0.12724(8)	0.68569(14)	0.0388(3)
C10	0.14520(17)	0.11483(9)	0.55352(15)	0.0482(4)
C11	0.19309(15)	0.18974(7)	0.74538(14)	0.0385(3)
C12	0.40100(19)	0.24225(8)	0.84021(16)	0.0477(4)
C13	0.46027(17)	0.22701(7)	0.97327(15)	0.0422(4)
C14	0.40050(15)	0.11749(8)	0.79609(14)	0.0373(3)
C15	0.45854(14)	0.10458(7)	0.93071(14)	0.0350(3)
C16	0.61897(14)	0.15284(7)	0.09561(13)	0.0326(3)
C17	0.57355(15)	0.11064(8)	0.18657(14)	0.0388(3)
C18	0.65342(18)	0.10030(8)	0.29894(14)	0.0451(4)
C19	0.77781(18)	0.13015(9)	0.32166(15)	0.0472(4)
C20	0.82138(16)	0.17269(8)	0.23206(15)	0.0439(4)
C21	0.74435(14)	0.18528(7)	0.11842(14)	0.0380(3)

	<b>x/a</b>	<b>y/b</b>	<b>z/c</b>	<b>U(eq)</b>
C22	0.79683(18)	0.23146(10)	0.02258(18)	0.0557(4)

**Table 26.** Bond lengths (Å) for **11a**.

Cl-C18	1.7425(16)	O-C11	1.2231(19)
F1-C1	1.353(2)	N1-C11	1.348(2)
N1-C14	1.4625(19)	N1-C12	1.4682(19)
C1-C2	1.374(2)	C1-C6	1.375(3)
N2-C16	1.4318(18)	N2-C15	1.4627(18)
N2-C13	1.4704(19)	F2-C10	1.330(2)
C2-C3	1.383(2)	C2-H2	0.96(2)
C3-C4	1.390(2)	C3-H3	0.94(2)
F3-C10	1.344(2)	F4-C10	1.326(2)
C4-C5	1.394(2)	C4-C7	1.491(2)
C5-C6	1.387(3)	C5-H5	0.92(2)
C6-H6	0.94(2)	C7-C8	1.503(2)
C7-C9	1.535(2)	C7-H7	1.000(18)
C8-C9	1.504(2)	C8-H8A	1.01(2)
C8-H8B	0.91(2)	C9-C10	1.496(2)
C9-C11	1.521(2)	C12-C13	1.517(2)
C12-H12A	0.95(2)	C12-H12B	0.99(2)
C13-H13A	1.01(2)	C13-H13B	0.98(2)
C14-C15	1.520(2)	C14-H14A	0.976(19)
C14-H14B	0.97(2)	C15-H15A	0.990(19)
C15-H15B	0.95(2)	C16-C17	1.387(2)
C16-C21	1.402(2)	C17-C18	1.389(2)
C17-H17	0.92(2)	C18-C19	1.372(3)
C19-C20	1.373(3)	C19-H19	0.91(3)
C20-C21	1.394(2)	C20-H20	0.92(2)
C21-C22	1.501(2)	C22-H22A	0.97
C22-H22B	0.97	C22-H22C	0.97

**Table 27.** Bond angles (°) for **11a**.

C11-N1-C14	126.78(12)	C11-N1-C12	119.94(13)
C14-N1-C12	113.18(12)	F1-C1-C2	118.39(16)
F1-C1-C6	119.32(15)	C2-C1-C6	122.28(15)
C16-N2-C15	115.16(11)	C16-N2-C13	112.78(11)
C15-N2-C13	109.76(11)	C1-C2-C3	118.29(15)
C1-C2-H2	120.5(12)	C3-C2-H2	121.2(12)
C2-C3-C4	121.65(14)	C2-C3-H3	119.8(11)
C4-C3-H3	118.5(12)	C3-C4-C5	118.13(14)
C3-C4-C7	118.02(13)	C5-C4-C7	123.84(14)
C6-C5-C4	120.99(15)	C6-C5-H5	119.4(13)
C4-C5-H5	119.6(13)	C1-C6-C5	118.65(15)
C1-C6-H6	117.8(13)	C5-C6-H6	123.5(13)
C4-C7-C8	122.38(14)	C4-C7-C9	122.59(12)
C8-C7-C9	59.32(10)	C4-C7-H7	114.5(10)
C8-C7-H7	114.5(10)	C9-C7-H7	112.5(10)
C7-C8-C9	61.38(10)	C7-C8-H8A	115.4(13)
C9-C8-H8A	116.2(14)	C7-C8-H8B	117.2(14)
C9-C8-H8B	113.4(14)	H8A-C8-H8B	120.(2)
C10-C9-C8	115.37(14)	C10-C9-C11	113.28(13)
C8-C9-C11	116.80(14)	C10-C9-C7	119.18(14)
C8-C9-C7	59.30(10)	C11-C9-C7	121.93(12)
F4-C10-F2	107.45(16)	F4-C10-F3	105.39(14)
F2-C10-F3	105.80(14)	F4-C10-C9	114.07(13)
F2-C10-C9	112.94(14)	F3-C10-C9	110.59(15)
O-C11-N1	122.75(14)	O-C11-C9	118.91(13)
N1-C11-C9	118.31(12)	N1-C12-C13	110.12(12)
N1-C12-H12A	108.9(13)	C13-C12-H12A	109.8(13)
N1-C12-H12B	105.8(12)	C13-C12-H12B	112.2(12)
H12A-C12-H12B	109.8(17)	N2-C13-C12	110.20(13)
N2-C13-H13A	112.9(11)	C12-C13-H13A	108.9(12)
N2-C13-H13B	109.8(12)	C12-C13-H13B	109.5(12)
H13A-C13-H13B	105.4(17)	N1-C14-C15	109.81(12)
N1-C14-H14A	111.1(10)	C15-C14-H14A	111.0(10)
N1-C14-H14B	110.4(11)	C15-C14-H14B	108.9(11)

H14A-C14-H14B	105.6(15)	N2-C15-C14	110.00(11)
N2-C15-H15A	113.7(10)	C14-C15-H15A	105.3(10)
N2-C15-H15B	109.5(12)	C14-C15-H15B	106.8(11)
H15A-C15-H15B	111.2(15)	C17-C16-C21	119.76(13)
C17-C16-N2	121.67(12)	C21-C16-N2	118.55(12)
C16-C17-C18	119.64(14)	C16-C17-H17	121.3(12)
C18-C17-H17	118.9(12)	C19-C18-C17	121.42(15)
C19-C18-Cl	119.47(13)	C17-C18-Cl	119.10(14)
C18-C19-C20	118.65(15)	C18-C19-H19	119.6(17)
C20-C19-H19	121.8(17)	C19-C20-C21	122.05(15)
C19-C20-H20	120.7(14)	C21-C20-H20	117.2(14)
C20-C21-C16	118.43(14)	C20-C21-C22	120.19(14)
C16-C21-C22	121.37(14)	C21-C22-H22A	109.5
C21-C22-H22B	109.5	H22A-C22-H22B	109.5
C21-C22-H22C	109.5	H22A-C22-H22C	109.5
H22B-C22-H22C	109.5		

**Table 28.** Anisotropic atomic displacement parameters ( $\text{\AA}^2$ ) for **11a**.

The anisotropic atomic displacement factor exponent takes the form:  $-2\pi^2 [ h^2 a^{*2} U_{11} + \dots + 2 h k a^* b^* U_{12} ]$

	$U_{11}$	$U_{22}$	$U_{33}$	$U_{23}$	$U_{13}$	$U_{12}$
Cl	0.0992(4)	0.0921(4)	0.0536(3)	0.0316(3)	0.0128(3)	-0.0040(3)
O	0.0527(7)	0.0372(6)	0.0775(9)	0.0061(5)	-0.0065(6)	0.0108(5)
F1	0.0807(8)	0.0980(9)	0.0336(5)	0.0024(5)	0.0045(5)	-0.0134(7)
N1	0.0399(6)	0.0314(6)	0.0439(7)	0.0047(5)	-0.0071(5)	-0.0008(5)
C1	0.0419(8)	0.0624(10)	0.0330(7)	-0.0006(6)	0.0081(6)	-0.0125(7)
N2	0.0326(6)	0.0318(6)	0.0371(6)	0.0022(4)	-0.0028(5)	-0.0029(5)
F2	0.0931(9)	0.0898(8)	0.0462(6)	-0.0154(6)	0.0005(6)	-0.0374(7)
C2	0.0388(7)	0.0444(8)	0.0424(8)	0.0093(6)	0.0066(6)	-0.0038(7)
C3	0.0343(7)	0.0329(7)	0.0383(7)	-0.0014(6)	0.0069(5)	-0.0034(6)
F3	0.0861(8)	0.0938(9)	0.0494(6)	0.0305(6)	-0.0032(5)	0.0141(7)
F4	0.0507(6)	0.0957(9)	0.0412(5)	-0.0031(5)	0.0027(4)	0.0013(5)
C4	0.0284(6)	0.0337(7)	0.0393(7)	0.0007(5)	0.0040(5)	-0.0038(6)
C5	0.0380(7)	0.0349(7)	0.0516(9)	-0.0043(6)	0.0089(6)	0.0000(6)
C6	0.0458(8)	0.0515(9)	0.0478(9)	-0.0158(7)	0.0143(7)	-0.0109(7)
C7	0.0350(7)	0.0391(8)	0.0403(8)	0.0014(6)	-0.0006(6)	-0.0051(6)

	<b>U<sub>11</sub></b>	<b>U<sub>22</sub></b>	<b>U<sub>33</sub></b>	<b>U<sub>23</sub></b>	<b>U<sub>13</sub></b>	<b>U<sub>12</sub></b>
C8	0.0339(8)	0.0566(10)	0.0533(10)	0.0089(8)	-0.0053(7)	0.0006(7)
C9	0.0344(7)	0.0394(7)	0.0405(8)	0.0061(6)	-0.0051(6)	0.0001(6)
C10	0.0441(8)	0.0579(10)	0.0398(8)	0.0080(7)	-0.0077(6)	-0.0057(7)
C11	0.0404(8)	0.0339(7)	0.0398(7)	0.0092(6)	-0.0011(6)	0.0024(6)
C12	0.0540(9)	0.0310(7)	0.0540(9)	0.0086(6)	-0.0121(8)	-0.0063(7)
C13	0.0475(8)	0.0291(7)	0.0473(8)	0.0004(6)	-0.0072(7)	-0.0005(6)
C14	0.0335(7)	0.0359(7)	0.0415(8)	-0.0016(6)	-0.0003(6)	0.0008(6)
C15	0.0304(7)	0.0301(7)	0.0429(8)	0.0006(5)	-0.0027(6)	0.0014(6)
C16	0.0325(6)	0.0289(6)	0.0357(7)	-0.0019(5)	0.0005(5)	0.0023(5)
C17	0.0360(7)	0.0392(7)	0.0411(8)	0.0026(6)	0.0037(6)	-0.0004(6)
C18	0.0560(9)	0.0429(8)	0.0365(8)	0.0032(6)	0.0050(7)	0.0072(7)
C19	0.0548(9)	0.0464(8)	0.0372(8)	-0.0077(7)	-0.0090(7)	0.0099(8)
C20	0.0374(8)	0.0430(8)	0.0488(9)	-0.0117(7)	-0.0068(6)	-0.0014(7)
C21	0.0356(7)	0.0337(7)	0.0440(8)	-0.0046(6)	0.0003(6)	-0.0030(6)
C22	0.0476(9)	0.0544(10)	0.0642(11)	0.0070(8)	0.0029(8)	-0.0181(8)

**Table 29.** Hydrogen atomic coordinates and isotropic atomic displacement parameters ( $\text{\AA}^2$ ) for **11a**.

	<b>x/a</b>	<b>y/b</b>	<b>z/c</b>	<b>U(eq)</b>
H2	0.240(2)	-0.0586(11)	0.1031(19)	0.049(5)
H3	0.1745(18)	-0.0407(10)	-0.1109(18)	0.043(5)
H5	0.076(2)	0.1564(11)	-0.0425(19)	0.052(5)
H6	0.139(2)	0.1382(11)	0.173(2)	0.056(5)
H7	0.0742(18)	0.0209(9)	-0.2829(18)	0.042(4)
H8A	-0.090(3)	0.1017(12)	-0.362(2)	0.068(6)
H8B	-0.052(2)	0.1507(11)	-0.236(2)	0.053(5)
H12A	0.343(2)	0.2814(11)	-0.161(2)	0.055(5)
H12B	0.471(2)	0.2505(10)	-0.216(2)	0.054(5)
H13A	0.385(2)	0.2242(10)	0.0284(19)	0.051(5)
H13B	0.516(2)	0.2662(11)	0.0055(19)	0.056(5)
H14A	0.3453(18)	0.0784(9)	-0.2364(16)	0.038(4)
H14B	0.474(2)	0.1201(9)	-0.2560(18)	0.043(5)
H15A	0.3801(19)	0.0968(9)	-0.0229(16)	0.038(4)
H15B	0.512(2)	0.0638(10)	-0.0696(17)	0.045(5)
H17	0.489(2)	0.0916(10)	0.1764(17)	0.045(5)



	<b>x/a</b>	<b>y/b</b>	<b>z/c</b>	<b>U(eq)</b>
H19	0.829(3)	0.1219(12)	0.396(3)	0.075(7)
H20	0.905(2)	0.1926(11)	0.244(2)	0.062(6)
H22A	0.7795	0.2102	-0.0593	0.067
H22B	0.8926	0.2378	0.0431	0.067
H22C	0.7524	0.2762	0.0220	0.067

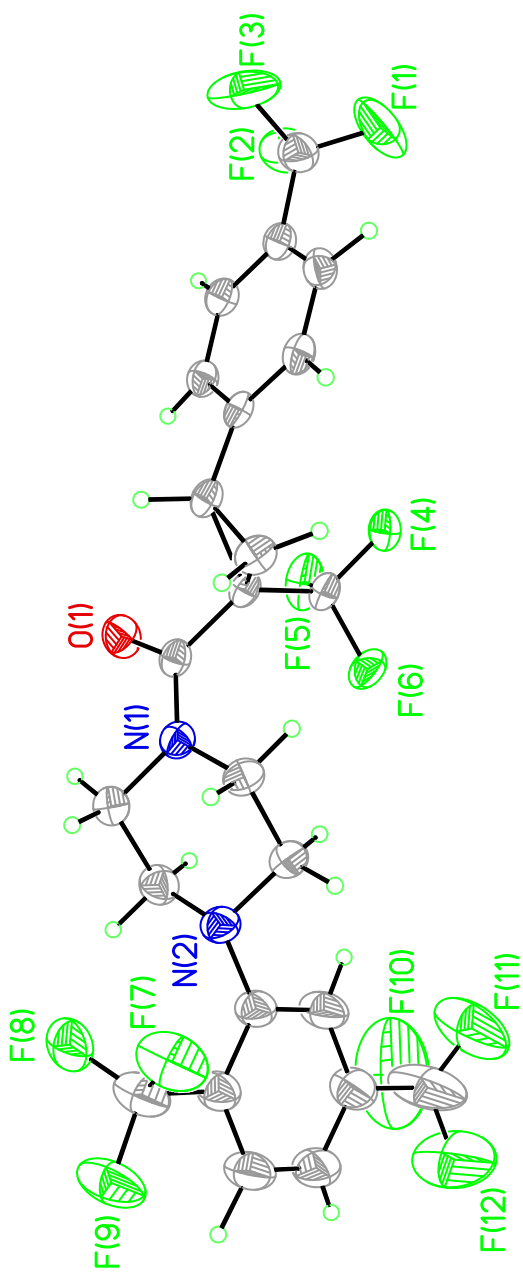


Figure 61. X-ray structural information for *rac*-15.

**Table 30.** Crystal data for **15**.

<b>Chemical formula</b>	C <sub>24</sub> H <sub>18</sub> F <sub>12</sub> N <sub>2</sub> O	
<b>Formula weight</b>	578.40 g/mol	
<b>Temperature</b>	230(2) K	
<b>Wavelength</b>	1.54178 Å	
<b>Crystal size</b>	0.050 x 0.090 x 0.190 mm	
<b>Crystal system</b>	triclinic	
<b>Space group</b>	P -1	
<b>Unit cell dimensions</b>	a = 5.9316(2) Å	α = 79.476(2)°
	b = 9.3304(3) Å	β = 83.146(2)°
	c = 23.4340(8) Å	γ = 78.234(3)°
<b>Volume</b>	1243.78(7) Å <sup>3</sup>	
<b>Z</b>	2	
<b>Density (calculated)</b>	1.544 g/cm <sup>3</sup>	
<b>Absorption coefficient</b>	1.414 mm <sup>-1</sup>	
<b>F(000)</b>	584	

**Table 31.** Data collection and structure refinement for **15**.

<b>Diffractometer</b>	Bruker Apex II CCD	
<b>Radiation source</b>	Bruker X8 Prospector Ultra, IMuS Cu K/α	
<b>Theta range for data collection</b>	1.92 to 68.24°	
<b>Index ranges</b>	-7<=h<=7, -11<=k<=11, -28<=l<=28	
<b>Reflections collected</b>	19374	
<b>Independent reflections</b>	4443 [R(int) = 0.0329]	
<b>Absorption correction</b>	multi-scan	
<b>Max. and min. transmission</b>	0.9300 and 0.7800	
<b>Structure solution technique</b>	direct methods	
<b>Structure solution program</b>	SHELXT 2014/4 (Sheldrick, 2014)	
<b>Refinement method</b>	Full-matrix least-squares on F <sup>2</sup>	
<b>Refinement program</b>	SHELXL-2016/6 (Sheldrick, 2016)	
<b>Function minimized</b>	Σ w(F <sub>o</sub> <sup>2</sup> - F <sub>c</sub> <sup>2</sup> ) <sup>2</sup>	
<b>Data / restraints / parameters</b>	4443 / 0 / 424	
<b>Goodness-of-fit on F<sup>2</sup></b>	2.234	
<b>Final R indices</b>	3652 data; I>2σ(I)	R1 = 0.0689, wR2 = 0.2059
	all data	R1 = 0.0799, wR2 = 0.2143

<b>Weighting scheme</b>	$w=1/[\sigma^2(F_o^2)+(0.0680P)^2]$ ; where $P=(F_o^2+2F_c^2)/3$
<b>Largest diff. peak and hole</b>	0.907 and -0.558 eÅ <sup>-3</sup>
<b>R.M.S. deviation from mean</b>	0.062 eÅ <sup>-3</sup>

**Table 32.** Atomic coordinates and equivalent isotropic atomic displacement parameters (Å<sup>2</sup>) for **15**.

U(eq) is defined as one third of the trace of the orthogonalized U<sub>ij</sub> tensor.

	<b>x/a</b>	<b>y/b</b>	<b>z/c</b>	<b>U(eq)</b>
C1	0.1387(6)	0.0949(4)	0.68813(14)	0.0593(8)
F1	0.1790(7)	0.1909(5)	0.71821(12)	0.1347(14)
N1	0.4022(4)	0.3430(3)	0.28993(10)	0.0450(5)
O1	0.1494(4)	0.2140(3)	0.34568(10)	0.0612(6)
C2	0.2077(5)	0.1298(3)	0.62488(12)	0.0440(6)
F2	0.9125(4)	0.0979(3)	0.70028(10)	0.0865(7)
N2	0.4347(4)	0.5411(3)	0.18436(10)	0.0509(6)
C3	0.4069(5)	0.1864(3)	0.60637(14)	0.0488(7)
F3	0.2312(6)	0.9583(4)	0.71066(11)	0.1278(14)
C4	0.4775(5)	0.2125(3)	0.54724(13)	0.0434(6)
F4	0.2722(4)	0.49915(18)	0.46309(8)	0.0595(5)
C5	0.3495(4)	0.1846(2)	0.50639(11)	0.0360(5)
F5	0.9961(3)	0.4641(2)	0.42056(11)	0.0704(6)
C6	0.1466(4)	0.1309(3)	0.52569(12)	0.0403(6)
F6	0.2436(3)	0.58778(17)	0.37316(8)	0.0601(5)
C7	0.0774(5)	0.1021(3)	0.58414(12)	0.0428(6)
F7	0.8490(4)	0.5045(4)	0.10095(12)	0.1072(10)
C8	0.4318(4)	0.1965(3)	0.44338(12)	0.0395(6)
F8	0.5839(5)	0.3950(3)	0.08522(11)	0.0926(8)
C9	0.6089(5)	0.2854(3)	0.41434(13)	0.0455(6)
F9	0.7417(5)	0.5293(4)	0.01498(11)	0.1069(10)
C10	0.3637(4)	0.3295(3)	0.39644(11)	0.0360(5)
F10	0.8120(12)	0.0407(9)	0.1129(5)	0.291(5)
C11	0.2201(5)	0.4676(3)	0.41380(12)	0.0412(6)
F11	0.0081(13)	0.0817(5)	0.16276(19)	0.218(3)
C12	0.2963(4)	0.2910(3)	0.34117(12)	0.0399(6)
F12	0.0278(15)	0.1585(5)	0.0731(2)	0.244(4)
C13	0.5732(5)	0.4390(3)	0.27959(13)	0.0469(6)

	<b>x/a</b>	<b>y/b</b>	<b>z/c</b>	<b>U(eq)</b>
C14	0.4865(6)	0.5795(3)	0.23806(13)	0.0496(7)
C15	0.3407(7)	0.3071(4)	0.23611(14)	0.0552(7)
C16	0.2560(6)	0.4499(4)	0.19546(15)	0.0563(8)
C17	0.3826(6)	0.6660(4)	0.13831(13)	0.0554(7)
C18	0.4880(6)	0.6564(4)	0.08244(14)	0.0595(8)
C19	0.4337(8)	0.7732(5)	0.03745(16)	0.0761(11)
C20	0.2823(9)	0.8992(5)	0.04746(18)	0.0835(13)
C21	0.1852(9)	0.9122(4)	0.10287(17)	0.0866(13)
C22	0.2351(8)	0.7950(5)	0.14818(16)	0.0766(12)
C23	0.6650(7)	0.5192(6)	0.07090(16)	0.0760(11)
C24	0.0372(18)	0.0559(8)	0.1153(3)	0.167(4)

**Table 33.** Bond lengths (Å) for **15**.

C1-F1	1.310(4)	C1-F3	1.319(4)
C1-F2	1.334(4)	C1-C2	1.485(4)
N1-C12	1.343(4)	N1-C13	1.457(4)
N1-C15	1.466(4)	O1-C12	1.222(3)
C2-C3	1.382(4)	C2-C7	1.387(4)
N2-C17	1.446(4)	N2-C14	1.452(4)
N2-C16	1.462(4)	C3-C4	1.391(4)
C3-H3	0.99(4)	C4-C5	1.380(4)
C4-H4	0.95(4)	F4-C11	1.328(3)
C5-C6	1.392(4)	C5-C8	1.490(4)
F5-C11	1.325(3)	C6-C7	1.376(4)
C6-H6	0.92(3)	F6-C11	1.351(3)
C7-H7	0.91(4)	F7-C23	1.339(5)
C8-C9	1.494(4)	C8-C10	1.522(3)
C8-H8	0.96(4)	F8-C23	1.317(6)
C9-C10	1.516(4)	C9-H9A	0.90(3)
C9-H9B	1.01(4)	F9-C23	1.328(4)
C10-C11	1.488(4)	C10-C12	1.523(4)
F10-C24	1.381(13)	F11-C24	1.166(7)
F12-C24	1.243(7)	C13-C14	1.519(4)
C13-H13A	1.01(4)	C13-H13B	1.00(4)
C14-H14A	1.00(4)	C14-H14B	0.97(3)

C15-C16	1.521(4)	C15-H15A	0.99(5)
C15-H15B	0.99(5)	C16-H16A	1.03(4)
C16-H16B	1.00(4)	C17-C22	1.375(5)
C17-C18	1.392(5)	C18-C19	1.386(5)
C18-C23	1.525(5)	C19-C20	1.365(6)
C19-H19	1.05(5)	C20-C21	1.372(6)
C20-H20	0.83(5)	C21-C22	1.389(5)
C21-C24	1.501(7)	C22-H22	0.93(5)

**Table 34.** Bond angles (°) for **15**.

F1-C1-F3	110.9(3)	F1-C1-F2	103.0(3)
F3-C1-F2	103.1(3)	F1-C1-C2	113.4(3)
F3-C1-C2	112.2(3)	F2-C1-C2	113.4(3)
C12-N1-C13	127.7(2)	C12-N1-C15	119.3(2)
C13-N1-C15	113.0(2)	C3-C2-C7	119.6(3)
C3-C2-C1	119.9(3)	C7-C2-C1	120.5(3)
C17-N2-C14	114.6(2)	C17-N2-C16	112.1(2)
C14-N2-C16	111.1(2)	C2-C3-C4	119.9(3)
C2-C3-H3	121.(2)	C4-C3-H3	119.(2)
C5-C4-C3	120.9(3)	C5-C4-H4	117.(2)
C3-C4-H4	122.(2)	C4-C5-C6	118.4(2)
C4-C5-C8	122.3(2)	C6-C5-C8	119.0(2)
C7-C6-C5	121.1(3)	C7-C6-H6	122.(2)
C5-C6-H6	117.(2)	C6-C7-C2	120.0(3)
C6-C7-H7	120.(2)	C2-C7-H7	120.(2)
C5-C8-C9	124.3(2)	C5-C8-C10	125.9(2)
C9-C8-C10	60.36(17)	C5-C8-H8	111.(2)
C9-C8-H8	115.(2)	C10-C8-H8	111.(2)
C8-C9-C10	60.72(16)	C8-C9-H9A	118.(2)
C10-C9-H9A	118.2(19)	C8-C9-H9B	115.(2)
C10-C9-H9B	118.(2)	H9A-C9-H9B	116.(3)
C11-C10-C9	117.7(2)	C11-C10-C8	119.1(2)
C9-C10-C8	58.92(17)	C11-C10-C12	113.7(2)
C9-C10-C12	122.0(2)	C8-C10-C12	114.6(2)
F5-C11-F4	106.3(2)	F5-C11-F6	105.8(2)
F4-C11-F6	105.5(2)	F5-C11-C10	112.8(2)

F4-C11-C10	114.1(2)	F6-C11-C10	111.7(2)
O1-C12-N1	123.3(3)	O1-C12-C10	118.4(2)
N1-C12-C10	118.3(2)	N1-C13-C14	109.7(2)
N1-C13-H13A	109.8(19)	C14-C13-H13A	110.(2)
N1-C13-H13B	109.(2)	C14-C13-H13B	109.(2)
H13A-C13-H13B	110.(3)	N2-C14-C13	109.7(3)
N2-C14-H14A	112.(2)	C13-C14-H14A	107.(2)
N2-C14-H14B	113.1(18)	C13-C14-H14B	104.2(18)
H14A-C14-H14B	110.(3)	N1-C15-C16	109.4(3)
N1-C15-H15A	109.(2)	C16-C15-H15A	111.(2)
N1-C15-H15B	107.(2)	C16-C15-H15B	111.(2)
H15A-C15-H15B	109.(3)	N2-C16-C15	109.3(3)
N2-C16-H16A	112.(2)	C15-C16-H16A	109.(2)
N2-C16-H16B	113.(2)	C15-C16-H16B	106.(2)
H16A-C16-H16B	108.(3)	C22-C17-C18	118.9(3)
C22-C17-N2	122.1(3)	C18-C17-N2	119.0(3)
C19-C18-C17	119.7(3)	C19-C18-C23	120.1(3)
C17-C18-C23	120.2(3)	C20-C19-C18	120.8(4)
C20-C19-H19	117.(3)	C18-C19-H19	122.(3)
C19-C20-C21	119.9(4)	C19-C20-H20	122.(4)
C21-C20-H20	118.(4)	C20-C21-C22	119.8(4)
C20-C21-C24	120.2(4)	C22-C21-C24	119.9(4)
C17-C22-C21	120.8(4)	C17-C22-H22	118.(3)
C21-C22-H22	121.(3)	F8-C23-F9	106.9(4)
F8-C23-F7	107.4(3)	F9-C23-F7	107.0(3)
F8-C23-C18	113.5(3)	F9-C23-C18	111.3(3)
F7-C23-C18	110.4(4)	F11-C24-F12	120.4(8)
F11-C24-F10	94.8(8)	F12-C24-F10	93.0(7)
F11-C24-C21	119.8(4)	F12-C24-C21	114.3(5)
F10-C24-C21	105.8(8)		

**Table 35.** Anisotropic atomic displacement parameters ( $\text{\AA}^2$ ) for **15**.

The anisotropic atomic displacement factor exponent takes the form:  $-2\pi^2[ h^2 a^{*2}U_{11} + \dots + 2 h k a^* b^* U_{12} ]$

	<b>U<sub>11</sub></b>	<b>U<sub>22</sub></b>	<b>U<sub>33</sub></b>	<b>U<sub>23</sub></b>	<b>U<sub>13</sub></b>	<b>U<sub>12</sub></b>
C1	0.0647(19)	0.0578(18)	0.0530(17)	-0.0120(14)	-0.0047(14)	-0.0034(16)
F1	0.193(3)	0.187(3)	0.0657(15)	-0.0610(19)	0.0213(17)	-0.112(3)
N1	0.0476(12)	0.0413(12)	0.0470(12)	-0.0070(10)	-0.0020(9)	-0.0120(10)
O1	0.0632(13)	0.0715(14)	0.0616(13)	-0.0192(11)	0.0041(10)	-0.0396(12)
C2	0.0465(14)	0.0343(12)	0.0491(15)	-0.0095(11)	-0.0041(11)	-0.0001(11)
F2	0.0824(15)	0.1058(18)	0.0630(13)	-0.0102(12)	0.0180(10)	-0.0155(14)
N2	0.0558(14)	0.0452(13)	0.0461(13)	-0.0028(10)	-0.0030(10)	-0.0010(11)
C3	0.0518(16)	0.0433(14)	0.0557(16)	-0.0140(12)	-0.0139(12)	-0.0085(13)
F3	0.152(3)	0.111(2)	0.0654(15)	0.0239(15)	0.0115(15)	0.057(2)
C4	0.0400(14)	0.0344(12)	0.0581(16)	-0.0085(11)	-0.0061(11)	-0.0106(11)
F4	0.0840(13)	0.0377(8)	0.0586(10)	-0.0159(7)	-0.0088(9)	-0.0071(8)
C5	0.0339(12)	0.0234(10)	0.0495(14)	-0.0038(9)	-0.0038(10)	-0.0041(9)
F5	0.0360(9)	0.0584(11)	0.1188(17)	-0.0353(11)	0.0101(9)	-0.0045(8)
C6	0.0376(13)	0.0364(12)	0.0491(15)	-0.0077(11)	-0.0068(11)	-0.0098(11)
F6	0.0768(12)	0.0303(8)	0.0647(11)	-0.0007(7)	0.0013(9)	-0.0007(8)
C7	0.0369(13)	0.0393(13)	0.0521(15)	-0.0072(11)	0.0005(11)	-0.0092(11)
F7	0.0691(14)	0.146(3)	0.0902(17)	-0.0214(17)	-0.0139(12)	0.0236(16)
C8	0.0366(13)	0.0280(12)	0.0514(15)	-0.0061(10)	0.0001(10)	-0.0031(10)
F8	0.118(2)	0.0663(14)	0.0815(16)	-0.0256(12)	-0.0061(13)	0.0218(14)
C9	0.0320(13)	0.0484(15)	0.0528(16)	-0.0024(13)	0.0014(11)	-0.0082(12)
F9	0.0976(17)	0.137(2)	0.0613(13)	-0.0218(14)	0.0102(11)	0.0314(17)
C10	0.0321(12)	0.0291(11)	0.0463(13)	-0.0036(10)	0.0007(9)	-0.0094(10)
F10	0.176(6)	0.212(7)	0.469(16)	-0.170(9)	-0.013(7)	0.095(5)
C11	0.0406(13)	0.0305(12)	0.0528(15)	-0.0062(11)	0.0000(10)	-0.0103(11)
F11	0.366(8)	0.128(3)	0.099(3)	-0.044(2)	-0.031(4)	0.126(4)
C12	0.0355(12)	0.0337(12)	0.0498(14)	-0.0095(10)	0.0009(10)	-0.0056(11)
F12	0.384(9)	0.094(3)	0.151(4)	0.021(3)	0.055(5)	0.106(4)
C13	0.0404(14)	0.0493(15)	0.0489(15)	-0.0013(12)	-0.0012(11)	-0.0111(13)
C14	0.0534(16)	0.0453(15)	0.0492(15)	-0.0026(12)	-0.0032(12)	-0.0122(14)
C15	0.069(2)	0.0493(16)	0.0505(16)	-0.0102(13)	-0.0066(14)	-0.0154(16)
C16	0.0594(18)	0.0562(18)	0.0533(17)	-0.0101(14)	-0.0116(14)	-0.0058(15)
C17	0.0637(18)	0.0510(16)	0.0452(16)	-0.0032(13)	-0.0051(13)	0.0004(15)
C18	0.0644(19)	0.0595(18)	0.0494(17)	-0.0069(14)	-0.0071(14)	-0.0001(16)
C19	0.092(3)	0.080(3)	0.0461(18)	-0.0025(17)	-0.0027(16)	-0.001(2)
C20	0.123(4)	0.062(2)	0.053(2)	0.0052(17)	-0.014(2)	0.002(2)
C21	0.128(4)	0.057(2)	0.059(2)	-0.0059(17)	-0.012(2)	0.020(2)



	<b>U<sub>11</sub></b>	<b>U<sub>22</sub></b>	<b>U<sub>33</sub></b>	<b>U<sub>23</sub></b>	<b>U<sub>13</sub></b>	<b>U<sub>12</sub></b>
C22	0.101(3)	0.064(2)	0.0462(18)	-0.0047(16)	-0.0010(17)	0.020(2)
C23	0.068(2)	0.097(3)	0.0510(19)	-0.0131(19)	-0.0072(15)	0.014(2)
C24	0.235(9)	0.126(5)	0.066(3)	0.009(3)	-0.002(4)	0.113(6)

**Table 36.** Hydrogen atomic coordinates and isotropic atomic displacement parameters ( $\text{\AA}^2$ ) for **15**.

	<b>x/a</b>	<b>y/b</b>	<b>z/c</b>	<b>U(eq)</b>
H3	0.496(7)	0.216(5)	0.6342(18)	0.073(11)
H4	0.615(7)	0.249(5)	0.5330(18)	0.073(11)
H6	0.060(6)	0.118(4)	0.4977(15)	0.050(8)
H7	-0.056(6)	0.067(4)	0.5957(15)	0.052(9)
H8	0.438(6)	0.104(4)	0.4297(15)	0.053(9)
H9A	0.720(6)	0.244(4)	0.3894(14)	0.041(7)
H9B	0.660(7)	0.348(5)	0.4396(19)	0.076(12)
H13A	0.602(6)	0.465(4)	0.3176(15)	0.053(9)
H13B	0.719(6)	0.386(4)	0.2614(15)	0.058(9)
H14A	0.609(7)	0.642(5)	0.2315(18)	0.074(11)
H14B	0.352(5)	0.628(4)	0.2594(13)	0.041(7)
H15A	0.477(7)	0.248(5)	0.2176(18)	0.071(11)
H15B	0.217(7)	0.247(5)	0.2472(18)	0.076(12)
H16A	0.215(6)	0.424(4)	0.1574(16)	0.058(9)
H16B	0.110(6)	0.498(4)	0.2157(16)	0.059(9)
H19	0.493(8)	0.765(5)	-0.006(2)	0.095(14)
H20	0.238(8)	0.967(6)	0.020(2)	0.089(14)
H22	0.160(9)	0.798(6)	0.185(2)	0.095(15)

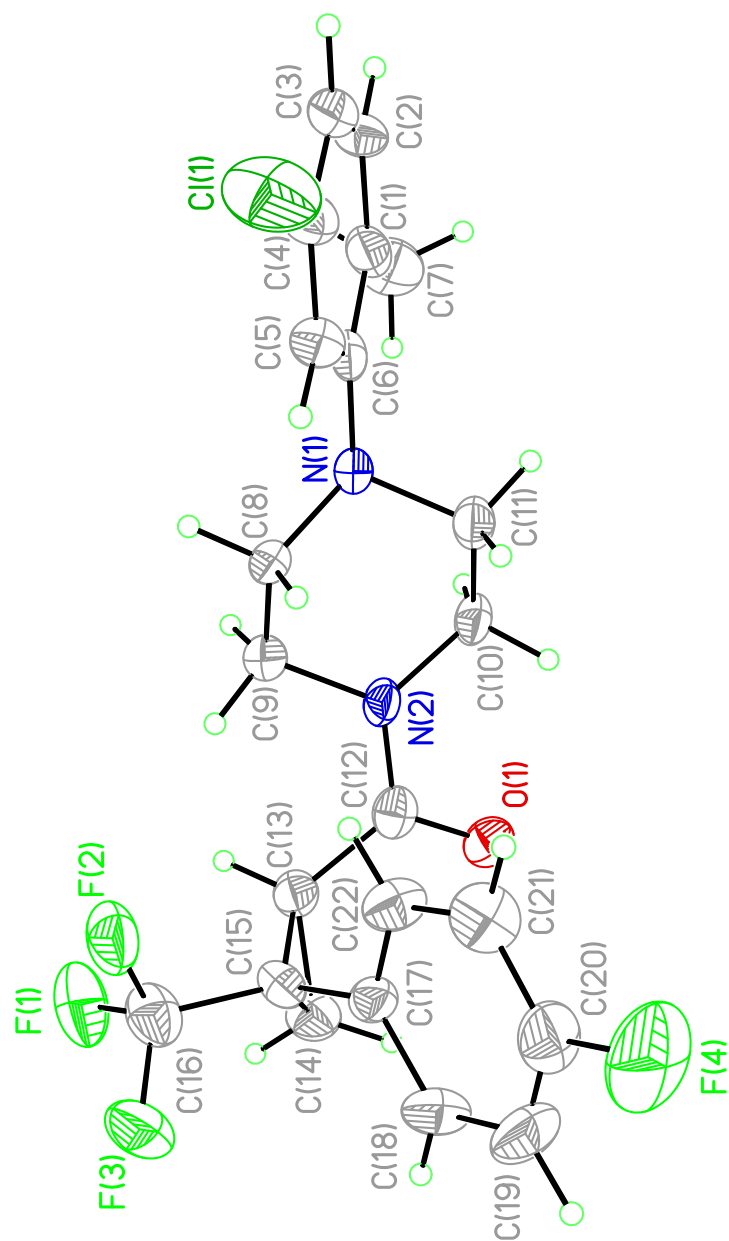


**Figure 62.** X-ray structural information for (-)-**6b**.

**Table 37.** Crystal data for (-)-**6b**.

<b>Chemical formula</b>	C <sub>22</sub> H <sub>21</sub> ClF <sub>4</sub> N <sub>2</sub> O	
<b>Formula weight</b>	440.86 g/mol	
<b>Temperature</b>	230(2) K	
<b>Wavelength</b>	1.54178 Å	
<b>Crystal size</b>	0.040 x 0.090 x 0.180 mm	
<b>Crystal system</b>	orthorhombic	
<b>Space group</b>	P 21 21 21	
<b>Unit cell dimensions</b>	a = 6.8983(15) Å	α = 90°
	b = 15.715(4) Å	β = 90°
	c = 19.766(5) Å	γ = 90°
<b>Volume</b>	2142.8(8) Å <sup>3</sup>	
<b>Z</b>	4	
<b>Density (calculated)</b>	1.367 g/cm <sup>3</sup>	
<b>Absorption coefficient</b>	2.030 mm <sup>-1</sup>	
<b>F(000)</b>	912	

**Table 38.** Data collection and structure refinement for (-)-**6b**.

<b>Diffractometer</b>	Bruker Apex II CCD	
<b>Radiation source</b>	Bruker X8 Prospector Ultra, Cu K <sub>α</sub>	
<b>Theta range for data collection</b>	4.47 to 50.54°	
<b>Index ranges</b>	-6 ≤ h ≤ 6, -13 ≤ k ≤ 15, -19 ≤ l ≤ 14	
<b>Reflections collected</b>	3721	
<b>Independent reflections</b>	2051 [R(int) = 0.0606]	
<b>Absorption correction</b>	multi-scan	
<b>Max. and min. transmission</b>	0.9230 and 0.7110	
<b>Structure solution technique</b>	direct methods	
<b>Structure solution program</b>	SHELXT 2014/4 (Sheldrick, 2014)	
<b>Refinement method</b>	Full-matrix least-squares on F <sup>2</sup>	
<b>Refinement program</b>	SHELXL-2016/6 (Sheldrick, 2016)	
<b>Function minimized</b>	Σ w(F <sub>o</sub> <sup>2</sup> - F <sub>c</sub> <sup>2</sup> ) <sup>2</sup>	
<b>Data / restraints / parameters</b>	2051 / 0 / 273	
<b>Goodness-of-fit on F<sup>2</sup></b>	1.182	
<b>Final R indices</b>	1683 data; I > 2σ(I)	R1 = 0.0614, wR2 = 0.1569
	all data	R1 = 0.0724, wR2 = 0.1644

<b>Weighting scheme</b>	$w=1/[\sigma^2(F_o^2)+(0.0680P)^2]$ ; where $P=(F_o^2+2F_c^2)/3$
<b>Absolute structure parameter</b>	0.00(7)
<b>Extinction coefficient</b>	0.0050(10)
<b>Largest diff. peak and hole</b>	0.251 and -0.263 eÅ <sup>-3</sup>
<b>R.M.S. deviation from mean</b>	0.061 eÅ <sup>-3</sup>

**Table 39.** Atomic coordinates and equivalent isotropic atomic displacement parameters (Å<sup>2</sup>) for (-)-**6b**.

U(eq) is defined as one third of the trace of the orthogonalized U<sub>ij</sub> tensor.

	<b>x/a</b>	<b>y/b</b>	<b>z/c</b>	<b>U(eq)</b>
C1	0.9793(15)	0.5959(6)	0.4443(4)	0.048(3)
C2	0.8428(15)	0.6608(6)	0.4445(5)	0.054(3)
C3	0.7900(14)	0.7020(6)	0.5012(5)	0.057(3)
C4	0.8724(16)	0.6795(6)	0.5628(5)	0.056(3)
C5	0.0102(15)	0.6149(6)	0.5656(5)	0.052(3)
C6	0.0665(12)	0.5735(5)	0.5068(4)	0.038(2)
C7	0.0282(17)	0.5478(7)	0.3812(5)	0.073(3)
C8	0.2014(14)	0.4538(5)	0.5685(4)	0.040(2)
C9	0.3138(14)	0.3731(5)	0.5555(4)	0.044(2)
C10	0.5292(14)	0.4559(6)	0.4796(5)	0.048(3)
C11	0.4031(13)	0.5327(6)	0.4948(5)	0.047(2)
C12	0.6598(16)	0.3375(6)	0.5443(4)	0.045(2)
C13	0.6304(15)	0.2662(5)	0.5926(4)	0.047(3)
C14	0.7970(15)	0.2181(6)	0.6192(4)	0.053(3)
C15	0.6882(14)	0.2766(5)	0.6648(4)	0.043(2)
C16	0.5605(18)	0.2351(7)	0.7177(6)	0.064(3)
C17	0.7815(14)	0.3565(6)	0.6902(4)	0.044(3)
C18	0.9623(18)	0.3544(7)	0.7197(5)	0.065(3)
C19	0.0461(19)	0.4270(10)	0.7461(6)	0.086(4)
C20	0.946(2)	0.5012(9)	0.7440(5)	0.075(4)
C21	0.7658(18)	0.5079(7)	0.7157(5)	0.067(3)
C22	0.6833(17)	0.4334(6)	0.6896(5)	0.056(3)
Cl1	0.8111(6)	0.73345(19)	0.63604(15)	0.0989(13)
F1	0.4828(11)	0.1637(4)	0.6959(4)	0.100(3)
F2	0.4145(9)	0.2852(4)	0.7339(3)	0.083(2)
F3	0.6530(11)	0.2171(4)	0.7745(3)	0.090(2)
F4	0.0308(13)	0.5730(6)	0.7688(4)	0.134(4)

	<b>x/a</b>	<b>y/b</b>	<b>z/c</b>	<b>U(eq)</b>
N1	0.2033(10)	0.5059(4)	0.5086(3)	0.0388(18)
N2	0.5097(11)	0.3912(4)	0.5302(3)	0.0413(19)
O1	0.8198(10)	0.3492(4)	0.5166(3)	0.0577(18)

**Table 40.** Bond lengths (Å) for (-)-**6b**.

C1-C2	1.388(13)	C1-C6	1.418(12)
C1-C7	1.498(13)	C2-C3	1.346(13)
C2-H2A	0.94	C3-C4	1.388(13)
C3-H3A	0.94	C4-C5	1.392(13)
C4-C11	1.731(10)	C5-C6	1.387(12)
C5-H5A	0.94	C6-N1	1.422(10)
C7-H7A	0.97	C7-H7B	0.97
C7-H7C	0.97	C8-N1	1.441(10)
C8-C9	1.507(12)	C8-H8A	0.98
C8-H8B	0.98	C9-N2	1.469(11)
C9-H9A	0.98	C9-H9B	0.98
C10-N2	1.432(11)	C10-C11	1.519(12)
C10-H10A	0.98	C10-H10B	0.98
C11-N1	1.467(10)	C11-H11A	0.98
C11-H11B	0.98	C12-O1	1.246(11)
C12-N2	1.365(12)	C12-C13	1.486(12)
C13-C14	1.473(13)	C13-C15	1.492(12)
C13-H13A	0.99	C14-C15	1.492(12)
C14-H14A	0.98	C14-H14B	0.98
C15-C17	1.497(12)	C15-C16	1.515(13)
C16-F1	1.317(12)	C16-F2	1.317(12)
C16-F3	1.321(12)	C17-C18	1.378(13)
C17-C22	1.384(13)	C18-C19	1.381(16)
C18-H18A	0.94	C19-C20	1.354(17)
C19-H19A	0.94	C20-F4	1.361(13)
C20-C21	1.370(16)	C21-C22	1.400(14)
C21-H21A	0.94	C22-H22A	0.94

**Table 41.** Bond angles (°) for (-)-**6b**.

C2-C1-C6	117.9(8)	C2-C1-C7	121.7(9)
C6-C1-C7	120.4(9)	C3-C2-C1	122.6(9)
C3-C2-H2A	118.7	C1-C2-H2A	118.7
C2-C3-C4	119.8(9)	C2-C3-H3A	120.1
C4-C3-H3A	120.1	C3-C4-C5	120.1(9)
C3-C4-C11	120.5(8)	C5-C4-C11	119.4(8)
C6-C5-C4	119.9(9)	C6-C5-H5A	120.0
C4-C5-H5A	120.0	C5-C6-C1	119.7(9)
C5-C6-N1	121.1(8)	C1-C6-N1	119.2(8)
C1-C7-H7A	109.5	C1-C7-H7B	109.5
H7A-C7-H7B	109.5	C1-C7-H7C	109.5
H7A-C7-H7C	109.5	H7B-C7-H7C	109.5
N1-C8-C9	109.4(7)	N1-C8-H8A	109.8
C9-C8-H8A	109.8	N1-C8-H8B	109.8
C9-C8-H8B	109.8	H8A-C8-H8B	108.2
N2-C9-C8	111.7(7)	N2-C9-H9A	109.3
C8-C9-H9A	109.3	N2-C9-H9B	109.3
C8-C9-H9B	109.3	H9A-C9-H9B	108.0
N2-C10-C11	111.9(7)	N2-C10-H10A	109.2
C11-C10-H10A	109.2	N2-C10-H10B	109.2
C11-C10-H10B	109.2	H10A-C10-H10B	107.9
N1-C11-C10	110.2(7)	N1-C11-H11A	109.6
C10-C11-H11A	109.6	N1-C11-H11B	109.6
C10-C11-H11B	109.6	H11A-C11-H11B	108.1
O1-C12-N2	119.4(8)	O1-C12-C13	121.0(9)
N2-C12-C13	119.6(9)	C14-C13-C12	120.6(9)
C14-C13-C15	60.4(6)	C12-C13-C15	119.7(8)
C14-C13-H13A	115.1	C12-C13-H13A	115.1
C15-C13-H13A	115.1	C13-C14-C15	60.4(6)
C13-C14-H14A	117.7	C15-C14-H14A	117.7
C13-C14-H14B	117.7	C15-C14-H14B	117.7
H14A-C14-H14B	114.8	C14-C15-C13	59.2(6)
C14-C15-C17	120.3(8)	C13-C15-C17	121.9(7)
C14-C15-C16	116.4(8)	C13-C15-C16	117.2(9)
C17-C15-C16	112.3(7)	F1-C16-F2	106.1(10)

F1-C16-F3	107.0(9)	F2-C16-F3	106.9(9)
F1-C16-C15	112.2(9)	F2-C16-C15	110.8(9)
F3-C16-C15	113.4(10)	C18-C17-C22	117.9(9)
C18-C17-C15	120.7(9)	C22-C17-C15	121.3(9)
C17-C18-C19	121.2(11)	C17-C18-H18A	119.4
C19-C18-H18A	119.4	C20-C19-C18	119.2(11)
C20-C19-H19A	120.4	C18-C19-H19A	120.4
C19-C20-F4	119.1(13)	C19-C20-C21	122.7(11)
F4-C20-C21	118.2(13)	C20-C21-C22	117.1(11)
C20-C21-H21A	121.5	C22-C21-H21A	121.5
C17-C22-C21	121.9(10)	C17-C22-H22A	119.1
C21-C22-H22A	119.1	C6-N1-C8	116.0(7)
C6-N1-C11	113.8(6)	C8-N1-C11	109.0(7)
C12-N2-C10	120.7(8)	C12-N2-C9	120.6(7)
C10-N2-C9	117.5(7)		

**Table 42.** Anisotropic atomic displacement parameters ( $\text{\AA}^2$ ) for (-)-**6b**.

The anisotropic atomic displacement factor exponent takes the form:  $-2\pi^2[ h^2 a^{*2}U_{11} + \dots + 2 h k a^* b^* U_{12} ]$

	<b>U<sub>11</sub></b>	<b>U<sub>22</sub></b>	<b>U<sub>33</sub></b>	<b>U<sub>23</sub></b>	<b>U<sub>13</sub></b>	<b>U<sub>12</sub></b>
C1	0.053(7)	0.045(6)	0.047(6)	0.009(5)	-0.007(5)	-0.012(5)
C2	0.050(7)	0.055(6)	0.055(7)	0.019(5)	-0.014(6)	0.002(6)
C3	0.046(7)	0.049(6)	0.075(8)	0.021(6)	0.010(6)	0.008(5)
C4	0.059(8)	0.044(6)	0.066(7)	0.010(5)	0.011(6)	0.012(5)
C5	0.049(7)	0.056(6)	0.052(6)	0.012(5)	-0.004(5)	0.002(6)
C6	0.037(6)	0.035(5)	0.042(5)	0.003(4)	0.010(5)	-0.008(4)
C7	0.088(10)	0.079(8)	0.052(6)	-0.002(6)	-0.014(7)	0.003(7)
C8	0.029(6)	0.047(5)	0.043(5)	0.007(4)	0.001(5)	-0.002(4)
C9	0.040(7)	0.042(5)	0.051(5)	0.006(4)	-0.001(5)	-0.003(5)
C10	0.034(6)	0.058(6)	0.051(5)	0.008(5)	0.009(5)	-0.010(5)
C11	0.041(7)	0.043(6)	0.057(6)	0.003(5)	0.006(5)	-0.008(5)
C12	0.046(7)	0.046(6)	0.043(6)	-0.009(4)	0.002(6)	-0.008(6)
C13	0.040(7)	0.043(6)	0.059(6)	0.006(5)	0.007(5)	0.005(5)
C14	0.052(7)	0.048(6)	0.060(6)	0.000(5)	0.005(5)	0.016(5)
C15	0.053(7)	0.038(5)	0.039(5)	0.006(4)	0.006(5)	0.006(5)
C16	0.074(9)	0.045(7)	0.073(8)	0.003(6)	0.013(7)	0.004(6)

	<b>U<sub>11</sub></b>	<b>U<sub>22</sub></b>	<b>U<sub>33</sub></b>	<b>U<sub>23</sub></b>	<b>U<sub>13</sub></b>	<b>U<sub>12</sub></b>
C17	0.037(7)	0.057(6)	0.037(5)	0.005(4)	-0.001(5)	0.001(5)
C18	0.069(9)	0.072(8)	0.054(6)	0.006(6)	-0.020(6)	0.010(7)
C19	0.057(10)	0.117(12)	0.084(9)	0.002(8)	-0.032(7)	-0.019(9)
C20	0.086(11)	0.082(10)	0.056(7)	-0.004(6)	-0.017(7)	-0.034(8)
C21	0.087(10)	0.056(7)	0.059(7)	-0.017(5)	-0.003(6)	0.000(6)
C22	0.051(7)	0.055(6)	0.063(6)	-0.011(5)	-0.012(6)	0.007(6)
Cl1	0.127(3)	0.085(2)	0.084(2)	-0.0091(16)	0.024(2)	0.051(2)
F1	0.115(6)	0.071(5)	0.115(6)	0.010(4)	0.027(5)	-0.031(5)
F2	0.070(5)	0.071(4)	0.107(5)	0.024(4)	0.040(4)	0.008(4)
F3	0.095(5)	0.111(5)	0.064(4)	0.036(4)	-0.001(4)	0.009(5)
F4	0.140(9)	0.129(7)	0.134(7)	-0.050(6)	-0.023(6)	-0.063(6)
N1	0.033(5)	0.038(4)	0.045(4)	0.007(3)	0.003(4)	-0.005(4)
N2	0.030(5)	0.041(5)	0.053(5)	0.005(4)	0.012(4)	-0.001(4)
O1	0.042(5)	0.062(4)	0.070(4)	0.004(3)	0.004(4)	0.005(4)

**Table 43.** Hydrogen atomic coordinates and isotropic atomic displacement parameters ( $\text{\AA}^2$ ) for (-)-**6b**.

	<b>x/a</b>	<b>y/b</b>	<b>z/c</b>	<b>U(eq)</b>
H2A	-0.2150	0.6766	0.4033	0.064
H3A	-0.3024	0.7459	0.4992	0.068
H5A	0.0650	0.5993	0.6074	0.063
H7A	0.1260	0.5053	0.3912	0.11
H7B	-0.0873	0.5200	0.3640	0.11
H7C	0.0777	0.5869	0.3474	0.11
H8A	0.0675	0.4398	0.5807	0.048
H8B	0.2599	0.4850	0.6063	0.048
H9A	0.3232	0.3404	0.5976	0.053
H9B	0.2441	0.3384	0.5223	0.053
H10A	0.4928	0.4323	0.4355	0.057
H10B	0.6651	0.4738	0.4771	0.057
H11A	0.4548	0.5631	0.5341	0.056
H11B	0.4047	0.5717	0.4561	0.056
H13A	0.5114	0.2322	0.5851	0.057
H14A	0.9269	0.2355	0.6046	0.064
H14B	0.7808	0.1567	0.6261	0.064



	<b>x/a</b>	<b>y/b</b>	<b>z/c</b>	<b>U(eq)</b>
H18A	1.0300	0.3025	0.7220	0.078
H19A	1.1707	0.4250	0.7652	0.103
H21A	0.7000	0.5602	0.7139	0.081
H22A	0.5578	0.4356	0.6713	0.067

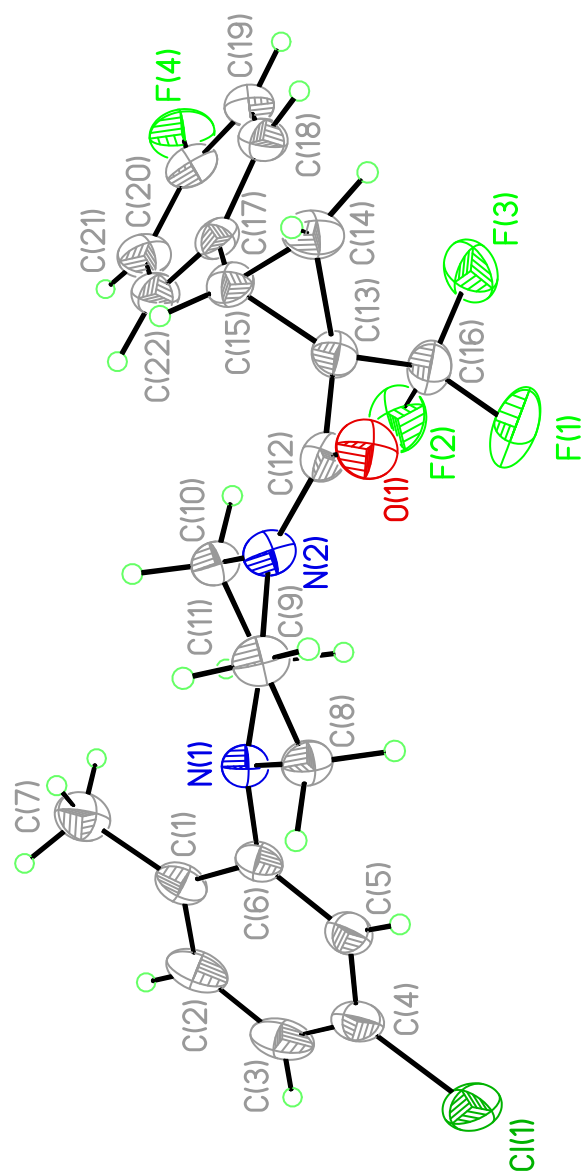


**Figure 63.** X-ray structural information for (-)-11a.

**Table 44.** Crystal data for (-)-11a.

<b>Chemical formula</b>	C <sub>22</sub> H <sub>21</sub> ClF <sub>4</sub> N <sub>2</sub> O	
<b>Formula weight</b>	440.86 g/mol	
<b>Temperature</b>	230(2) K	
<b>Wavelength</b>	1.54178 Å	
<b>Crystal size</b>	0.130 x 0.150 x 0.220 mm	
<b>Crystal system</b>	orthorhombic	
<b>Space group</b>	P 21 21 21	
<b>Unit cell dimensions</b>	a = 10.0283(6) Å	α = 90°
	b = 13.7511(8) Å	β = 90°
	c = 15.1078(8) Å	γ = 90°
<b>Volume</b>	2083.4(2) Å <sup>3</sup>	
<b>Z</b>	4	
<b>Density (calculated)</b>	1.406 g/cm <sup>3</sup>	
<b>Absorption coefficient</b>	2.088 mm <sup>-1</sup>	
<b>F(000)</b>	912	

**Table 45.** Data collection and structure refinement for (-)-11a.

<b>Diffractometer</b>	Bruker Aoex II CCD	
<b>Theta range for data collection</b>	4.35 to 68.55°	
<b>Index ranges</b>	-12 ≤ h ≤ 11, -16 ≤ k ≤ 16, -18 ≤ l ≤ 18	
<b>Reflections collected</b>	17703	
<b>Independent reflections</b>	3828 [R(int) = 0.0491]	
<b>Absorption correction</b>	multi-scan	
<b>Max. and min. transmission</b>	0.7700 and 0.6600	
<b>Structure solution technique</b>	direct methods	
<b>Structure solution program</b>	SHELXT 2014/4 (Sheldrick, 2014)	
<b>Refinement method</b>	Full-matrix least-squares on F <sup>2</sup>	
<b>Refinement program</b>	SHELXL-2016/6 (Sheldrick, 2016)	
<b>Function minimized</b>	Σ w(F <sub>o</sub> <sup>2</sup> - F <sub>c</sub> <sup>2</sup> ) <sup>2</sup>	
<b>Data / restraints / parameters</b>	3828 / 0 / 357	
<b>Goodness-of-fit on F<sup>2</sup></b>	0.914	
<b>Final R indices</b>	3484 data; I > 2σ(I)	R1 = 0.0293, wR2 = 0.0865
	all data	R1 = 0.0329, wR2 = 0.0899
<b>Weighting scheme</b>	w = 1/[σ <sup>2</sup> (F <sub>o</sub> <sup>2</sup> ) + (0.0680P) <sup>2</sup> ]; where P = (F <sub>o</sub> <sup>2</sup> + 2F <sub>c</sub> <sup>2</sup> )/3	

<b>Absolute structure parameter</b>	0.02(2)
<b>Extinction coefficient</b>	0.0055(6)
<b>Largest diff. peak and hole</b>	0.165 and -0.154 eÅ <sup>-3</sup>
<b>R.M.S. deviation from mean</b>	0.026 eÅ <sup>-3</sup>

**Table 46.** Atomic coordinates and equivalent isotropic atomic displacement parameters (Å<sup>2</sup>) for (-)-**11a**.

U(eq) is defined as one third of the trace of the orthogonalized U<sub>ij</sub> tensor.

	<b>x/a</b>	<b>y/b</b>	<b>z/c</b>	<b>U(eq)</b>
C1	0.7000(3)	0.66744(18)	0.02808(17)	0.0481(6)
Cl1	0.92547(9)	0.63048(8)	0.77098(5)	0.0865(3)
F1	0.2877(2)	0.5075(2)	0.25638(15)	0.0984(8)
N1	0.8377(2)	0.54237(13)	0.09626(12)	0.0399(4)
O1	0.1065(2)	0.32358(13)	0.27177(13)	0.0572(5)
C2	0.6698(3)	0.7229(2)	0.9541(2)	0.0598(7)
F2	0.1736(2)	0.62440(14)	0.30840(15)	0.0823(6)
N2	0.9640(2)	0.44444(14)	0.23766(12)	0.0431(5)
C3	0.7367(3)	0.7130(2)	0.87433(19)	0.0632(8)
F3	0.31977(19)	0.55688(16)	0.38888(14)	0.0817(6)
C4	0.8368(3)	0.6451(2)	0.86905(16)	0.0565(7)
F4	0.0751(2)	0.83459(14)	0.63672(12)	0.0809(6)
C5	0.8715(3)	0.5880(2)	0.94092(16)	0.0479(6)
C6	0.8047(2)	0.59981(17)	0.02126(15)	0.0406(5)
C7	0.6177(3)	0.6766(3)	0.1110(2)	0.0662(8)
C8	0.9092(3)	0.45211(17)	0.07964(15)	0.0439(5)
C9	0.9081(3)	0.38989(18)	0.16295(16)	0.0480(6)
C10	0.8994(3)	0.53848(17)	0.25265(14)	0.0421(5)
C11	0.9023(3)	0.59703(17)	0.16777(15)	0.0416(5)
C12	0.0632(2)	0.40545(17)	0.28563(14)	0.0414(5)
C13	0.1240(2)	0.46550(17)	0.36023(16)	0.0425(5)
C14	0.1517(3)	0.4100(2)	0.44391(18)	0.0569(7)
C15	0.0451(3)	0.48547(18)	0.44470(15)	0.0440(5)
C16	0.2259(3)	0.5374(2)	0.32882(18)	0.0548(7)
C17	0.0552(2)	0.57782(18)	0.49689(14)	0.0433(5)
C18	0.1551(3)	0.5944(2)	0.55924(17)	0.0537(6)
C19	0.1623(3)	0.6803(2)	0.60632(17)	0.0577(7)

	<b>x/a</b>	<b>y/b</b>	<b>z/c</b>	<b>U(eq)</b>
C20	0.0672(3)	0.7496(2)	0.59128(15)	0.0559(6)
C21	0.9645(3)	0.7358(2)	0.53322(18)	0.0592(7)
C22	0.9591(3)	0.6494(2)	0.48593(16)	0.0516(6)

**Table 47.** Bond lengths (Å) for (-)-**11a**.

C1-C2	1.386(4)	C1-C6	1.406(4)
C1-C7	1.505(4)	C11-C4	1.740(3)
F1-C16	1.323(3)	N1-C6	1.420(3)
N1-C8	1.455(3)	N1-C11	1.467(3)
O1-C12	1.225(3)	C2-C3	1.387(5)
C2-H2	0.96(4)	F2-C16	1.342(4)
N2-C12	1.343(3)	N2-C10	1.464(3)
N2-C9	1.466(3)	C3-C4	1.373(5)
C3-H3	1.00(4)	F3-C16	1.334(4)
C4-C5	1.385(4)	F4-C20	1.358(3)
C5-C6	1.396(4)	C5-H5	0.90(3)
C7-H7A	0.99(4)	C7-H7B	1.01(4)
C7-H7C	0.99(4)	C8-C9	1.522(3)
C8-H8A	1.03(3)	C8-H8B	0.99(3)
C9-H9A	1.00(3)	C9-H9B	0.90(3)
C10-C11	1.514(3)	C10-H10A	1.00(3)
C10-H10B	0.99(3)	C11-H11A	0.97(3)
C11-H11B	1.02(3)	C12-C13	1.525(3)
C13-C16	1.499(4)	C13-C14	1.503(3)
C13-C15	1.526(3)	C14-C15	1.490(4)
C14-H14A	1.01(4)	C14-H14B	1.01(4)
C15-C17	1.498(4)	C15-H15	0.98(3)
C17-C22	1.388(4)	C17-C18	1.394(4)
C18-C19	1.380(4)	C18-H18	0.91(3)
C19-C20	1.367(4)	C19-H19	0.96(4)
C20-C21	1.366(4)	C21-C22	1.387(4)
C21-H21	0.89(4)	C22-H22	0.99(4)

**Table 48.** Bond angles (°) for (-)-**11a**.

C2-C1-C6	117.9(3)	C2-C1-C7	120.3(3)
C6-C1-C7	121.7(2)	C6-N1-C8	116.83(19)
C6-N1-C11	113.92(18)	C8-N1-C11	110.26(19)
C1-C2-C3	122.7(3)	C1-C2-H2	117.(2)
C3-C2-H2	120.(2)	C12-N2-C10	126.7(2)
C12-N2-C9	119.6(2)	C10-N2-C9	113.7(2)
C4-C3-C2	118.1(2)	C4-C3-H3	120.(2)
C2-C3-H3	122.(2)	C3-C4-C5	121.6(3)
C3-C4-C11	120.1(2)	C5-C4-C11	118.3(2)
C4-C5-C6	119.7(3)	C4-C5-H5	120.(2)
C6-C5-H5	120.(2)	C5-C6-C1	119.9(2)
C5-C6-N1	121.1(2)	C1-C6-N1	118.9(2)
C1-C7-H7A	108.7(19)	C1-C7-H7B	110.(2)
H7A-C7-H7B	105.(3)	C1-C7-H7C	111.(2)
H7A-C7-H7C	112.(3)	H7B-C7-H7C	110.(3)
N1-C8-C9	109.47(19)	N1-C8-H8A	113.4(16)
C9-C8-H8A	107.4(16)	N1-C8-H8B	107.3(17)
C9-C8-H8B	111.8(16)	H8A-C8-H8B	108.(2)
N2-C9-C8	110.3(2)	N2-C9-H9A	107.7(18)
C8-C9-H9A	111.8(17)	N2-C9-H9B	110.(2)
C8-C9-H9B	105.(2)	H9A-C9-H9B	112.(3)
N2-C10-C11	109.29(19)	N2-C10-H10A	110.1(17)
C11-C10-H10A	108.2(18)	N2-C10-H10B	108.6(15)
C11-C10-H10B	109.6(15)	H10A-C10-H10B	111.(2)
N1-C11-C10	110.05(19)	N1-C11-H11A	110.(2)
C10-C11-H11A	110.(2)	N1-C11-H11B	108.3(15)
C10-C11-H11B	109.7(15)	H11A-C11-H11B	109.(3)
O1-C12-N2	122.5(2)	O1-C12-C13	118.8(2)
N2-C12-C13	118.6(2)	C16-C13-C14	118.4(2)
C16-C13-C12	113.3(2)	C14-C13-C12	114.9(2)
C16-C13-C15	120.0(2)	C14-C13-C15	58.93(17)
C12-C13-C15	120.5(2)	C15-C14-C13	61.33(16)
C15-C14-H14A	116.(2)	C13-C14-H14A	114.(2)
C15-C14-H14B	121.(2)	C13-C14-H14B	117.(2)
H14A-C14-H14B	116.(3)	C14-C15-C17	123.1(2)

C14-C15-C13	59.74(16)	C17-C15-C13	123.9(2)
C14-C15-H15	113.1(18)	C17-C15-H15	115.3(18)
C13-C15-H15	110.2(18)	F1-C16-F3	107.2(2)
F1-C16-F2	105.7(3)	F3-C16-F2	104.7(2)
F1-C16-C13	112.1(2)	F3-C16-C13	113.4(2)
F2-C16-C13	113.2(2)	C22-C17-C18	117.6(2)
C22-C17-C15	119.4(2)	C18-C17-C15	122.9(2)
C19-C18-C17	121.7(3)	C19-C18-H18	115.(2)
C17-C18-H18	123.(2)	C20-C19-C18	118.3(3)
C20-C19-H19	121.(2)	C18-C19-H19	121.(2)
F4-C20-C21	119.2(3)	F4-C20-C19	118.4(3)
C21-C20-C19	122.4(3)	C20-C21-C22	118.6(3)
C20-C21-H21	121.(3)	C22-C21-H21	120.(3)
C21-C22-C17	121.2(3)	C21-C22-H22	117.1(19)
C17-C22-H22	121.6(19)		

**Table 49.** Anisotropic atomic displacement parameters ( $\text{\AA}^2$ ) for (-)-**11a**.

The anisotropic atomic displacement factor exponent takes the form:  $-2\pi^2 [ h^2 a^{*2} U_{11} + \dots + 2 h k a^* b^* U_{12} ]$

	$U_{11}$	$U_{22}$	$U_{33}$	$U_{23}$	$U_{13}$	$U_{12}$
C1	0.0517(13)	0.0375(13)	0.0551(13)	-0.0070(10)	-0.0151(11)	0.0007(11)
Cl1	0.0816(6)	0.1331(8)	0.0447(3)	0.0170(4)	-0.0013(3)	-0.0318(5)
F1	0.0873(14)	0.1165(18)	0.0915(14)	-0.0407(13)	0.0496(12)	-0.0383(13)
N1	0.0467(10)	0.0329(10)	0.0401(9)	-0.0022(7)	-0.0028(8)	0.0029(8)
O1	0.0668(12)	0.0363(10)	0.0685(10)	-0.0005(8)	-0.0035(9)	0.0143(8)
C2	0.0705(19)	0.0390(15)	0.0700(17)	0.0011(12)	-0.0321(15)	-0.0003(13)
F2	0.0828(12)	0.0603(11)	0.1038(14)	0.0294(10)	0.0145(11)	-0.0173(10)
N2	0.0571(12)	0.0310(10)	0.0411(9)	0.0002(7)	-0.0013(8)	0.0072(8)
C3	0.082(2)	0.0491(16)	0.0586(16)	0.0156(13)	-0.0305(15)	-0.0167(15)
F3	0.0547(10)	0.1015(16)	0.0889(13)	-0.0164(11)	-0.0043(9)	-0.0198(10)
C4	0.0592(16)	0.0672(19)	0.0430(12)	0.0087(11)	-0.0114(12)	-0.0229(14)
F4	0.1158(17)	0.0623(11)	0.0645(9)	-0.0160(8)	-0.0108(10)	0.0042(11)
C5	0.0461(14)	0.0527(16)	0.0448(12)	0.0030(10)	-0.0063(10)	-0.0070(12)
C6	0.0452(12)	0.0342(12)	0.0426(11)	-0.0007(9)	-0.0088(9)	-0.0044(9)
C7	0.0613(19)	0.071(2)	0.0659(17)	-0.0158(15)	-0.0100(14)	0.0229(15)
C8	0.0531(14)	0.0380(12)	0.0407(11)	-0.0044(9)	-0.0017(10)	0.0066(10)

	<b>U<sub>11</sub></b>	<b>U<sub>22</sub></b>	<b>U<sub>33</sub></b>	<b>U<sub>23</sub></b>	<b>U<sub>13</sub></b>	<b>U<sub>12</sub></b>
C9	0.0637(16)	0.0333(13)	0.0470(12)	-0.0028(9)	-0.0024(12)	0.0021(12)
C10	0.0527(14)	0.0331(12)	0.0405(11)	-0.0019(8)	0.0000(10)	0.0074(10)
C11	0.0503(13)	0.0326(12)	0.0419(10)	0.0004(9)	-0.0068(10)	0.0021(10)
C12	0.0473(12)	0.0322(12)	0.0446(11)	0.0060(8)	0.0062(9)	0.0020(9)
C13	0.0434(12)	0.0367(12)	0.0473(12)	0.0049(9)	0.0003(9)	0.0058(9)
C14	0.0713(18)	0.0438(16)	0.0558(14)	0.0078(11)	-0.0103(13)	0.0136(14)
C15	0.0503(14)	0.0390(13)	0.0428(11)	0.0116(9)	0.0023(10)	0.0008(10)
C16	0.0485(15)	0.0602(17)	0.0557(14)	-0.0064(12)	0.0100(12)	-0.0054(12)
C17	0.0503(13)	0.0438(13)	0.0357(9)	0.0097(9)	0.0059(9)	0.0010(10)
C18	0.0541(15)	0.0602(18)	0.0469(12)	0.0053(11)	-0.0050(11)	0.0082(13)
C19	0.0598(16)	0.0701(19)	0.0433(12)	-0.0021(12)	-0.0053(12)	-0.0007(14)
C20	0.0783(18)	0.0493(15)	0.0401(11)	0.0000(10)	0.0055(12)	-0.0003(14)
C21	0.0724(19)	0.0546(18)	0.0507(13)	0.0017(11)	-0.0038(13)	0.0180(14)
C22	0.0535(14)	0.0552(16)	0.0461(12)	0.0036(10)	-0.0037(11)	0.0080(11)

**Table 50.** Hydrogen atomic coordinates and isotropic atomic displacement parameters ( $\text{\AA}^2$ ) for (-)-**11a**.

	<b>x/a</b>	<b>y/b</b>	<b>z/c</b>	<b>U(eq)</b>
H2	0.598(4)	0.769(3)	-0.040(2)	0.076(11)
H3	0.716(3)	0.755(2)	-0.178(2)	0.068(9)
H5	0.933(3)	0.541(2)	-0.065(2)	0.053(8)
H7A	0.525(4)	0.693(2)	0.094(2)	0.063(9)
H7B	0.612(4)	0.611(3)	0.142(3)	0.083(11)
H7C	0.657(4)	0.725(3)	0.152(3)	0.085(12)
H8A	1.007(3)	0.463(2)	0.0620(19)	0.048(7)
H8B	0.864(3)	0.419(2)	0.0298(19)	0.047(7)
H9A	0.962(3)	0.329(2)	0.1555(19)	0.058(8)
H9B	0.821(3)	0.376(2)	0.173(2)	0.058(9)
H10A	0.804(3)	0.529(2)	0.270(2)	0.054(8)
H10B	0.949(3)	0.5737(19)	0.2997(18)	0.041(7)
H11A	0.857(3)	0.659(2)	0.176(2)	0.068(10)
H11B	0.999(3)	0.610(2)	0.1498(17)	0.048(7)
H14A	1.239(4)	0.428(3)	0.474(2)	0.070(10)
H14B	1.128(4)	0.339(3)	0.444(2)	0.072(10)
H15	0.955(3)	0.458(2)	0.440(2)	0.051(8)



	<b>x/a</b>	<b>y/b</b>	<b>z/c</b>	<b>U(eq)</b>
H18	1.215(4)	0.548(2)	0.575(2)	0.062(9)
H19	1.233(4)	0.692(3)	0.648(2)	0.074(10)
H21	0.900(4)	0.780(3)	0.527(3)	0.082(11)
H22	0.882(3)	0.641(2)	0.445(2)	0.062(9)

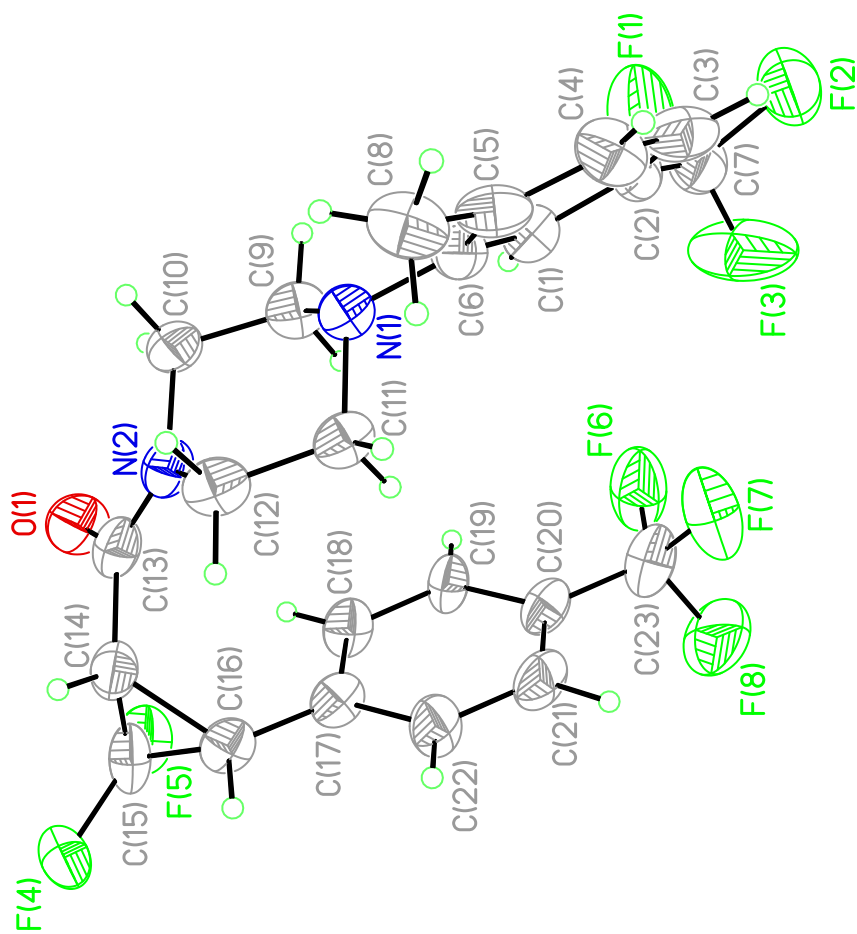


**Figure 64.** X-ray structural information for (-)-34.

**Table 51.** Crystal data for (-)-**34**.

<b>Identification code</b>	st769031	
<b>Chemical formula</b>	C <sub>23</sub> H <sub>20</sub> F <sub>8</sub> N <sub>2</sub> O	
<b>Formula weight</b>	492.41 g/mol	
<b>Temperature</b>	230(2) K	
<b>Wavelength</b>	1.54178 Å	
<b>Crystal size</b>	0.020 x 0.120 x 0.200 mm	
<b>Crystal system</b>	monoclinic	
<b>Space group</b>	P 1 21 1	
<b>Unit cell dimensions</b>	a = 10.9909(9) Å	α = 90°
	b = 10.5085(10) Å	β = 99.376(7)°
	c = 20.090(2) Å	γ = 90°
<b>Volume</b>	2289.4(4) Å <sup>3</sup>	
<b>Z</b>	4	
<b>Density (calculated)</b>	1.429 g/cm <sup>3</sup>	
<b>Absorption coefficient</b>	1.173 mm <sup>-1</sup>	
<b>F(000)</b>	1008	

**Table 52.** Data collection and structure refinement for (-)-**34**.

<b>Diffractometer</b>	Bruker Apex II CCD
<b>Radiation source</b>	Bruker X8 Prospector Ultra, IμS Cu K/α
<b>Theta range for data collection</b>	2.23 to 68.39°
<b>Index ranges</b>	-13 ≤ h ≤ 12, -12 ≤ k ≤ 11, -24 ≤ l ≤ 24
<b>Reflections collected</b>	32756
<b>Independent reflections</b>	8340 [R(int) = 0.1472]
<b>Absorption correction</b>	multi-scan
<b>Max. and min. transmission</b>	0.9770 and 0.7990
<b>Structure solution technique</b>	direct methods
<b>Structure solution program</b>	SHELXT 2014/4 (Sheldrick, 2014)
<b>Refinement method</b>	Full-matrix least-squares on F <sup>2</sup>
<b>Refinement program</b>	SHELXL-2016/6 (Sheldrick, 2016)
<b>Function minimized</b>	Σ w(F <sub>o</sub> <sup>2</sup> - F <sub>c</sub> <sup>2</sup> ) <sup>2</sup>
<b>Data / restraints / parameters</b>	8340 / 1 / 616
<b>Goodness-of-fit on F<sup>2</sup></b>	1.231

$\Delta/\sigma_{\max}$	0.001
<b>Final R indices</b>	3994 data; $I > 2\sigma(I)$ R1 = 0.1068, wR2 = 0.2497 all data R1 = 0.1921, wR2 = 0.2934
<b>Weighting scheme</b>	$w=1/[\sigma^2(F_o^2)+(0.0680P)^2]$ ; where $P=(F_o^2+2F_c^2)/3$
<b>Absolute structure parameter</b>	0.1(5)
<b>Largest diff. peak and hole</b>	0.584 and -0.347 eÅ <sup>-3</sup>
<b>R.M.S. deviation from mean</b>	0.096 eÅ <sup>-3</sup>

**Table 53.** Atomic coordinates and equivalent isotropic atomic displacement parameters (Å<sup>2</sup>) for (-)-**34**.

U(eq) is defined as one third of the trace of the orthogonalized U<sub>ij</sub> tensor.

	<b>x/a</b>	<b>y/b</b>	<b>z/c</b>	<b>U(eq)</b>
C1	0.9924(12)	0.3615(12)	0.3377(6)	0.058(3)
C2	0.0956(13)	0.4129(12)	0.3155(7)	0.061(4)
C3	0.0860(17)	0.5264(14)	0.2815(7)	0.081(5)
C4	0.9739(16)	0.5835(13)	0.2674(8)	0.076(4)
C5	0.8663(15)	0.5334(12)	0.2857(6)	0.066(4)
C6	0.8793(13)	0.4189(11)	0.3226(6)	0.059(3)
C7	0.2092(16)	0.3451(15)	0.3345(9)	0.080(4)
C8	0.7431(15)	0.5970(14)	0.2655(7)	0.082(5)
C9	0.7698(13)	0.2305(10)	0.3574(7)	0.062(3)
C10	0.6428(13)	0.1860(12)	0.3613(7)	0.063(4)
C011	0.5365(12)	0.5951(10)	0.8257(6)	0.052(3)
C11	0.7286(13)	0.4352(11)	0.4006(6)	0.057(3)
C12	0.6000(13)	0.3955(11)	0.4080(7)	0.064(4)
C13	0.5532(12)	0.1938(12)	0.4656(7)	0.061(3)
C14	0.5112(13)	0.2716(12)	0.5202(7)	0.062(3)
C15	0.5325(12)	0.2293(12)	0.5886(8)	0.067(4)
C16	0.6076(12)	0.3390(10)	0.5758(6)	0.056(3)
C17	0.7398(12)	0.3361(10)	0.5768(6)	0.054(3)
C18	0.8048(12)	0.2245(10)	0.5642(6)	0.059(3)
C19	0.9302(11)	0.2296(11)	0.5608(7)	0.056(3)
C20	0.9946(13)	0.3464(11)	0.5699(6)	0.061(3)
C21	0.9305(14)	0.4527(12)	0.5843(7)	0.071(4)
C22	0.8048(14)	0.4486(11)	0.5864(7)	0.069(4)
C23	0.1272(16)	0.3522(15)	0.5669(9)	0.085(5)
C24	0.4322(12)	0.6502(11)	0.8452(6)	0.057(3)

	<b>x/a</b>	<b>y/b</b>	<b>z/c</b>	<b>U(eq)</b>
C25	0.3173(13)	0.5958(11)	0.8234(6)	0.059(3)
C26	0.3079(14)	0.4858(11)	0.7846(6)	0.064(4)
C27	0.4131(14)	0.4335(12)	0.7656(7)	0.066(4)
C28	0.5278(13)	0.4875(11)	0.7845(6)	0.056(3)
C29	0.2093(15)	0.6538(13)	0.8428(9)	0.071(4)
C30	0.6371(14)	0.4330(13)	0.7592(7)	0.072(4)
C31	0.6613(12)	0.7835(10)	0.8661(7)	0.061(3)
C32	0.7962(12)	0.8300(12)	0.8731(7)	0.066(4)
C33	0.7331(11)	0.5733(11)	0.9012(6)	0.055(3)
C34	0.8685(13)	0.6172(11)	0.9105(6)	0.061(3)
C35	0.9383(12)	0.8094(11)	0.9790(7)	0.057(3)
C36	0.0103(12)	0.7189(12)	0.0293(6)	0.059(3)
C37	0.0312(13)	0.7503(11)	0.1002(7)	0.060(3)
C38	0.9448(11)	0.6473(10)	0.0821(6)	0.050(3)
C39	0.8090(11)	0.6576(10)	0.0800(5)	0.046(3)
C40	0.7434(12)	0.7717(10)	0.0748(6)	0.055(3)
C41	0.6171(14)	0.7720(12)	0.0729(8)	0.069(4)
C42	0.5551(12)	0.6584(12)	0.0748(7)	0.060(3)
C43	0.6201(14)	0.5440(12)	0.0783(7)	0.069(4)
C44	0.7446(15)	0.5464(12)	0.0814(7)	0.071(4)
C45	0.4175(16)	0.6583(17)	0.0736(10)	0.089(5)
F1	0.2082(10)	0.2228(11)	0.3167(7)	0.139(4)
F2	0.3040(9)	0.3860(10)	0.3019(5)	0.114(3)
F3	0.2619(12)	0.3495(18)	0.3968(6)	0.181(7)
F4	0.4416(7)	0.2475(8)	0.6278(4)	0.085(2)
F5	0.5870(7)	0.1189(6)	0.6101(4)	0.078(2)
F6	0.1712(9)	0.2497(10)	0.5443(7)	0.124(4)
F7	0.1540(10)	0.4491(11)	0.5272(6)	0.126(4)
F8	0.1947(10)	0.3803(13)	0.6264(6)	0.139(4)
F9	0.1873(13)	0.6264(18)	0.8990(6)	0.188(8)
F10	0.1035(10)	0.6201(13)	0.8052(7)	0.148(5)
F11	0.2045(11)	0.7757(10)	0.8354(9)	0.160(6)
F12	0.9980(7)	0.8614(7)	0.1271(4)	0.075(2)
F13	0.1443(7)	0.7174(8)	0.1393(4)	0.082(2)
F14	0.3640(10)	0.7617(11)	0.0543(9)	0.164(6)
F15	0.3608(10)	0.5672(12)	0.0368(7)	0.141(5)

	<b>x/a</b>	<b>y/b</b>	<b>z/c</b>	<b>U(eq)</b>
F16	0.3902(12)	0.6337(17)	0.1348(8)	0.179(6)
N1	0.7698(10)	0.3683(9)	0.3427(5)	0.055(3)
N2	0.5977(10)	0.2558(9)	0.4167(5)	0.059(3)
N3	0.6582(10)	0.6479(8)	0.8461(5)	0.054(3)
N4	0.8739(10)	0.7547(9)	0.9237(6)	0.061(3)
O1	0.5486(10)	0.0755(8)	0.4683(5)	0.082(3)
O2	0.9430(10)	0.9245(8)	0.9875(5)	0.080(3)

**Table 54.** Bond lengths (Å) for (-)-**34**.

C1-C6	1.371(18)	C1-C2	1.393(18)
C1-H1A	0.94	C2-C3	1.370(19)
C2-C7	1.43(2)	C3-C4	1.36(2)
C3-H3A	0.94	C4-C5	1.40(2)
C4-H4A	0.94	C5-C6	1.408(17)
C5-C8	1.51(2)	C6-N1	1.433(16)
C7-F3	1.293(18)	C7-F1	1.334(18)
C7-F2	1.385(17)	C8-H8A	0.97
C8-H8B	0.97	C8-H8C	0.97
C9-N1	1.478(14)	C9-C10	1.486(19)
C9-H9A	0.98	C9-H9B	0.98
C10-N2	1.483(15)	C10-H10A	0.98
C10-H10B	0.98	C011-C28	1.395(16)
C011-C24	1.396(17)	C011-N3	1.444(15)
C11-N1	1.491(15)	C11-C12	1.504(18)
C11-H11A	0.98	C11-H11B	0.98
C12-N2	1.479(15)	C12-H12A	0.98
C12-H12B	0.98	C13-O1	1.246(14)
C13-N2	1.336(16)	C13-C14	1.501(18)
C14-C15	1.425(19)	C14-C16	1.577(18)
C14-H14A	0.99	C15-F5	1.345(14)
C15-F4	1.383(16)	C15-C16	1.465(17)
C16-C17	1.450(18)	C16-H16A	0.99
C17-C22	1.378(16)	C17-C18	1.418(16)
C18-C19	1.392(17)	C18-H18A	0.94
C19-C20	1.413(16)	C19-H19A	0.94

C20-C21	1.377(19)	C20-C23	1.47(2)
C21-C22	1.39(2)	C21-H21A	0.94
C22-H22A	0.94	C23-F6	1.293(18)
C23-F8	1.333(18)	C23-F7	1.354(18)
C24-C25	1.391(17)	C24-H24A	0.94
C25-C26	1.389(18)	C25-C29	1.442(19)
C26-C27	1.388(19)	C26-H26A	0.94
C27-C28	1.379(19)	C27-H27A	0.94
C28-C30	1.494(19)	C29-F9	1.229(17)
C29-F11	1.289(17)	C29-F10	1.327(18)
C30-H30A	0.97	C30-H30B	0.97
C30-H30C	0.97	C31-N3	1.479(14)
C31-C32	1.545(18)	C31-H31A	0.98
C31-H31B	0.98	C32-N4	1.452(16)
C32-H32A	0.98	C32-H32B	0.98
C33-N3	1.490(14)	C33-C34	1.540(18)
C33-H33A	0.98	C33-H33B	0.98
C34-N4	1.469(15)	C34-H34A	0.98
C34-H34B	0.98	C35-O2	1.222(14)
C35-N4	1.345(16)	C35-C36	1.514(17)
C36-C37	1.443(17)	C36-C38	1.567(17)
C36-H36A	0.99	C37-F12	1.361(13)
C37-F13	1.401(15)	C37-C38	1.447(17)
C38-C39	1.490(17)	C38-H38A	0.99
C39-C44	1.369(17)	C39-C40	1.395(16)
C40-C41	1.383(19)	C40-H40A	0.94
C41-C42	1.377(18)	C41-H41A	0.94
C42-C43	1.394(19)	C42-C45	1.51(2)
C43-C44	1.36(2)	C43-H43A	0.94
C44-H44A	0.94	C45-F14	1.267(19)
C45-F15	1.30(2)	C45-F16	1.34(2)

**Table 55.** Bond angles (°) for (-)-**34**.

C6-C1-C2	120.9(12)	C6-C1-H1A	119.5
C2-C1-H1A	119.5	C3-C2-C1	119.8(15)
C3-C2-C7	123.9(14)	C1-C2-C7	116.2(12)

C4-C3-C2	118.8(16)	C4-C3-H3A	120.6
C2-C3-H3A	120.6	C3-C4-C5	123.8(14)
C3-C4-H4A	118.1	C5-C4-H4A	118.1
C4-C5-C6	116.3(13)	C4-C5-C8	121.6(12)
C6-C5-C8	122.1(14)	C1-C6-C5	120.2(13)
C1-C6-N1	123.2(11)	C5-C6-N1	116.6(13)
F3-C7-F1	106.1(14)	F3-C7-F2	101.2(14)
F1-C7-F2	98.4(14)	F3-C7-C2	118.2(15)
F1-C7-C2	116.0(14)	F2-C7-C2	114.2(13)
C5-C8-H8A	109.5	C5-C8-H8B	109.5
H8A-C8-H8B	109.5	C5-C8-H8C	109.5
H8A-C8-H8C	109.5	H8B-C8-H8C	109.5
N1-C9-C10	110.4(10)	N1-C9-H9A	109.6
C10-C9-H9A	109.6	N1-C9-H9B	109.6
C10-C9-H9B	109.6	H9A-C9-H9B	108.1
N2-C10-C9	108.4(10)	N2-C10-H10A	110.0
C9-C10-H10A	110.0	N2-C10-H10B	110.0
C9-C10-H10B	110.0	H10A-C10-H10B	108.4
C28-C011-C24	121.5(12)	C28-C011-N3	116.8(12)
C24-C011-N3	121.7(11)	N1-C11-C12	110.9(10)
N1-C11-H11A	109.5	C12-C11-H11A	109.5
N1-C11-H11B	109.5	C12-C11-H11B	109.5
H11A-C11-H11B	108.1	N2-C12-C11	108.7(10)
N2-C12-H12A	109.9	C11-C12-H12A	109.9
N2-C12-H12B	109.9	C11-C12-H12B	109.9
H12A-C12-H12B	108.3	O1-C13-N2	122.7(12)
O1-C13-C14	119.5(12)	N2-C13-C14	117.8(11)
C15-C14-C13	120.9(12)	C15-C14-C16	58.2(8)
C13-C14-C16	120.7(11)	C15-C14-H14A	115.1
C13-C14-H14A	115.1	C16-C14-H14A	115.1
F5-C15-F4	105.2(11)	F5-C15-C14	124.9(13)
F4-C15-C14	119.1(12)	F5-C15-C16	120.0(11)
F4-C15-C16	118.1(11)	C14-C15-C16	66.1(9)
C17-C16-C15	125.0(10)	C17-C16-C14	123.8(11)
C15-C16-C14	55.7(9)	C17-C16-H16A	113.5
C15-C16-H16A	113.5	C14-C16-H16A	113.5
C22-C17-C18	118.1(13)	C22-C17-C16	118.6(11)
C18-C17-C16	123.2(11)	C19-C18-C17	120.5(11)



C19-C18-H18A	119.7	C17-C18-H18A	119.7
C18-C19-C20	120.4(12)	C18-C19-H19A	119.8
C20-C19-H19A	119.8	C21-C20-C19	118.0(13)
C21-C20-C23	121.3(12)	C19-C20-C23	120.7(12)
C20-C21-C22	121.8(12)	C20-C21-H21A	119.1
C22-C21-H21A	119.1	C17-C22-C21	121.1(12)
C17-C22-H22A	119.4	C21-C22-H22A	119.4
F6-C23-F8	108.3(15)	F6-C23-F7	107.0(15)
F8-C23-F7	102.7(13)	F6-C23-C20	114.2(13)
F8-C23-C20	112.5(15)	F7-C23-C20	111.5(13)
C25-C24-C011	119.1(12)	C25-C24-H24A	120.4
C011-C24-H24A	120.4	C26-C25-C24	119.9(13)
C26-C25-C29	120.9(13)	C24-C25-C29	119.1(12)
C27-C26-C25	119.7(14)	C27-C26-H26A	120.1
C25-C26-H26A	120.1	C28-C27-C26	121.7(13)
C28-C27-H27A	119.1	C26-C27-H27A	119.1
C27-C28-C011	118.0(12)	C27-C28-C30	119.9(12)
C011-C28-C30	122.1(13)	F9-C29-F11	109.1(15)
F9-C29-F10	100.1(15)	F11-C29-F10	100.6(15)
F9-C29-C25	116.3(14)	F11-C29-C25	114.2(13)
F10-C29-C25	114.7(13)	C28-C30-H30A	109.5
C28-C30-H30B	109.5	H30A-C30-H30B	109.5
C28-C30-H30C	109.5	H30A-C30-H30C	109.5
H30B-C30-H30C	109.5	N3-C31-C32	108.0(10)
N3-C31-H31A	110.1	C32-C31-H31A	110.1
N3-C31-H31B	110.1	C32-C31-H31B	110.1
H31A-C31-H31B	108.4	N4-C32-C31	109.7(10)
N4-C32-H32A	109.7	C31-C32-H32A	109.7
N4-C32-H32B	109.7	C31-C32-H32B	109.7
H32A-C32-H32B	108.2	N3-C33-C34	109.8(9)
N3-C33-H33A	109.7	C34-C33-H33A	109.7
N3-C33-H33B	109.7	C34-C33-H33B	109.7
H33A-C33-H33B	108.2	N4-C34-C33	109.0(10)
N4-C34-H34A	109.9	C33-C34-H34A	109.9
N4-C34-H34B	109.9	C33-C34-H34B	109.9
H34A-C34-H34B	108.3	O2-C35-N4	122.8(12)
O2-C35-C36	121.6(12)	N4-C35-C36	115.5(11)
C37-C36-C35	119.8(11)	C37-C36-C38	57.3(8)

C35-C36-C38	120.4(11)	C37-C36-H36A	115.6
C35-C36-H36A	115.6	C38-C36-H36A	115.6
F12-C37-F13	105.1(10)	F12-C37-C36	125.3(11)
F13-C37-C36	118.7(11)	F12-C37-C38	122.3(11)
F13-C37-C38	116.2(10)	C36-C37-C38	65.7(9)
C37-C38-C39	124.5(10)	C37-C38-C36	57.0(8)
C39-C38-C36	121.0(10)	C37-C38-H38A	114.2
C39-C38-H38A	114.2	C36-C38-H38A	114.2
C44-C39-C40	118.2(12)	C44-C39-C38	117.2(11)
C40-C39-C38	124.6(10)	C41-C40-C39	120.6(11)
C41-C40-H40A	119.7	C39-C40-H40A	119.7
C42-C41-C40	119.8(11)	C42-C41-H41A	120.1
C40-C41-H41A	120.1	C41-C42-C43	119.8(12)
C41-C42-C45	120.0(13)	C43-C42-C45	120.3(13)
C44-C43-C42	119.3(12)	C44-C43-H43A	120.3
C42-C43-H43A	120.3	C43-C44-C39	122.4(13)
C43-C44-H44A	118.8	C39-C44-H44A	118.8
F14-C45-F15	107.5(17)	F14-C45-F16	106.5(18)
F15-C45-F16	102.8(15)	F14-C45-C42	114.7(14)
F15-C45-C42	113.3(15)	F16-C45-C42	111.1(15)
C6-N1-C9	116.6(10)	C6-N1-C11	114.9(9)
C9-N1-C11	107.3(9)	C13-N2-C12	125.8(10)
C13-N2-C10	121.2(10)	C12-N2-C10	112.9(10)
C011-N3-C31	115.3(10)	C011-N3-C33	112.5(9)
C31-N3-C33	108.6(9)	C35-N4-C32	121.1(10)
C35-N4-C34	124.7(11)	C32-N4-C34	114.0(11)

**Table 56.** Anisotropic atomic displacement parameters ( $\text{\AA}^2$ ) for (-)-**34**.

The anisotropic atomic displacement factor exponent takes the form:  $-2\pi^2 [ h^2 a^{*2} U_{11} + \dots + 2 h k a^* b^* U_{12} ]$

	$U_{11}$	$U_{22}$	$U_{33}$	$U_{23}$	$U_{13}$	$U_{12}$
C1	0.063(9)	0.046(7)	0.062(8)	0.003(6)	0.002(7)	0.008(6)
C2	0.068(10)	0.060(8)	0.054(8)	0.009(6)	0.007(7)	-0.017(7)
C3	0.118(15)	0.066(10)	0.062(10)	-0.012(7)	0.022(10)	0.006(9)
C4	0.094(13)	0.053(8)	0.086(11)	0.011(7)	0.029(9)	0.005(8)
C5	0.095(12)	0.056(8)	0.049(8)	0.001(6)	0.014(8)	0.022(7)
C6	0.073(10)	0.048(7)	0.058(9)	-0.002(5)	0.016(7)	-0.008(6)
C7	0.089(13)	0.072(11)	0.077(11)	0.018(8)	0.011(10)	-0.012(9)

	<b>U<sub>11</sub></b>	<b>U<sub>22</sub></b>	<b>U<sub>33</sub></b>	<b>U<sub>23</sub></b>	<b>U<sub>13</sub></b>	<b>U<sub>12</sub></b>
C8	0.094(13)	0.080(10)	0.075(11)	0.016(7)	0.024(9)	0.022(8)
C9	0.077(10)	0.038(7)	0.071(9)	-0.003(5)	0.013(7)	0.010(6)
C10	0.072(10)	0.056(8)	0.062(9)	-0.018(6)	0.014(7)	-0.007(6)
C011	0.057(9)	0.043(6)	0.051(8)	0.005(5)	-0.003(6)	-0.005(5)
C11	0.077(10)	0.037(6)	0.057(8)	0.000(5)	0.005(7)	0.001(6)
C12	0.076(10)	0.046(7)	0.069(9)	-0.004(6)	0.009(7)	0.022(6)
C13	0.055(9)	0.049(8)	0.075(10)	-0.007(6)	-0.003(7)	-0.005(6)
C14	0.052(8)	0.067(8)	0.065(10)	-0.002(7)	0.002(7)	-0.011(6)
C15	0.039(8)	0.054(8)	0.102(12)	0.005(7)	-0.003(8)	-0.005(6)
C16	0.066(10)	0.033(6)	0.068(9)	-0.004(5)	0.007(7)	0.005(5)
C17	0.068(9)	0.035(6)	0.057(8)	0.005(5)	0.003(6)	0.000(5)
C18	0.061(9)	0.030(6)	0.083(9)	-0.003(5)	0.006(7)	0.002(5)
C19	0.043(8)	0.042(6)	0.081(9)	-0.005(5)	-0.001(6)	-0.005(5)
C20	0.070(10)	0.043(7)	0.065(8)	-0.006(5)	-0.002(7)	-0.010(6)
C21	0.083(12)	0.042(8)	0.087(11)	-0.020(6)	0.010(9)	-0.016(7)
C22	0.070(11)	0.037(7)	0.102(12)	-0.013(6)	0.024(9)	-0.012(6)
C23	0.075(12)	0.065(10)	0.108(13)	-0.003(9)	-0.009(10)	-0.014(8)
C24	0.060(9)	0.050(7)	0.058(8)	0.004(6)	-0.001(7)	0.003(6)
C25	0.069(10)	0.050(8)	0.058(8)	0.011(6)	0.013(7)	-0.010(6)
C26	0.078(11)	0.047(7)	0.061(9)	0.008(6)	-0.005(8)	-0.003(6)
C27	0.069(11)	0.055(8)	0.071(10)	-0.006(6)	0.004(8)	-0.002(7)
C28	0.079(10)	0.046(7)	0.042(8)	0.002(5)	0.005(7)	0.005(6)
C29	0.067(11)	0.055(9)	0.094(13)	-0.009(7)	0.016(9)	-0.001(7)
C30	0.087(11)	0.070(9)	0.061(9)	-0.008(6)	0.013(8)	0.003(7)
C31	0.055(9)	0.036(6)	0.087(10)	0.005(5)	0.002(7)	0.005(5)
C32	0.069(10)	0.053(8)	0.068(9)	0.014(6)	-0.015(7)	-0.008(6)
C33	0.061(9)	0.040(6)	0.060(8)	0.004(5)	-0.004(7)	-0.005(5)
C34	0.082(10)	0.042(7)	0.057(8)	-0.002(5)	0.004(7)	-0.004(6)
C35	0.061(9)	0.049(8)	0.060(9)	0.000(6)	0.007(7)	-0.008(6)
C36	0.056(8)	0.054(7)	0.065(9)	-0.004(6)	0.005(7)	-0.007(6)
C37	0.058(9)	0.048(8)	0.070(10)	-0.008(6)	0.002(7)	0.009(6)
C38	0.051(8)	0.041(6)	0.059(8)	0.001(5)	0.012(6)	0.005(5)
C39	0.060(9)	0.037(6)	0.042(7)	0.002(4)	0.005(6)	-0.001(5)
C40	0.064(9)	0.035(6)	0.065(9)	-0.009(5)	0.008(7)	-0.007(6)
C41	0.072(11)	0.042(7)	0.099(11)	-0.008(6)	0.024(9)	0.015(6)
C42	0.047(9)	0.060(8)	0.073(9)	-0.006(6)	0.010(7)	-0.003(6)

	<b>U<sub>11</sub></b>	<b>U<sub>22</sub></b>	<b>U<sub>33</sub></b>	<b>U<sub>23</sub></b>	<b>U<sub>13</sub></b>	<b>U<sub>12</sub></b>
C43	0.070(11)	0.049(8)	0.092(11)	-0.002(6)	0.028(9)	-0.014(7)
C44	0.083(12)	0.039(7)	0.089(11)	0.006(6)	0.010(9)	-0.011(7)
C45	0.075(13)	0.071(11)	0.124(15)	0.021(10)	0.025(11)	-0.004(9)
F1	0.081(7)	0.091(8)	0.245(14)	0.007(8)	0.026(8)	0.019(5)
F2	0.091(8)	0.130(9)	0.123(8)	0.015(6)	0.020(6)	-0.020(6)
F3	0.120(10)	0.35(2)	0.068(8)	-0.001(10)	-0.006(7)	0.098(13)
F4	0.057(5)	0.098(6)	0.102(6)	-0.011(5)	0.026(5)	-0.011(4)
F5	0.079(6)	0.052(4)	0.099(6)	0.017(4)	0.004(5)	-0.005(4)
F6	0.069(7)	0.097(8)	0.208(12)	-0.040(7)	0.027(7)	-0.001(5)
F7	0.079(7)	0.109(8)	0.196(12)	0.023(7)	0.040(7)	-0.013(5)
F8	0.079(8)	0.197(13)	0.128(9)	-0.040(8)	-0.023(7)	-0.005(7)
F9	0.147(12)	0.33(2)	0.100(9)	0.068(11)	0.062(9)	0.139(13)
F10	0.067(7)	0.167(12)	0.215(14)	-0.058(10)	0.038(8)	-0.009(7)
F11	0.108(9)	0.078(7)	0.318(18)	-0.011(9)	0.109(11)	0.007(6)
F12	0.090(6)	0.056(4)	0.081(5)	-0.014(4)	0.017(4)	-0.013(4)
F13	0.057(5)	0.104(6)	0.080(6)	0.003(4)	-0.003(4)	-0.004(4)
F14	0.071(8)	0.089(8)	0.33(2)	0.044(10)	0.028(9)	0.004(6)
F15	0.076(8)	0.121(9)	0.222(14)	-0.005(9)	0.010(8)	-0.028(6)
F16	0.090(9)	0.271(19)	0.192(14)	0.032(13)	0.066(9)	0.015(10)
N1	0.060(7)	0.046(6)	0.059(6)	-0.001(4)	0.009(5)	0.004(5)
N2	0.061(7)	0.043(6)	0.069(7)	-0.006(5)	0.003(6)	-0.004(5)
N3	0.063(7)	0.039(5)	0.055(6)	0.001(4)	-0.009(5)	-0.009(5)
N4	0.061(7)	0.047(6)	0.073(7)	-0.005(5)	0.009(6)	-0.011(5)
O1	0.105(8)	0.047(6)	0.099(8)	-0.015(5)	0.031(6)	-0.015(5)
O2	0.107(9)	0.043(5)	0.086(7)	-0.001(4)	0.006(6)	-0.022(5)

**Table 57.** Hydrogen atomic coordinates and isotropic atomic displacement parameters ( $\text{\AA}^2$ ) for (-)-**34**.

	<b>x/a</b>	<b>y/b</b>	<b>z/c</b>	<b>U(eq)</b>
H1A	1.0006	0.2863	0.3635	0.069
H3A	1.1557	0.5641	0.2682	0.097
H4A	0.9684	0.6613	0.2440	0.091
H8A	0.6801	0.5328	0.2532	0.123
H8B	0.7463	0.6524	0.2272	0.123
H8C	0.7237	0.6469	0.3030	0.123
H9A	0.8237	0.2134	0.4003	0.074

	<b>x/a</b>	<b>y/b</b>	<b>z/c</b>	<b>U(eq)</b>
H9B	0.8021	0.1837	0.3219	0.074
H10A	0.5884	0.2022	0.3184	0.075
H10B	0.6432	0.0943	0.3702	0.075
H11A	0.7306	0.5274	0.3934	0.069
H11B	0.7852	0.4154	0.4422	0.069
H12A	0.5754	0.4376	0.4473	0.077
H12B	0.5419	0.4204	0.3678	0.077
H14A	0.4332	0.3188	0.5065	0.075
H16A	0.5777	0.4206	0.5918	0.067
H18A	0.7629	0.1463	0.5581	0.07
H19A	0.9724	0.1550	0.5524	0.068
H21A	0.9729	0.5302	0.5929	0.086
H22A	0.7633	0.5239	0.5945	0.082
H24A	0.4396	0.7231	0.8727	0.069
H26A	0.2308	0.4470	0.7712	0.077
H27A	0.4059	0.3593	0.7391	0.079
H30A	0.6114	0.3976	0.7145	0.109
H30B	0.6733	0.3664	0.7895	0.109
H30C	0.6975	0.4995	0.7570	0.109
H31A	0.6312	0.7933	0.9091	0.073
H31B	0.6084	0.8338	0.8318	0.073
H32A	0.8252	0.8219	0.8296	0.08
H32B	0.8009	0.9199	0.8862	0.08
H33A	0.7280	0.4825	0.8900	0.066
H33B	0.7005	0.5856	0.9434	0.066
H34A	0.9169	0.5716	0.9484	0.073
H34B	0.9034	0.5983	0.8697	0.073
H36A	1.0777	0.6716	1.0131	0.071
H38A	0.9789	0.5618	1.0946	0.06
H40A	0.7854	0.8491	1.0727	0.066
H41A	0.5736	0.8493	1.0703	0.083
H43A	0.5783	0.4660	1.0785	0.082
H44A	0.7879	0.4690	1.0847	0.085

## BIBLIOGRAPHY

1. Siegel, R. L.; Miller, K. D.; Jemal, A. *CA-Cancer J. Clin.* **2017**, *67*, 7–30.
2. Thompson, I. M.; Goodman, P. J.; Tangen, C. M.; Parnes, H. L.; Minasian, L. M.; Godley, P. A.; Lucia, S.; Ford, L. G. *N. Engl. J. Med.* **2013**, *369*, 603–610.
3. Hamdy, F. C.; Donovan, J. L.; Lane, J. A.; Mason, M.; Metcalfe, C.; Holding, P.; Davis, M.; Peters, T. J.; Turner, E. L.; Martin, R. M.; Oxley, J.; Robinson, M.; Staffurth, J.; Walsh, E.; Bollina, P.; Catto, J.; Doble, A.; Doherty, A.; Gillatt, D.; Kockelbergh, R.; Kynaston, H.; Paul, A.; Powell, P.; Prescott, S.; Rosario, D. J.; Rowe, E.; Neal, D. E. *N. Engl. J. Med.* **2016**, *377*, 132–142.
4. Wilt, T. J.; Jones, K. M.; Barry, M. J.; Andriole, G. L.; Culkin, D.; Wheeler, T.; Aronson, W. J.; Brawer, M. K. *N. Engl. J. Med.* **2017**, *375*, 1415–1424.
5. Denmeade, S. R.; Isaacs, J. T. *Nat. Rev. Cancer* **2002**, *2*, 389–396.
6. Hotte, S. J.; Saad, F. *Curr. Oncol.* **2010**, *17*, 72–79.
7. Evans, R. M. *Science* **1988**, *240*, 889–895.
8. Mangelsdorf, D. J.; Thummel, C.; Beato, M.; Herrlich, P.; Schütz, G.; Umesono, K.; Blumberg, B.; Kastner, P.; Mark, M.; Chambon, P.; Evans, R. M. *Cell* **1995**, *83*, 835–839.
9. De Mol, E.; Fenwick, R. B.; Phang, C. T. W.; Buzón, V.; Szulc, E.; de la Fuente, A.; Escobedo, A.; García, J.; Bertoncini, C. W.; Estébanez-Perpiñá, E.; McEwan, I. J.; Riera, A.; Salvatella, X. *ACS Chem. Biol.* **2016**, *11*, 2499–2505.
10. Lavery, D. N.; McEwan, I. J. *Biochem.* **2008**, *47*, 3360–3369.
11. Reid, J.; Kelly, S. M.; Watt, K.; Price, N. C.; McEwan, I. J. *J. Biol. Chem.* **2002**, *277*, 20079–20086.
12. Jenster, G.; van der Korput, H. A.; Trapman, J.; Brinkmann, A. O. *J. Biol. Chem.* **1995**, *270*, 7341–7346.
13. Tan, M. E.; Li, J.; Xu, H. E.; Melcher, K.; Yong, E. *Acta Pharmacol. Sin.* **2015**, *36*, 3–23.
14. Shaffer, P. L.; Jivan, A.; Dollins, D. E.; Claessens, F.; Gewirth, D. T. *Proc. Natl. Acad. Sci. U S A* **2004**, *101*, 4758–4763.

15. Centenera, M. M.; Harris, J. M.; Tilley, W. D.; Butler, L. M. *Mol. Endocrinol.* **2008**, *22*, 2373–2382.
16. Helsen, C.; Dubois, V.; Verfaillie, A.; Young, J.; Trekels, M.; Vancraenenbroeck, R.; De Maeyer, M.; Claessens, F. *Mol. Cell. Biol.* **2012**, *32*, 3033–3043.
17. Yu, X.; Gupta, A.; Wang, Y.; Suzuki, K.; Mirosevich, J.; Orgebin-Crist, M.; Matusik, R. *Ann. N. Y. Acad. Sci.* **2005**, *1061*, 77–93.
18. Mellinghoff, I. K.; Vivanco, I.; Kwon, A.; Tran, C.; Wongvipat, J.; Sawyers, C. *Cancer cell* **2004**, *6*, 517–527.
19. Ni, L.; Llewellyn, R.; Kesler, C. T.; Kelley, J. B.; Spencer, A.; Snow, C. J.; Shank, L.; Paschal, B. M. *Mol. Cell. Biol.* **2013**, *33*, 4766–4778.
20. Nadal, M.; Prekovic, S.; Gallastegui, N.; Helsen, C.; Abella, M.; Zielinska, K.; Gay, M.; Vilaseca, M.; Taulès, M.; Houtsmuller, A. B.; van Royen, M. E.; Claessens, F.; Fuentes-Prior, P.; Estébanez-Perpiñá, E. *Nat. Commun.* **2017**, *8*, 14388.
21. Feng, W.; Ribeiro, R. C.; Wagner, R. L.; Nguyen, H.; Apriletti, J. W.; Fletterick, R. J.; Baxter, J. D.; Kushner, P. J.; West, B. L. *Science* **1998**, *280*, 1747–1749.
22. Wilson, E. M. *Methods Mol. Biol.* **2011**, *776*, 113–129.
23. Saporita, A. J.; Zhang, Q.; Navai, N.; Dincer, Z.; Hahn, J.; Cai, X.; Wang, Z. *J. Biol. Chem.* **2003**, *278*, 41998–42005.
24. Grishkovskaya, I.; Avvakumov, G. V.; Hammond, G. L. *J. Biol. Chem.* **2002**, *277*, 32086–32093.
25. Bennett, N. C.; Gardiner, R. A.; Hooper, J. D.; Johnson, D. W.; Gobe, G. C. *Int. J. Biochem. Cell. Biol.* **2010**, *42*, 813–827.
26. Lonergan, P. E.; Tindall, D. J. *J. Carcinog.* **2011**, *10*, 20.
27. Huggins, C.; Hodges, C. V. *Cancer Res.* **1941**, *1*, 293–297.
28. de Voogt, H. J. *Prostate Suppl.* **1992**, *4*, 91–95.
29. Gao, W.; Bohl, C. E.; Dalton, J. T. *Chem. Rev.* **2005**, *105*, 3352–3370.
30. Wirth, M. P.; Hakenberg, O. W.; Froehner, M. *Eur. Urol.* **2007**, *51*, 306–314.
31. Chen, Yu.; Clegg, N. J.; Scher, H. I. *Lancet Oncol.* **2009**, *10*, 981–991.
32. Haendler, B.; Cleve, A. *Mol. Cell. Endocrin.* **2012**, *352*, 79–91.
33. Wong, Y.; Ferraldeschi, R.; Attard, G.; de Bono, J. *Nat. Rev. Clin. Oncol.* **2014**, *11*, 365–376.

34. Janknegt, R. A.; Abbou, C. C.; Bartoletti, R.; Bernstein-Hahn, L.; Bracken, B.; Brisset, J. M.; Calais Da Silva, F.; Chisholm, G.; Crawford, E. D.; Debruyne, F. M. J.; Dijkman, G. D.; Frick, J.; Goedhals, J.; Knönagel, H.; Venner, P. M. *J. Urol.* **1993**, *149*, 77–82.
35. Schellhammer, P. F.; Sharifi, R.; Block, N. L.; Soloway, M. S.; Venner, P. M.; Patterson, A. L.; Sarosdy, M. F.; Vogelzang, N. J.; Chen, Y.; Kolvenbag, G. J. *Cancer* **1996**, *78*, 2164–2169.
36. Zhou, Y.; Bolton, E. C.; Jones, J. O. *J. Mol. Endocrinol.* **2015**, *54*, 15–29.
37. Chandrasekar, T.; Yang, J. C.; Gao, A. C.; Evanc, C. P. *Transl. Androl. Urol.* **2015**, *4*, 365–380.
38. Coutinho, I.; Day, T. K.; Tilley, W. D.; Selth, L. A. *Endocr. Relat. Cancer* **2016**, *23*, 179–197.
39. Bohl, C. E.; Gap, W.; Miller, D. D.; Bell, C. E.; Dalton, J. T. *Proc. Natl. Acad. Sci. U S A* **2005**, *102*, 6201–6206.
40. Tran, C.; Ouk, S.; Clegg, N. J.; Chen, Y.; Watson, P. A.; Arora, W.; Wongvipat, J.; Smith-Jones, P.; Yoo, D.; Kwon, A.; Wasielewska, T.; Welsbie, D.; Chen, C.; Higano, C. S.; Beer, T. M.; Hung, D. T.; Scher, H. I.; Jung, M.; Sawyers, C. L. *Science*, **2009**, *324*, 787–790.
41. Pinto, A. *Cancer Biol. Ther.* **2014**, *15*, 149–155.
42. Merseburger, A. S.; Haas, G. P.; von Klot, C. *Ther. Adv. Urol.* **2015**, *7*, 9–21.
43. Mostaghel, E. A. *Cancer Manag. Res.* **2014**, *6*, 39–51.
44. Claessens, F.; Helsen, C.; Prekovic, S.; Van den Broeck, T.; Spans, L.; Van Poppel, H.; Joniau, S. *Nat. Rev. Urol.* **2014**, *11*, 712–716.
45. Kregel, S.; Chen, J. L.; Tom, W.; Krishnan, V.; Kach, J.; Brechka, H.; Fessenden, T. B.; Isikbay, M.; Paner, G. P.; Szmulewitz, R. Z.; Vander Griend, D. J. *Oncotarget* **2016**, *7*, 26259–26274.
46. Johnston, P. A.; Nguyen, M. M.; Dar, J. A.; Ai, J.; Wang, Y.; Masoodi, K. Z.; Shun, T.; Shinde, S.; Camarco, D. P.; Hua, Y.; Hury, D. M.; Wilson, G. M.; Lazo, J. S.; Nelson, J. B.; Wipf, P.; Wang, Z. *Assay Drug Dev. Technol.* **2016**, *14*, 226–239.
47. Johnson, J. K.; Skoda, E. M.; Zhou, J.; Parrinello, E.; Wang, D.; O'Malley, K.; Eyer, B. R.; Kazancioglu, M.; Eisermann, K.; Johnston, P. A.; Nelson, J. B.; Wang, Z.; Wipf, P. *ACS Med. Chem. Lett.* **2016**, *7*, 785–790.
48. Fried, J.; Sabo, E. F. *J. Am. Chem. Soc.* **1954**, *76*, 1455–1456.
49. Isanbor, C.; O'Hagan, D. *J. Fluorine Chem.* **2006**, *127*, 303–319.
50. Liang, T.; Neumann, C. N.; Ritter, T. *Angew. Chem. Int. Ed.* **2013**, *52*, 8214–8264.



51. Wang, J.; Sánchez-Roselló, M.; Aceña, J. L.; del Pozo, C.; Sorochinsky, A. E.; Fustero, S.; Soloshonok, V. D.; Liu, H. *Chem. Rev.* **2014**, *114*, 2432–2506.
52. Purser, S.; Moore, P. R.; Swallow, S.; Gouverneur, V. *Chem. Soc. Rev.*; **2008**, *37*, 320–330.
53. Lu, H.; Xie, C.; Chang, J.; Lin, G.; Sun, X. *Eur. J. Med. Chem.* **2011**, *46*, 1743–1748.
54. Miao, Z.; Zhu, L.; Dong, G.; Zhuang, C.; Wu, Y.; Wang, S.; Guo, Z.; Wu, S.; Zhu, S.; Fang, K.; Yao, J.; Li, J.; Sheng, C.; Zhang, W. *J. Med. Chem.* **2013**, *56*, 7902–7910.
55. Gillis, E. P.; Eastman, K. J.; Hill, M. D.; Donnelly, D. J.; Meanwell, N. A. *J. Med. Chem.* **2015**, *58*, 8315–8359.
56. O'Hagan, D. *Chem. Soc. Rev.* **2008**, *37*, 308–319.
57. Rosenblum, S. B.; Huynh, T.; Adriano, A.; Davis, Jr., H. R.; Yumibe, N.; Clader, J. W.; Burnett, D. A. *J. Med. Chem.* **1998**, *41*, 973–980.
58. Rosen, T. C.; Yoshida, S.; Frohlich, R.; Kirk, K. L.; Haufe, G. *J. Med. Chem.* **2004**, *47*, 5860–5871.
59. Schlosser, M.; Brugger, N.; Schmidt, W.; Amrhein, N. *Tetrahedron* **2004**, *60*, 7731–7742.
60. Haufe, G.; Rosen, T. C.; Meyer, O. G. J.; Frohlich, R.; Rissanen, K. *J. Fluorine Chem.* **2002**, *114*, 189–198.
61. Shi, G.; Xu, Y. *J. Chem. Soc., Chem. Commun.* **1989**, 607.
62. Shi, G.; Xu, Y. *J. Org. Chem.* **1990**, *55*, 3383–3386.
63. Bartrum, H. E.; Blakemore, D. C.; Moody, C. J.; Hayes, C. J. *Chem. Eur. J.* **2011**, *17*, 9586–9589.
64. Muller, P.; Grass, S.; Shahi, S. P.; Bernardinelli, G. *Tetrahedron* **2004**, *60*, 4755 – 4763.
65. Feit, B. A.; Elser, R.; Melamed, U.; Goldberg, I. *Tetrahedron* **1984**, *40*, 5177–5180.
66. Brahm, D. L. S.; Dailey, W. P. *Chem. Rev.* **1996**, *96*, 1585–1632.
67. Dolbier, Jr., W. R.; Battiste, M. A. *Chem. Rev.* **2003**, *103*, 1071–1098.
68. Ni, C.; Hu, J. *Synthesis* **2014**, *64*, 842–863.
69. Oshiro, K.; Morimoto, Y.; Amii, H. *Synthesis* **2010**, 2080–2084.
70. Eusterwiemann, S.; Martinez, H.; Dolbier, Jr., W. R. *J. Org. Chem.* **2012**, *77*, 5461–5464.
71. Thomason, C. S.; Martinez, H.; Dolbier, Jr., W. R. *J. Fluorine Chem.* **2013**, *150*, 53–59.
72. Wang, F.; Luo, T.; Hu, J.; Wang, Y.; Krishnan, H. S.; Jog, P. V.; Ganesh, S. K.; Prakash, G. K. S.; Olah, G. A. *Angew. Chem. Int. Ed.* **2011**, *50*, 7153–7157.

73. Wang, F.; Zhang, W.; Zhu, J.; Li, H.; Huang, K.; Hu, J. *Chem. Commun.* **2011**, *47*, 2411–2413.
74. Li, L.; Wang, F.; Ni, C.; Hu, J. *Angew. Chem. Int. Ed.* **2013**, *52*, 12390–12394.
75. Zheng, Z.; Dolbier, Jr., W. R. *J. Fluorine Chem.* **2013**, *149*, 119–124.
76. Baker, B. A.; Bošković, Z. V.; Lipshutz, B. H. *Org. Lett.* **2008**, *10*, 289–292.
77. Bessard, Y.; Schlosser, M. *Tetrahedron* **1991**, *47*, 123–1238.
78. Stepan, A. F.; Subramanyam, C.; Efremov, I. V.; Dutram J. K.; O’Sullivan, T. J.; DiRico, K. J.; McDonald, W. S.; Won, A.; Dorff, P. H.; Nolan, C. E.; Becker, S. L.; Pustilnik, L. R.; Riddell, D. R.; Kauffman, G. W.; Kormos, B. L.; Zhang, L.; Lu, Y.; Capetta, S. H.; Green, M. E.; Karki, K.; Sibley, E.; Atchison, K. P.; Hallgreen, A. J.; Oborski, C. E.; Robshaw, A. E.; Sneed, B.; O’Donnell, C. J. *J. Med. Chem.* **2012**, *55*, 3414–3424.
79. Nicolaou, K. C.; Vourloumis, D.; Totokotsopoulos, S.; Papakyriakou, A.; Karsunky, H.; Fernando, H.; Gavriljuk, J.; Webb, D.; Stepan, A. *ChemMedChem* **2016**, *11*, 31–37.
80. Measom, N. D.; Down., K. D.; Hirst, D. J.; Jamieson, C.; Manas, E. S.; Patel, V. K.; Somers, D. O. *ACS Med. Chem. Lett.* **2017**, *8*, 43–48.
81. Makarov, I. S.; Brocklehurst, C. E.; Karaghiosoff, K.; Koch, G.; Knochel, P. *Angew. Chem. Int. Ed.* **2017**, *56*, 12774–12777.
82. Wiberg, K. B.; Waddell, S. T.; Laidig, K. *Tetrahedron Lett.* **1986**, *27*, 1553–1556.
83. Kaszynski, P.; Michl, J. *J. Org. Chem.* **1988**, *53*, 4593–4594.
84. Della, E. W.; Taylor, D. K.; Tsanaktsidis, J. *Tetrahedron Lett.* **1990**, *31*, 5219–5220.
85. Messner, M.; Kozhushkov, S. I.; de Meijere, A. *Eur. J. Org. Chem.* **2000**, 1137–1155.
86. Applequist, D. E.; Renken, T. L.; Wheeler, J. W. *J. Org. Chem.* **1982**, *47*, 4985–4995.
87. Della, E. W.; Taylor, D. K. *J. Org. Chem.* **1994**, *59*, 2986–2996.
88. Semmler, K.; Szeimies, G.; Belzner, J. *J. Am. Chem. Soc.* **1985**, *107*, 6410–6411.
89. Concellón, J. M.; Rodríguez-Solla, H.; Méjica, C.; Blance, E. G. *Org. Lett.* **2007**, *9*, 2981–2984.
90. Anson, C. W.; Thamattoor, D. M. *J. Org. Chem.* **2012**, *77*, 1693–1700.
91. Lebel, H.; Marcoux, J.; Molinaro, C.; Charette, A. B. *Chem. Rev.* **2003**, *103*, 977–1050.
92. Ebner, C.; Carreira, E. M. *Chem. Rev.* **2017**, *117*, 11651–11679.
93. Zhang, J. L.; Zou, H. B.; Huang, J. S.; Che, C. M. *Chem. Eur. J.* **2002**, *8*, 1554–1562.
94. Dai, H.; Hu, X.; Chen, H.; Bai, C.; Zheng, Z. *J. Mol. Catal. A* **2004**, *211*, 17–21.

95. Doyle, M. P. *Angew. Chem. Int. Ed.* **2009**, *48*, 850–852.
96. Hoang, V. D. M.; Reddy, P. A. N.; Kim, T. J. *Tetrahedron Lett.* **2007**, *48*, 8014 – 8017.
97. Rosenberg, M. L.; Vlasana, K.; Gupta, N. S.; Wragg, D.; Tilset, M. J. *Org. Chem.*; **2011**, *76*, 2465–2470.
98. Uchida, T.; Irie, R.; Katsuki, T. *Synlett.* **1999**, 1163–1165.
99. Nakamura, A.; Konishi, A.; Tatsuno, Y.; Otsuka, S. *J. Am. Chem. Soc.* **1978**, *100*, 3443–3448.
100. Fukuda, T.; Katsuki, T. *Synlett* **1995**, 825–826.
101. Niimi, T.; Uchida, T.; Irie, R.; Katsuki, T. *Tetrahedron Lett.* **2000**, *41*, 3647–3651.
102. Uchida, T.; Katsuki, T. *Synthesis* **2006**, *10*, 1715–1723.
103. Kanchiku, S.; Suematsu, H.; Matsumoto, K.; Uchida, T.; Katsuki, T. *Angew. Chem. Int. Ed.* **2007**, *46*, 3889–3891.
104. Sasaki, H.; Irie, R.; Hamada, T.; Suzuki, K.; Katsuki, T. *Tetrahedron Lett.* **1994**, *50*, 11827–11838.
105. Smith, K.; Liu, C. H.; El-Hiti, G. A. *Org. Biomol. Chem.* **2006**, *4*, 917–927.
106. Hashihayata, T.; Punniyamurthy, P.; Irie, R.; Katsuki, T.; Akita, M.; Moro-oka, Y. *Tetrahedron* **1999**, *55*, 14599–14610.
107. Hirotsu, M.; Kojima, M.; Nakajima, K.; Kashino, S.; Yoshikawa, Y. *Bull. Chem. Soc. Jpn.* **1996**, *69*, 2549–2557.
108. Niimi, T.; Uchida, T.; Irie, R.; Katsuki, T. *Adv. Synth. Catal.* **2001**, *343*, 79–88.
109. Gianatassio, R.; Lopchuck, J. M.; Wang, J.; Pan, C. M.; Malins, L. R.; Prieto, L.; Brandt, T. A.; Collins, M. R.; Gallego, G. M.; Sach, N. W.; Spangler, J. E.; Zhu, H.; Zhu, J.; Baran, P. S. *Science* **2016**, *351*, 241–246.